Theoretical Studies of Novel Radon-Containing Molecules

by

Amelia Fitzsimmons

A thesis submitted in partial fulfillment of the requirements for the degree of

Doctor of Philosophy

Department of Chemistry

University of Alberta

Abstract

The chemistry of radon is best understood in the context of the periodic relationship between radon and its lighter cousin xenon. I have studied several classes of radon-containing small molecules, many of which are related to extant xenon-containing molecules. These studies began with an investigation into the structure and properties of HRnF, which I have studied at levels of theory which account for electron correlation and with large pseudopotentials basis sets. My results demonstrated that HRnF is more stable than was previously supposed. Structures and properties of radon halohydrides of the heavier halogens: fluorine, chlorine, bromine, and iodine were also studied with correlated methods and larger pseudopotentials basis sets in order to better understand their chemistry. These compounds have been studied with population analysis methods that analyze the electron density.

In the fourth Chapter, I present results of studies of small organic molecules containing radon. Pseudopotentials basis sets and correlated methods were used to predict the stability of several organic compounds of the type ARgB containing heavy rare gas atoms, where Rg is either xenon or radon, and A and B are fluoride or any of the following organic ligands: methyl -CH_3, perfluoromethyl -CF_3, ethynyl -CCH, fluoroethynyl -CCF, and cyano -CN. The effect of solvents upon the kinetic stability of these molecules was also studied, and I found that the radon-containing organic molecules are equally stable as xenon-containing organic molecules.

Related compounds composed of radon with either a methyl or perfluoromethyl

group on either side (CX_3RgCX_3, where X=H, F and Rg=Xe, Rn) were studied with a variety of computational methods, including correlated methods for computing structures and population analysis methods for analyzing bonding. I found that bonding in the radon-containing compounds matches the bonding in xenon-containing compounds.

Continuing my studies of organic radon-containing compounds, I examined molecules of the type C_6H_5RgA and C_6F_5RgA, where Rg is either radon or xenon and A is one of F, CN, CCH, or CCF using correlated methods and pseudopotentials basis sets. I computed structures and properties of these molecules and analyzed their free energies of formation. Analysis of the electron density of these molecules indicates that they are stabilized by π-electron transfer from the aromatic ring to the bond between the rare gas and the aromatic group. Radon-containing molecules of this type were found to be more stable than xenon-containing molecules, which is unsurprising based on the results of the previous chapters.

The effects of confinement within a harmonic potential upon the decomposition pathway of molecules of the type HRgX (Rg=Xe Rn; X=F, Cl) were studied next, with both planar and cylindrical confinements used. The reaction was followed both in the gas phase and in confined environments in order to evaluate the effects of confinement on the energy barrier ΔE_{TS} and kinetic stability of the HRgX compounds. Confinement does not affect the angle at which the HRgX transition state occurs and results in a slight increase in the energy barrier to decomposition of the HRgX species.

This same decomposition reaction was also studied in the context of confinement within a pair of planar helium sheets, and the effect of the location of the HRgX molecule within the sheets upon the structure of the transition state and the energy barrier to decomposition was studied. The effect of confinement within helium sheets

on the electron density of HRgX molecules was studied as well.

Anharmonic vibrational frequencies were computed for radon-containing inorganic compounds. Structures of molecules HRnAH and HRnAF(A=O, S), $HRnZH_2$ and $HRnZF_2$ (Z=N, P) were optimized and anharmonic vibrational frequencies computed with the correlation corrected vibrational self-consistent field method. Spectra of HRnSH and $HRNPH_2$ are analyzed and dominant features of each highlighted. The HRnSH spectrum includes the three IR active fundamentals, two overtones, and one combination band. The $HRnPH_2$ spectrum features three high-intensity fundamentals and many intense combination bands and overtones. The quartic force field approximation has large errors with respect to the direct method in computation of overtones.

Preface

All of the research reported in Chapters 2-9 of this thesis was accomplished in a collaborative environment at the University of Alberta.

A version of Chapter 2 has been previously published as "Model core potential and all-electron studies of molecules containing rare gas atoms" in the *Journal of Physical Chemistry A*, **2010**, *114*, 8786 by A. Fitzsimmons, H. Mori, E. Miyoshi, and M. Klobukowski. H. Mori and E. Miyoshi provided new basis functions and pseudopotentials for the study.

A version of Chapter 3 has previously been published as "Basis set effects in simple compounds of heavy rare gases" in the *Canadian Journal of Chemistry*, **2013**, *91*, 894-901 by A. Fitzsimmons and M. Klobukowski. A. Fitzsimmons carried out computations, analyzed data, and composed the article. M. Klobukowski wrote scripts to aid in data analysis, provided paragraphs in the article and assisted with the editing process.

A version of Chapter 4 was previously published as "Structure and stability of organic molecules containing heavy rare gas atoms" in *Theoretical Chemistry Accounts*, **2013**, *132*, 1413 by A. Fitzsimmons and M. Klobukowski. A. Fitzsimmons carried out the gas-phase computations, analyzed data, and composed the sections of the article reporting gas-phase results. M. Klobukowski carried out solvent-phase computations, analyzed solvent-phase data, and wrote the section of the article reporting solvent-phase results.

Data from Chapter 5 are being prepared for publication as "Symmetric and asymmetric methyl and perfluoromethyl compounds of heavy rare gases" by A. Fitzsimmons, S. Turner, and M. Klobukowski. Perturbation theory geometry optimizations in GAMESS-US were carried out by A. Fitzsimmons and S. Turner, a WISEST student under A. Fitzsimmons' supervision in the summer of 2012, and density functional theory geometry optimizations were carried out by M. Klobukowski. QTAIM computations were carried out by S. Turner. Data was analyzed by A. Fitzsimmons, and the article was written by A. Fitzsimmons.

Data from Chapter 6 are being prepared for publication under its present title by A. Fitzsimmons, C. Chiasson, and M. Klobukowski. Computations of optimized structures were done by C. Chiasson, a WISEST student under A. Fitzsimmons' supervision in the summer of 2013. A. Fitzsimmons carried out the QTAIM computations and data analysis and wrote the paper. Editorial comments were provided by M. Klobukowski.

Data from Chapter 7 are being prepared for publication under its present title in the *Journal of Physics B* by A. Fitzsimmons and M. Klobukowski. A. Fitzsimmons carried out computations in the planar confinement and M. Klobukowski carried out computations in the cylindrical confinement. M. Klobukowski and A. Fitzsimmons both wrote scripts to aid in the analysis of data. I analyzed all data and composed the manuscript.

A version of Chapter 8 is being prepared for publication in *J. Phys. B.* I carried out computations for configurations A and B; M.Klobukowski carried out computations for configuration C. Figure 8.1 was made by M. Klobukowski. M. Klobukowski and A. Fitzsimmons both wrote scripts to aid in the analysis of data. A. Fitzsimmons analyzed all data and composed the manuscript.

A version of Chapter 9 has been published under its present title in *Chemical*

Physics Letters, **2014**, *612*, 73 as an article by A. Fitzsimmons and M. Klobukowski. A. Fitzsimmons computed optimized structures, vibrational frequencies and analyzed data. M. Klobukowski optimized transition states and computed energies of decomposition and of the transition state. M. Klobukowski and A. Fitzsimmons both wrote scripts to aid in the collection and analysis of data. A. Fitzsimmons wrote the manuscript with the editorial help of M. Klobukowski.

Magic is just science we don't understand yet.–Arthur C. Clarke

The Lord is subtle but he is not malicious.–Albert Einstein

Discovery of the quantum mechanics could arguably be the most fantastic event in the entire history of physics.–Sigeru Huzinaga

At the same time that we are earnest to explore and learn all things, we require that all things be mysterious and unexplorable, that land and sea be indefinitely wild, unsurveyed and unfathomed by us because unfathomable. We can never have enough of nature.–Henry David Thoreau

The most exciting phrase to hear in science, the one that heralds new discoveries, is not "Eureka!" but "That's funny..."–Isaac Asimov

Acknowledgements

"It is now well understood that we may learn to make our own lives good and honest and true, by carefully and diligently following the example of the good and honest and true who have gone before us." –*The Story of the Herschels, a Family of Astronomers*

I am grateful to so many people, for reasons big and small that all contributed to my finishing this thesis. For the past five years it has been my privilege to work in the research group of Mariusz Klobukowski. The love that Mariusz has for his work and the joy that he takes in teaching his students are evident in all he does. I particularly want to thank him for all of the wise advice, both about science and life, that he has shared.

Thank you to my coworkers, and to past and present group members: Cassandra Churchill, Melis Gedik, Shuai Sun, Farnaz Shakib, Melissa Gajewski, Toby Zeng, Stephanie Wong, Mohammed Momeni, Arianne Krekoski, Enrico Medina, and Ahmed Ayoub: your conversation and friendship have made work days pleasant. I appreciate the time and care that the members of my examining committee have taken in reading the preliminary version of this thesis and in giving me their comments. To Alex Brown, for suggesting that I do the anharmonic computations in the first place and to Jon Veinot, for your encouragement and advice.

No academic work exists in a vacuum, and I am thankful for the many friends outside of the University of Alberta who have made the time that I have spent in Edmonton a joy in spite of the often bitter climate. I am happy to have been a part of the community at St. George's Anglican church for the past three years. Thank you to everyone there, especially to the ladies of the altar guild, for your wonderful

stories and for being willing to let me share in the work that you take such pride and diligence in, to Joan–you brightened all of our lives with your kindness and grace; to Sue, Alex, and Scott, for leading this community with such love and care; to Cedric and all the choir, for the fun that we have had making music together; to Sineen and Natasha, for all of the fun times we have had together; to Elise, for the times in Rutherford we spent working on our theses; to Heather, with love; to Kristian, to Julie and Kelsey, Kirsti, Alison, Joe, Lewis, Sarah and Grant, to Alexis, Sarah and Stu: you have made my time in Edmonton such a delight.

To my parents, Dennis and Marylou, who are the ones who first introduced me to the wonder and joy of science: thank you for your love and support, for helping me with everything from elementary school science fair projects to moving to Alberta to start graduate school, for all that you have sacrificed in raising Bonnie and Nathan and myself, I will always be grateful. To my siblings Bonnie and Nathan, who are simultaneously two of the silliest and wisest people I know: peace and blessings. Thank you to all of the Enix and Benner clans: to Dale and Chloe; to Nancy and Alan; to Ryan, Lisa, and the girls; to Caitie and Aiden; to Cody; to Mark, Michelle and Rachel; to Tom and Emily, Tommy and Laurie: I am proud to be one of you. To my grandparents, Mary Alice and Louie and Gene and Clyde: I will always treasure the memories of all the time that you spent with my siblings and I. I am so grateful for all of your encouragement to further my education and to write: I love and miss you so much.

I am fortunate to have wonderful inlaws; to all the Fitzsimmons, thank you for your love and friendship. To Hannah and Naomi, for all of the fun that we had while working on our bachelor's degrees; to Sharon, for all of your wise advice; to Dan and Betty, for your love.

Finally, I thank Luke, for more than there is space here to name. For your willingness to move across the continent with me less than a year after we were married, and then to stay here through five Alberta winters, for all the article and thesis chapter drafts that you proofread, for all of your love and faith in me, for your support while I worked on this.

Table of Contents

List of Tables

List of Figures

List of Abbreviations and Acronyms

BSSE	*Basis Set Superposition Error*
CEBE	*Core Electron Binding Energy*
CCSD	*Coupled Clusters: Single and Double excitations*
CCSD(T)	*Coupled Clusters: Single, Double, and non-iterative Triple excitations*
cc-VSCF	*Correlation-Corrected Vibrational Self-Consistent Field*
CI	*Configuration Interaction*
CP	*Counterpoise*
CR-CC(2,3)	*Completely Renormalized Coupled Clusters (2,3)*
DFT	*Density Functional Theory*
GGA	*Generalized Gradient Approximation*
HF	*Hartree-Fock*
HFRH	*Hartree-Fock Roothaan Hall*
HOMO	*Highest Occupied Molecular Orbital*
iMCP	*Improved Model Core Potentials*
IR	*Infrared*
IUPAC	*International Union of Pure and Applied Chemistry*
IRC	*Intrinsic Reaction Coordinate*
LUMO	*Lowest Unoccupied Molecular Orbital*
MP2	*Møller-Plesset Perturbation Theory, Second Order*

MCP	*Model Core Potentials*
NBO	*Natural Bond Orbitals*
NPA	*Natural Population Analysis*
NMR	*Nuclear Magnetic Resonance*
PBE	*Perdew-Burke-Enzerhof Functional*
PBE0	*Perdew-Burke-Enzerhof Functional, without parameters*
QFF	*Quartic Force Field Approximation*
RHF	*Restricted Hartree-Fock*
ROHF	*Restricted Open Shell Hatree-Fock*
SCF	*Self-Consistent Field*
UHF	*Unrestricted Hartree-Fock*
VSCF	*Vibrational Self-Consistent Field*
WISEST	*Women in Scholarship, Engineering, Science and Technology*
ZFK	*Zeng-Fedorov-Klobukowski basis set*
ωB97	*A Long-Range Corrected GGA Functional*

List of Symbols

Roman Symbols

Å	*Angstrom*
$\hat{a}$	*Annhilation Operator*
$\hat{a}^+$	*Creation Operator*
a.u.	*Atomic Units*
cm^{-1}	*Wavenumbers*
°C	*Degrees Celsius*
$\hat{C}_n$	*Excitation Operator*
e	*Charge of an Electron*
eV	*Electron Volts*
$\hat{f}$	*Fock Operator*
h	*Planck's Constant*
$\hat{h}$	*One-Electron Hamiltonian Operator*
$\mathcal{H}$	*Hamiltonian*
$\hat{J}$	*Exchange Operator*
$\hat{K}$	*Coulomb Operator*
$kJ{\cdot}mol^{-1}$	*Kilojoules per mol*
$km{\cdot}mol^{-1}$	*Kilometers per mol*
N_c	*Number of Core Electrons*
n_K^d	*Contracted d-type basis function*

n_K^f	*Contracted f-type basis function*
n_K^p	*Contracted p-type basis function*
n_K^s	*Contracted s-type basis function*
$\mathcal{P}$	*Property*
q	*Charge*
r_e	*Equilibrium Bond Length*
r	*Bond Length*
Rg	*Rare Gas*
$\hat{T}_n$	*Cluster Operator*
$\hat{V}$	*Potential Operator*
Z	*Atomic Number*

Greek Symbols

ΔE	*Change in Energy*
ΔG	*Change in Gibbs Free Energy*
Δ_{h-q}	*Difference between Harmonic and QFF Frequencies*
Δ_{q-d}	*Difference between QFF and Direct Frequencies*
δ_s ABC	*in-plane bend (scissor) of atoms A, B, and C*
ϵ_c	*Energy of Core Atomic Orbital*
Θ	*Bond Angle*
μ	*Dipole Moment*
ν	*Vibrational Normal Mode*
ρ(r)	*Electron Density*

ρ ABC	*in-plane bend (rock) of atoms A, B, and C*
τ ABC	*out-of-plane bend (twist) of atoms A, B, and C*
υ_s AB	*symmetric stretch between atoms A and B*
υ_{as} AB	*asymmetric stretch between atoms A and B*
ϕ	*Orbital*
$\chi_p(r)$	*Basis Function*
ψ	*Spin Orbital*
Ψ	*Wavefunction*
Ω	*MCP Projection Operator*
ω	*Coefficient of Confining Potential Strength*
ω ABC	*out-of-plane bend (wag) of atoms A, B, and C*

Non-Alphabetical Symbols

∇^2	*Laplacian*

Chapter 1

Introduction

1.1 A Brief History of Heavy Rare Gas Chemistry

Radon chemistry has a rich history, beginning with the discovery of the element in 1900 by Friederich Ernst Dorn and its isolation in 1910 by Sir William Ramsay and Robert Whytlaw-Gray.[1] Following the preparation of the first xenon-containing compound by Bartlett[2] there was a flurry of activity as chemists synthesized related xenon-containing compounds. Bartlett originally believed he had synthesized $Xe(PtF_6)$, but the compound was later shown to be a mixture of two xenon-fluoride cations: XeF^+ and $Xe_2F_3^+$.[3] More important than the exact chemical makeup of the compound was the implication – one rare gas, at least, was no longer inert. This discovery set the stage for further investigation into the nature of rare gas chemistry. Having surmounted the first hurdle – is there anything at all with which xenon can react? – inorganic chemists now searched for other conditions and reagents capable of reacting with xenon. Several simple xenon fluorides were soon prepared: XeF_2[4], XeF_4, and XeF_6.[5] All of these syntheses were accomplished at very low temperatures – -78° C was standard – and characterized the resulting compounds using infrared spectroscopy and mass spectrometry. These xenon-containing compounds were first studied as an object of curiosity, as xenon was the first rare gas to be proven to be able to reactive. Later, as xenon chemistry developed further, small xenon-containing compounds such as XeF_2 began to be useful as reactants in further syntheses of xenon-containing organic compounds.

Applying the tools of xenon chemistry to radon, Fields, Stein, and Zirin found that while radon reacted with fluorine at the conditions described above, it was unreactive with chlorine and water. The radon fluoride of unknown empirical formula[6] was the first radon-containing molecule to be synthesized. From its inception, radon chemistry developed by mimicking known xenon chemistry. The periodic relationship of the two elements together with the periodic trend in polarizability suggest that in any way that xenon can react, radon should be more reactive. But radon chemistry was limited in ways that xenon chemistry was not; working with a radioactive gas whose longest-lived isotope decayed by α-decay in 3.8 days[7] was a daunting prospect. In an almost prophetic comment in *Noble Gas Compounds*, Weinstock noted that "the lack of volatility of the radon fluoride would be explained if radon formed an ionic fluoride".[8] Several years down the road, a new class of radon-containing fluorohydrides would indeed be shown to be primarily ionic in character.

Haseltine and Moser discovered that when ^{220}Rn and ^{226}Rn were in secular equilibrium, or being produced by their parent isotopes at the same rate as they were decaying, in an ionic, aqueous solution, they could be oxidized and then extracted into hexane, and proposed the formula RnO_3 for the species at pH < 11 and $HRnO_4^-$ at pH > 11.[9] A few years later, Stein prepared some form of radon fluoride at -78° C in an ionic solution. While still unable to nail down the formula for the species, he succeeded in determining that upon oxidation in solution, the radon fluoride was a cation.[10] Four years later, in 1974, the Bartlett group measured binding energies of core electrons for xenon-containing compounds.[11] Even in 1975, the formula of the original radon fluoride was elusive. Was it RnF_2 or RnF_4? Based on computed excitation energies, Pitzer hypothesized that it could even be RnF.[12]

The late 1970s through the 1990s saw renewed interest in heavy rare gas chemistry, with research focusing on organic xenon-containing compounds and small molecules with less than seven atoms. The organic chemistry of the heavy rare gases during these years will be discussed first, with a discussion of progress in small, inorganic compounds to follow. In Germany, Seppelt reviewed recent developments in xenon chemistry as part of a survey of recent work with electronegative elements,[13] and dis-

cussed the structures of higher-order xenon fluorides.[14] In the United States, Turbini and coworkers were the first to report synthesis of "a stable σ-bonded xenon-carbon compound"[15], as they titled their article, and indeed did characterize their $Xe(CF_3)_2$ with ^{19}F NMR. However, the lack of an infrared spectrum for the molecule and unsuccessful attempts by the larger scientific community to duplicate this synthesis lead other researchers to doubt the existence of $Xe(CF_3)_2$, and interest in organoxenon chemistry dwindled.

Two reviews of radon chemistry appeared in the early 1980s. Avrorin et al. reviewed progress in radon chemistry with an emphasis on properties of known compounds, the clathrate radon compounds, their stability, and specific challenges associated with their synthesis – notably the short half life of ^{220}Rn.[16] Stein reviewed current progress in radon chemistry the next year, focusing on the developments in four main categories of radon-containing compounds extant at that time: clathrates, both in the gas phase and in solid states; simple radon fluorides of the type RnF_n; complex radon fluorides involving a non-metal or transition metal; and ionic solutions of radon.[17]

It would be another decade before Frohn and Jakobs in Germany synthesized $[C_6F_5Xe]^+$ and confirmed its existence with ^{129}Xe NMR.[18] Frohn and Jakobs confirmed that xenon was a good leaving group, and that their aryl xenon compounds, as they dubbed the new class of molecules, were reactive with both halides and water. In the same year, Naumann and Tyrra synthesized the first neutral compounds with a xenon-carbon bond since 1979: $[C_6F_5XeF][B(C_6F_5)_3F]$, characterizing it with both ^{19}F NMR and ^{129}Xe NMR.[19] Continuing the quest for compounds containing a σ-bond to xenon, in 1990 Turowsky and Seppelt created the inorganic xenon-containing polymer (-Xe-O-TeF_4-O-)$_n$ and confirmed this structure with X-ray crystallography.[20] In 1992, Wells and Weitz synthesized $Cr(CO)_5Xe$, $Mo(CO)_5Xe$, and $W(CO)_5Xe$ by photolyzing metal hexa-carbon monoxides in the presence of xenon and determined dissociation energies and rates of formation.[21]

The review "Organic Chemistry of Noble Gases" published in 1993 focused mainly on the many alkyl and aryl xenon-containing compounds that had been discovered

since the still-contested $Xe(CF_3)_2$.[22] Aryl xenon compounds were found to be kinetically stable at temperatures up to 125 °C and electrophilic, reacting with nucleophilic ligands such as AsF_6^-.[23] By removing two fluorines from tetrafluorovinylidene, xenon difluorovinylidine was successfully synthesized and characterized by Kötting et al. in 1998,[24] who also computed optimized geometries of xenon difluorivinylidene and determined through Natural Population Analysis (NPA) that the xenon atom interacted electrostatically with difluorovinylidene. Continuing interest in aryl xenon tetrafluoroborates led Naumann et al. to synthesize several more species in this class: $[(2,6\text{-}F_2C_6H_3)Xe][BF_4]$, $[(4\text{-}FC_6H_4)Xe][BF_4]$, $[(2\text{-}F_2C_6H_4)Xe][BF_4]$ by hydrolyzing $[XeAr][BF_4]$ in ether, pyridine, and dimethylformamide, any characterized with ^{129}Xe NMR.[25] Frohn et al. continued their work on aryl xenon compounds with the isolation and characterization of $[C_6F_5Xe]Cl$ and $[C_6F_5XeCl][AsF_6]$ from solution in dichloromethane at low temperatures.[26] Frohn and Theissen reported synthesis of derivatives of the pentalfuorophenylxenon(II) ligand they had previously synthesized in 2000 as well.[27] Maggiarosa et al. synthesized bis(pentafluorophenyl)xenon in 2000, verifying this with ^{129}Xe NMR.[28] Progress in organoxenon chemistry up to this point was reviewed by Brel et al. in 2001, highlighting the variety of compounds that could be made mainly by replacing one or more of the fluorides in XeF_2 or XeF_4 with other nucleophiles such as amines, aryl, allene, and oxygen-containing ligands.[29]

1995 was a significant year for inorganic rare gas chemistry in Finland: it saw studies of XeH_2 and $XeAu^+$ as well as the first instance of the synthesis of HXeX (X=Cl, Br, I) compounds. XeH_2 was revisited both theoretically and experimentally in 1995: Pettersson, Lundell, and Räsänen synthesized it inside solid xenon matrices at low temperatures[30] and assigned peaks in their infrared spectra with the aid of computed spectra at the MP2/LANLDZ[31,32] level of theory. Runeberg, Seth, and Pyykkö computed spectroscopic constants for XeH_2 at a variety of levels of theory up to CCSD(T).[33,34] An Xe-Au-Xe compound was also predicted on the basis of relativistic effects alone; lighter rare gases appeared unable to bond with gold.[35] HXeCl, HXeBr, and HXeI were synthesized through photodissociation of HCl, HBr, or HI in solid xenon matrices and studied computationally at the MP2/LANLDZ[31,32]

level of theory.[36] Pettersson et al. studied the mechanism of formation of one of these compounds, HXeI, inside a solid xenon matrix and determined that the most likely formation mechanism is the infrared photodissociation route, in which the H–I bond is lengthened through infrared excitation and a xenon atom from the solid matrix is inserted between the hydrogen and iodine.[37] They hypothesized that this mechanism should hold true for related xenon hydrides and later this was confirmed to be the case: one year later, Pettersson et al. applied the same photoionization-inside-matrix method to synthesize HXeSH: this was the first instance of a xenon-sulfur bond reported in the scientific literature.[38] The photoionization method was also employed to synthesize HXeCN and HXeNC in solid xenon matrices, expanding the library of known xenon species considerably.[39] Further computational studies of heavy rare gas-noble metal compounds revealed that PdXe and PtXe had large enough dissociation energies that they should be thermodynamically stable.[40] Neutral xenon halides XeX as well as their cations and anions were studied in the gas phase and computationally by Schröder et al. in 1998. While the cations were found to be bonded species, the anions and neutral compounds turned out to be weakly interacting van der Waals complexes rather than covalently bound.[41]

By this point, it was clear that at low temperatures, xenon could be coaxed into being far more reactive than previously expected and interest in this new class of molecules grew. Pettersson et al. continued to explore new xenon hydrides, synthesizing HXeCN and HXeNC by the photoionization method in solid xenon matrices in 1998[42] and computationally studying the energy barrier to conversion of HXeNC to HXeCN, finding that while the latter structure is more thermodynamically stable, the barrier to conversion is so low that vibrational excitation of either of the Xe-H or C-N stretching modes provides enough energy to fuel conversion. HXeOH was the next new xenon hydride found, with its synthesis reported in 1999 by Pettersson et al. As with the xenon hydrides already discovered, HXeOH was synthesized through photoionization of a precursor – in this instance, water – inside a solid xenon matrix at low temperatures.[43] The Räsänen group also studied the bonding in HXeX molecules by computing Mulliken charges, which indicated that there was a positively

charged (H-Xe) group interacting with the nucleophile X.[44] Johansson et al. studied the excited states of HXeCl in 1999, computing potential energy surfaces with the CISD method for both the ground state and the four lowest-lying excited states (two singlets, followed by two triplets).[45] Koskinen and Cooks observed BXe^+ and similar ions of lighter rare gases via exchange reactions inside of a mass spectrometer and studied them computationally, finding that the bond order increases with the size of the rare gas and that the energy required to produce BXe^+ from the BBr^+ radical and neutral xenon was less than the collision energy of the system.[46] Crépin-Gilbert and Tramer found that complexes of xenon with alkali, alkaline earth, or noble metals had significantly higher dissociation energies than similar complexes of lighter rare gases in both their ground and excited electronic states.[47] Computational investigations of radon-containing compounds resumed in 1998 when Runeberg and Pyykkö computed structural parameters, dissociation energies, and vibrational frequencies for Xe_2, RnXe, and Rn_2 with a variety of methods, including CCSD(T) and a variety of pseudopotential basis sets, finding that radon was capable of forming van der Waals dimers with both another radon atom and a xenon atom.[48] That same year, Liao and Zhang used a crystal field model to compute properties of several heavy rare gas di- and tetra-fluorides, among then RnF_2, finding that RnF_2 was among the most thermodynamically stable of the surveyed compounds.[49] A year later, radon chemistry continued with the computation of the structures of RnF_2 and RnF_4 along with XeF_2 and XeF_4 by Han and Lee in Korea who used effective core potentials and several methods from HF to CCSD(T), finding that bond lengths in radon hydrides are only 0.09 Å longer than those of the well known xenon hydrides.[50] Experimantally, Eichler et al. found that at 100 K, ^{220}Rn adsorbs onto ice surfaces with an enthalpy of adsorption of -19.2 $kJ \cdot mol^{-1}$,[51] and Lee and Wright computed the interaction energy of the ($Rn \cdot H_2O$) complex.[52]

In their chapter in the 1999 issue of *Advances in Inorganic Chemistry*, Holloway and Hope reviewed progress in rare gas chemistry from 1979-1999, touching on "the possibility of argon chemistry" and briefly on krypton chemistry, but focusing on the significant progress in xenon chemistry that had been made in the previous two

decades. At the start of the 1980s, xenon chemistry could be classified within two rather narrow categories: cations or excited-state molecules in the gas phase, and complexes involving xenon sterically trapped rather than chemically bound inside of a structure.[53] But even within these narrow categories, the large number of papers published on xenon chemistry demonstrate that xenon chemistry progressed significantly in the intervening years, and work continued into the next millennium.

Interest in heavy rare gas chemistry continued to grow in the 21st century. Seidel and Seppelt found that xenon is capable of forming a complex cation with gold, and were able to link this ligand to a bulky polyatomic anion of fluorine and antimony, forming $[AuXe_4{}^{2+}][(Sb_2F_{11}{}^-)_2]$.[54] Grills et al. characterized several organoxenon compounds at room temperature with infrared spectroscopy and examined the lifetimes of these species in order to propose a suggested mechanism for formation.[55] Lundell et al. found that anharmonic effects are significant in the infrared spectrum of the previously studied HXeI, and obtained new IR absorption spectra of HXeI in a solid xenon matrix.[56] Lundell, Chaban, and Gerber computed anharmonic infrared spectra of other xenon containing compounds: HXeH, HXeCl, HXeBr, and HXeOH were all found to have significant anharmonicity.[57] Electronic excitation spectra of HXeCl, HXeBr, HXeI, and HXeCN in xenon matrices were reported by Ahokas et al. in 2000 and the excited state assigned as $A^1\Sigma$ with the help of multireference configuration interaction computations.[58] Lundell et al. also computed optimized geometries and anharmonic vibrational frequencies for fluorohydrides of all rare gases, finding that xenon fluorohydride was the most likely to be thermodynamically stable, and that HRnF had an unusually large r(Rn-F), which lead to the conclusion that HRnF was not a chemically bound species.[59] The only other study of radon chemistry in the year 2000 was that done by Lee et al., in which structures, harmonic vibrational frequencies and interaction energies of the $RnNO^+$ cation were computed.[60] Ball computed heats of formation for xenon sulphides and oxysulfides, finding that their extremely large (positive) heats of formation made it unlikely the species could be synthesized.[61] Eloranta and Kunttu computed excited electronic states for the compounds XeH, linear Xe_2H, triangular Xe_2H, and XeHXe with good agreement

with previous experimental data where it existed.[62] Structures and potential energy surfaces of Xe_2 were computed in 2000 with a comparison between relativistic and non-relativistic methods.[63] The synthesis of $XePtF_6$ by the Bartlett group was reviewed in 2000.[64] Theoretical work by Lundell, Pettersson, and Räsänen indicated that bonding in HXeY-type molecules followed a $[HXe]^+Y^-$ pattern when Y is an organic group or halogen.[65] Lundell et al. computed dissociation energies of HXeY (where Y is an electronegative group) compounds, finding that these energies are high enough that it is likely the molecules could be synthesized in the gas phase in addition to in solid xenon matrices.[66] Pettersson et al. studied the photochemistry of HNCO in xenon matrices, finding that the species can be produced through photolysis of HNCO at low temperatures in a similar manner as several xenon compounds already known.[67] Pyykkö also reviewed recent developments in rare gas chemistry in 2000, focusing on the discoveries of neutral, heavy rare gas containing species in solid rare gas matrices and compounds containing both noble gases and noble metals.[68] Gerken and Schrobilgen reviewed the influence of NMR spectrometry on rare gas chemistry up to the year 2000.[69]

In 2001, Malli predicted that unlike XeF_6, neither RnF_6, nor RnF_6^+, nor RnF_6^- should exist as a chemically bound species due to the large distances between the radon and fluorines.[70] Yu and Chen evaluated several structural isomers of XeF_6, determining that the C_{3v} isomer was the most stable.[71]

Reviews of both organoxenon chemistry and xenon general chemistry were published in 2001, summarizing recent progress in the field. Frohn and Bardin reviewed the state of organoxenon chemistry, focusing on new developments in carbon-xenon bonds.[72] The same year, Christe published a review of the state of rare gas chemistry, highlighting the discoveries of the past thirty years, specifically the existence of Xe-C bonds, the capability of xenon to bond with noble metals, the existence of xenon-containing polyatomic ligands, and other developments in the chemistry of lighter rare gases.[73] Grills et al. continued their work on organometallic xenon compounds, characterizing several more compounds of alkanes and xenon at room temperature.[74] Cohen et al. computed potential energy surfaces and dynamics of the xenon halohy-

drides interacting with the surfaces of xenon matrices in 2001.[75] Machado et al. computed electronic structures of several xenon fluorides, finding equilibrium structural parameters and dissociation energies.[76] Cunje et al. found that in gas phase reactions, xenon could bond with SiF_3^+ to form a SiF_3Xe^+ cation.[77] A chapter on the organic chemistry of xenon appeared in the 2002 issue of *Inorganic Chemistry Highlights* and covered synthetic methods, crystallographic and spectroscopic characteristics, and reactions that use organoxenon compounds as starting materials.[78] In 2002, Panek et al. computed dissociation energies, harmonic vibrational frequencies, and electron densities of rare gas halohydrides for all rare gases except radon, finding that results of Density Functional Theory (DFT) computations were often wildly divergent from results of standard *ab initio* computations.[79] Bihary et al. picked up the study of HXeCl, HXeI, and lighter rare gas halohydrides inside solid rare gas matrices in 2002 when they computed potential energy surfaces and anharmonic vibrational frequencies for these molecules, finding that the ambient rare gas matrix had a significant effect upon the vibrational spectrum.[80] Nemukhin et al. computed the interaction strengths and vibrational spectra of HXeOH and HXeOH-H_2O complexes.[81] Himmel et al. reviewed reactions of ground and excited state atoms and included reactions of xenon – by this point, xenon had been demonstrated to be reactive with water, Cl_2, H_2S, HCN, HNCO, and halohydrides.[82] Lovallo and Klobukowski computed energies of formation and decomposition for several xenon-containing compounds: XeF_2, $Xe(CN)_2$, $Xe(CCH)_2$, $Xe(CCF)_2$, $Xe(C_6H_5)_2$, $Xe(C_6F_5)_2$, $Xe(CF_3)_2$, and $Xe(CH_3)_2$, predicting thermodynamic stability for many of these compounds.[83] Lundell, Cohen, and Gerber predicted the existence of HXeCCH, $HXeC_6H_5$, and $HXeOC_6H_5$ in 2002, and experimental confirmation of HXeCCH in particular would appear within one year.[84] Drews, Seidel, and Seppelt continued their investigations of $AuXe_4^{2+}$ cations in 2002 with crystallographic studies of gold-xenon cations.[85] Based on computed dissociation energies, atomic charges, and optimized geometries, Malli predicted that HRnCO should exist as a stable, bound species.[86] Similarly, Khriachtchev et al. predicted that the neutral HXeO radical should be stable inside a xenon matrix at 7 K.[87] Tanskanen et al. identified $HXeC_4H$ inside a xenon matrix and analyzed the infrared

absorption spectrum of the molecule.[88] Theoretical studies of nonmetal fluorides and analysis of their electron density by Tsvetkov et al. revealed that xenon fluorides are most stable when complexed with heavier transition metals and nonmetals.[89]

A significant development in 2003 was the publication of two unique routes to synthesize xenon-containing organic compounds in the solid state. Organoxenon compounds without fluorine were also studied by Khriachtchev et al. in 2003, with HXeCCH, HXeCC, and HXeCCXeH synthesized by photolyzing acetylene in xenon matrices.[90] Feldman et al. also synthesized HXeCCH in 2003, but did not use the photolysis technique favoured by the Finnish group – instead, they used high speed electrons to dissociate the acetylene molecule inside solid xenon, producing HXeCCH.[91] Slavíček et al. computed high level potential energy curves of Xe_2.[92] Buth et al. found that ionization potentials for xenon n-fluorides increase as n increases from two to four to six, and that inclusion of relativistic and correlation effects also increase computed ionization potentials.[93] Lein and Frenking determined that electrostatic interactions play a significant role in the bonding of XeF_6, and that on the basis of purely quantum contributions to the energy of formation, the species would not exist.[94] Gerken et al. characterized xenon di- tetra- and hexafluorides with both ^{129}Xe and ^{19}F NMR spectroscopy in the gas phase for all fluorides and the solid state for XeF_2.[95] Cooke and Gerry reported the microwave-region rotational spectrum of XeAuF, a compound which would attract significant interest in the coming years.[96] Ginter and Eden computed Rydberg states of Xe_2 in 2004, reporting dissociation energies, equilibrium bond distances, and spectroscopic constants.[97] Also in 2004, Yen et al. computed energies of intermolecular H—H and H—F bonding between two HXeF molecules and lighter rare gas halohydrides, finding that these intermolecular interactions decreased the energy barrier to decomposition into HF and atomic Xe.[98] Tanskanen et al. computed formation mechanisms and vibrational spectra for HXeCCH, HXeCC, and HXeCCXeH in solid xenon matrices, finding a mechanism to explain previous experimental results and the first case of "a noble gas hydride [...] formed from another noble gas molecule".[99] Gerber published a chapter in the Annual Review of Physical Chemistry highlighting the HRgX class of molecules, with attention to their mech-

anisms of formation in cold rare gas matrices and the predicted stability of specific molecules. Additionally, he noted that the two-body dissociation channel, or

$$\mathrm{HRgX}_{(g)} \rightarrow \mathrm{HX}_{(g)} + \mathrm{Rg}_{(g)} \tag{1.1}$$

is the proposed dissociation mechanism for HRgX borne out by experimental data for several compounds.[100] Semenov and Sigolaev computed energies of formation and spin-spin coupling constants for the pentafluorophenylxenonium ion and fluoro(pentafluorophenylxenon) in a vacuum and in a solution of acetonitrile, finding that solvent effects stabilize the molecule and coupling constants were in good agreement with experimental values.[101] They also computed energies of formation of $Xe(CF_3)_2$, $FXe(CF_3)$, and XeF_2, finding that the perfluoroethane molecules decompose spontaneously to produce atomic xenon and perfluoroethane.[102] Frohn and Theissen revisited the study of $(C_6H_5)XeF$, demonstrating that it can be used as a starting material in the synthesis of multiple organic xenon-containing compounds.[103]

Forgeron et al. studied the level of magnetic shielding present in XeF_2 both computationally and experimentally with ^{129}Xe NMR spectra, finding that when spin-orbit coupling is included in DFT computations, theoretical results are in accord with experimental results.[104] In 2005 Chaban computed that glycine with a xenon inserted at the carboxylic O-H bond should be stable.[105] Brown et al. computed that an organic xenon-containing polymer with monomers of –(XeCC)– should be stable according to electronic structure computations at several levels of theory.[106] AuXeF, AuXeOH, and other compounds of gold and lighter rare gases were computed to be unstable, dissociating into free atoms spontaneously.[107] Khriachtchev et al. obtained infrared spectra of xenon halohydrides inside solid, low-temperature xenon matrices, finding characteristic fingerprint regions and examining the effect of the Xe–HXeX (X=Cl, Br) intermolecular interaction upon the infrared spectrum.[108] Gerber reviewed the recent developments in rare gas chemistry in 2005, with emphasis on compounds of argon and xenon.[109]

Ball et al. synthesized the interesting organometallic xenon-containing molecule $Re(C_5H_4CH(CH_3)_2)COPF_3Xe$ in 2005 and characterized it with ^{129}Xe NMR and in-

frared spectroscopy.[110] The next year, McMaster et al. studied this compound computationally, analyzing the topology of the electron density and its implications for bonding.[111] Computed interaction energies between CuXeF and AgXeF revealed both compounds to be unstable, but with high energy barriers to the triangular transition state.[112] Buck and Fárník reviewed progress in the synthesis and characterization of gas phase xenon hydrides.[113] Khriachtchev et al. found that xenon could be inserted into acetylene inside of a xenon matrix, and reported both experimental and computed infrared absorption frequencies.[114] This group also demonstrated that HXeCCH could be synthesized inside of argon or krypton matrices, again characterizing the species with infrared spectroscopy.[115] Lignell et al. evaluated theoretical methods commonly employed in computations of heavy rare gas containing molecules, determining that results of single-reference computations may not give accurate results for energies. Consequently, Lignell et al. recommended that computed values of the dissociation energy of the products of reactions such as Reaction 1.1 should be compared with experimental values, and that multireference methods should be used in computations involving weaker interactions.[116] Ansbacher and Gerber computed potential energy surfaces of HCCXeCCH, predicting it to be stable at up to 200 K.[117] Semenov and Sigolaev computed that the secondary carbon of $[XeC_6F_7]^+$ is the most reactive site for addition of a fluoride ion.[118] Tramšek and Žemva reviewed the chemistry of xenon difluoride and enumerated both organic and inorganic compounds that had been synthesized using XeF_2 as a precursor.[119] Krouse et al. computed the dissociation energy of XeF_3^- into Xe_2 and F^- in 2007,[120] and Straka et al. computed chemical shifts and quadrupole couplings for the increasingly well-studied HXeCCH.[121] Takayanagi et al. computed vibrational energy levels of HXeH, HXeD, and DXeD.[122] Brock et al. synthesized $XeOF_2$, $F_2OXeNCCH_3$, and $XeOF_2 \cdot HF$ – unique compounds in that they involved xenon in its (IV) state, unlike the more usual xenon(II) found in organoxenon compounds.[123] Sheng and Gerber investigated the stability of HXeCCH in small clusters, finding that they form a crystalline structure through electrostatic intermolecular interactions.[124] Computational studies by Antoniotti et al. found that while $FXeBN^-$ is unstable, the high energy barrier to

decomposion may be sufficient to preserve the compound from decomposition.[125] The next two years produced a plethora of new xenon-containing small molecules, with many different groups contributing to the field. Grochala reviewed the state of xenon chemistry in 2007, focusing on developments since the year 2000,[126] and in 2008 computed phase diagrams for XeAuF at varying pressures.[127] Belpassi et al. reported high-level computations on the structures of XeAuF and $XeAuF^+$ in 2008, analyzing the bonding in terms of charge transfer and the electron density.[128] Continuing the study of metal gas halides, Mou and Witek computed structures and properties of compounds involving xenon, noble metals, and halides, finding that AuXeF and AuXeCl should be kinetically stable.[129] Breckenridge et al. computed bond orders and analyzed the extent to which covalent effects are present in the bonding between xenon and gold in the Xe-Au cations studied previously by Seppelt et al.[13,14,20,54,85,130] Poterya et al. synthesized HXeCCH in the gas phase rather than in a solid xenon matrix and computed excitation energies for its lower-lying excited electronic states.[131] Khriachtchev et al. demonstrated that HXeOXeH can be synthsized inside a xenon matrix via photodissociation of water at warmer temperatures than other xenon-containing compounds.[132] Potential energy surfaces of the already well-studied HXeI were computed in 2008 as well.[133] Fang and Zhang predicted stability of XeAuCl and xenon metal bromides based on DFT computations.[134] Lignell et al. studied vibrational spectra for xenon halohydrides complexed with halohydrides in xenon matrices experimentally as well as computationally, finding that complexation significantly increases the frequencies at which vibrational modes are excited.[135] Tanskanen et al. found that, as with smaller organoxenon compounds, propiolic acid could be photolyzed inside of a solid xenon matrix to produce an HXeCCH–CO_2 complex, which has characteristic infrared peaks similar to those of HXeCCH. *Ab initio* computations for the complex provided minimum energy structures and accompanying vibrational spectra.[136] This was also the year that Tsivion et al. predicted HXeCCH to be stable at 273 K – a significant finding for a compound previously thought to be stable only at low temperatures.[137] Binding energies and dissociation energies for $HXeCO^+$ were computed in 2008.[138] In 2009, Feldman et al. observed an isotopic shift in infrared

spectra of HXeCCH, HXeCC, and HXeH for ^{129}Xe and ^{136}Xe – the first such shift to be reported for xenon.[139] Tsivion and Gerber computed that the recently discovered compounds HXeOH and HXeOXeH should have hour-long half lives at triple-digit Kelvin temperatures.[140] Domanskaya et al. reported both experimental and computed infrared spectra of HXeCCH-acetylene complexes, highlighting the additional peaks produced by the complex as compared to the already known HXeCCH infrared spectrum.[141] Mück et al. examined the extent to which donor-acceptor complexes of rare gases are formed with various ligands,[142] and Jiménez-Halla et al. computed properties of a compound with a xenon-xenon bond: HXeXeF.[143] Fang and Zhang computed properties of compounds of xenon and noble metal halides,[134] and Huang et al. computed potential energy surfaces and vibrational frequencies of HXeBr.[144] Pérez-Peralta et al. computed structures and stabilities of several neon halohydrides and organoxenon compounds and found them to be metastable with respect to decomposition into atomic xenon and a hydride.[145] Misochko et al. obtained infrared spectra of the XeF_3 radical inside a low-temperature argon matrix.[146] Khriachtchev et al. reviewed the state of rare gas chemistry in 2009, focusing on such newly-discovered compounds at HXeCCH and compounds of lighter rare gases.[147]

A decade into the 21st century, the field of xenon chemistry was burgeoning with novel compounds and high-level computational results, but progress in radon chemistry had slowed considerably compared to the late 1990s. Gardner et al. computed potential energy curves for the $^2\Sigma^+$ ground state of CuRn, AgRn, and AuRn, as well as for xenon-containing analogs. Interestingly, they found that equilibrium bond distances decreased as the size of the rare gas increased as a consequence of increasing ionic character in the metal-rare gas bonds.[148]

In xenon chemistry, Torigoe et al. identified $XeCu^+$ with x-ray absorption spectroscopy inside zeolite and determined its heat of adsorption.[149] Maroulis computed multipole moments, polarizability, and hyperpolarizability of HXeH with the DFT method.[150] Khriachtchev et al. isolated both HXeCCF and HCCXeF in solid xenon matrices using the photoionization method and characterized them with infrared spectra and anharmonic *ab initio* computations.[151] Grant et al. computed heats of for-

mation for several XeF_n cations and anions, finding then to be thermodynamically unstable when n is odd for both cations and anions.[152] Borocci et al. computed structures and bond properties of the $HXeFXeH^+$ cation and determined that it was thermodynamically unstable and likely to decompose spontaneously into HF, atomic xenon, and the HXe^+ ion.[153] The CH_3XeF molecule was studied theoretically in this year as well and predicted to have an energy barrier to dissociation of 16.8 $kcal{\cdot}mol^{-1}$.[154] Rodrigues, de Sá, and Haiduke analyzed xenon copper halides with the Quantum Theory of Atoms in Molecules (QTAIM), computing bond properties and atomic properties.[155] In another theoretical study, Sun et al. found that the $XeNO_2^-$ and $XeNO_3^-$ had high energy barriers to dissociation.[156] Studies of heavy rare gas chemistry in 2010 concluded with the publication of electronic structure computations by Kobayashi et al. on $XeBe_2O_2$ and $XeBe_2O_2Xe$, where the binding energies of xenon containing compounds were found to be significantly higher than similar compounds of the lighter rare gases.[157] Tsivion and Gerber predicted radon to be capable of forming compounds with water and acetylene, and computed the half-lives of these compounds to be an hour and 3.8 days.[158]

In 2011, two studies on radon chemistry appeared, hinting that more could be possible in radon chemistry than was currently known. Jacobson et al. determined that radon had a much larger association constant for binding to tris-(triethazole ethylamine) cryptophane than did xenon at room temperatures: a significant finding because out of all molecules that association constants for xenon have been measured for, this constant for radon with cryptophane is even higher.[159] Juarez et al. computed energies of decomposition and formation for xenon and radon hydrides containing many of the ligands already studied by the Khriachtchev group, finding the compounds to be thermodynamically unstable.[160]

Xenon chemistry continued to flourish, and the current state of rare gas chemistry was reviewed in *Physics and Chemistry at Low Temperatures* by Grochala, Khriachtchev, and Räsänen.[161] Khriachtchev et al. synthesized HXeOBr in a solid xenon matrix and characterized it with infrared spectra and computed anharmonic vibrational frequencies.[162] Tsivion and Gerber simulated HXeCCH inside clusters of acety-

lene in an effort to computationally represent a possible solvent in which HXeCCH could be used, finding that interactions between the HXeCCH molecule and the solvent increased its stability.[163] Borocci et al. computed that the $HXeHXeH^+$ cation should be marginally thermodynamically stable.[164] Zins et al. found that when toluene is ionized to a 2+ cation, it is reactive with xenon and forms $C_7H_6Xe^{2+}$.[165]

Zins and Schröder characterized several new organoxenon dications in the gas phase.[166] Tonner et al. computed that six xenon atoms will fit inside of a buckminster fullerene (C_{60}) molecule without bursting the C-C bonds.[167] Liu et al. reported computed dipole moments for familiar organoxenon compounds and predicted structural parameters.[168] Lai et al. chose several xenon-containing molecules as part of their benchmark study of density functionals.[169]

From 2011 to 2013, Schrobilgen and Brock published a review of the year's progress in rare gas chemistry.[170–172] In 2012, Peterson et al. revisited the study of XeF_6 with high-level methods and confirmed that the C_{3v} geometry is the minimum energy structure.[173] Computed bond properties of $HXeC_2H_3$ and $HXeC_2H_5$ were reported in 2013 by Zhang and Sheng,[174] and Ma et al. computed interaction energies and optimized structures for HXeCCH—H_2O and HXeCCH—HF, analyzing the role of π-bonding in these systems.[175] Most recently, Cohen et al. optimized the structure of HXeBr inside a carbon dioxide shell and analyzed its anharmonic vibrational frequencies.[176]

1.2 The Quantum Chemistry Toolbox

The work described in this thesis required a variety of quantum chemical methods. The quantum chemical methods used in subsequent chapters will be described first, followed by the Model Core Potentials (MCP) basis sets. Finally, two methods of population analysis will be introduced.

1.2.1 The Hartree-Fock Method

The Hartree-Fock (HF) method is the most basic tool of the computational chemist. In this method, a Slater determinant becomes the trial wavefunction in a variational

method computation. The Hartree-Fock equations are solved iteratively until both the total energy of the system and its density matrix converge following the self-consistent field (SCF) algorithm. In modern quantum chemistry software packages, the"Hartree-Fock" method is available in several flavours: Restricted Hartree-Fock (RHF), Restricted Open Shell Hartree-Fock (ROHF), or Unrestricted Hartree-Fock (UHF). As all three of these methods are variants of the Hartree-Fock Roothaan Hall (HFRH) equations, I will discuss these in some detail. All calculations carried out in this work used the Born-Oppenheimer approximation, which states that as nuclei are much heavier than electrons and move orders of magnitude more slowly than electrons, their motion can be neglected in the Hamiltonian. Therefore, "the kinetic energy of the nuclei can be neglected [...] and the repulsion between the nuclei can be considered to be constant." [177]

1951 – the same year that saw the introduction of the comic "Dennis the Menace" in American newspapers and the show "I Love Lucy" on American televisions – also saw two men independently invent a way to incorporate basis sets in order to make the HF equations much simpler to solve on a computer. The operator used in the HF equations, the Fock operator, contains three terms: a one-electron Hamiltonian operator $\hat{h}$, an exchange operator $\hat{J}$, and a Coulomb operator $\hat{K}$.[177] The Fock operator and its component operators take the following forms:

$$\hat{f} = \hat{h} + \sum_{b=1}^{N} \left[\hat{J}_b(r) - \hat{K}_b\right](r) \tag{1.2}$$

$$\hat{J}_b(1)\psi_a(1) = \int \left[\frac{|\psi_b(2)|^2}{r_{12}} d\xi_2\right] = |\hat{J}_b|\psi_a\rangle \tag{1.3}$$

$$\hat{K}_b(1)\psi_a(1) = \int \left[\frac{\psi_b^*(2)\psi_a(2)}{r_{12}} d\xi_2\right] \psi_b(1) = |\hat{K}_b|\psi_a\rangle \tag{1.4}$$

In the above equations, $\psi_a(2)$=$\psi_a(r_2)$ and $\psi_b(2)$ are spin orbitals, r_1 and r_2 refer to electronic, not nuclear, coordinates, and $\xi = (r, \sigma)$ refers to space-spin coordinates.

The HF equation may be written in terms of a set of orbitals $\{\phi_a\}$.

$$\hat{f}(R)\phi_a(r) = \epsilon_a\phi_a(r), a = 1, 2, ..., n(N/2) \tag{1.5}$$

When solving this equation variationally, the energies $\{\epsilon_a\}$ and the orbitals $\{\phi_a(r)\}$

would be the eigenvalues and eigenfunctions of the Hermition Fock operator $\hat{f}$. Roothaan and Hall, however, applied an idea from mathematics to greatly simplify these equations: any function, for example $\phi_a(r)$, may be expressed as a function of some basis functions. Molecular orbitals are composed of linear combinations of these basis functions. All of the basis functions that I have used in this work are gaussian-type functions.

This led to the HFRH equations, also called the matrix HF method. In this method, a series of basis functions $\chi_p(r)$ whose coefficients $\{A\}$ have been optimized replace the set of orbitals $\{\phi_a\}$, with:

$$\phi_a(r) = \sum_{p=1}^{k} \chi_p(r) A_{ap} \tag{1.6}$$

Four matrices result: The Fock matrix, in which each element comes from the Fock operator acting on a pair of basis functions; the matrix of orbital expansion coefficients $\{A\}$; the overlap matrix, whose elements are the expectation values of the overlap integrals of pairs of basis functions; and finally the diagonal matrix of orbital energies, which are the eigenvalues of this equation. Properties of matrices are used to greatly speed up the calculation of the eigenvalues.

What then distinguishes the RHF, ROHF, and UHF methods from one another? The key is the way that they treat Pauli correlation. In the RHF method, all spin orbitals are required to be doubly occupied with two electrons of opposite spin; no other condition is allowed. This is accomplished through requiring that the number of electrons in the system is even and the spin multiplicity is equal to one, and each orbital is occupied by two electrons of opposite spin. Many systems of practical interest contain one or more unpaired electrons, and so in 1954 Pople and Nesbet created the UHF method, a version of the HFRH equations, in which electrons of opposite spins are not required to be in the same orbital – electrons are not paired and each molecular orbital is broken down into α and β components.[178] The ROHF method is the most complex of the three, and was only completed in 1960. It divides the electrons into two groups: those paired in closed-shell spin orbitals, and those unpaired in open-shell spin orbitals.

The following sections describe Møller-Plesset Perturbation Theory, coupled cluster methods, and Density Functional Theory, all of which account for effects of electron correlation beyond the Pauli correlation already included in the Hartree-Fock method. The correlation energy for a system is the difference between the exact, non-relativistic energy of the system and the HF energy. The correlation energy is necessarily basis set dependent.

1.2.2 Møller-Plesset Perturbation Theory

Møller-Plesset Perturbation Theory is best known in its second-order incarnation, MP2. It is widely used in a variety of contexts and prized for its size consistency, computational efficiency, and availability of analytical gradients, which are useful for computing structures and properties of molecules. Unlike the HFRH method, which is variational, MP2 is a perturbation theory. The foundational principle of perturbation theories in general is that there is an unperturbed state which undergoes some alteration, or perturbation, which is assumed to be small. Corrections to the unperturbed state are then computed to a specified order. As MP2 is built upon the HF method, the unperturbed Hamiltonian is none other than the Fock operator, designated $\hat{\mathcal{H}}^{(0)}$. The solution to Equation 1.7, therefore, is the HFRH solution.

$$\hat{\mathcal{H}}^{(0)}\Psi^{(}0)_n = E_n^{(0)}\Psi^{(}0)_n \tag{1.7}$$

The next step in an MPn computation is to expand a Taylor series around E_n which is then truncated at the desired level. For an MP2 computation, it is truncated after the second derivative term. The first and second derivative terms represent the perturbation – the way in which the system Hamiltonian is different from the pure HFRH Hamiltonian. These terms in the Taylor expansion are grouped together into the perturbation operator $\hat{V}$, which contains effects of electron correlation beyond the simple Pauli correlation already accounted for in the HFRH Hamiltonian. $\hat{V}$ acts on the HFRH wavefunction, producing the first-order energy correction.

$$\Psi_n^{(1)} = \sum_{m\neq n} \frac{\langle\Psi_m^{(0)}|\hat{V}|\Psi_n^{(0)}\rangle}{E_n^{(0)} - E_m^{(0)}}\Psi_m^{(1)} = \sum_{m\neq n} \frac{\hat{V}_{mn}}{E_n^{(0)} - E_m^{(0)}}\Psi_m^{(0)} \tag{1.8}$$

Once the first-order corrected wavefunction is available, it can be used to compute the second-order energy correction:

$$E_n^{(2)} = \sum_{m \neq n} \frac{\langle \Psi_m^{(0)} | \hat{V} | \Psi_n^{(0)} \rangle \langle \Psi_n^{(0)} | \hat{V} | \Psi_m^{(0)} \rangle}{E_n^{(0)} - E_m^{(0)}} = \sum_{m \neq n} \frac{|\hat{V}_{mn}^{(0)}|^2}{E_n^{(0)} - E^{(0)}} \tag{1.9}$$

The first-order corrected wavefunction may now also be used to compute atomic or molecular properties.

1.2.3 Coupled Cluster Methods

Coupled Cluster methods are the current gold standard in computational chemistry. Their size consistency and ability to accurately describe tricky phenomena such as bond breaking make them the method of choice for nearly any system – provided that the system is small enough. The main limitation of coupled cluster methods is the large number of nonlinear, high-dimensioned equations necessary to compute amplitudes, and currently these methods are impractical for systems containing more than one hundred atoms on most computer installations.[179] The goal of the method is to explicitly include interactions between pairs of electrons (clusters) and pairs of clusters in order to better describe excited states and to reap the benefits that inclusion of excited states has on the ground state wavefunction.[180]

In these methods, a cluster operator $\hat{T}$ acts on a reference wavefunction that describes non-interacting electrons:

$$|0\rangle = e^{\hat{T}} |0^0\rangle \tag{1.10}$$

The reference wavefunction $|0^0\rangle$ is usually chosen to be a single Slater determinant. The form of the cluster operator is as follows:

$$T_1 = \sum_{r}^{unocc} \sum_{\alpha}^{occ} t_\alpha^r \hat{a}_r^+ \hat{a}_\alpha \tag{1.11}$$

$$T_2 = \frac{1}{4} \sum_{\alpha,\beta,r,s} t_{\alpha\beta}^{rs} \hat{a}_r^+ \hat{a}_s^+ \hat{a}_\alpha \hat{a}_\beta \tag{1.12}$$

Where α, β are occupied spin orbitals and r, s are unoccupied spin orbitals. The coupled cluster wavefunction $|0^0\rangle$ is acted upon by the cluster operator, producing a

series of one- and two-electron clusters and corresponding excitation operators, $\hat{C}_n$:

$$e^{\hat{T}}|0^0\rangle = (1 + \hat{C}_1 + \hat{C}_2 + ...)|0^0\rangle \tag{1.13}$$

$$\hat{C}_1 = \hat{T}_1 \tag{1.14}$$

$$\hat{C}_2 = \hat{T}_2 + \frac{1}{2!}\hat{T}_1^2 \tag{1.15}$$

The most important term in Equation 1.13 is the $\hat{T}_2$ term which represents interactions between two electrons in different molecular orbitals; the least important is $\hat{T}_4$. Evaluation of the total electronic energy of a system requires the $t_{\alpha\beta}^{rs}$ amplitudes, which are obtained by solving the following equation:

$$\mathcal{H}e^{\hat{T}}|0^0\rangle = e^{\hat{T}}|0^0\rangle \tag{1.16}$$

where $\mathcal{H}$ is the Hamiltonian for the system. In solving Equation 1.16, it is necessary to choose where to truncate the cluster operator. The system of equations generated by Equation 1.16 after truncation of the cluster operator will have as many elements as there are amplitudes needing to be solved, as these amplitudes are the solutions to the system of nonlinear equations.

The next step in obtaining the total electronic energy of a system is to project the $\mathcal{H}e^{\hat{T}}$ onto the reference wavefunction. While this shares a similar form as the HF equations, it is a non-variational procedure as the cluster operator is truncated.

$$E = \langle 0^0|e^{-\hat{T}_2}\mathcal{H}e^{\hat{T}_2}|0^0\rangle \tag{1.17}$$

There are many variants of coupled cluster methods currently extant; I will provide more details for each method that I have used in the chapters where the methods have been applied.

1.2.4 Density Functional Theory

There are a plethora of density functionals in common use, and I will not open the Pandora's box that is the discussion of their relative merits and weaknesses here. Instead, I will outline the basics of functionals as it pertains to those that I have used in this work, and state my reasoning in choosing them.

An advantage of DFT is that its pure functionals scale as K^3, where K is the number of basis functions – it technically scales as faster than HF, which formally scales as K^4. Hybrid functionals scale as the same as HF. Even in programs where it is slower than HF, such as Gaussian09, DFT is one of the fastest correlated methods. Another advantage of DFT is the broad palette of functionals available to choose from. Several classes of functionals, including localized density approximation, pure exchange, pure correlation, generalized gradient approximation, hybrid generalized gradient, and meta-generalized gradient, are implemented in many quantum chemistry programs; each type of functional has an application for which it is best suited. However, it is impossible to know *a priori* which functional this will be. No one functional is better than all others across all applications, and the choice of functionals for any given system is an important decision. The "wrong" functional may produce bizarre or nonsensical results; for example, a functional may fail to produce a transition state for a molecule that does appear in *ab initio* calculations.[181] Looking into the way the functional was originally parametrized is a good way to determine if it is appropriate for a given system.[182]

Some of the work described in later chapters involves the PBE0 (Perdew-Burke-Ernzerhof zero) functional. It is as hybrid functional and incorporates the generalized gradient approximation, which takes into account the fact that the electron density is not homogenous over the entire molecule. Mathematically this is accounted for by including the gradient of the electron density. In general, functionals of this type include parameters fitted from experimental data. The Perdew-Burke-Ernzerhof (PBE) functional is a hybrid functional, with all its parameters being fundamental constants except for those in its exchange-correlation term.[183] This represents a significant advancement in DFT, as it begins to move away from highly parameterized functionals and begins to approach the true functional. Adamo and Barone extended this work by removing all the adjustable parameters from the PBE functional. This was accomplished through the addition of an adiabatic correction functional to represent the exchange correlation component of PBE. The result was a version of the PBE functional free from any empirical parameters: PBE0.[184]

1.2.5 Model Core Potentials Basis Sets

All-electron basis sets become impractical in certain limits. Among these are molecules, however small, involving atoms larger than argon. Theoretical chemists have invented a number of ways to deal with this problem, including semiempirical methods and effective core potentials, the latter of which MCPs are a subset. In effective core potentials basis sets, a number of core electrons are removed from explicit treatment and instead a potential that mimics the effect of these electrons is added to the Hamiltonian. The number of electrons to be removed, the manner by which they are removed, the basis set chosen to represent the valence electrons, and the specific form of the potential distinguish one effective core potentials method from another. A comment about the terms "core" and "valence" is warranted here, as I do not use them in the standard sense. By "core" electrons, I mean any electrons that have been replaced by the potential, and consequently I use "valence" to refer to all electrons which have been explicitly kept in calculations.

In any quantum chemical computation, a Hamiltonian is involved. The one-electron MCP Hamiltonian operator contains terms for the kinetic energy ($-\frac{1}{2}\nabla_i^2$), the potential energy ($V_{MCP}(r_i)$), and the MCP projection operator ($\hat{\Omega}$):[185–188]

$$\hat{h}_{MCP}(r_i) = -\frac{1}{2}\nabla_i^2 + V_{MCP}(r_i) + \hat{\Omega}, \qquad i = 1, 2, ...N_v \tag{1.18}$$

where N_v is the number of valence electrons. The potential ($V_{MCP}(r_i)$) is defined as:

$$V_{MCP}(r_i) = -\frac{Z - N_c}{r_i} \left[1 + \sum_{I=1}^{3} A_I e^{-\alpha_I {r_i}^2} + \sum_{J=1}^{3} A_J r_i e^{-\alpha_J r_i^2}\right]. \tag{1.19}$$

In Equation 1.19, Z represents the atomic number of an atom, N_c is the number of electrons in the core orbitals $\{\psi_c\}$, i.e. the number of electrons to be removed, and the $\{A_j, \alpha_j\}$ terms are fitted parameters of the model. The choice of N_c is significant– it determines which electrons will be explicitly included and which will be replaced by the potential $V_{MCP}(r_i)$. The parameters of the projection operator are computed systematically. Numerical Hartree-Fock computations on free atoms produce the set of radial orbital functions, which become the reference functions in a least-squares

fit of the exponents and expansion coefficients for Gaussian-type functions. The minimized exponents and expansion coefficients $\{\alpha_I, \alpha_J\}$ and $\{A_I, A_J\}$ become the variables upon which the energies of the atomic orbitals depend.

This shift, accomplished through the action of the projection operators, will be illustrated following the example for beryllium from Chapter 2 of the 1999 edition of *Computational Chemistry: Review of Current Trends* by Klobukowski et al.[189] For a ground state (^1S) beryllium atom, the Hamiltonian is as follows:

$$\hat{H}(1,2,3,4) = \sum_{i=1}^{4} \hat{h}(i) + \sum_{i>j}^{4} \frac{1}{r_{ij}} \tag{1.20}$$

where $(1,2,3,4)$ refer to the electrons i, j. The one-electron operator $\hat{h}(i)$, is:

$$\hat{h}(i) = -\frac{1}{2}\nabla_i^2 - \frac{4}{r_i} \tag{1.21}$$

In the Hartree-Fock approximation, the resulting four-electron Schrödinger equation $\hat{H}(1,2,3,4)\Psi(1,2,3,4) = E\Psi(1,2,3,4)$ can be written as the following four-electron Slater determinant:

$$\Psi(1,2,3,4) = \frac{1}{\sqrt{4!}}\det[\phi_{1s}(1)\alpha(1)\phi_{1s}(2)\beta(2)\phi_{2s}(3)\alpha(3)\phi_{2s}(4)\beta(4)] \tag{1.22}$$

Each orbital in this determinant is a solution of the following Hartree-Fock equations:

$$\hat{F}|\phi_{1s}\rangle = \epsilon_{1s}|\phi_{1s}\rangle \tag{1.23}$$

$$\hat{F}|\phi_{2s}\rangle = \epsilon_{2s}|\phi_{2s}\rangle \tag{1.24}$$

The Fock operator $\hat{F}$ in Equations 1.23 and 1.24 takes the following form,

$$\hat{F} = -\frac{1}{2}\nabla^2 - \frac{4}{r} + (2\hat{J}[1s] - \hat{K}[1s]) + (2\hat{J}[2s] - \hat{K}[2s]) \tag{1.25}$$

and contains the Coulomb and exchange operators described by Equations 1.3 and 1.4. The core orbitals must be removed to a virtual space so that the potential function containing the above parameters may be added to the Hamiltonian in their stead (Equation 1.19). To do this, a new Fock operator is defined which includes a projection operator whose function is to shift the core orbitals to virtual space:

$$\hat{F}_p = \hat{F} + \Delta_\epsilon|\phi_{1s}\rangle\langle\phi_{1s}| \tag{1.26}$$

This produces a new set of Hartree-Fock equations, with the core orbitals shifted to virtual space:

$$\hat{F}_p|\phi_{1s}\rangle = (\epsilon_{1s} + \Delta_\epsilon)|\phi_{1s}\rangle \tag{1.27}$$

$$\hat{F}_p|\phi_{2s}\rangle = \epsilon_{2s}|\phi_{2s}\rangle \tag{1.28}$$

The ϕ_{2s} retains its original orbital energy, but the orbital energy of ϕ_{1s} has now been increased by Δ_ϵ and is therefore shifted to virtual space. The core orbital ϕ_{1s} is now assumed to be frozen, ($\bar{\phi}_{1s}$), and appears in the HF equation in the following way:

$$\hat{F}_p|\phi\rangle = \epsilon|\phi\rangle \tag{1.29}$$

$$\hat{F}_p = \hat{h}_p + 2\hat{J}[\phi] - \hat{K}[\phi] \tag{1.30}$$

$$\hat{h}_p = -\frac{1}{2}\nabla_i^2 - \frac{4}{r} + 2\hat{J}[\bar{\phi}_1 s] - \hat{K}[\bar{\phi}_1 s] + \Delta_E|\bar{\phi}_1 s\rangle\langle\bar{\phi}_1 s| \tag{1.31}$$

The final three terms of Equation 1.31 constitute the frozen core approximation. For a general case, the $V_{MCP}(r_i)$ term in Equation 1.18 contains exchange and Coulomb operators, which now take into account that the core orbitals ϕ_c have been shifted to a virtual space. The exchange ($\hat{V}_X^{core}(r_i)$) and Coulomb ($\hat{V}_C^{core}(r_i)$) operators have the following forms:

$$\hat{V}_X^{core}(r_i) = -\sum_c \hat{K}(\bar{\phi}_c) \tag{1.32}$$

$$\hat{V}_C^{core}(r_i) = \frac{-N_c}{r_i} + 2\sum_c \hat{J}(\bar{\phi}_c) \tag{1.33}$$

The last term of Equation 1.31 is the projection operator, $\hat{\Omega}$. This is the operator responsible for shifting the core orbitals high enough in energy so that they occupy virtual space. For a general case, it has the following form:

$$\sum_c B_c\ |\bar{\psi}_c\rangle\langle\bar{\psi}_c|, \tag{1.34}$$

With the parameter B_c often set as $\mathrm{B}_c = -2\epsilon_c$, where ϵ_c is the energy of a frozen core orbital $\bar{\phi}_c$.)[190]

There are a variety of MCP basis sets available, with two general choices for the definitions of core and valence electrons. In the basis sets that I used in this work, valence electrons are defined as $(n-1)d\ ns\ np$. In the other option, valence electrons include only $ns\ np$. Some MCP basis sets are made more computationally efficient through the use of an L-shell, in which the $ns\ np$ basis functions share exponents. The L-shell reduces computational time required to compute one- and two-electron integrals.

In the following chapters, I describe work that involves a number of MCP basis sets which which can be described in three main groups: the MCP-$n$zp series, the improved MCP (iMCP) series, and the Zeng-Fedorov-Klobukowski (ZFK) series. The MCP-$n$zp series are the basic MCP basis sets. They come in double, triple, and quadruple ζ valence sizes, and include a suitable set of polarization and correlation functions. Diffuse functions may also be added to each to create an aug-MCP-$n$zp basis set. Of this series of basis sets, I have primarily used the aug-MCP-TZP basis set.[185–188,191–194] The iMCPs were created by reoptimizing the parameters to create the L-shell structure for the valence s and p electrons. These basis sets are more compact than the MCP-$n$zp series, and come in both scalar relativistic and non-relativistic flavours.[83,195,196] The ZFK series are the newest MCP basis sets. They currently have been made for the elements main-group Li through Rn, and have $(n-1)p\ (n-1)d\ ns\ np$ as the valence space for p-block atoms and $(n-1)p\ ns\ np$ as the valence space for s-block atoms. They are designated ZFK-$n$zp, where n=2,3,4.[197,198] For all three series of basis sets, the correlation consistent cc-pVNZ basis set for hydrogen is chosen to match the value of n in the MCP basis set name.

1.2.6 Special Methods for Specific Properties

Some of the work I discuss in the following chapters uses the results of special or uncommon methods in quantum chemistry. In this section, I will outline the mathematical or chemical basis for each such method. These methods, Natural Bond Orbitals (NBO) and Quantum Theory of Atoms in Molecules (QTAIM) are modern methods of population analysis. Specifics related to how the computations were

carried out will appear in subsequent chapters.

Natural Bond Orbitals

The acronym NBO generally refers to both the group of Natural Population Analysis (NPA) methods developed by Reed, Weinstock, and Weinhold, and the Natural Bond Orbitals method itself, which is included in this group. These include Natural Atomic Orbitals (NAO), Natural Hybridized Orbitals (NHO), NBOs themselves, and Natural Localized Molecular Orbitals (NLMO). An advantage over other population analysis methods that is common to all NPA methods is that these methods are not heavily basis set dependent, and NPA methods can therefore be included in many types of quantum chemical calculations. Population analysis and bond properties can be computed from NBOs.

Quantum Theory of Atoms in Molecules

The basis of QTAIM is analysis of the topology of the electron density.[199,200] Through computation of various critical points and evaluation of properties of the electron density at those critical points, chemists can gain insight into the nature of bonding within a molecule. One advantage of this method over other methods of population analysis is that through calculation of a series of gradient vectors terminating at the nuclei in a molecule, one can assign the specific volume elements of the molecule to individual atoms.

Chapter 2

Is Radon Reactive?*

2.1 Introduction

Once some compounds in the general category HRgX (Rg=Ar-Xe; X=electronegative group) were isolated inside a low-temperature rare gas matrix, many research groups became interested in the design and synthesis of related compounds.[22,29,126] The lighter rare gas hydrides garnered the attention of experimental chemists and theoretical chemists alike, and their properties and means of synthesis were soon enumerated in detail.[30,36,39,44,151,201–203] However, HRnF received little attention. This can be attributed to a number of factors: isotopes of radon are radioactive, and the longest-lived isotope of radon has a half-life of only 3.8 days[7], which makes experimental studies more challenging than those of lighter rare gases. Additionally, radon was thought to be much less reactive than xenon. In their 2000 study, Lundell et al. found that in HRnF, the Rn-F distance was almost three angstroms – much too far for a chemical bond to exist. However, this was incongruent with results of earlier studies, which seemed to indicate that radon should be more reactive than xenon. Already in 1975, Liebman wrote that "extrapolation from the trend of Ar, Kr and Xe suggests Rn compounds will be even more stable."[204] A 2001 review of rare gas chemistry by Christe quoted Frenking, stating that radon fluorohydrides "are only kinetically stable; their stability depends on the energy barriers toward decomposition which can be quite low, particularly in the condensed neat phase."[73,205] The work

*A version of this chapter was published in *J. Phys. Chem. A*, **2010**, *33*, 8786.

described in this chapter applies MCPs to the study of the heaviest rare gas fluoride, HRnF, as well as its lighter relatives, in order to settle the question "is radon reactive in the same way as xenon?".

2.2 Computational Methods

Many pieces of evidence were necessary to answer this question, and consequently many different quantum chemical methods were employed to obtain this evidence. Structures of HRgF (Rg=Ar-Rn) were optimized with three different methods and a variety of basis sets including MCPs, all-electron non-relativistic basis sets, and scalar-relativistic basis sets.

The MCP basis set used in this project was the augmented-MCP-TZP (hereafter abbreviated acp3) basis set; its composition is as follows, in [S/P/D/F]: for fluorine, $(5s\,5p\,4d\,3f)$ were contracted to $[4s\,4p\,3d\,2f]$ = (2111/2111/211/21); for argon, $(5s\,5p\,5d\,3f)$ were contracted to $[4s\,4p\,3d\,2f]$ = (2111/2111/311/21); for krypton, $(8s\,7p\,9d\,3f)$ were contracted to $[5s\,5p\,4d\,2f]$ = (41111/31111/5211/21); for xenon, $(9s\,8p\,9d\,3f)$ were contracted to $[5s\,5p\,4d\,2f]$ = (51111/41111/6111/21); for radon, $(10s\,9p\,11d\,4f)$ were contracted to $[5s\,5p\,4d\,2f]$ = (61111/51111/7211/31). The resulting sizes of variational space (in terms of spherical Gaussian functions) were 113 for HArF and 122 for HKrF, HXeF, and HRnF. For hydrogen, a (411/21/2) segmented basis set by Matsuoka[206] was used. In all cases, the source of the correlating functions was the work of Noro et al.[207] The valence space for these MCPs is $ns\,np$ for fluorine and argon and $(n-1)d\,ns\,np$ for the heavier rare gases. All MCP basis sets were used as spherical Gaussian functions.

The all-electron non-relativistic basis sets include the triple-ζ correlation-consistent basis set cc-pVTZ augmented with correlating functions for H, F, Ar, and Kr. These basis sets have been abbreviated accT. These basis sets do not exist for xenon or radon.[208–210] For atoms up to xenon, the non-relativistic aug-TK/NOSeC-TZP basis set (abbreviated nasT) was used.[193,206,207,211–216] Finally, for xenon and radon, the relativistic correlating-function augmented basis set aug-DK3-Gen-TK/NOSeC-TZP

(abbreviated rasT) was used.[217] All of the basis sets described in this paragraph may be found online; the correlation-consistent basis sets may be downloaded from the EMSL Basis Set Exchange[32] and the aug-TK basis sets, as well as the MCP basis sets described above, may be found at the Segmented Gaussian Basis Set Exchange.[218] Finally, an all-electron basis set matching the one used by Lundell et al was used and is abbreviated LCG.[59]

The basis sets described above were used in conjunction with a variety of methods. Geometry optimizations were done with three different methods: MP2, Coupled Clusters with Single and Double excitations (CCSD), and Coupled Clusters with Singles, Doubles, and non-iterative Triples (CCSD(T)). The coupled cluster methods used in this study were added to GAMESS-US by the Piecuch group in 2002.[219] Additionally, single-point evaluations of energies were computed with the CCSD(T) and MP2 optimized structures with the Completely Renormalized Coupled Clusters CR-CC(2,3) method, a more recently developed coupled clusters method, again from the Piecuch group. Computation of energies of formation and decomposition of HRgF required the computation of the energy of the open-shell atom F. This was accomplished using the MP2 implementation for open-shell systems[220,221] and the CCSD method, which can treat open-shells. All computations on radon-containing compounds presented in this and subsequent chapters use the atomic mass of the longest-lived isotope of radon, which is 222.0176 amu for ^{222}Rn, as is the standard in GAMESS-US.

2.3 Results and Discussion

Properties computed with the above methods and basis sets include structural parameters for optimized geometries, harmonic vibrational frequencies, energies of formation and decomposition, and Natural Population Analysis (NPA) charges for HRgF. These will be discussed in detail for each molecule in the following sections. The model of intramolecular interaction in HRgF is generally accepted to be an $(HRg)^+$ group interacting with an F^-.[59,222,223] This was taken into consideration when the basis sets described in the Methods section were chosen: they needed to be able to

represent the first ionization energies of the rare gases. Computed values of first ionization energies for the four rare gases involved in this study at the MP2/aug-MCP-TZP, CCSD/aug-MCP-TZP, and CR-CC(2,3)/aug-MCP-TZP levels of theory with an ROHF Hamiltonian[224–226] are presented in Table 2.1 alongside spin-corrected experimental values.[227–229] Computations of these first ionization energies were carried out in C_{2v} symmetry.

Table 2.1: *First ionization energies of rare gas atoms (in eV); values in parentheses correspond to frozen* n*d subshell*[(a)]

atom	MP2	CCSD	CR-CC(2,3)	exp.[(b)]
Ar	15.691	15.494	15.541	15.814
Kr	14.102 (14.033)	13.954 (13.911)	13.996	14.218
Xe	12.424 (12.327)	12.284 (12.226)	12.325	12.562
Rn	11.655 (11.534)	11.521 (11.457)	11.562	12.023

[(a)] aug-MCP-TZP basis set; call computations were carried out in C_{2v} symmetry [(b)] Ref.[7].

Computed first ionization energies agree well with experiment, with both indicating that ionization energy decreases with an increase in size of the rare gas. Of all the rare gases, radon's *p*-electrons are most easily ionized, indicating that it should be the most reactive. Additionally, increasing the quality of the treatment of effects of electron correlation for the *n*d electrons has little effect on the first ionization energy.

Energies of formation and decomposition of HRgF species are computed according to the following reactions:

$$\mathrm{H}_{(g)} + \mathrm{F}_{(g)} + \mathrm{Rg}_{(g)} \rightarrow \mathrm{HRgF}_{(g)}, \qquad \Delta E_1 \tag{2.1}$$

$$\mathrm{HRgF}_{(g)} \rightarrow \mathrm{HF}_{(g)} + \mathrm{Rg}_{(g)}, \qquad \Delta E_2 \tag{2.2}$$

$$\mathrm{H}_{(g)} + \mathrm{F}_{(g)} \rightarrow \mathrm{HF}_{(g)}, \qquad \Delta \mathrm{E}_1 + \Delta \mathrm{E}_2 = -\Delta\ \mathrm{E}_{\mathrm{HF}} \tag{2.3}$$

Basis set superposition error (BSSE), or the tendency for the more diffuse functions of basis sets belonging to neighbouring atoms to overlap in the region of space between adjacent nuclei, affecting the quality of the description of the neighbouring atom,[230,231] was accounted for in the calculation of the energy difference ΔE_1 through a counterpoise (CP) correction.[232] Such a correction entails computing the energy of

each atom in proximity to ghost atoms with the basis sets belonging to the true atoms they represent centred on them. This is a common and established method to dealing with BSSE in cases where the spatial arrangement of a group of atoms in the interacting fragment does not change. However, because the atoms rearrange during Reaction 2, this method was inapplicable to that reaction and could not be applied to the computation of ΔE_2, nor to the computation of ΔE_{HF}. ΔE_{HF} was computed as a check, because the HF molecule has been well-studied and comparison may therefore be made between computed values and experimental values.

In the sections that follow, results for each HRgF will be discussed individually, followed by conclusions for all molecules.

2.3.1 HArF

The computed bond lengths of HArF at the MP2/aug-MCP-TZP level of theory method agree with MP2/all-electron results, differing only by 0.01 Å and 0.02 Å for the Ar-H and Ar-F bond distances. This data and other data discussed in this section is collected in Table 2.2. The computed MP2/aug-MCP-TZP energy of formation (ΔE_1) is larger by about 20 kJ·mol^{-1} than the MP2/all-electron ΔE_1, but this decreases to only 7 kJ·mol^{-1} after applying the counterpoise correction. However, ΔE_1 is heavily influenced by basis sets. The present MP2/aug-MCP-TZP results are 40 kJ·mol^{-1} less exothermic than previously reported results which used the 6-311G basis set.[59] This could result from a fault in the 6-311G basis set, which is not of true triple-zeta quality in the *s*-shell – a relevant region of valence space for the molecules considered in this study. The *s*-shell in the 6-311G basis set is more accurately described as 6-311G: a double-zeta valence basis set.[233] The 6-311G basis set as it was applied in this case had only a few polarization and correlating functions added to it, whereas the aug-MCP-TZP basis set has several carefully designed contracted polarization and correlating functions. This is clear when comparing values of ΔE_1 computed with the CR-CC(2,3)/aug-MCP-TZP level of theory and with the CCSD(T)/LCG level of theory which agrees well with the LCG result.[59]

Thus far, counterpoise corrections have reduced the value of ΔE_1 significantly.

The energy of formation is further decreased by taking into account the zero-point energy correction. Including the zero-point energy for HArF from MP2/aug-MCP-TZP calculations, where it was found to be 26.3 kJ·mol^{-1}, the corrected values of the best ΔE_1 from CR-CC(2,3)/aug-MCP-TZP//MP2/aug-MCP-TZP calculation become essentially zero. This correction will increase the value of ΔE_2 only marginally by about 1 kJ·mol^{-1}, as the zero-point energy for hydrogen fluoride equals 24.9 kJ·mol^{-1} (MP2/aug-MCP-TZP).

Table 2.2: *Bond lengths (in Å) in HArF and energies (in kJ·mol^{-1}) of reactions involving H, Ar, and F*

method/basis	r_e(Ar-H)	r_e(Ar-F)	ΔE_1 [a]	ΔE_2 [b]	ΔE_{HF} [c]
MP2/aug-MCP-TZP	1.304	1.954	-66.8 (-43.2)	-546.7	613.5
MP2/accT	1.313	1.968	-49.2 (-40.2)	-551.1	600.3
MP2/nasT	1.314	1.976	-48.2 (-35.4)	-552.8	601.0
MP2/rasT	1.314	1.975	-46.7 (-36.3)	-553.4	600.1
MP2/LCG[d]	1.326	1.996	-6.8	-584.3	591.1
MP2/LCG[e]	1.326	1.998	-4.0 (7.8)	-585.2	589.2
CCSD/aug-MCP-TZP	1.296	1.970	-21.2 (-0.4)	-546.6	567.8
CCSD(T)/aug-MCP-TZP[f]	1.319	1.964	N/A	-545.8	N/A
CCSD(T)/LCG[d]	1.355	2.005	-49.2	-579.6	628.8
CR-CC(2,3)/aug-MCP-TZP[g]			-41.6 (-23.5)	-551.0	592.6
CR-CC(2,3)/aug-MCP-TZP[h]			-41.5 (-22.6)	-551.1	592.6

[a] energy change in the formation reaction H + F + Rg → HRgF (values in parentheses are corrected for BSSE); [b] energy change in the decomposition reaction HRgF → Rg + HF; [c] molecular total atomization energy, Eq. (3); [d] values from Ref.[59] [e] this work; [f] present implementation of CCSD(T) in GAMESS-US is restricted to closed-shell RHF reference wavefunction (entries N/A in the table); [g] at CCSD(T)/aug-MCP-TZP optimized geometry; [h] at MP2/aug-MCP-TZP optimized geometry.

Several values of ΔE_1 are available computed at a variety of levels of theory, for comparison. In 2001 Runeberg et al.[202] found the CCSD(T)/acp3 value of $-\Delta E_1$ equal to 23.2 kJ·mol^{-1} which was reduced to 13.5 kJ·mol^{-1} when basis set extension corrections were added. One year later Panek et al.[79], using the MP2 method as well as several density functionals with the accT basis set, found the range for the energy of HArF relative to the neutral atom dissociation limit (ΔE_1) to be from

-30.3 kJ·mol^{-1} to -11.4 kJ·mol^{-1}; their MP2/accT value was -40.5 kJ·mol^{-1}, fairly close to the MP2/acp3 value of -49.2 kJ·mol^{-1}. In 2004 Xie and coworkers reported[234] that the combined energy of the three free atoms Hr, Ar, and F relative to the minimum energy of HArF ($-\Delta E_1$) equals 17.6 kJ·mol^{-1} when evaluated at the MR-AQCC/accT level of theory. Three years later Hu and coworkers[235] calculated the atomization energy of HArF to be 40.6 kJ·mol^{-1} at the MP2/accT level of theory.

2.3.2 HKrF

Results for HKrF are tabulated in Table 2.3. Structural parameters computed at the MP2/acp3 level of theory agree very well (within mÅ) with relativistic all-electron structural parameters, as do their energies of formation and decomposition, which differ by less than 10 kJ·mol^{-1}. When a relativistic basis set is used, bond lengths are shortened, as expected. The MP2/LCG level of theory slightly overestimates the Kr-F bond length as compared to the all-electron value from the most complete all-electron basis set included in this study. Additionally, this level of theory underestimates the energy of formation of HKrF, ΔE_1. This can be attributed to the deficiency in polarization functions on krypton and correlating functions on fluorine of the basis set, as described in the Methods section. Application of a counterpoise correction reduces ΔE_1 values as with HArF. This correction is largest for the MP2/LCG ΔE_1. Adding the zero-point energy correction to the counterpoise correction continues to reduce ΔE_1 of HKrF but has no affect on the ΔE_2 as HKrF and HF have almost equal zero-point energies.

2.3.3 HxeF

As with HKrF, MCP and all-electron results for HXeF computed with the MP2 method agree well for HXeF. These results are found in Table 2.4, and indicate that the energy of formation for HXeF, ΔE_1, is underestimated at the MP2/LCG level and, given the energy balance of Eq. (3), leads to an increased value of the energy in the dissociation reaction (2). Counterpoise corrections decrease the ΔE_1 by 30-50 kJ·mol^{-1} and zero-point energy corrections decrease it by another 23.6 kJ·mol^{-1}

Table 2.3: *Bond lengths (in Å) in HKrF and energies (in kJ·mol^{-1}) of reactions involving H, Kr, and F*

method/basis	r_e(Kr-H)	r_e(Kr-F)	ΔE_1	ΔE_2	Δ E$_{HF}$ $^{(*)}$
MP2/aug-MCP-TZP	1.456	2.034	-137.6 (-105.4)	-475.8	613.4
MP2/accT	1.461	2.035	-128.5 (-110.1)	-471.8	600.3
MP2/nasT	1.459	2.036	-133.3 (-109.6)	-467.7	601.0
MP2/rasT	1.454	2.031	-133.7 (-110.4)	-466.3	600.0
MP2/LCG	1.423	2.134	-91.5	-499.6	591.1
MP2/LCG	1.423	2.134	-90.2 (-33.7)	-499.1	589.3
CCSD/aug-MCP-TZP	1.455	2.039	-93.2 (-65.0)	-492.5	585.7
CCSD(T)/aug-MCP-TZP	1.474	2.040	N/A	-474.3	N/A
CCSD(T)/LCG	1.439	2.138	-131.8	-497.0	628.8
CR-CC(2,3)/aug-MCP-TZP			-114.5 (-88.0)	-478.1	592.6
CR-CC(2,3)/aug-MCP-TZP			-114.4 (-87.1)	-478.3	592.7

$^{(*)}$ See footnotes to Table 2.2

at the MP2/aug-MCP-TZP level of theory. For decomposition into Xe + HF, the zero-point energy correction is insignificant: only about 1 kJ·mol^{-1} .

Table 2.4: *Bond lengths (in Å) in HXeF and energies (in kJ·mol^{-1}) of reactions involving H, Xe, and F*

method/basis	r_e(Xe-H)	r_e(Xe-F)	ΔE_1	ΔE_2	Δ E$_{HF}$ $^{(*)}$
MP2/aug-MCP-TZP	1.633	2.100	-240.3 (-190.6)	-373.1	613.4
MP2/nasT	1.644	2.100	-240.2 (-204.4)	-360.8	601.0
MP2/rasT	1.638	2.102	-234.7 (-199.1)	-365.3	600.0
MP2/LCG	1.665	2.146	-188.7	-402.2	590.9
MP2/LCG	1.666	2.147	-187.4 (-157.1)	-401.8	589.2
CCSD/aug-MCP-TZP	1.639	2.096	-199.7 (-155.7)	-386.1	585.8
CCSD(T)/aug-MCP-TZP	1.651	2.102	N/A	-369.7	N/A
CCSD(T)/LCG	1.681	2.150	-231.1	-397.7	628.8
CR-CC(2,3)/aug-MCP-TZP			-220.0 (-177.4)	-372.6	592.6
CR-CC(2,3)/aug-MCP-TZP			-219.9 (-176.3)	-372.8	592.7

$^{(*)}$ See footnotes to Table 2.2

2.3.4 HRnF

Relativistic (DK3) and MCP results agree well for HRnF for both bond lengths and energies. The Rn-H bond length, for example, differs by only 0.02 Å between

MP2/acp3 and MP2/rasT computations. A large discrepancy exists between the Rn-F bond length computed at the MP2/acp3 level of theory and the MP2/LCG level of theory.[59] This bond length is significantly shorter at the MP2/acp3 level of theory, and is certainly short enough to indicate that the two atoms must be interacting. As this is in direct contrast to previously reported results, further investigation is warranted. A possible explanation is that there are multiple local minima on the HRnF potential energy surface, one with each Rn-F bond length. In order to check this, the geometry of HRnF was optimized using the structure of Lundell et al. as a starting point.[59] However, optimization converged to the geometry reported in Table 2.5. As present computations with the LCG basis set were able to reproduce the results of Lundell et al. using the GAMESS program, the difference may be attributed to the different pseudopotentials used by Lundell et al. and in the present work.

The CP corrections lead to the reduction of ΔE_1, with the vibrational correction due to the zero-point energy of 21.8 kJ·mol^{-1} for HRnF (MP2/acp3) reducing it further. Zero-point energy corrections for ΔE_2 will slightly decrease its value by about 3 kJ·mol^{-1}.

Table 2.5: *Bond lengths (in Å) in HRnF and energies (in kJ·mol^{-1}) of reactions involving H, Rn, and F*

method/basis	r_e(Rn-H)	r_e(Rn-F)	ΔE_1	ΔE_2	ΔE_e[(*)]
MP2/aug-MCP-TZP	1.736	2.175	-287.0 (-223.2)	-326.4	613.4
MP2/rasT	1.716	2.163	-277.7 (-224.8)	-322.3	600.0
MP2/LCG	1.868	2.809	+39.7	-630.7	591.0
MP2/LCG	1.870	2.808	+40.7 (53.3)	-629.9	589.2
CCSD/aug-MCP-TZP	1.743	2.173	-245.8 (-190.2)	-340.0	585.8
CCSD(T)/aug-MCP-TZP	1.755	2.177	N/A	-323.7	N/A
CCSD(T)/LCG	1.942	2.849	-2.5	-626.2	628.7
CR-CC(2,3)/aug-MCP-TZP			-266.3 (-211.9)	-326.4	592.7
CR-CC(2,3)/aug-MCP-TZP			-266.0 (-210.7)	-326.6	592.6

[(*)] See footnotes to Table 2.2

2.3.5 Summary for All HRgX

For all HRgF, bond lengths obtained using the model core potentials at MP2 and CCSD(T) levels of theory agree reasonably well, with the largest difference for the Rg-H bond smaller than 0.02 Å, and the largest difference for the Rg-F bond smaller than 0.01 Å. The Rg-H bond length increases systematically by about 0.1 Å as the size of the Rg increases; similarly, the bond length Rg-F increases by about 0.07 Å.

In Figure 2.1, trends in computed geometry of the HRgF molecules are correlated with the first ionization energies of the rare gases. As the rare gas becomes heavier and more easily ionized, the increase in bond lengths becomes less dramatic, and bond lengths in HRnF are very close to those in XeF.

Figure 2.1: *MP2/aug-MCP-TZP Rg-X bond lengths (in Å)*

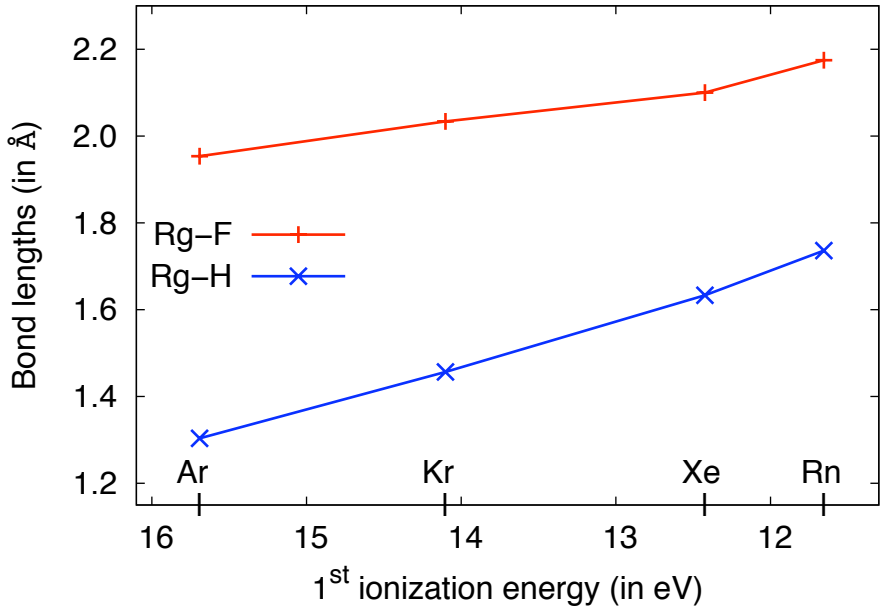

Structures of HRgX computed herein agree well with those previously obtained by other researchers for argon, krypton, and xenon containing halohydrides.[59] For HRnF, however, there is a major difference in the computed value of the Rn-F bond length between the MP2/LCG level of theory and all other levels of theory used in this work. It is possible that the basis set and pseudopotentials in the LCG basis

set were not sufficient to describe the chemistry of radon. The averaged relativistic core potentials by Christiansen et al.[236–238] have a small valence space compared to the MCPs: only three s- and p-type primitive Gaussian functions and four d-type primitives. This deficient description of the valence space of radon is responsible for the excessively large Rn-F bond length, as well as the increase in the energy of dissociation of HRnF (ΔE_2).

Figure 2.2: *Energy change in the reactions involving Rg, H, and F (in kJ/mol); data from CR-CC(2,3)/mcpT//MP2/mcpT calculations. (CP) refers to CP-corrected energies.*

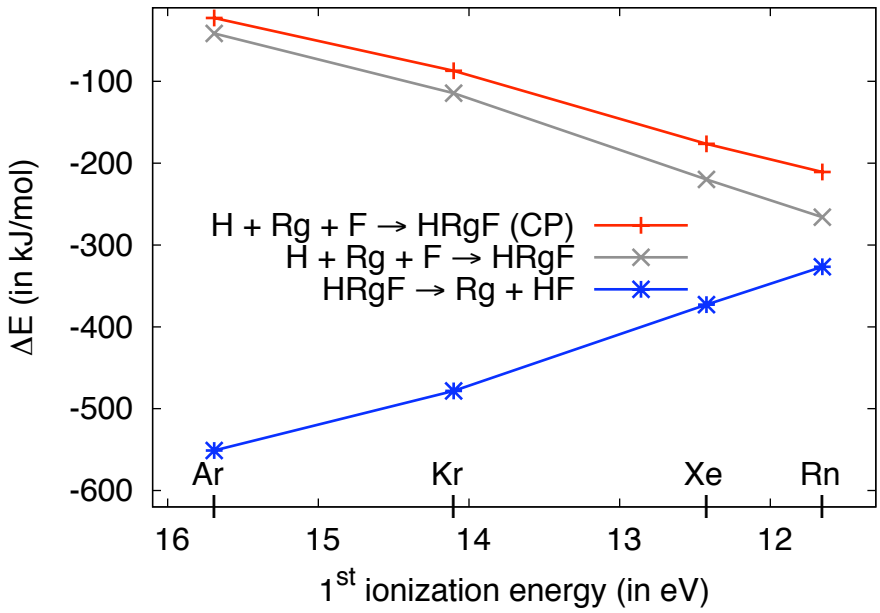

As shown in Tables 2.2-2.5 and in Figures 2.2, increase in size of the rare gas in HRgF correlates with a more exothermic formation reaction and a less exothermic reaction for dissociation into Rg + HF. All of the HRgF compounds are thermodynamically unstable, but the possibility of kinetic stability must also be considered. Frenking et al.[205] stated that if the energy barrier to the dissociation reaction is high enough, kinetic stability for these molecules may be possible.

The highest level of theory at which ΔE_1 and ΔE_2 were computed in this study is the CR-CC(2,3)/acp3//MP2/acp3 level. For the lighter four rare gases these com-

puted energies of formation and decomposition agree well with previously reported results.[59] For HRnF, it is expected that the ΔE_1 and ΔE_2 values would differ greatly as they were computed for a different optimized geometry than were the ΔE_1 and ΔE_2 values computed at the MP2/LCG level of theory.

ΔE_{HF}, determined through subtraction of ΔE_1 and ΔE_2 depends on the basis set and method at which ΔE_1 and ΔE_2 were computed. The closest ΔE_{HF} to the experimental value of 591 kJ·mol^{-1} reported by Martin[239] is the CR-CC(2,3)/aug-MCP-TZP value of 593 kJ·mol^{-1}. Other values are about 613 kJ·mol^{-1}at the MP2/aug-MCP-TZP level of theory, and is reduced to about 600 kJ·mol^{-1} when the all-electron basis sets are employed (accT, nasT, and rasT). The CCSD(T)/LCG value of ΔE_{HF} is about 590 kJ·mol^{-1}.

Harmonic vibrational frequencies for each HRgF were computed at the MP2/aug-MCP-TZP level of theory. In Table 2.6 these results are compared to those of Lundell et al.[59]. As with the energies of formation and decomposition, harmonic vibrational frequencies for the lighter four rare gases agree well with previous results. Harmonic vibrational frequencies for HRnF cannot be expected to agree, as they were computed for the optimized geometry at the MP2/aug-MCP-TZP level of theory which differs significantly from the MP2/LCG optimized geometry. In general, the Rg-H stretch has the largest intensity which is decreasing from the lightest (718.4 km·mol^{-1}) to the heaviest (376.1 km·mol^{-1}) congener. The intensity of the Rg-F stretch changes less, from 262.0 km·mol^{-1} for HArF to 185.9 km·mol^{-1}) for HRnF. Smaller vibrational frequencies corresponding to the bond stretches correlate with the longer bond lengths Rg-H and Rg-F obtained in previous studies[59].

Table 2.6: *Harmonic vibrational frequencies (in cm^{-1})* [(a),(b)]

molecule	$\nu_1(\Sigma^+)$	$\nu_2(\Pi)$	$\nu_3(\Sigma^+)$
HArF	483.8 (481.2)	772.4 (743.4)	2371.4 (2148.9)
HKrF	455.0 (396.1)	708.0 (695.2)	2230.5 (2315.9)
HXeF	463.2 (438.9)	660.2 (657.8)	2160.1 (2068.9)
HRnF	461.8 (312.6)	572.2 (601.2)	2046.3 (1575.0)

[(a)] values in parentheses are from Ref.[59] [(b)] modes $\nu_1(\Sigma^+)$, $\nu_2(\Pi)$, and $\nu_3(\Sigma^+)$ correspond to Rg-F stretch, degenerate bend, and Rg-H stretch, respectively.

In order to better understand the bonding in HRnF, and to confirm that the geometry resulting from MP2/acp3 level optimizations has the same general type of intramolecular interactions as the lighter HRgF, population analysis for all atoms was carried out with three different methods. The most basic of these is Mulliken population analysis, in which half of the electron density between two atoms is assigned to each atom.[240,241] The simplest extant method of population analysis, the Mulliken method suffers from a number of disadvantages. First, it can produce negative overlap population values, which are unphysical if they are produced for any population other than the population of an antibonding orbital. Second, it is heavily dependent on the basis set chosen, and is notoriously unreliable for compounds involving lithium, due to the very small valence space of the atom. However, it is often worth some attention as the way electrons are assigned in this method is fairly intuitive to chemists. A more mathematically rigorous, but still problematic method of population analysis is the Löwdin population analysis, in which the basis sets are orthogononalized following Löwdin's symmetric orthogonalization procedure developed in 1950, and then the density matrix constructed from these basis functions is partitioned between atoms over the entire space of the molecule.[242] The advantage of this method is inability to produce negative population values. Two main disadvantages of the Löwdin method are its basis set dependency and its inconsistency with the Mulliken method: the two methods may produce populations of opposite sign for the same atom in the same molecule! Results for all HRgF from both of these methods, as well as the NPA method described in the previous chapter[243,244] are presented in Table 2.7.

With the exception of HArF, the Mulliken charges agree quite well with the NPA charge distribution. Electron densities from both MP2 and CCSD methods yield similar charge distribution for all atoms. The Löwdin charges attribute a smaller partial negative charge to fluorine than do NPA and Mulliken, but in all three cases the model of bonding is of a fluorine with a large partial negative charge of about -0.8e (NPA) interacting with the positively charged Rg-H complex, whose partial positive charge that is predominantly localized on the rare gas atom, especially for the heavier atoms. As the size of the rare gas atom increases, the magnitude of the

Table 2.7: *Atomic charges computed according to various population analyses* [(a)]

molecule/method	population analysis									μ/D [(b)]
			H			Rg			F	
	MPA	LPA	NPA	MPA	LPA	NPA	MPA	LPA	NPA	
HArF/MP2	0.67	-0.46	0.21	0.13	1.10	0.55	-0.80	-0.64	-0.76	6.686
HArF/CCSD	0.61	-0.44		0.20	1.09		-0.81	-0.65		6.797
HKrF/MP2	0.13	-0.46	0.11	0.67	1.12	0.65	-0.80	-0.66	-0.76	6.118
HKrF/CCSD	0.11	-0.45		0.70	1.12		-0.81	-0.67		6.179
HXeF/MP2	0.11	-0.51	-0.02	0.66	1.23	0.79	-0.77	-0.72	-0.77	5.125
HXeF/CCSD	0.09	-0.50		0.69	1.23		-0.79	-0.73		5.126
HRnF/MP2	-0.11	-0.54	-0.07	0.89	1.31	0.86	-0.78	-0.76	-0.79	4.971
HRnF/CCSD	-0.12	-0.53		0.91	1.30		-0.80	-0.77		4.980

[(a)] aug-MCP-tzp basis set; [(b)] dipole moment in Debye

dipole moment decreases, with the dipole moments of Rn and Xe being very close to each other both in charge distribution and dipole moment. The charge distribution clearly supports the accepted model of bonding in the HRgF systems, $[HRg]^+$ F^-. The Rg-H bond lengths in HRgF are only 3-4% longer than the ones found of the ions HRg^+: 1.271 Å, 1.406 Å, 1.578 Å, and 1.662 Å for Rg = Ar, Kr, Xe, and Rn, respectively, with the values reported above coming from MP2/acp3 results. The amount of electron transfer from the valence *np*-subshell of the rare gas increase with the increases in size of the rare gas atom. The decreased dipole moment of radon fluorohydride as compared to the lighter rare gas fluorohydrides is likely a result of the increased magnitude of the charges on the radon and the fluorine, as they form a stronger interaction with more electron density shared between them.

Analysis of the bonding in HRgF with the NBO method confirms that there is only one bond between the rare gas and the hydrogen, and another between the rare gas and the fluoride. Other associated valence electrons exist as lone pairs, with four on the fluoride and three on the rare gas. Computed bond orders[245,246] for each of these bonds for each HRgF indicate that as the size of the rare gas increases, the order of the Rg-H bond increases and the order of the Rg-F bond decreases. Bond order analysis reveals that in all cases, the interaction between the rare gas and the hydrogen is much stronger than the interaction between the rare gas and the fluoride.

HArF has an Ar-H bond order of only 0.31, while HKrF has a corresponding Kr-H bond order of 0.81, demonstrating that bonding in HKrF is dramatically different than in HArF. When the size of the rare gas increases further to Xe, this bond order increases to 0.86, and finally to 0.89 for HRnF. The Ar-F bond order is 0.20, and as the rare gas increases this continues to decrease: 0.17 for Kr-F, 0.11 for Xe-F, and less than 0.05 for Rn-F.

2.4 Conclusions

In this chapter, it has been demonstrated the HRnF is indeed a chemically bonded compound. This claim is substantiated through optimized geometries energies of formation and decomposition of the HRgF species, charge distributions, and computed dipole moments. A variety of quantum chemical methods and basis sets have been employed in this study in order to put the existence of HRnF beyond doubt. These methods include the MP2, CCSD, CCSD(T), and CR-CC(2,3) methods. Both all-electron basis sets and MCPs have been used in conjunction with these methods. The bonding behaviour of radon is consistent with the periodic trends for the rare gases, with radon binding more strongly than the lighter rare gas atoms. Examination of calculated dissociation energies shows that the HRgF compounds are thermodynamically more stable than the free atoms but less stable than HF + Rg. It is relevant to note here that the structures obtained from the economical MP2 method are quite similar to those obtained with the CCSD(T) method, making it reasonable to compute reaction energies with the CR-CC(2,3) method from structures optimized at the MP2/acp3 level of theory. The charge distribution for all the rare gas systems studied is similar, with large partial negative charge being localized on the fluorine atom and a positive charge distributed across the RgH^+ group. The dipole moment of these molecules decreases with increasing rare gas atom size. This work agrees with previous work in its description of the four lighter HRgF; but for HRnF, it is clear the the Rn-F bond length must be a maximum of 2.177 Å. This difference in geometry affects computed properties for HRnF such as harmonic vibrational frequencies and

energies of formation and decomposition. The problem in the Rn-F bond length has clearly been attributed to a deficient basis set. Population analysis of HRgF confirms that in these molecules the positively charged rare gas and hydrogen together interact electrostatically with the fluoride.

Chapter 3

Compounds of Heavy Rare Gases and the Halogens*

3.1 Introduction

After demonstrating that HRnF is as stable as any other HRgF-type compound, the logical next step is to extend the investigation to related compounds with the heavier halogens, termed HRgX, where X= F, Cl, Br, and I. In this chapter, properties and structures of HRgX compounds and the dependence on various basis sets will be discussed. As radon chemistry rapidly becomes an area of general interest, chemists turn to high-level computational methods using extensive basis sets to gain insight. Reliable predictions require the use of state-of-the-art methods where, for larger systems, extensive basis sets are often prohibitively expensive. Consequently, the practicality of using large basis sets becomes a pressing concern. In order to efficiently study rare gas compounds of increasing size and complexity, it is essential to find the balance between speed of calculations and completeness of description. Model core potentials (MCP) and their basis sets[189] are ideal for this task, as they are known for having a high degree of computational efficiency without compromising the quality of results[185]. In this chapter, several MCP basis sets are compared as well as the effect of the addition of extensive correlation, polarization, and diffuse functions on the quality of results for energetics and geometry, both for the hydride itself and for the tran-

*A version of this chapter was published in *Can. J. Chem.*, **2013**, *91*, 894.

sition state along the hydride decomposition pathway. The goal is to find the most efficient MCP basis set that will provide results of a high calibre, and will therefore be ideal in computations on other systems that contain both rare gases and other heavy atoms. Toward this end, the Møller-Plesset (MP2)[247] and density functional theory (DFT) with the PBE0[184] functional were used to compute fundamental properties of the hydrides, such as geometry, energetics of formation, decomposition, formation of the transition state, and examined bonding by computing atomic charges via Natural Population Analysis (NPA). Energy of formation of the transition state is examined with particular interest, since it provides a measure of the kinetic stability of the hydride and is consequently useful for predictive purposes.

In the interest of characterizing the radon analogs of xenon halohydrides, the recommended basis set was then used to compute critical points, bond paths, electron density, and atomic basins with the Quantum Theory of Atoms in Molecules (QTAIM)[199,200]. The QTAIM method has long been applied to a wide variety of problems of chemical interest, including the study and characterization of small molecules that contain rare-gas atoms[248].

The rare gas hydrides studied herein share common pathways for their formation and decomposition reactions. The atomic hydrogen, halogen, and rare gas react to exothermically produce a bound, triatomic rare gas hydride that is metastable (Reaction 3.1). This study has been framed around this mechanism rather than around a reaction of ions as indicated by early experiments[36], as later experiments support the triatomic formation mechanism.[37] After formation of HRgX, the product decays producing an HX molecule and rare gas atom. This is accomplished via rearrangement of the hydrogen, which moves through a triangular transition state in order to bond with the halogen. The formation and subsequent dissociation of the HRgX species in the gas phase can be summarized by the following reactions:

$$\mathrm{H}_{(g)} + \mathrm{F}_{(g)} + \mathrm{Rg}_{(g)} \rightarrow \mathrm{HRgF}_{(g)}, \qquad \Delta E_1 \tag{3.1}$$

$$\mathrm{HRgF}_{(g)} \rightarrow \mathrm{HF}_{(g)} + \mathrm{Rg}_{(g)}, \qquad \Delta E_2 \tag{3.2}$$

$$\mathrm{HRgX}_{(g)} \rightarrow \mathrm{HRgX}^{\mathrm{TS}}_{(g)}, \qquad \Delta E_{\mathrm{TS}}. \tag{3.3}$$

The relationships between the three reaction energies are illustrated in Figure 3.1.

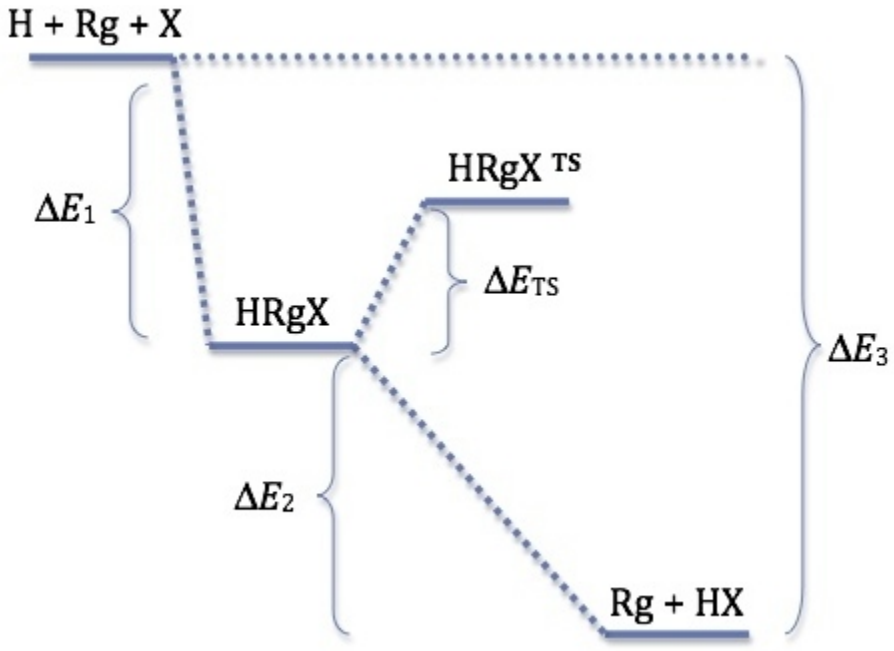

Figure 3.1: *Energy diagram for the reactions involved in formation and dissociation of HRgX species.* ΔE_1, ΔE_2, *and* ΔE_{TS} *are described in text;* ΔE_3 *is the energy of formation of HX from atoms.*

3.2 Computational Methods

Six MCP basis sets were used in this study in order to examine the effect of basis set size on the structure and properties of HRgX. Shared characteristics of all MCP basis sets have been described in Chapter 1. The basis sets used in this chapter are, in order of increasing complexity, (a) improved scalar-relativistic MCP with an extremely compact basis set (abbreviated ims2)[196]; (b) three MCPs from a recent compilation:[185] MCP-TZP with a triple zeta valence basis set (denoted mcp3), the mcp3 basis set with added diffuse functions, aug-MCP-TZP (acp3), and the augmented quadruple-zeta valence basis setaug-MCP-QZP (acp4); (c) two new, large MCP basis sets, ZFK3LDK3 (zfk3) and ZFK4LDK3 (zfk4)[198], which contain extensive sets

of diffuse, polarization, and correlating functions. Detailed information about the composition of these basis sets is presented in Table 3.1, in [ns.np.nd.nf.ng] format.

All electrons outside of the pseudopotential were correlated in the MP2 calculations. The DFT(PBE0) computations used a radial grid of 116 points and angular Lebedev grid with 770 points. The hybrid generalized gradient approximation functional PBE0 was chosen as it has performed favourably in structure and kinetics computations, as shown by Adamo and Barone[184]. Optimized geometries of HRgX and the corresponding transition state and energies of formation and decomposition were computed using each basis set with the MP2 and DFT(PBE0) methods. In addition, as discussed below, computed energies of formation and decomposition for each hydride and energy barriers to the transition states at the CCSD/zfk4 level using geometries optimized at the MP2/zfk4 level.

Charges on all atoms were computed using Natural Population Analysis (NPA) at the MP2/aug-MCP-TZP level. In order to present a more complete picture of the structure of the HRgX molecule, the QTAIM approach was employed to analyze the electron density distribution for all HRgX species. Densities were generated for QTAIM computations using the MP2 method and a modified aug-MCP-TZP basis set, which contained no f-type polarization functions, abbreviated acp3-f. Removal of the additional f-type functions from the acp3 basis set was necessary to ensure that the Poincaré-Hopf relationship was satisfied during the QTAIM integrations,[200] and that the molecular graph displayed the correct bond paths. QTAIM properties were computed from the results of GAMESS-US[249] calculations using the AIMAll program[250]. AIM extended wavefunction files (file extension ".wfx") for AIMAll input are needed when pseudopotentials are used[251,252]. These files were generated with a locally-modified version of the GAMESS-US program. Additional electron density functions, which modelled the core electron density replaced by the pseudopotential, were obtained from the extended wavefunction files produced by Gaussian09[253] in energy calculations using the SBKJC[254–256] basis set on the free atoms, and scaled to match the core size of the acp3-f basis set. Figures representing QTAIM results were generated in the AIMStudio environment[250]. Electronic structure computations were

Table 3.1: *Composition of contracted basis functions*

Atom	ims2 iMCP-SR2	mcp3 MCP-TZP	acp3 MCP-ATZP	acp4 MCP-AQZP	zfk3 ZFK3LDK3	zfk4 ZFK4LDK3
H	$[3s.2p.1d]$	$[3s.2p.1d]$	$[4s.3p.2d]$	$[5s.4p.3d.2f]$	$[4s.3p.2d]$	$[5s.4p.3d.2f]$
F	$[3s.3p.1d.1f]$	$[3s.3p.2d.1f]$	$[4s.4p.3d.2f]$	$[4s.4p.4d.3f.2g]$	$[8s.7p.3d.2f]$	$[8s.7p.4d.3f.2g]$
Cl	$[3s.3p.1d.1f]$	$[3s.3p.2d.1f]$	$[4s.4p.3d.2f]$	$[4s.4p.4d.3f.2g]$	$[8s.8p.3d.2f]$	$[8s.8p.4d.3f.2g]$
Br	N/A	$[4s.4p.3d.1f]$	$[5s.5p.4d.2f]$	$[5s.5p.5d.3f.2g]$	$[8s.8p.5d.2f]$	$[8s.8p.6d.3f.2g]$
I	N/A	$[4s.4p.3d.1f]$	$[5s.5p.4d.2f]$	$[5s.5p.4d.3f.2g]$	$[11s.11p.9d.2f]$	$[11s.11p.9d.3f.2g]$
Xe	$[3s.3p.3d.1f]$	$[4s.4p.3d.1f]$	$[5s.5p.4d.2f]$	$[5s.5p.4d.3f.2g]$	$[11s.11p.9d.2f]$	$[11s.11p.9d.3f.2g]$
Rn	$[3s.3p.2d.1f]$	$[4s.4p.3d.1f]$	$[5s.5p.4d.2f]$	$[5s.5p.5d.3f.2g]$	$[11s.11p.8d.2f]$	$[11s.11p.8d.3f.2g]$

Table 3.2: *Reference MP2/ZFK-QZP values of structural parameters* [(a)]

Species	HRgX		Transition state		
	Rg-H	Rg-X	Rg-H	Rg-X	H-Rg-X
HXeF	1.638	2.117	1.564	2.373	100.0
HXeCl	1.659	2.597	1.568	2.931	99.1
HXeBr	1.674	2.743	1.569	3.091	98.5
HXeI	1.699	2.956	1.571	3.333	97.5
HRnF	1.731	2.189	1.644	2.430	95.3
HRnCl	1.748	2.659	1.647	2.984	93.3
HRnBr	1.762	2.802	1.648	3.144	92.4
HRnI	1.786	3.010	1.649	3.388	90.9

[(a)] bond lengths in Å, bond angles in degrees

carried out with GAMESS-US[249], Gaussian09[253], and NBO 5.G[257] on dual core and dual-quad core Apple Macintosh computers and Linux clusters at the University of Alberta.

3.3 Results and Discussion

An evaluation of basis set performance requires comparison of results at each level of theory to a chosen standard. Meaningful comparison requires the use of a method as a standard which both considers electron correlation effects and can handle open-shell species. The CCSD(T) method is considered such a standard. However, the current implementation[219] of the CCSD(T) method in GAMESS-US cannot treat the open-shell species which comprise the starting materials for the formation of HRgX and the CR-CC(2,3)[179] method does not have analytical gradients. In the previous chapter I have shown that with the aug-MCP-TZP basis set, the MP2 and CCSD(T) geometries differ by about 0.02 Å for the Rg-H bonds and are essentially the same for the Rg-F bonds. Consequently, geometries and energies computed at the MP2/ZFK-QZP level of theory became the reference standard.

Table 3.4 and Table 3.5 contain, in addition to the reference values, the differences between the DFT(PBE0) and MP2 reference values. These deviations show that the PBE0 functional brings about results that are fairly close to the ones obtained with

Table 3.3: *Reference MP2/ZFK-QZP values of reaction energies* [(a)]

Species	ΔE_1	ΔE_2	ΔE_{TS}
HXeF	-234	-374	155
HXeCl	-126	-325	132
HXeBr	-92	-305	131
HXeI	-51	-291	130
HRnF	-266	-341	160
HRnCl	-165	-287	142
HRnBr	-131	-266	141
HRnI	-91	-250	141

[(a)] Δ E$_n$ are defined in Figure 3.1; Δ E$_n$ are given in kJ·mol^{-1}

Table 3.4: *Reference DFT(PBE0)/ZFK-QZP values of structural parameters* [(a,b)]

Species	HRgX		Transition state		
	Rg-H	Rg-X	Rg-H	Rg-X	$\Theta_{H\,Rg\,X}$
HXeF	1.682 (0.044)	2.108 (-0.009)	1.596 (0.032)	2.366 (-0.007)	99.6 (-0.4)
HXeCl	1.705 (0.046)	2.603 (0.006)	1.607 (0.039)	2.951 (0.020)	96.5 (-2.6)
HXeBr	1.720 (0.046)	2.758 (0.015)	1.615 (0.046)	3.125 (0.034)	94.6 (-3.9)
HXeI	1.743 (0.044)	2.979 (0.023)	1.629 (0.058)	3.388 (0.055)	91.1 (-6.4)
HRnF	1.784 (0.053)	2.182 (-0.007)	1.684 (0.040)	2.424 (-0.006)	94.9 (-0.4)
HRnCl	1.802 (0.054)	2.666 (0.007)	1.691 (0.044)	3.010 (0.026)	90.2 (-3.1)
HRnBr	1.815 (0.053)	2.819 (0.017)	1.696 (0.048)	3.182 (0.038)	87.7 (-4.7)
HRnI	1.835 (0.049)	3.037 (0.027)	1.704 (0.055)	3.437 (0.049)	84.0 (-6.9)

[(a)] bond lengths in Å, bond angles in degrees [(b)] The values in parentheses are differences with respect to the MP2 values: $\mathcal{P}$(PBE0) - $\mathcal{P}$(MP2)

the MP2 method: The largest deviations in structural parameters are for the Rg-H bond lengths (up to 0.06 Å) while the agreement for the Rg-X bond and H-Rg-X angle in the transition state is slightly poorer. The energies ΔE_1 and ΔE_2 are very similar in the two approaches, while the PBE0 energies ΔE_{TS} are systematically larger (by about 20 kJ·mol^{-1}) than the MP2 ones.

It is worth mentioning that the DFT methodology brings about savings in computing time: for example, in the saddle point calculations for HRgI using the reference ZFK-QZP basis set the DFT(PBE0) method was found to be up to 1.5 times faster than the MP2 method: 19.5 minutes for HRnI at MP2/ZFK-QZP vs. 12.9 minutes for DFT(PBE0)/ZFK-QZP on seven cores of a 3.2 GHz Mac Pro. Tables 3.3 and 3.5 show

Table 3.5: *Reference DFT(PBE0)/ZFK-QZP values of reaction energies*[a,b]

Species	ΔE_1	ΔE_2	ΔE_{TS}
HXeF	-198 (36)	-366 (8)	173 (18)
HXeCl	-127 (-1)	-315 (10)	149 (17)
HXeBr	-93 (-1)	-292 (13)	147 (16)
HXeI	-53 (-2)	-277 (14)	144 (14)
HRnF	-225 (41)	-340 (1)	179 (19)
HRnCl	-158 (7)	-284 (3)	159 (17)
HRnBr	-124 (7)	-261 (5)	158 (17)
HRnI	-85 (6)	-244 (6)	157 (16)

[a] The values in parentheses are differences with respect to the MP2 values: $\mathcal{P}$(PBE0) - $\mathcal{P}$(MP2)
[b] Δ E$_n$ are defined in Figure 3.1 and are given in units of kJ·mol^{-1}

energies of formation, formation of the transition state, and decomposition for HRgX. Due to the higher reactivity of fluorine, as compared to the heavier halogens, ΔE_1 for HRgF are consistently larger across MP2 and DFT/PBE0 computations. However, HRgX compounds of the heavier halogens have a significant barrier (ΔE_{TS}) to decomposition which stabilizes the triatomic HRgX species. Computed bond lengths for HRgX have been compared with published data where available[36,57,59,169]. For HXeF, the percent difference in bond lengths is between -0.0004% and 0.13% with a standard deviation between 0.0007 and 0.1. For HXeCl, the percent difference in bond lengths varies between 0.008-0.06% and the standard deviation is between 0.01-0.13. For HXeBr, percent different varies between 0.05-0.10% and the standard deviation is between 0.07-0.19. HXeI compounds have a percent difference that ranges from 0.06-0.16% and a standard deviation ranging from 0.08-0.21. These values were computed using the standard deviation formula:

$$s = \sqrt{\frac{\sum (x - \bar{x})^2}{(n-1)}} \tag{3.4}$$

where n is the sample size, $\bar{x}$ is the average value of the data, and x is the given data point. In all cases, the bond lengths computed herein agree extremely well with those determined previously.

To assess energy differences between the MP2 and CCSD methods and ascertain the validity of selecting the MP2 method for computing reference values, differences

in the energy of formation (ΔE_1) and energy of decomposition (ΔE_2) were computed from MP2/ZFK-QZP//MP2/ZFK-QZP and CCSD/ZFK-QZP//MP2/ZFK-QZP results.

Table 3.6: *Energy differences $\Delta(\Delta E_n)$ (in kJ·mol^{-1}) between MP2/ZFK-QZP and CCSD/ZFK-QZP* [a,b,c]

Atom	$\Delta\Delta E_1$	$\Delta\Delta E_2$	$\Delta\Delta E_{TS}$
HXeX			
F	-45	16	-2
Cl	-25	17	4
Br	-22	17	5
I	-23	20	7
HRnX			
F	-43	14	-3
Cl	-25	17	3
Br	-22	17	4
I	-23	21	6

[a] $\Delta(\Delta E_n) = \Delta E_n$(MP2/ZFK-QZP) - ΔE_n(CCSD/ZFK-QZP) [b] ΔE_n are defined in Figure 3.1
[c] Errors are computed as: $\mathcal{P}$(basis) - $\mathcal{P}$(ZFK-QZP)

These results, collected in Table 3.6, show that the MP2 energy for Reaction 3.1 is too negative by up to 45 kJ·mol^{-1}, overstabilizing the HRgX product, while that of Reaction (2) is too small by about 14 kJ·mol^{-1}, again overestimating the stability of HRgX. On the other hand, the transition state energies calculated at MP2/ZFK-QZP level agreed well with CCSD/ZFK-QZP values. The tendency of the MP2 method to overstabilize a compound as compared with the coupled clusters method has been shown for other rare-gas containing systems.[50] The CCSD energies of formation of HRgCl (ΔE_1) increase in magnitude as the size of the rare gas increases. This is consistent with past findings, which indicate that radon may bond more strongly than xenon.[258] Comparison of data in Tables 3.5 and 3.6 shows that the energies evaluated using the DFT(PBE0) method are satisfactorily close to the CCSD values. $\Delta(\Delta E_1)$ are found to be larger than $\Delta(\Delta E_2)$ due to the greater effect of basis set superposition error in the calculation of ΔE_1. As ΔE_1 is computed as the difference between the sum of the energies of the free atoms and the energy of the triatomic HRgX species, the overlap of the basis functions from the atoms in the HRgX species

leads effectively to a larger basis set, resulting in a better value for ΔE_1. As the MP2 method is a perturbative method, this does not necessarily coincide with a decrease in the energy of the HRgX species as would be the case for a variational method. The same is true of the CCSD method, and so a standard of reference must be chosen in order to qualitatively differentiate between results of 'higher' or 'poorer' quality. In this case, the ZFK-QZP basis set is chosen for its extensive size, including many polarization and diffuse functions.

When evaluating quality of results against basis set efficiency, it is important to be able to distinguish basis sets that meet both these criteria from the ones that appear efficient through fortuitous cancellation of errors and are in reality inadequate to describe the chemistry of the system. This holds especially true in the present work, where the heavy rare gas atoms require basis sets capable of accounting for relativistic effects. In light of this, the effect of basis set size on the completeness of description of molecular geometry with respect to the chosen standard is examined. Calculated errors in the values of several properties $\mathcal{P}$, such as bond lengths, bond angles in transition states, energies of formation, and the energy barriers to the transition state complex with respect to the DFT(PBE0)/ZFK-QZP values are shown in Tables 3.9 and 3.10. Calculated errors for these properties with respect to those computed at the MP2/ZFK-QZP level of theory are shown in Tables 3.7 and 3.8. The errors for each property $\mathcal{P}$, shown in subsequent tables, were evaluated for each basis B as $\mathcal{P}$(B) - $\mathcal{P}$(ZFK-QZP), where B = iMCP-SR2, MCP-TZP, aug-MCP-TZP, aug-MCP-QZP, and ZFK-TZP.

Errors in the MP2 results with respect to the reference values are shown in Table 3.7 for the Reaction (1) product molecules HRgX and in Table 3.8 for the transition states. Errors computed for the DFT(PBE0) method are shown in Table 3.9 for the products of Reaction (1) and in Table 3.10 for the transition states.

The addition of diffuse functions to the MCP-TZP basis set can have a noticeable effect on the results of geometry optimization. The MCP-TZP basis set produces accurate results for geometry, but diverges greatly from the MP2/ZFK-QZP reference for energetics. In both cases, aug-MCP-TZP produces values which are more

Table 3.7: *Errors in structural parameters of the linear systems (in Å) computed with the MP2 method* [(a)]

	H-Rg					Rg-X				
	ims2	mcp3	acp3	zfk3	acp4	ims2	mcp3	acp3	zfk3	acp4
HXeX										
F	0.004	0.009	-0.005	0.016	-0.013	-0.002	-0.037	-0.017	-0.001	-0.017
Cl	0.013	0.010	-0.000	0.015	-0.008	0.002	-0.002	0.021	0.017	-0.005
Br		0.002	-0.003	0.016	-0.010		0.018	0.029	0.016	0.000
I		0.004	-0.001	0.017	-0.005		0.007	0.017	0.017	-0.019
	ims2	mcp3	acp3	zfk3	acp4	ims2	mcp3	acp3	zfk3	acp4
HRnX										
F	0.030	0.021	0.005	0.019	-0.004	0.016	-0.034	-0.014	-0.002	-0.023
Cl	0.044	0.021	0.007	0.019	-0.006	0.021	-0.009	0.010	0.017	-0.003
Br		0.013	0.004	0.018	-0.010		0.009	0.025	0.017	0.004
I		0.013	0.002	0.018	-0.010		0.006	0.023	0.021	-0.010

[(a)] Errors are computed as: $\mathcal{P}$(basis) - $\mathcal{P}$(zfk4)

consistent across halogen and rare gas atoms than either of the smaller MCP basis sets and ZFK-TZP. Differences in r(Xe-H) in xenon chlorides at the MP2/aug-MCP-TZP level are half of those at the MP2/MCP-TZP level, and are a third of those at the MP2/ZFK-TZP level. A similar trend is evident for the radon bromides; the difference in r(Rn-H) at the MP2/aug-MCP-TZP level is about a third of that at the MP2/MCP-TZP level, and is less than a fourth of the variance at the MP2/ZFK-TZP level. In nearly all cases, aug-MCP-TZP produces results of higher consistency with the MP2/ZFK-QZP reference.

At the DFT(PBE0) level both aug-MCP-TZP and aug-MCP-QZP significantly overestimate r(Xe-H), while ZFK-TZP underestimates it by only about a tenth as much, yielding a more consistent result. The aug-MCP basis sets provide improved results for r(Rn-H), but still overestimate this bond length by up to double the error in the ZFK-TZP basis. Both the aug-MCP-QZP and the ZFK-TZP basis sets produce results of comparable accuracy of r(Rn-Br) at the DFT(PBE0) level, and the aug-MCP-TZP basis set overestimates this property by double the error of the two larger basis sets.

While computations with the iMCP-SR2 basis set are significantly faster than

Table 3.8: *Errors in structural parameters of the transition state (in Å and degrees) computed with the MP2 method* [(a)]

	H-Rg					Rg-X					$\Theta_{H\,Rg\,X}$				
	ims2	mcp3	acp3	zfk3	acp4	ims2	mcp3	acp3	zfk3	acp4	ims2	mcp3	acp3	zfk3	acp4
HXeX															
F	-0.005	-0.001	-0.002	0.013	-0.014	0.057	-0.047	-0.006	0.011	-0.018	1.0	0.2	0.8	-0.1	0.8
Cl	-0.006	0.000	-0.001	0.014	-0.013	0.060	-0.002	0.034	0.031	-0.006	0.8	-0.3	0.9	-0.1	0.8
Br		0.001	-0.001	0.014	-0.013		0.040	0.041	0.029	0.005		0.6	0.9	-0.2	0.9
I		0.001	-0.001	0.014	-0.013		0.034	0.025	0.032	-0.017		0.5	1.0	-0.2	1.0
HRnX															
F	0.013	0.011	0.004	0.017	-0.006	0.066	-0.050	-0.023	0.009	-0.031	1.2	0.1	0.6	-0.0	0.7
Cl	0.012	0.011	0.005	0.018	-0.005	0.104	-0.007	0.041	0.036	0.008	0.6	-0.7	1.0	-0.0	0.7
Br		0.012	0.005	0.018	-0.005		0.035	0.055	0.034	0.016		0.4	1.3	-0.1	0.9
I		0.012	0.005	0.018	-0.005		0.028	0.039	0.035	-0.016		0.3	1.3	0.0	0.9

[(a)] Errors are computed as: $\mathcal{P}$(basis) - $\mathcal{P}$(zfk4)

Table 3.9: *Errors in structural parameters of the linear systems (in Å) computed with the DFT(PBE0) method* [(a)]

	H-Rg					Rg-X				
	ims2	mcp3	acp3	zfk3	acp4	ims2	mcp3	acp3	zfk3	acp4
HXeX										
F	-0.002	0.001	-0.011	0.001	-0.013	-0.002	-0.023	0.000	0.004	-0.005
Cl	-0.004	0.004	-0.007	0.002	-0.009	-0.118	-0.011	0.003	0.003	-0.002
Br		-0.005	-0.006	0.001	-0.007		0.005	0.019	0.002	0.016
I		-0.003	-0.008	0.002	-0.011		-0.009	-0.005	0.002	-0.008
	ims2	mcp3	acp3	zfk3	acp4	ims2	mcp3	acp3	zfk3	acp4
HRnX										
F	0.025	0.006	-0.005	0.001	-0.008	-0.006	-0.025	-0.003	0.004	-0.013
Cl	0.038	0.008	-0.001	0.002	-0.005	0.065	-0.012	-0.001	0.003	-0.010
Br		-0.002	-0.005	0.002	-0.010		0.001	0.004	0.002	-0.002
I		0.001	-0.003	0.002	-0.008		-0.012	-0.009	0.002	-0.015

[(a)] Errors are computed as: $\mathcal{P}$(basis) - $\mathcal{P}$(zfk4)

computations with any of the larger basis sets (4 minutes to locate the saddle point of HRnCl at the DFT(PBE0)/iMCP-SR2 level vs 80 minutes to locate the same saddle point at the DFT(PBE0)/ZFK-QZP level on a 3.2 GHz Mac Pro, in each case starting from a structure optimized at the same level of theory as was used in the saddle point computation), the ims2 basis set lacks sufficient polarization, diffuse, and correlating functions (see Table 3.1), and it brought about the largest errors in structural parameters of all the basis sets examined. While this basis set may be used for initial geometry optimizations, it is not recommended for energy evaluations for rare-gas containing molecules, except perhaps in preliminary investigations.

Several trends are evident in the reaction energetics of HRgX. As the size of the rare gas increases, the energy of formation of the transition state decreases slightly. Energies of formation for HRgX are significantly larger in magnitude for radon hydrides than for xenon hydrides: this is most noticeable in the bromides. While a heavier rare gas leads to a more stable molecule, increasing the size of the halogen results in decreased stability due to the lesser electronegativities of the heavy halogens. The lower first ionization energy of radon correlates with its greater polarizability as compared to xenon, and both are contributing factors in the greater reactivity of

Table 3.10: *Errors in structural parameters of the transition state (in Å and degrees) computed with the DFT(PBE0) method* [(a)]

	H-Rg					Rg-X					$\Theta_{H\,Rg\,X}$				
	ims2	mcp3	acp3	zfk3	acp4	ims2	mcp3	acp3	zfk3	acp4	ims2	mcp3	acp3	zfk3	acp4
HXeX															
F	-0.001	-0.003	-0.009	0.002	-0.013	0.017	-0.043	0.001	-0.003	-0.003	0.9	0.4	0.9	-0.1	0.9
Cl	0.026	0.006	-0.007	0.003	-0.011	0.015	-0.020	0.005	0.003	-0.002	-0.1	-0.1	1.1	-0.1	1.1
Br		-0.002	-0.008	0.003	-0.013		0.013	0.011	0.002	0.007		-0.1	1.1	-0.1	1.1
I		0.002	-0.006	0.003	-0.011		0.003	-0.004	0.003	-0.010		0.9	1.4	-0.2	1.5
HRnX															
F	0.027	0.003	-0.003	0.003	-0.006	0.023	-0.491	-0.004	0.005	-0.012	0.9	0.3	0.7	-0.1	0.9
Cl	0.062	0.011	-0.001	0.003	-0.004	0.066	-0.029	0.004	0.003	-0.007	-1.1	-0.2	0.9	-0.1	1.1
Br		0.004	-0.001	0.004	-0.005		0.004	0.009	0.003	0.001		0.9	1.1	-0.1	1.5
I		0.009	0.002	0.004	-0.002		0.000	-0.006	0.003	-0.013		1.0	1.2	-0.1	1.5

[(a)] Errors are computed as: $\mathcal{P}$(basis) - $\mathcal{P}$(ZFK-QZP)

radon as compared with xenon. Although the higher polarizability of radon as compared with that of xenon facilitates bonding with the readily ionizable fluorine, when paired with a less reactive halogen both radon and xenon react less readily. Consequently, HXeI and HRnI have comparable energies of formation. Errors in reaction energies are collected in Table 3.11 and Table 3.12 for MP2 and DFT(PBE0) results, respectively.

Differences in computed energies for formation and decomposition at the MP2/aug-MCP-TZP level are significantly smaller in magnitude than differences for any other MP2/basis combinations. In the case of ΔE_1 for HRnI, the difference at the MP2/aug-MCP-TZP level is 8 kJ·mol^{-1}, while for the same molecule it is 30 and 17 kJ·mol^{-1} at the MP2/MCP-TZP and MP2/ZFK-TZP levels, respectively. The same comparison can be made for ΔE_2. The difference in this property computed at the MP2/aug-MCP-TZP level for HRnCl is 0 kJ·mol^{-1}, whereas for the same molecule it is -77, -20, and 9 kJ·mol^{-1} for MP2/iMCP-SR2, MP2/MCP-TZP, and MP2/aug-MCP-QZP, respectively. In most cases, differences in the energy of formation of the transition state are significantly smaller than the differences in ΔE_1 and ΔE_2. Energies of formation for the transition states of the heavier halides are essentially identical, while ΔE_{TS} for the fluorides are much larger. For the heavier halogens, the activation energy barrier remains approximately constant as size of the rare gas increases, indicating that there is no great difference in stability of HXeBr and HRnBr. For compounds containing fluorine, the radon hydride has a higher energy barrier to the transition state than xenon hydride, indicating possible greater kinetic stability for the radon species.

Atomic charges and natural valence electronic configurations were computed for HRgX molecules using both the natural population analysis as well as the QTAIM method. In all cases, the model of bonding was found to be a positively charged rare gas-hydrogen moiety which interacts electrostatically with a negatively charged halogen. This is consistent with the model of interaction which has been proposed by Chaban et al.[259] in their study of the HArF and HKrF systems. For a given rare gas, as the halogen bonded to it becomes larger, the magnitude of the positive charge assigned to the rare gas decreases slightly. Likewise, the negative charge on

Table 3.11: *Errors in reaction energies (in kJ·mol^{-1}) computed with the MP2 method* [a,b]

	ΔE_1					ΔE_2					ΔE_{TS}				
	ims2	mcp3	acp3	zfk3	acp4	ims2	mcp3	acp3	zfk3	acp4	ims2	mcp3	acp3	zfk3	acp4
HXeX															
F	62	45	-6	10	-18	-60	-35	0	-2	-7	7	23	1	3	-1
Cl	78	43	18	15	-6	-64	-26	-6	-5	2	15	10	-9	-0	-3
Br		33	15	14	-6		-24	-12	-3	-0		-3	-9	0	-5
I		33	11	16	-9		-26	-12	-3	-4		-3	-8	-0	-3
HRnX															
F	73	39	-21	10	-27	-71	-29	15	-2	2	8	24	6	4	3
Cl	91	38	12	16	-12	-77	-20	0	-6	9	12	13	-7	-0	1
Br		29	12	16	-13		-20	-10	-4	6		1	-9	0	-2
I		30	8	17	-16		-23	-9	-4	3		0	-8	-0	0

[a] Δ E$_n$ are defined in Figure3.1 [b] Errors are computed as: $\mathcal{P}$(basis) - $\mathcal{P}$(ZFK-QZP)

Table 3.12: *Errors in reaction energies (in kJ·mol^{-1}) computed with the DFT(PBE0) method* [a,b]

	ΔE_1					ΔE_2					ΔE_{TS}				
	ims2	mcp3	acp3	zfk3	acp4	ims2	mcp3	acp3	zfk3	acp4	ims2	mcp3	acp3	zfk3	acp4
HXeX															
F	31	26	8	2	4	-28	-23	8	-2	-14	6	12	-6	0	-5
Cl	39	36	28	2	22	-35	-25	-15	0	-12	12	7	-6	0	-5
Br		16	12	1	10		-17	-15	-1	-13		-5	-8	0	-7
I		33	11	1	8		-32	-13	0	-12		-4	-6	0	-5
HRnX															
F	51	13	-3	3	-9	-48	-10	-3	-2	-1	6	13	-2	0	1
Cl	56	26	18	2	12	-52	-11	-6	-1	-2	11	10	-2	0	1
Br		6	4	2	0		-8	-7	-1	-3		-2	-5	0	-3
I		6	4	1	-1		-7	-5	0	-4		-1	-3	0	-1

[a] Δ E$_n$ are defined in Figure3.1 [a] Errors are computed as: $\mathcal{P}$(basis) - $\mathcal{P}$(ZFK-QZP)

Table 3.13: *Atomic charges from population analysis at the MP2/aug-MCP-TZP-f level of theory*

	H		Rg		X	
Molecule	NPA	QTAIM	NPA	QTAIM	NPA	QTAIM
HXeF	-0.02	-0.09	0.79	0.84	-0.77	-0.76
HRnF	-0.07	-0.10	0.85	0.88	-0.80	-0.78
HXeCl	0.00	-0.06	0.68	0.71	-0.68	-0.65
HRnCl	-0.05	-0.08	0.74	0.71	-0.69	-0.65
HXeBr	-0.00	-0.06	0.65	0.66	-0.64	-0.61
HRnBr	-0.05	-0.08	0.71	0.68	-0.65	-0.60
HXeI	-0.02	-0.07	0.60	0.59	-0.58	-0.52
HRnI	-0.06	-0.08	0.66	-0.61	-0.59	-0.52

the halogen decreases in magnitude, indicating that the compounds of the heaviest halogens have the greatest covalent bonding character. Comparisons between the NPA and QTAIM charges are shown in Table 3.13. It is worth noticing that the NPA charges on the rare gas atoms are very similar and that the charge on radon is systematically greater (by a constant 0.06 e).

Natural valence electronic configurations computed at the MP2/aug-MCP-TZP level, shown in Table 3.14, explain the origin of the NPA charges: The positive charge on the rare gas results from the transfer of about 0.8 e from the np subshell of the rare gas to the np subshell on the halogen atom, accompanied by additional transfer to virtual (correlating) nd orbitals both on the rare gas and halogen atoms. This effect is very slight for chlorides, but appreciably large for iodides. The nd virtual orbital of the halogen contains only a small portion of the electron density. The $(n-1)d$ orbital of both the rare gas and the halogen contain minimal electron density; even less than the nd orbitals. For this reason, the $(n-1)d$ orbitals are not presented here.

The results of QTAIM analysis both corroborate and expand upon the insights provided by the NPA results. Atomic charges computed at the QTAIM level are consistent with the NPA charges to $\pm$ 0.07 e. The NPA charges indicate that the bonding in HRgX molecules takes the form of a positively charged H-Rg group interacting electrostatically with a negatively charged halogen. This is confirmed by

Table 3.14: *Natural valence electron configurations MP2/aug-MCP-TZP*

Molecule	H	Rg	X
HXeCl	$1s^{0.97}$	$5s^{1.96}5p^{5.19}5d^{0.12}$	$3s^{1.97}3p^{5.55}3d^{0.10}$
HRnCl	$1s^{1.02}$	$6s^{1.97}6p^{5.14}6d^{0.07}$	$3s^{1.96}3p^{5.56}3d^{0.10}$
HXeBr	$1s^{0.97}$	$5s^{1.96}5p^{5.22}5d^{0.12}$	$4s^{1.97}4p^{5.52}4d^{0.06}$
HRnBr	$1s^{1.02}$	$6s^{1.97}6p^{5.17}6d^{0.03}$	$4s^{1.97}4p^{5.53}4d^{0.10}$
HXeI	$1s^{0.99}$	$5s^{1.96}5p^{5.27}5d^{0.12}$	$5s^{1.97}5p^{5.45}5d^{0.08}$
HRnI	$1s^{1.03}$	$6s^{1.97}6p^{5.22}6d^{0.10}$	$5s^{1.97}5p^{5.46}5d^{0.07}$

QTAIM computations of the value of $\nabla^2\rho$, the Laplacian of the electron density, at each bond critical point (BCP). A value of $\nabla^2\rho \geq 0$ at a BCP indicates that the bond is predominantly ionic in character, while a value of $\nabla^2\rho \leq 0$ at a BCP indicates that the bond is covalent[200]. Figure 3.2 shows the values of $\nabla^2\rho$ at each BCP in HRgX molecules, and it is clear that the bond between the hydrogen and the rare gas atom in each case is covalent, and then the entire group forms ionic bond with the halogen atom. Increasing the size of the halogen from chlorine through iodine shows a larger $\nabla^2\rho$ at the BCP for halogens bonded to radon than for halogens bonded to xenon. Fluorine compounds do not follow this trend; HRnF has a $\nabla^2\rho$ at the Rn-F BCP of 0.03 e less than that of HXeF.

It should be noted that while the aug-MCP-TZP and aug-MCP-QZP basis sets treat relativistic effects at a lower order than the ZFK-TZP and ZFK-QZP basis sets: the Cowan-Griffin approximation[260] for the acp basis sets and the third order Douglas-Kroll approximation[261,262] for the ZFK basis sets, despite occasionally producing results for geometry and energies which are disharmonius with values determined with the ZFK-QZP basis set, past comparisons to experiment and all-electron calculations have established that these basis sets perform quite well.[185] The rare gas hydrides studied herein behave as expected for the trends evident in the lighter rare gas fluorides.[147,258] Of notable interest is the energetics of the dissociation pathway transition state, which may shed some light on the question of kinetic stability for these HRgX systems. In accordance with the periodic trends in polarizability and the first ionization energy, it is reasonable to expect that for a given halogen, HRnX

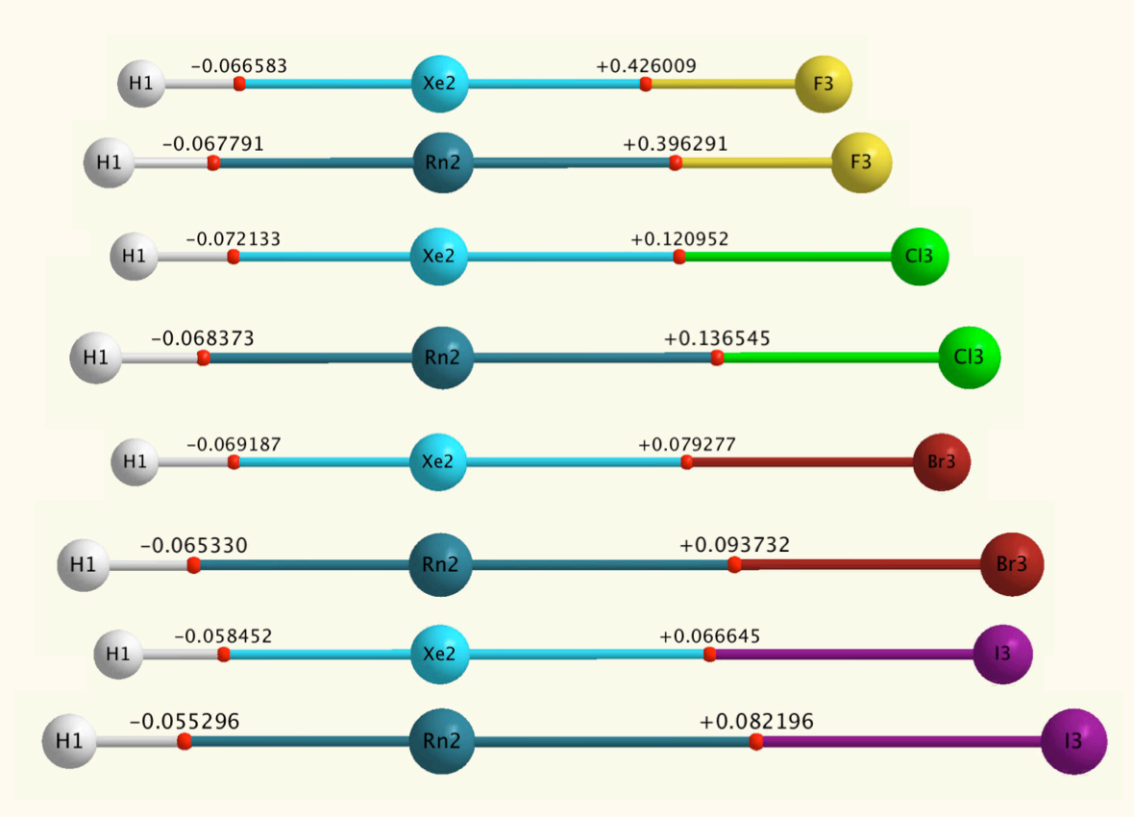

Figure 3.2: *Values of $\nabla^2(\rho)$ at bond critical points, computed at the MP2/aug-MCP-TZP level.*

would bind more strongly than HXeX. This is exemplified in the energies of formation, ΔE_1, of the HRgX compound. For the heavier radon halides, the ΔE_1 is around 40 kJ·mol^{-1} more negative than ΔE_1 for the corresponding xenon halide, indicating greater probable stability for the radon compound, especially when accompanied by slightly higher (by about 10 kJ·mol^{-1}) reaction barriers. The hydrogen rare gas iodides were found to be less stable. The most illustrative example of this is radon iodohydride; as computed at both the DFT(PBE0)/ZFK-QZP and MP2/ZFK-QZP levels of theory, the bond between Rn and I is quite long (about 3.4 Å) and the energy of formation of HRnI is small.

3.4 Conclusions

Geometrical properties and energetics of the formation and dissociation reactions for rare gas halohydrides were computed in order to identify the MCP basis set that combines the greatest computational efficiency with quality of results. The augmented MCP-TZP basis set, aug-MCP-TZP, produced results of the greatest consistency with the reference MP2/ZFK-QZP data, and is recommended for use in studying larger rare gas systems. Paired with the PBE0 functional, the aug-MCP-TZP basis set provides both accuracy in calculated properties and computational efficiency. Comparison of results obtained using the DFT and MP2 methodologies shows that while accuracy of structural parameters and energy results are similar, the DFT implementation in GAMESS-US code is substantially faster than MP2. Computed reaction energies suggest that the most kinetically stable of the molecules I studied is hydrogen radon bromide, which has the largest energy barrier between the bonded HRnBr and the transition state along its decomposition pathway. Radon halides were found to be universally more strongly bound than corresponding xenon halides.

Chapter 4

Small Organic Compounds of Heavy Rare Gases*

4.1 Introduction

The earliest rare gas containing compound to be synthesized was an organic compound[2] and to this day the design and synthesis of novel organic, xenon-containing compounds has been an important part of rare gas chemistry. Several types of organoxenon compounds have already been discovered. Experimentalists have prepared bis(pentafluorophenyl)xenon at 215.15 K[28] and 233.15 K to 213.15 K[72] and confirmed its presence via ^{129}Xe NMR[28]. FXe(C_6H_5), an intermediate in the synthesis of bis(pentafluorophenyl)xenon, has also been characterized with ^{19}F NMR at the same temperature[27]. Several reviews[22,29,126] demonstrate that the organic chemistry of xenon has become a diverse field of study, and many neutral and cationic compounds with carbon-xenon bonds have been synthesized[78]. HXeSH was synthesized in 1998 by Pettersson et al.[38] and shown via infrared (IR) spectroscopy to exist at temperatures up to 100 K. In the same year, Kötting et al.[24] synthesized F_2CC^*Xe in solid argon at 7 K. HXeOH was synthesized at 48 K in 1999 by Pettersson et al.[43] and characterized with IR spectroscopy. In 2008, Tsivion et al.[137] predicted that HXeCCH should be stable below 253.15 K; the compound was subsequently synthesized by Domanskaya et al. at 45 K[141]. Properties of the species CH_3RgF, for all rare

*A version of this chapter was published in *Theor. Chem. Acc.*, **2013**, *132*, 1314.

gases except radon, were computed in 2010 by Liu et al.[154] The isoelectronicity of xenon(II), in the most common oxidation state of xenon, with iodine(III), a common ligand in organic compounds, has lead to the synthesis of many new organoxenon compounds[22]. Alkyl xenon(II) compounds and aryl xenon(II) salts were synthesized by Frohn and Jakobs[18], Turbini et al.[15], Maggiarosa et al.[28], Frohn et al.[23], and Frohn and Theissen[27].

Alongside experimental work, formation reactions for organoxenon(II) compounds have been studied computationally to determine their viability based on the height of potential energy barriers[102]. An earlier computational investigation of organoxenon compounds of high symmetry[83] examined geometrical properties and energetics of the formation of these compounds from perfluoromethyl silanes and rare gas difluorides[27,28]. This chapter discusses results of studies of rare gas-containing organic compounds formed via the following reactions:

$$(CH_3)_3SiA + RgF_2 \longrightarrow (CH_3)_3SiF + ARgF, \qquad \Delta G_1 \tag{4.1}$$

$$(CH_3)_3SiB + ARgF \longrightarrow (CH_3)_3SiF + ARgB, \qquad \Delta G_2 \tag{4.2}$$

where A and B stand for the entire organic ligand, with a carbon atom directly bonded to the Rg atom.

While both synthetic and computational organoxenon chemistry experienced a true renaissance in the last decade[73], organoradon chemistry developed less dynamically. However, the larger atomic radius of radon, a lower first ionization energy, and lower promotion energy than that of xenon[7] hint that radon-containing compounds could be bound even more strongly than corresponding xenon-containing compounds[258]. A plethora of possibly stable molecules is now open to investigation, including radon hydrides[160] and small organic molecules[158]. Due to the short half-life of radon (3.30×10^5 s for ^{222}Rn)[7], it appears advantageous to study potentially stable radon compounds computationally before attempting an experimental investigation, whose scope would necessarily be limited by the rapid decay of the rare gas. For the computations discussed in this chapter, several carbon-containing ligands that could

form compounds with xenon or radon were selected. The organic ligands chosen, -CCH, -CCF, -CH_3, -CF_3, and -CN, were selected for their compact size and, in some cases, because experimentalists have already synthesized compounds containing these ligands and xenon[15,23,27,28].

In this chapter, computed structures, energetics, and bond properties are analyzed for radon-containing analogs of well-studied xenon-containing organic compounds.

4.2 Computational Methods

The basis set used in this study, the model core potential (MCP)[189] method with augmented triple-zeta valence basis set aug-MCP-TZP[191], was chosen due to the computational efficiency which is characteristic of the MCP family of basis sets. The acug-MCP-TZP basis set provides extensive polarization/correlating space: $3p\,2d$ for hydrogens and $3d\,2f$ for all other atoms. With this basis set, optimized geometries, harmonic vibrational frequencies at local minima, and thermodynamic properties were computed using the Møller-Plesset second-order perturbation theory (MP2)[31], with all electrons correlated. The aug-MCP-TZP basis set, along with other MCP basis sets, has been described in detail in Chapter 1. These basis sets are included in the internal libraries of GAMESS-US[249] and may also be found at the Segmented Gaussian Basis Set database[218]. Geometry optimizations were carried out in the symmetries listed in Table 4.1.

Table 4.1: *Symmetry constraints chosen for geometry optimizations*

C_{2v}	C_{3v}	D_{2h}
CNRgF	CF_3RgF	CNRgCN
CCFRgF	CH_3RgF	CCFRgCCF
CCHRgF	CF_3RgCN	CCHRgCCH
CCFRgCN	CF_3RgCCF	
CCHRgCN	CF_3RgCCH	
CCHRgCCF	CH_3RgCN	
	CH_3RgCCF	
	CH_3RgCCH	

In addition to computed structural parameters and reaction energetics, bonding

in these molecules was evaluated through Natural Population Analysis (NPA)[243,244] at each optimized geometry in order to delineate the nature of the chemical bonds by inspecting natural charges and natural bond orbitals (NBOs). The following parameters were changed from the defaults in MacMolPlt when generating all figures of NBOs: number of grid points = 105; grid size = 180; contour value = 0.035. The specific goal of this analysis was to understand the relationship between bonding behaviour in organoxenon compounds and their organoradon analogues, in order to gauge the predictive power of knowledge of xenon compounds in related radon chemistry using, as indicators, the Gibbs free energies for all reactions.

Furthermore, core electron binding energies (CEBE) were computed using the ΔMP2/mix method calibrated by Shim et al.[263]. In that method, all rare gas atoms and any atoms that are not ionized are described by the MCP-dzp[191] basis set, while the ionized atom is described by the cc-pCVTZ basis[208]. This approach offers twofold advantage: the computational efficiency characteristic of the MCP-family of basis sets and localization of the core hole on the ionized target atom, as the MCP method replaces core electrons with a pseudopotential.

All computations were carried out using the GAMESS-US[249] software package running on multi-core Apple MacPro computers and Linux clusters at the University of Alberta. The NBO 5.G program[257] was used in conjunction with GAMESS-US (version May 2008, release R1) for computation of the NBO and NPA properties. The MacMolPlt[264] program was used to generate the figures from NBO results.

4.3 Results and Discussion

In this section, results for the formation of ARgF species will be discussed first, followed by an analysis of the effect of solvent upon this reaction. Next, results for the ARgB formation reaction will be discussed, and the section will conclude with a discussion of computed CEBEs.

4.3.1 ARgF Formation Reaction

The reactions chosen in this study were inspired by the experimental work of Frohn et al.[27,72] who synthesized both symmetrically and asymmetrically substituted organoxenon complexes. Results of calculations for Reaction 4.1 are collected in Table 4.2 and presented graphically in Figure 4.1.

Table 4.2: *Free energy of reaction 4.1, bond lengths between Rg and the adjacent atoms, and NPA atomic charges*

A-Rg-F	ΔG_1/kJ $\cdot$ mol^{-1}	r(C-Rg)/Å	r(Rg-F)/Å	q_C	q_{Rg}	q_F
CNXeF	-116	2.080	2.021	-0.10	1.06	-0.68
CCFXeF	-120	2.053	2.045	-0.50	1.05	-0.71
CCHXeF	-131	2.053	2.051	-0.39	1.04	-0.72
CF_3XeF	-179	2.187	2.072	0.78	0.88	-0.71
CH_3XeF	-202	2.158	2.116	-0.80	0.88	-0.76
CNRnF	-112	2.181	2.098	-0.13	1.12	-0.70
CCFRnF	-114	2.154	2.120	-0.56	1.12	-0.73
CCHRnF	-124	2.155	2.125	-0.45	1.11	-0.74
CF_3RnF	-164	2.278	2.147	0.76	0.94	-0.74
CH_3RnF	-185	2.250	2.184	-0.84	0.95	-0.78

The free energy changes of the reactions that yield the radon-containing organic compounds are nearly 10% smaller than energy changes for their xenon-containing cousins. This mildly decreased stability of the radon products of Reaction 4.1 can be attributed to the increased stability that RnF_2 enjoys over XeF_2[258]. Considering that the smallest value of ΔG_1 is about -100 kJ/mol, this small difference should not be a significant impediment to possible synthesis of these radon-containing compounds with an organic ligand and fluorine.

In all the ARgF compounds, bond lengths and angles within the organic ligands are only minimally affected by the size of the rare gas atom, as can be seen in Tables A3 and A4 in the Appendix to this chapter. Bond lengths between the rare gas and ligand are larger in the case of radon compounds, as expected, due to the larger atomic radius of radon.

The Xe-C bond lengths vary between 2.05 Å and 2.08 Å for the smaller ligands (containing two or three atoms), while the bulkier methyl and perfluoromethyl groups

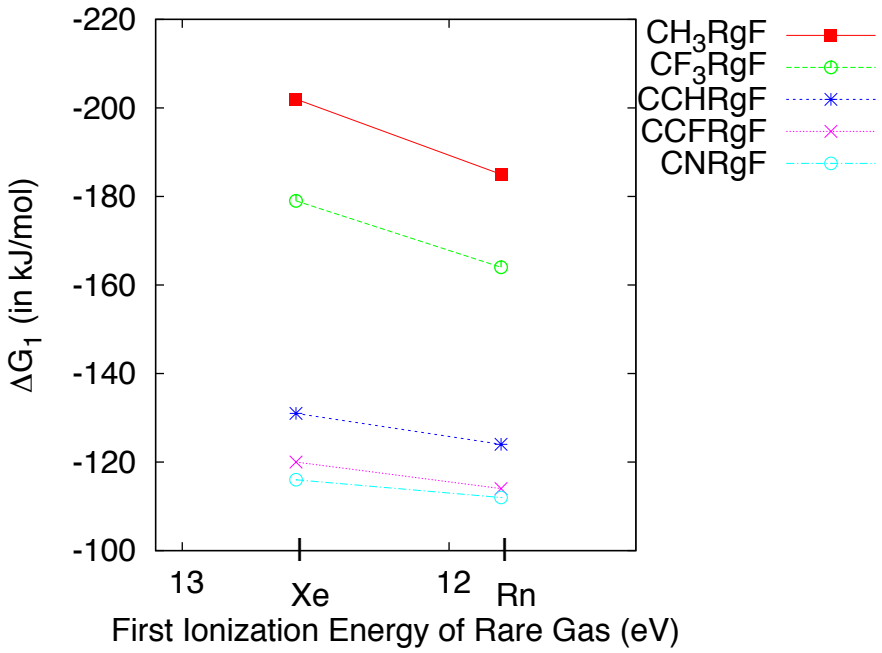

Figure 4.1: *Free energy change in the reaction* $(CH_3)_3SiA + RgF_2 \longrightarrow (CH_3)_3SiF + ARgF$

are almost 0.2 Å further away from xenon. The Rn-C bonds involving methyl or perfluoromethyl ligands are 0.1 Å longer than Rn-C bonds involving the smaller ligands. Inspection of bond radii of products of Reaction 4.1 for the two rare gases reveals that ratios of r(C-Rg) and r(Rg-F) are consistent with the ratios of the atomic radii of the rare gas atoms. The ratio of single-bond radii of xenon to radon may be calculated to be 0.92 using the data of Pyykkö and Atsumi[265–267]. The ratios of r(C-Rg) are about 0.95 for CNRgF, CH_3RgF, and CF_3RgF, and are only slightly larger (0.96) for the two bulkier ligands, indicating that the difference in atomic radii of the rare gases results in a slightly shorter and stronger bonds in cases of larger ligands bonding with radon. The bond lengths r(Rg-F) increase by about 0.08 Å as the ligands become larger, with CH_3RgF possessing the largest r(Rg-F).

The NPA charge on the fluorine remains essentially constant (within 0.03 e) regardless of the nature of the rare gas or the ligand. The charges on the carbon adjacent to the rare gas atom are slightly larger (by 0.03 – 0.06 e) for radon-containing molecules than for xenon-containing ones. In cases where there is a strong negative

charge from one ligand – flouride, for example – a methyl carbon takes on a negative charge as well in order to balance the charges on the molecule. This may be seen by comparing data for CH_3RnF and CF_3RnF in Table 4.2. The NBO results for the CNRgF system illustrate a classic feature of the NBOs – their transferability between "molecules having similar bonding features",[268] wherein molecules composed of atoms within the same period or column bonded to the same ligand will produce topographically similar orbitals. Occurrences of this phenomenon abound in ARgF systems; the most striking examples are the C-N π bond in CNRgF molecules and the Rg-C σ bond in CF_3RgF molecules.

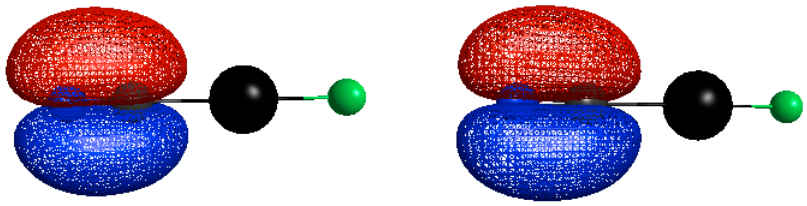

Figure 4.2: *The a_2 π_{CN} NBO Orbitals of CNXeF (left) and CNRnF (right)*

Figure 4.2 shows the a_2 orbital from the NBO analysis of CNRgF, with occupancies of 1.997 and 1.998 for CNXeF and CNRnF, respectively. Figure 4.3 depicts the 4th orbital of CF_3RgF, with occupancies of 1.793 for CF_3XeF and 1.790 for CF_3RnF.

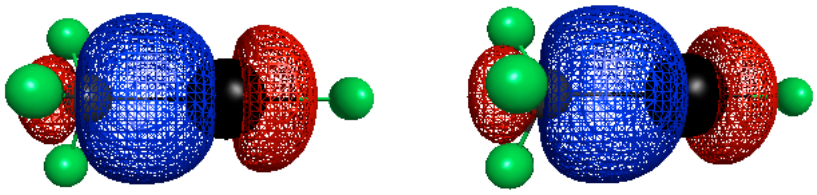

Figure 4.3: *The a_1 σ_{CRg} NBO Orbitals of CF_3XeF (left) and CF_3RnF (right)*

Increasing the size of the rare gas in Reaction 4.1 decreases the magnitude of ΔG_1 more significantly if group A is a methyl or perfluoromethyl than for any other of the

ligands studied. This effect is related to the charge distribution on the ligands: since radon has the highest polarizability among the rare gases and is prone to forming more ionic-like interactions with ligands, bonding in ARgF is moderately weaker for radon than it is for xenon. The methyl and perfluoromethyl ligands contain higher charges than does the cyano ligand, resulting in a Rn-CF_3 or Rn-CH_3 bond that exhibits more ionic character than a Rn-CN bond, which has overall lower charges and consequently greater covalent character.

4.3.2 Dissociation of ARgF in the gas phase and in solvents

In order to examine kinetic stability of the ARgF systems, transition states were located and the free energy change in the first step of this dissociation process was evaluated:

$$\mathrm{ARgF} \quad \stackrel{\Delta G^{\ddagger}}{\longrightarrow} \quad [\mathrm{A}\cdots\mathrm{Rg}\cdots\mathrm{F}]^{\ddagger} \quad \longrightarrow \quad \mathrm{AF} + \mathrm{Rg} \tag{4.3}$$

Transition state structures for CNRgF, CCFRgF, and CCHRgF were easily located and confirmed by harmonic vibrational analysis. In all six cases, the reactive vibrational mode (identified by the single imaginary frequency resulting from the hessian calculation) is a combined wagging motion of both the Rg-F and Rg-C_2 bonds that decreases the distance between the two groups. The nature of this transition state structure was analyzed by following the intrinsic reaction coordinate (IRC) in both the forward and backward directions, starting from the transition state. (The IRC computations employed the default values in GAMESS-US for all adjustable parameters.) Results of the IRC computations are shown in Figures 4.4 and 4.5 for CNXeF and CNRnF, respectively. The position of zero on the reaction coordinate axis corresponds to the transition state whose geometry is given in Table 4.3. The reaction coordinate displays the path distance parameter, with the values for the backward reaction multiplied by -1.

Lundell et al.[84] computed properties for related transition states using the MP2 method with an averaged relativistic core potential AREP and the 6-311G(2d,2p) basis set, and found a similar value of the H-Xe-C angle for the HXeCCF transition

Table 4.3: *Properties of the ARgF transition state*

Molecule	r(A-Rg)/Å	r(Rg-F)/Å	$\Theta_{A\,Rg\,F}/^\circ$	$\Delta G^\ddagger$/kJ·mol^{-1}	$\nu^\ddagger$/cm^{-1}
CNXeF	1.938	2.295	98.7	221	$123\,i$
CNRnF	2.035	2.348	93.9	229	$111\,i$
CCFXeF	1.930	2.347	99.3	198	$84.5\,i$
CCFRnF	2.026	2.389	94.0	209	$75.5\,i$
CCHXeF	1.932	2.341	98.8	191	$88.0\,i$
CCHRnF	2.029	2.385	93.4	203	$81.4\,i$

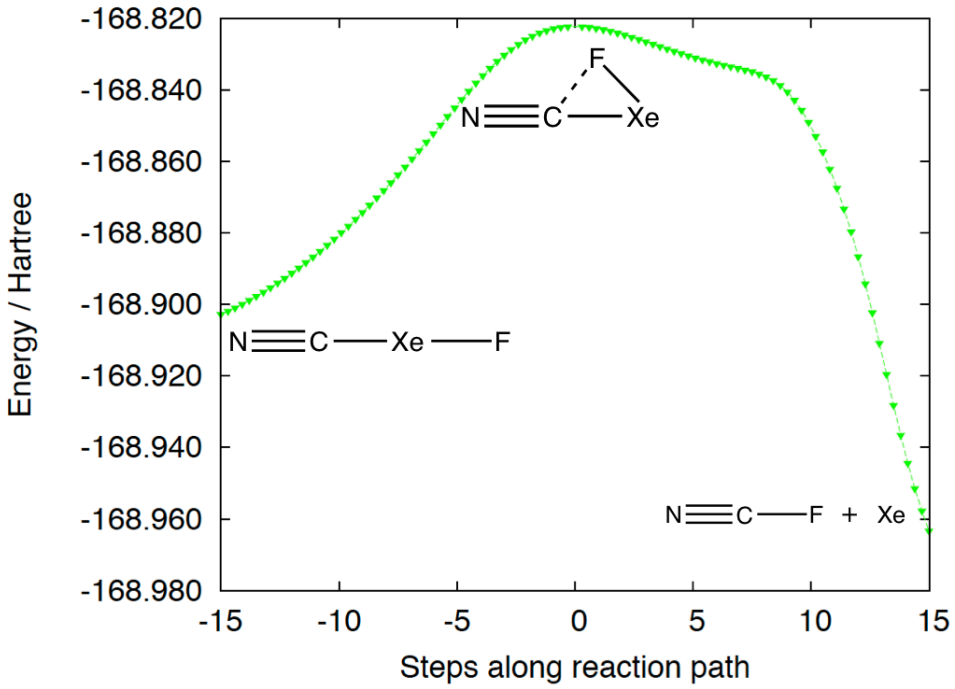

Figure 4.4: *Energy profile for decomposition of CNXeF along the IRC*

state as were found in the present computation for the F-Xe-C angle in the FXeCCF transition state. While the AREP/6-311G(2d,2p) basis set is not ideal for heavy rare gas-containing systems (discussed in detail in Chapter 2), these results do qualitatively support the assertion that the transition states and dissociation mechanisms of these ARgF compounds are closely related.

In the mechanism observed from these computations, the fluorine and the primary carbon belonging to the A group both swing inwards, decreasing the angle C-Rg-F

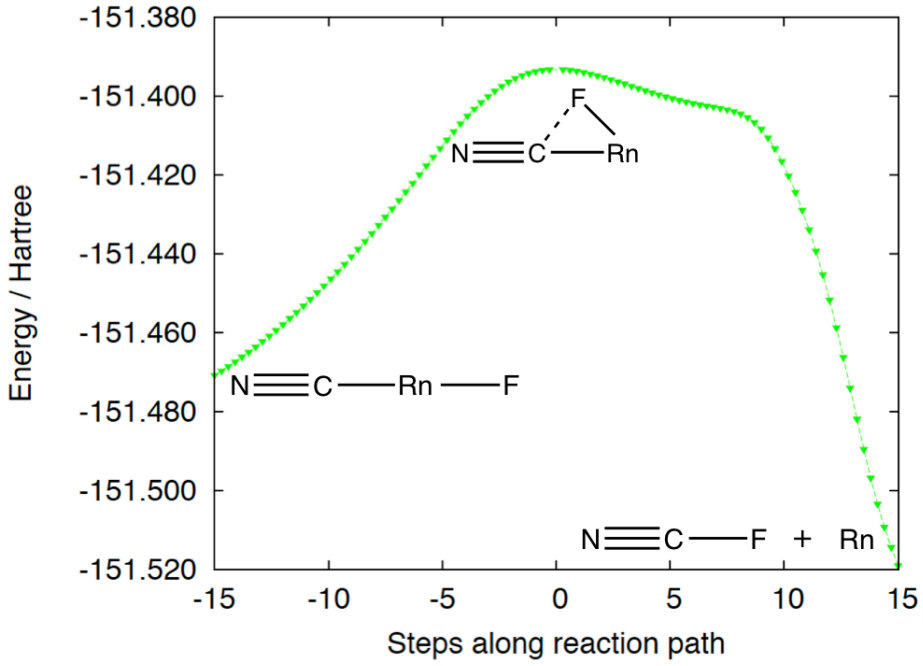

Figure 4.5: *Energy profile for decomposition of CNRnF along the IRC*

from 180° to between 93° and 99°. The fluorine subsequently attaches to the back of the primary carbon via an S_{N1}-like motion and the resulting organic molecule dissociates completely from the rare gas. In CNXeF, the Xe-F bond has shortened by 0.3 Å from its length at the transition state, the Xe-C bond has lengthened by 0.05 Å, while the C-Xe-F angle has decreased from 98.7° to 62.7° as the fluorine swings around the xenon to attach to the carbon. The same effect is exhibited by CNRnF: the Rn-F bond decreases by 0.2 Å as the Rn-C bond increases by 0.06 Å, with the C-Rn-F angle closing to 57.3° from its value of 98.3° at the transition state.

The transition states of CF_3RgF and CH_3RgF are more elusive. In their work on the molecules CF_3XeF and CF_3XeCF_3, Semenov and Sigolaev presented coordinates for similar transition states that correspond to the following decomposition reactions[102]:

$$CF_3XeF \longrightarrow CF_4 + Xe \tag{4.4}$$

$$CF_3XeCF_3 \longrightarrow C_2F_6 + Xe \tag{4.5}$$

However, examination of the transition state geometries and the associated reactive modes shows that these transition states do not lead to the decomposition products described above. The transition state for CF_3XeF identified in the present computations does contain the requisite one imaginary frequency characteristic of a saddle point on the potential energy surface, but upon visualization of this reactive mode it became apparent that motion along this mode would not lead to dissociation into the products predicted by Sigolaev and Semenov. Instead, the reactive mode appears to be a rotation. The IRC (in C_1 symmetry) from the transition state of CF_3XeF previously identified and the resulting energy profiles are merged and shown in Figure 4.6. As the computed reaction path demonstrates, the transition states previously located for CF_3XeF by Semenov and Sigolaev and the transition states found in the present work do not correspond to dissociation along the same pathway as the linear ARgF compounds. Instead, CF_3XeF rotates from the transition state geometry into an isomer of CF_3XeF with C_s symmetry and stability lower than that of the C_{3v} molecule. For CF_3XeF, the Gibbs energy difference between the staggered minimum and eclipsed transition state is about 24 kJ·mol^{-1}, while for CF_3RnF the barrier to rotation is 22 kJ·mol^{-1}. The structural parameters r(Rn-F) and $\Theta_{C\,Rn\,F}$ listed in Table 4.3 essentially do not change during the rotation, while r(Rn-C) varies by only 0.02 Å, making the two structures virtually indistinguishable. In comparison with the C_{3v} parent molecules, the staggered C_s isomer of CF_3XeF has Gibbs energy 123 kJ $\cdot$ mol^{-1} higher (134 kJ $\cdot$ mol^{-1} for the Rn system). The bond lengths in the C_s isomer of the xenon compound (values in parentheses are for the Rn congener) are r(Rg-F) = 2.354 Å (2.379 Å), r(Rg-C) = 2.224 Å (2.291 Å), and r(C-F) = 1.279 Å and 1.314 Å (1.285 Å and 1.319 Å). The angle $\Theta_{C\,Rn\,F}$ equals only 65.6° (64.7°).

Quite different results were found for CH_3XeF and CH_3RnF. It was expected that the CH_3RgF transition states would follow a decomposition pathway similar to that seen in the linear ARgF transition states. Following the IRC in the backward direction agrees with this expectation, with the C_s structure at the transition state returning to the C_{3v} structure of the reactant. However, the tracking of the IRC in

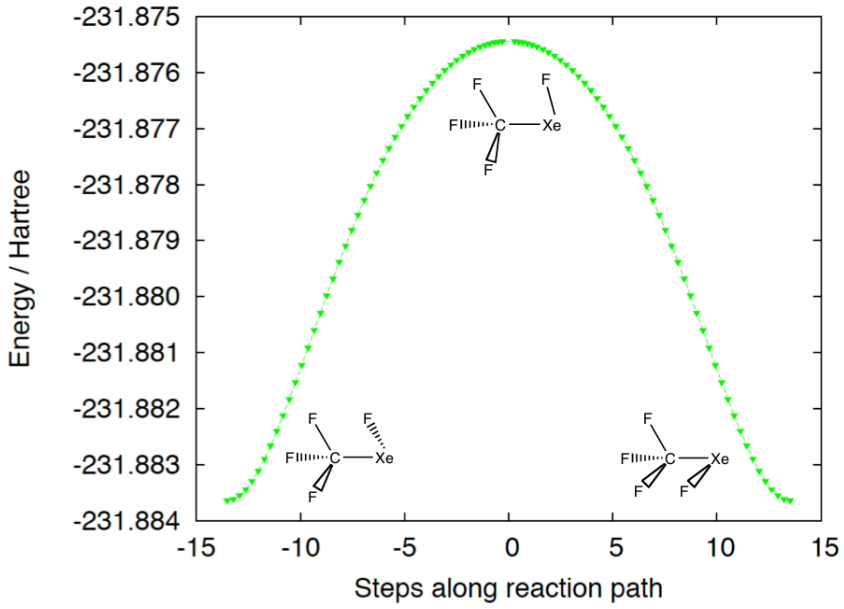

Figure 4.6: *Energy profile along the IRC for CF_3XeF*

the forward direction showed different products:

$$CH_3RgF \longrightarrow CH_2Rg + HF \tag{4.6}$$

The resulting reaction paths for CH_3XeF and CH_3RnF are quite similar and are shown in Figures 4.7 and 4.8, respectively. The structure of the rare-gas containing product of Reaction (4.6) in its singlet ground state was optimized at the MP2/acp3 level of theory. For CH_2Rn, the structural parameters are r(Rn-C) = 2.424 Å, r(C-H) = 1.102 Å, $\Theta_{H\,C\,H} = 102.6°$, and $\Theta_{C\,Rn\,H} = 93.1°$.

The structure of CH_2Xe is nearly identical: r(Xe-C) = 2.440 Å, r(C-H) = 1.102 Å, $\Theta_{H\,C\,H} = 102.5°$, and $\Theta_{C\,Xe\,H} = 91.5°$. The value of the angle C-Rg-H indicates that the plane of CH_2 is nearly perpendicular to the Rg-C bond. For the Xe case, the Gibbs energies of the products of Reaction 4.4 are 77 kJ·mol^{-1} lower than the energy at the transition state and 53 kJ·mol^{-1} higher that the Gibbs energy of the reactant CH_3XeF; for the Rn case, the corresponding values are 42 kJ·mol^{-1} and 95 kJ·mol^{-1}. The NBO analysis reveals that the interaction between the rare gas and the carbon in this molecule takes the form of a σ-bond, as shown in Figure 4.9.

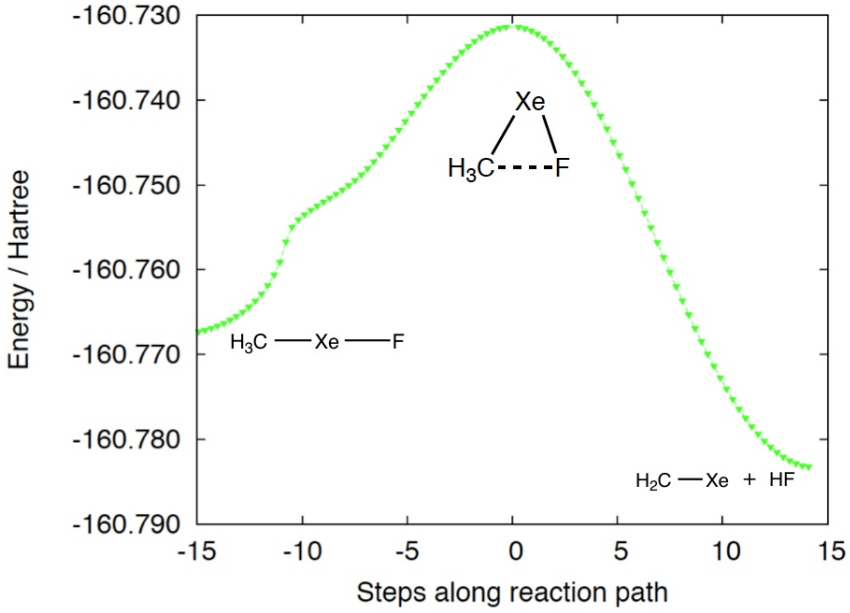

Figure 4.7: *Energy profile along the IRC for CH_3XeF*

Table 4.4: *Properties of the CX_3RgF transition state*

Molecule	r(C-Rg)/ Å	r(Rg-F) / Å	$\Theta_{C\,Rg\,F}$	$\Delta G^{\ddagger}$ / kJ·mol^{-1}	$\nu^{\ddagger}$ /cm^{-1}
CH_3XeF	2.105	2.414	106	130	176 i
CH_3RnF	2.189	2.446	102	137	169 i
CF_3XeF	2.330	2.220	76.6	146	53.4 i
CF_3RnF	2.366	2.290	74.9	156	50.4 i

The experiments that led to the synthesis of organoxenon compounds were carried out in solvents[27,72]. The presence of solvent may affect the barrier to decomposition of the products of Reaction 4.1 and change kinetic stability of the products. In order to establish the effect of solvent, the free energy change at the transition state in the first step of the dissociation process in Reaction 4.3 was studied. The polarizable continuum model (PCM)[269–271] was employed to estimate solvent effects on the dissociation processes that involved the ligands -CN, -CCF, and -CCH, using two solvents: dichloromethane (CH_2Cl_2) and acetonitrile (CH_3CN). The results, displayed in Figure 4.10, indicate that while solvent reduces the height of the reaction barrier (with acetonitrile being more effective than dichloromethane), the barrier to dissociation

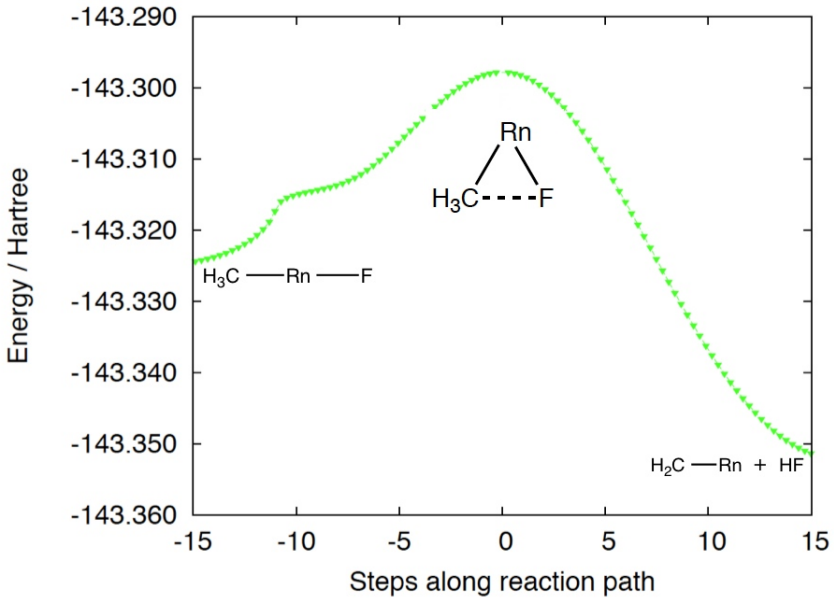

Figure 4.8: *Energy profile along the IRC for CH_3RnF*

remains higher for the radon-containing compounds than for the xenon-containing compounds.

4.3.3 ARgB Formation Reaction

The data for the products of Reaction 4.2 are collected in Table 4.5 and the free energy change in that reaction is displayed in Figure 4.11. The values of ΔG_2(Xe) display a wider range of energies than ΔG_2(Rn), as do ΔG_1, a consequence of the

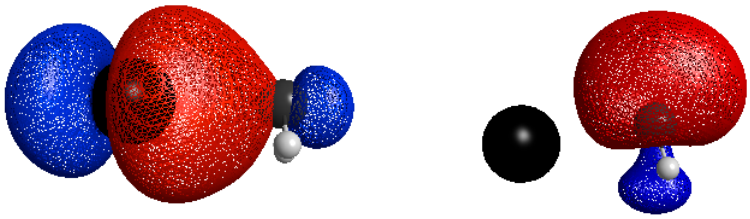

Figure 4.9: *Selected NBOs of CH_2Rn. Left = bonding σ orbital; right = carbon lone pair*

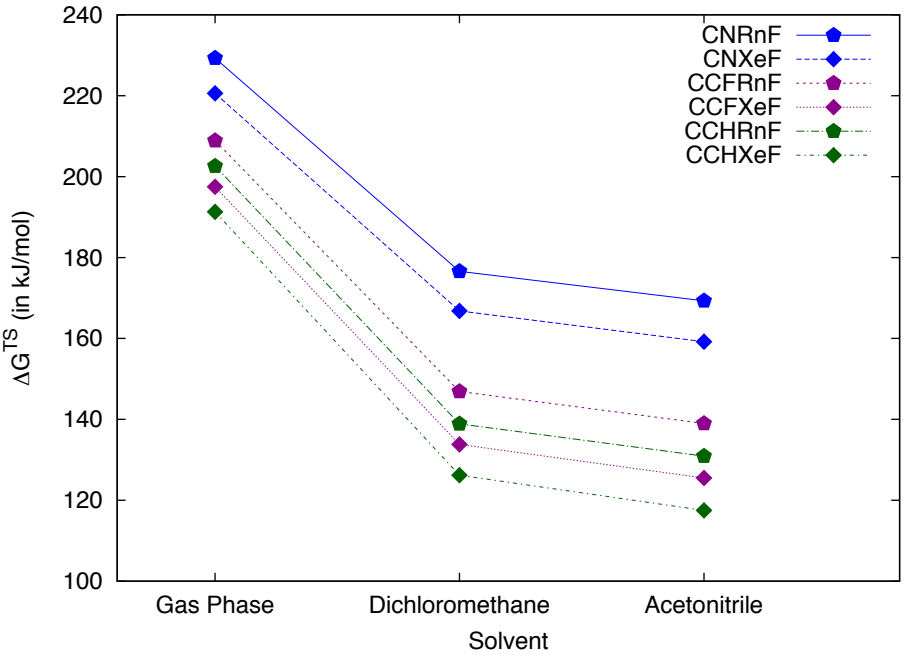

Figure 4.10: $\Delta G^{\ddagger}$ *for the dissociation reaction in various solvents*

fact that RnF_2 has a larger ΔG of formation than XeF_2. Compounds with any pairing of linear ligands display larger ΔG_2 for ARnB than for AXeB. The opposite is true for compounds containing one or more nonlinear ligands: if A, B, or both are the methyl or perfluoromethyl ligand, then ΔG_2 of ARnB is lesser than the ΔG_2 of AXeB. Depending on the energy of the ligand to be added to ARgF as B, ΔG_2 may decrease in magnitude by up to 150 kJ·mol^{-1} for ARnB, and by up to 170 kJ·mol^{-1} for AXeB compounds.

The bond lengths for a compound increase by a maximum of 0.1 Å when radon replaces xenon. The asymmetrically substituted compounds containing a larger group as ligand A and a smaller group as ligand B show a slight shortening of the bond Rg-A as compared to the symmetric compound ARgA. On the other hand, the bond length Rg-B in these compounds increases appreciably in comparison to its value in BRgB.

Natural Population Analysis (NPA) for the symmetric products of Reaction (2) shows symmetric negative charge distributions at the poles of the molecule, with the

Table 4.5: *Free energy of Reaction 4.2, bond lengths between Rg and the adjacent atoms, and NPA atomic charges*

A-Rg-B	ΔG_2/kJ · mol^{-1}	r(C-Rg)/Å	r(Rg-B)/Å	q_{A}	q_{Rg}	q_{B}
CNXeCN	-68	2.192	2.192	-0.05	0.84	-0.05
CCFXeCN	-69	2.135	2.238	-0.50	0.90	-0.17
CCFXeCCF	-53	2.178	2.178	-0.52	0.88	-0.52
CCHXeCN	-77	2.133	2.252	-0.43	0.87	-0.09
CCHXeCCF	-61	2.176	2.193	-0.44	0.88	-0.53
CCHXeCCH	-55	2.190	2.190	-0.36	0.78	-0.36
CF_3XeCN	-124	2.274	2.327	0.76	0.75	-0.18
CF_3XeCCF	-105	2.277	2.249	0.73	0.76	0.34
CF_3XeCCH	-100	2.287	2.251	0.72	0.75	-0.22
CH_3XeCN	-146	2.207	2.382	-0.82	0.79	-0.22
CH_3XeCCF	-114	2.239	2.318	-0.85	0.78	0.31
CH_3XeCCH	-107	2.251	2.318	-0.86	0.76	-0.48
CNRnCN	-71	2.268	2.268	-0.20	0.98	-0.20
CCFRnCN	-72	2.222	2.305	-0.61	0.99	-0.19
CCFRnCCF	-58	2.257	2.257	-0.61	0.99	-0.61
CCHRnCN	-79	2.224	2.322	-0.48	0.96	-0.20
CCHRnCCF	-65	2.258	2.269	-0.49	0.98	-0.63
CCHRnCCH	-60	2.269	2.269	-0.50	0.95	-0.50
CF_3RnCN	-116	2.334	2.371	0.74	0.82	-0.21
CF_3RnCCF	-100	2.350	2.316	0.71	0.84	0.37
CF_3RnCCH	-95	2.359	2.318	0.70	0.83	-0.23
CH_3RnCN	-136	2.289	2.436	-0.87	0.86	-0.24
CH_3RNCF	-108	2.316	2.378	-0.90	0.86	0.33
CH_3RNCCH	-100	2.327	2.379	-0.90	0.84	-0.51

rare gas carrying a positive charge of approximately one. Symmetrical compounds containing radon have slightly larger charges on the ligands than their xenon counterparts, but the overall bonding remains the same, as the positive charge on radon is also slightly higher than that on xenon. In all cases except CF_3RgB, the carbon adjacent to the rare gas bears a negative charge between -0.3e and -0.5e. In the case of CF_3RgB, this carbon takes on a large positive charge as a consequence of the three fluorines to which it is bonded and which carry a cumulative charge of about -0.75e. Charges on individual atoms within a ligand remain constant regardless of the rare gas. All ARnB systems studied herein display the same pattern of charge distribu-

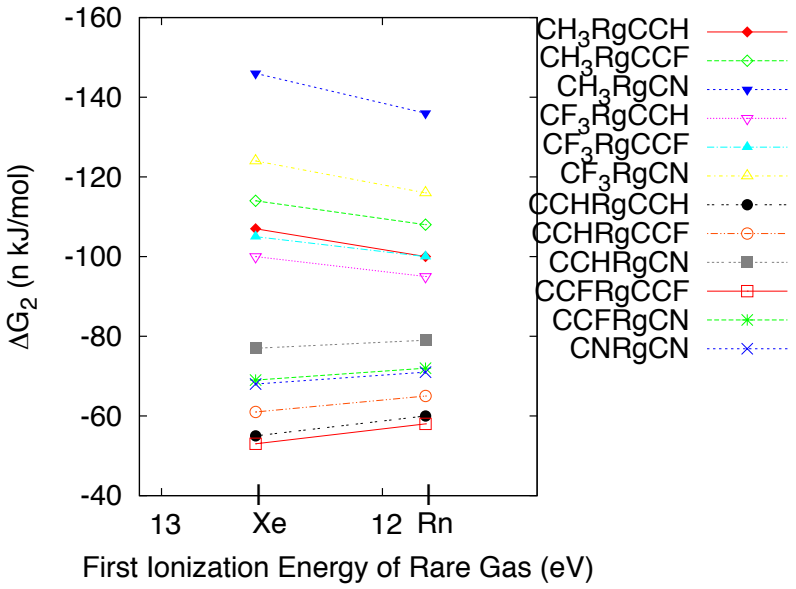

Figure 4.11: *Free energy change in the reaction* $(CH_3)_3SiB+ARgF \longrightarrow (CH_3)_3SiF+ARgB$

tions as the corresponding AXeB systems, indicating that any ARnB molecule related to AXeB which has already been synthesized is an ideal candidate for experimental study.

When the product of Reaction 4.2 belongs to the subset CF_3RgB or CH_3RgB, the reaction is more endergonic if the rare gas it contains is xenon rather than radon. All other products of Reaction 4.2 are more endergonic than the corresponding ARgF product of Reaction 4.1. However, an alternative reaction pathway shows a more encouraging result for organoradon chemistry. If the products of Reaction 4.1 undergo the following reaction:

$$(CH_3)_3SiA + FRgB \quad \rightarrow \quad (CH_3)_3SiF + ARgB, \qquad \Delta G_3 \tag{4.7}$$

then, as shown in Figure 4.12, the change in Gibbs energy for the reaction yielding ARnB is always more negative than for the analogous AXeB. In such cases, organoradon compounds are expected to react more spontaneously than similar organoxenon compounds.

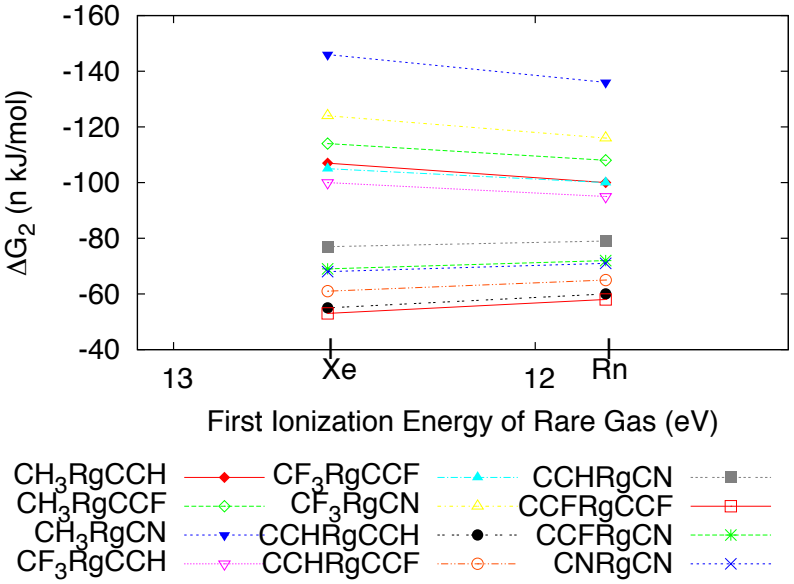

Figure 4.12: ΔG_3 *for Reaction 4.5:* $(CH_3)_3SiA + FRgB \rightarrow (CH_3)_3SiF + ARgB$

4.3.4 Core Electron Binding Energies

CEBEs were calculated using the method described in the Computational Methods section of this Chapter in order to corroborate the results of natural population analysis. CEBEs offer a particularly useful way to study bonding as they have been determined experimentally[11,272] for several xenon fluorides, thereby providing a basis for evaluating the accuracy of our own results. Results for simple xenon and radon fluorides are shown in Tables 4.6 and 4.7 and compared with experimental data when available. It may be seen that the agreement between experimental and computed values of the F 1s CEBEs is satisfactory.

Table 4.6: *F(1s) core electron binding energies (in eV) in xenon fluorides*

	CEBE		
Molecule	experiment	ΔMP2/mix	q(F)[c]
XeF_6	693.33[a]	693.57	-0.50
XeF_4	692.11[a]; 692.52[b]	692.75	-0.54
XeF_2	691.23[a]; 691.4[b]	691.62	-0.58
HXeF	N/A	688.62	-0.77

[a]Ref[11]. [b]Ref[272]. [c]q(F) computed as NPA charge at the MP2/acp3 level

Table 4.7: *F(1s) core electron binding energies (in eV) in radon fluorides*

Molecule	ΔMP2/mix	q(F)[a]
RnF_6	693.47	-0.56
RnF_4	692.43	-0.59
RnF_2	691.17	-0.62
HRnF	688.54	-0.79

[a] q(F) computed as NPA charge at the MP2/acp3 level

The ΔMP2/mix values of CEBEs were computed for all the light atoms in the molecules studied herein and extensive tables of CEBEs may be found in the Appendix to this Chapter. In general, as the size of the rare gas increases, the CEBE of another atom in the same molecules decreases by between 0.1 eV to 1.5 eV. This can be seen for the majority of molecules containing two ionizable atoms, and correlates with the larger NPA charges found on Rn-containing molecules: it is energetically easier to ionize a core electron from an atom with a larger negative charge atom than from a similar atom carrying a lesser negative charge.

4.4 Conclusion

Formation of compounds of the type ARgB from perfluorinated methyl silane and xenon difluoride precursors has been experimentally demonstrated to be a viable method of producing disubstituted organic xenon compounds. The chemical similarity between radon and xenon suggests this reaction as a possible route for synthesizing novel organoradon compounds. The present study shows that both radon and xenon compounds of this type are stable. The radon compounds may prove slightly more difficult to synthesize due to the higher stability of one of the precursors, RnF_2. This results in a slightly smaller Gibbs free energy change for the formation of radon-containing ARgB. The bonding in the two families of compounds is similar, with the majority of the positive charge localized on the rare gas and any hydrogens, with the exception of the carbon in perfluoromethyl groups which carries a positive charge as well. Computed core electron binding energies for the light atoms are usually slightly higher for a xenon compound than for an analogous radon compound.

Chapter 5

Chemistry of Organic Compounds Containing Heavy Rare Gases

5.1 Introduction

Organic xenon chemistry has been a field of interest to many chemists since the early days of xenon chemistry. CF_3XeCF_3 was synthesized in 1979 by Turbini et al.[15] and characterized by infrared (IR) spectroscopy, but subsequent attempts to synthesize this molecule have been frustrated.[273] The stability of the CF_3XeCF_3 species was confirmed computationally by Sigolaev and Semenov[102], but no recent attempts to synthesize this compound have been made. Due to the recently elucidated link between radon chemistry and xenon chemistry, it is probable that stable radon analogs of known, organoxenon compounds exist. The lifetime and stability of these compounds would necessarily be limited by the 3.8 day half-life of radon[7], making computational methods the ideal starting point for investigations into the structure and properties of these compounds. With a rich variety of organoxenon compounds already being synthesized, the natural next step in organic rare gas chemistry is the exploration of related organoradon compounds. These organic, radon-containing small molecules have yet to be synthesized experimentally, but recent computational studies have demonstrated that some of these molecules should be stable.[158,258] While Malli predicted the existence of a radon-carbonyl bond a decade ago,[86] it is only very recently that radon chemistry has become an area of active interest and study.

In this work, I have computed structural parameters and vibrational spectra for molecules of the type CX_3RgCX_3, where X=H,F and Rg=Xe,Rn with two different computational methods. In order to better understand the properties of these molecules, I have computed atomic charges, bond critical points, bond paths, and electron densities via the Quantum Theory of Atoms in Molecules (QTAIM)[199] method.

5.2 Computational Methods

The CX_3RgCX_3 compounds are studied in the context of the following reactions, which were previously used to study related compounds:[83,274]

$$(CH_3)_3SiA + RgF_2 \longrightarrow (CH_3)_3SiF + ARgF, \qquad \Delta G_1 \tag{5.1}$$

$$(CH_3)_3SiB + ARgF \longrightarrow (CH_3)_3SiF + ARgB, \qquad \Delta G_2 \tag{5.2}$$

Optimized geometries were computed with a Model Core Potential (MCP) basis set, chosen due to its computational efficiency and inclusion of relativistic effects, which are significant for molecules containing heavy atoms. MCP basis sets work with small-core pseudopotentials which are parametrized to retain the nodal structure of the core orbitals. In addition, MCP basis sets contain a specifically designed set of polarization and correlating functions which further improve the quality of results. The improved Model Core Potentials series of basis sets makes use of the L-shell contraction, in which the ns and np basis functions share common exponents, and a second-order scalar relativistic correction. This results in expediency of integrations and an overall decrease in computational cost by a half as compared to similar basis sets which do not use the L-shell structure.[83] The composition of the iMCP-SR2 basis set, in [S/P/D/F] format, where each integer indicates the number of primitives composing each contracted basis function,: for hydrogen, [311/11/1]; for carbon and fluorine, [311/311/2/1]; for xenon, [511/511/62/1] and for radon, [611/611/62/1]. The optimized structure of CH_3RnCH_3 is shown in Figure 5.1. Geometry optimizations and harmonic vibrational frequencies were computed with two methods: the Møller-Plesset second order (MP2) perturbation theory and the ωB97 functional, both in

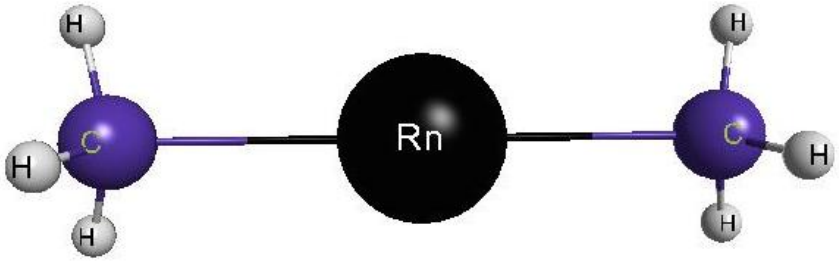

Figure 5.1: *Structure of CH_3RnCH_3*

the GAMESS-US[249] program suite. The MP2 method has already been described in detail in section 2 of Chapter 1, so an introduction of the ωB97 functional as it pertains to this Chapter is warranted here. The ωB97 functional is a newer functional, created in 2008 by Chai and Head-Gordon as an improved long-range corrected hybrid functional.[275] As a hybrid functionl, ωB97 treats exchange in two different ways: for long-range exchange, it uses the HF exchange term. For short-range exchange, it uses the generalized gradient approximation. This approximation states that because the electron density is not homogenous, both information about the density and the gradient of the density should be included at every grid point.[276] In their original paper introducing the ωB97 functional, Chai and Head-Gordon recommend their functional for computations involving thermochemistry, equilibrium geometries, dissociation, charge-transfer systems, and kinetics. While they caution that there are a few situations where the functional does not perform well, none of these are applicable to the goals of the current Chapter.[275]

In order to verify that computed geometries were indeed local minima on the potential energy surface, hessians were computed and the harmonic vibrational frequencies of CX_3RgCX_3 compounds analyzed. Local modifications to the GAMESS-US code[277] were used to generate extended wavefunction (".wfx" extension) files for QTAIM computations in the AIMAll program suite.[250] The QTAIM method, which was described briefly in Chapter 1, was applied in order to obtain information about the bonding, charge distribution, and electron density in CX_3RgCX_3 molecules. QTAIM properties were computed using the AIMQB program and the results were

analyzed in the AIMStudio environment. The compactness of the iMCP-SR2 basis set is an advantage in QTAIM computations, as basis sets with extremely diffuse functions can often produce additional critical points in the QTAIM computations which arise solely out of the overlap of the diffuse functions in empty regions of space within a molecule, and do not correspond to any nuclei. The iMCP-SR2 basis set does not produce these delusive critical points. All computations were carried out on Linux clusters and Apple Macintosh computers at the University of Alberta.

5.3 Results and Discussion

Results of geometry optimization for CX_3RgCX_3 molecules will be discussed first, with an analysis of the harmonic vibrational normal modes to follow. The Results section will conclude with a discussion of the results of QTAIM computations.

Structural parameters for CX_3RgCX_3 molecules optimized at the MP2/iMCP-SR2 level of theory are given in Table 5.1 and demonstrate several features which are characteristic of radon-containing molecules. First, bond lengths r(C-Rg) increase by up to 0.1 Å when radon is substituted for xenon. This is a typical relationship between radon- and xenon-containing molecules which has been seen in previous studies.[274] Second, r(H-C) and r(F-C) are unaffected by the substitution of radon for xenon. The irrelevance of the nature of the rare gas atom to the bond lengths within an organic ligand to which it is bonded is another characteristic feature of organic rare gas compounds which has been demonstrated in previous studies on related molecules. Finally, with the exception of angles in CH_3RgCH_3, which increase minimally by 0.1° when radon is substituted for xenon, angles in CX_3RgCX_3 molecules both within the ligand and between the ligand and the rare gas are unaffected by an increase in size of the rare gas.

Substitution of the more electronegative CF_3 group for both of the CH_3 groups in CX_3RnCX_3 at D_{3h} symmetry minimally contracts the r(C-Rn) bond length, hinting that the presence of the fluorines in the CF_3 group makes for a stronger bond. This will be discussed in more detail with the results of QTAIM analysis.

Structural data from MP2 computations will be discussed first, with DFT results to follow. It is also relevant to note that not all CX_3RgCX_3 molecules have a local minimum on their potential energy surface in equivalent symmetries. The highest order of point group possible for CX_3RgCX_3 molecules (when X=CF_3 or CH_3) is D_{3h}, and this is indeed the symmetry of the minimum-energy structure of both CH_3XeCH_3 and CH_3RnCH_3. CH_3XeCH_3 has a local minimum of D_{3d} symmetry that is 0.26 kJ·mol^{-1} higher in energy than the D_{3h} minimum: an energy barrier low enough that interconversion between the two structural isomers would occur at room conditions. For CH_3RnCH_3, however, there is no local minimum of D_{3d} symmetry.

Although this structural isomer does not situate the hydrogens at maximum distances from each other, this is not a problem when the ligands are small methyl groups. When a perfluoromethyl group is substituted for one or both of the methyl groups, however, the CF_3RgCH_3 molecule becomes sterically constrained in the eclipsed conformation and a staggered geometry analogous to D_{3d} is the optimal geometry for the molecule. Two local minima exist on the potential energy surfaces of CF_3RnCF_3 and CF_3XeCF_3: the lowest-energy of these being the D_{3d} structure, with a secondary local minimum in D_{3h} symmetry that is $1.06{\cdot}10^{-3}$ kJ·mol^{-1} higher in energy than the D_{3d} structure in the case of CF_3RnCF_3. As the two structures have essentially identical values of all tabulated structural parameters (given in Table 5.1), it appears from the perturbation theory computations that the actual configuration of CF_3RnCF_3 would exist as a nearly barrierless set of structural isomers. In the case of CF_3XeCF_3, the energy barrier to conversion between the lower-energy D_{3d} structure and the D_{3h} structure is higher: $7.11{\cdot}10^{-3}$ kJ·mol^{-1} , but still low enough to be achievable from the thermal energy available at room conditions.

A slightly different picture emerges from the ωB97/iMCP-SR2 level computations. With this method, there are local minima at both the D_{3h} and D_{3d} symmetries for every CX_3RgCX_3 species. As shown in Table 5.2, these structures have identical geometrical parameters. Angles computed at the ωB97/iMCP-SR2 level of theory are generally shorter than corresponding angles computed at the MP2/iMCP-SR2 level of theory; notable exceptions are the $\Theta_{H\,C_2\,H}$ in CH_3RnCH_3 which is 4 degrees

Table 5.1: *Structure of CX_3RgCX_3 computed at the MP2/iMCP-SR2 level of theory*[a]

CF_3XeCF_3 D_{3h}	r(F-C)	r(C-Xe)	$\Theta_{F\,C\,Xe}$	$\Theta_{F\,C\,F}$				
	1.3285	2.4566	110.31	108.62				
CF_3RnCF_3 D_{3h}	r(F-C)	r(Rn-C)	$\Theta_{F\,C\,Rn}$	$\Theta_{F\,C\,F}$				
	1.3317	2.5348	110.74	108.17				
CF_3XeCF_3 D_{3d}	r(F-C)	r(C-Xe)	∠(F-C-Xe)	$\Theta_{F\,C\,F}$				
	1.3285	2.4568	110.31	108.62				
CF_3RnCF_3 D_{3d}	r(F-C)	r(Rn-C)	$\Theta_{F\,C\,Rn}$	$\Theta_{F\,C\,F}$				
	1.3318	2.5349	110.74	108.17				
CH_3XeCF_3[b]	r(H-C_1)	r(C_1-Xe)	r(C_2-F)	r(C_2-Xe)	$\Theta_{H\,C_1\,Xe}$	$\Theta_{F_1\,C_2\,Xe}$	$\Theta_{F\,C_2\,F}$	$\Theta_{H\,C_2\,H}$
	1.0757	2.3456	1.3384	2.4173	106.08	111.50	107.37	112.64
CH_3RnCF_3[b]	r(H-C_1)	r(C_1-Rn)	r(C_2-F)	r(C_2-Rn)	$\Theta_{H\,C_1\,Rn}$	$\Theta_{F_1\,C_2\,Rn}$	$\Theta_{F\,C_2\,F}$	$\Theta_{H\,C_2\,H}$
	1.075	2.4502	1.3402	2.5165	105.98	111.77	107.08	112.73
CH_3XeCH_3 D_{3h}	r(H-C)	r(C-Xe)	$\Theta_{H\,C\,Xe}$	$\Theta_{H\,C\,H}$				
	1.0747	2.4994	104.11	114.26				
CH_3RnCH_3 D_{3h}	r(H-C)	r(Rn-C)	$\Theta_{H\,C\,Rn}$	$\Theta_{H\,C_2\,H}$				
	1.0745	2.5369	105.10	113.47				

[a] Bond lengths are given in Å; angles are given in degrees. [b] Structures of these molecules were optimized in a staggered C_3 configuration.

longer at the ωB97/iMCP-SR2 level of theory. For radon-containing CX_3RgCX_3, the Gibbs energies of formation of the D_{3h} and D_{3d} structures are very close: within 0.5 kJ·mol^{-1}. For these molecules, sufficient energy to drive conversion between the two symmetries is present at room conditions. For xenon-containing CX_3RgCX_3, Gibbs energies of formation differ only marginally (by 0.1 kJ·mol^{-1} for CF_3XeCF_3), by 1.3 kJ·mol^{-1} for CH_3XeCH_3, and by only 0.8 kJ·mol^{-1} CH $_3XeCF_3$ (in this case, the comparison is between the eclipsed and staggered configurations). While there are clearly two separate local minima for each compound, corresponding to slightly different structures, it is clear that the thermal energy available at room conditions is sufficient to fuel interconversion between these species. This is supported by both perturbation theory and density functional theory computations.

CX_3RgCX_3 molecules have 21 harmonic vibrational modes, 12 of which are doubly-degenerate, resulting in a total of 13 unique normal modes for the system. I have already demonstrated that the D_{3d} and D_{3h} configurations of CF_3RnCF_3 are energetically and geometrically close enough that it is sensible to view the two structural isomers as freely rotating between the two conformations; computed harmonic vibrational frequencies for CF_3RnCF_3 further support this hypothesis. Differences between normal modes computed for the two structures of CF_3RnCF_3 are minimal: for example, normal mode number 24, which occurs at 1173.70 cm^{-1} for the D_{3h} structure, differs by 0.10% from the frequency at which it occurs in the D_{3d} structure.

Computed Mayer bond orders, which use the non-classical component of the exchange operator's contribution to the total energy,[246] of CX_3RgCX_3 with the MP2 method also support the interpretation of their existence as a pair of interconverting structural isomers between the D_{3h} and D_{3d} structures (except for CH_3RnCH_3 and CF_3RgCH_3, which exist only in the D_{3h} and staggered configurations, respectively): when the symmetry of the molecule is changed, the order of the bond between the carbon and the rare gas is unaffected. This can be seen in Table 5.3. Additionally, all radon-containing CX_3RgCX_3 have higher bond orders than the corresponding CX_3XeCX_3. Previous chapters have demonstrated that smaller radon-containing compounds are more strongly bound than equivalent xenon-containing compounds;

Table 5.2: *Structure of CX_3RgCX_3 computed at the ωB97/iMCP-SR2 level of theory*[a]

CF_3XeCF_3 D_{3h}	r(F-C)	r(C-Xe)	$\Theta_{F\,C\,Xe}$	$\Theta_{F\,C\,F}$				
	1.3467	2.2792	111.47	107.41				
CF_3XeCF_3 D_{3d}	r(F-C)	r(C-Xe)	$\Theta_{F\,C\,Xe}$	$\Theta_{F\,C\,F}$				
	1.3467	2.2792	111.47	107.40				
CF_3RnCF_3 D_{3h}	r(F-C)	r(Rn-C)	$\Theta_{F\,C\,Rn}$	$\Theta_{F\,C\,F}$				
	1.3501	2.4026	111.97	106.87				
CF_3RnCF_3 D_{3d}	r(F-C)	r(C-Rn)	$\Theta_{F\,C\,Rn}$	$\Theta_{F\,C\,F}$				
	1.3502	2.4026	111.97	106.87				
CH_3XeCF_3[b]	r(H-C_1)	r(C_1-Xe)	r(C_2-F)	r(C_2-Xe)	$\Theta_{H\,C_1\,Xe}$	$\Theta_{F_1\,C_2\,Xe}$	$\Theta_{F\,C_2\,F}$	$\Theta_{H\,C_2\,H}$
	1.0832	2.1918	1.3654	2.3845	107.90	112.86	105.88	111.00
CH_3XeCF_3[c]	r(H-C_1)	r(C_1-Xe)	r(C_2-F)	r(C_2-Xe)	$\Theta_{H\,C_1\,Xe}$	$\Theta_{F_1\,C_2\,Xe}$	$\Theta_{F\,C_2\,F}$	$\Theta_{H\,C_2\,H}$
	1.0832	2.1918	1.3654	2.3844	107.90	112.86	105.88	111.00
CH_3RnCF_3[b]	r(H-C_1)	r(C_1-Rn)	r(C_2-F)	r(C_2-Rn)	$\Theta_{H\,C_1\,Rn}$	$\Theta_{F_1\,C_2\,Rn}$	$\Theta_{F\,C_2\,F}$	$\Theta_{H\,C_2\,H}$
	1.0822	2.3124	1.3685	2.4979	108.35	113.20	105.50	110.57
CH_3RnCF_3[c]	r(H-C_1)	r(C_1-Rn)	r(C_2-F)	r(C_2-Rn)	$\Theta_{H\,C_1\,Rn}$	$\Theta_{F_1\,C_2\,Rn}$	$\Theta_{F\,C_2\,F}$	$\Theta_{H\,C_2\,H}$
	1.0822	2.3123	1.3685	2.4979	108.35	113.20	105.50	110.57
CH_3XeCH_3 D_{3h}	r(H-C)	r(C-Xe)	$\Theta_{H\,C\,Xe}$	$\Theta_{H\,C\,H}$				
	1.0858	2.2753	108.74	110.19				
CH_3XeCH_3 D_{3d}	r(H-C)	r(C-Xe)	$\Theta_{H\,C\,Xe}$	$\Theta_{H\,C\,H}$				
	1.0858	2.2754	108.74	110.19				
CH_3RnCH_3 D_{3h}	r(H-C)	r(Rn-C)	$\Theta_{H\,C\,Rn}$	$\Theta_{H\,C_2\,H}$				
	1.0847	2.3952	109.25	109.69				
CH_3RnCH_3 D_{3d}	r(H-C)	r(Rn-C)	$\Theta_{H\,C\,Rn}$	$\Theta_{H\,C_2\,H}$				
	1.0847	2.3952	109.25	109.69				

[a] Bond lengths are given in Å; angles are given in degrees. [b] Structures of these molecules were optimized in a staggered C_3 configuration.
[c] Structures of these molecules were optimized in an eclipsed C_3 configuration.

this appears to be true as well for CX_3RgCX_3 molecules.

Table 5.3: *Bond order of CX_3RgCX_3*[a]

Molecule	Order (C_1-Rg)	Order (C_2-Rg)
CH_3RnCH_3 D_{3h}	0.260	0.260
CH_3XeCH_3 D_{3h}	0.200	0.200
CF_3RnCH_3	0.312	0.335
CF_3XeCH_3	0.304	0.288
CF_3RnCF_3 D_{3h}[b]	0.318	0.318
CF_3XeCF_3 D_{3h}[b]	0.263	0.263

[a] Computed at the MP2/iMCP-SR2 level of theory [b] For both of these molecules, bond orders in D_{3h} symmetry and in D_{3d} symmetry are identical.

Table 5.4: *$\rho(r)$ of CF_3XeCF_3 in D_{3h} and D_{3d} symmetry*

BCP:Symmetry	ρ(r)
(Xe-C): D_{3h}	0.079
(Xe-C): D_{3d}	0.073
(C-F): D_{3h}	0.278
(C-F): D_{3d}	0.281

The QTAIM method was used to compute both bond properties through analysis of the electron density of CX_3RgCX_3 molecules and to compute atomic charges, which are given in Table 5.5. The charge distribution in CX_3RgCX_3 molecules further supports the interpretation of the D_{3h} and D_{3d} forms of CF_3RgCF_3 existing as a pair of nearly identical structural isomers: charges between the two structural isomers of CF_3XeCF_3 and CF_3RnCF_3 are identical on all atoms except for the rare gas, which gains an additional $0.11e$ (for CF_3RnCF_3) and an additional $0.13e$ for CF_3XeCF_3 in the D_{3d} symmetry. For both molecules, this increase in charge does not qualitatively change the bonding in the molecule, nor does it alter the geometry, as has already been demonstrated.

For CH_3RgCF_3 and CH_3RgCH_3, the substitution of radon for xenon in the molecule does not alter the charge distribution at all. The two rare gas atoms interact with the

Table 5.5: *QTAIM atomic charges on CX_3RgCX_3*[a]

CF_3XeCF_3 D_{3h}	F	C	Xe		
	-0.81	2.08	0.67		
CF_3RnCF_3 D_{3h}	F	C	Rn		
	-0.81	2.02	0.80		
CF_3XeCF_3 D_{3d}	F	C	Xe		
	-0.73	1.95	0.45		
CF_3RnCF_3 D_{3d}	F	C	Rn		
	-0.73	1.91	0.56		
CH_3XeCF_3	H	C_1	Xe	C_2	F
	0.02	-0.10	0.65	1.87	-0.82
CH_3RnCF_3	H	C_1	Rn	C_2	F
	0.00	-0.18	0.78	1.85	-0.82
CH_3XeCH_3 D_{3h}	H	C	Xe		
	-0.04	-0.18	0.62		
CH_3RnCH_3 D_{3h}	H	C	Rn		
	-0.04	-0.19	0.63		

[a] Computed at the MP2/iMCP-SR2 level of theory

ligands in exactly the same way: an important feature of organic, rare-gas containing molecules which has been discussed in a previous chapter for smaller molecules.

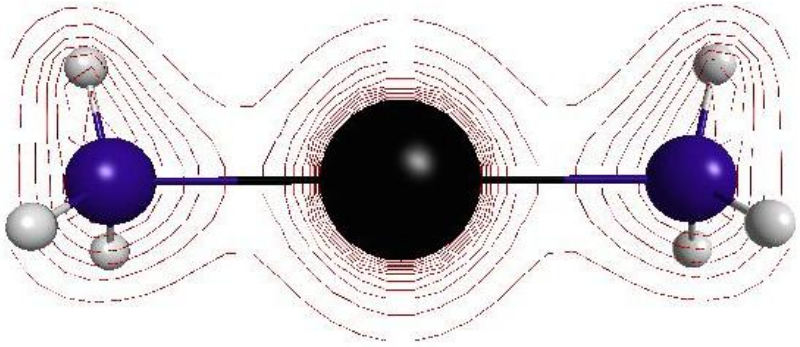

Figure 5.2: *$\rho(r)$ of CH_3RnCH_3, D_{3h} symmetry, MP2/iMCP-SR2 level of theory*

Analysis of the topology of the electron density, ρ(r) of CF_3RnCF_3 in D_{3h} and D_{3d} symmetry reveals that the ρ(r) is essentially unchanged between the two stereoisomers. The values of ρ(r) at bond critical points are nearly identical between the two configurations: at the (Rn-C) bond critical points, ρ(r) has a value of 0.071 in D_{3h} symmetry and a value of 0.067 in D_{3d}. Similarly, the value of ρ(r) at the (C-F)

bond critical points is 0.275 in D_{3h} symmetry and 0.280 in D_{3d}. Both of these values indicate that the behaviour of the electron density of CF_3RnCF_3 is the same at equivalent bond critical points in either symmetry, further supporting my interpretation that this compound, as well as CF_3XeCF_3, exists as a resonance of the two stereoisomers. Data for ρ(r) of CH_3XeCH_3 may be found in the Appendix to this chapter.

5.4 Conclusion

The CF_3XeCF_3 molecule has a checkered history, and to date it is still uncertain if it was indeed synthesized in 1979. More recently, computational studies have confirmed that the molecule should be stable, but little other work has been done on the molecule. As radon-containing molecules often have very similar chemistry to xenon-containing molecules, radon analogs of xenon-containing dimethyl and diperfluoromethyl compounds have been studied in this Chapter. In this work, I have computed structural parameters and vibrational spectra for molecules of the type CX_3RgCX_3, where X=H,F and Rg=Xe,Rn. Through analysis of the above properties and of the electron density in CX_3RgCX_3 molecules, I have demonstrated that the two stereoisomers of each CX_3RgCX_3 most likely exist as a pair of freely rotating structural isomers. This is evinced by the low energy barrier to conversion, the nearly identical structural parameters, the minute differences in the harmonic vibrational frequencies, very close values of atomic charges, and similar values of the electron density at specific bond critical points within the stereoisomers.

Chapter 6

Large Organic Compounds of Heavy Rare Gases

6.1 Introduction

Large organoxenon compounds have been one of the main foci of heavy rare gas chemistry since its beginning. Several types of molecules have been synthesized and studied both experimentally and computationally. Prominent among these are the perfluorophenyl xenon compounds studied by Frohn, Theissen, and Jakobs.[18,23,26,27,103] They have demonstrated that C_6F_5XeF makes an ideal starting material in the synthesis of both symmetric ($C_6F_5XeC_6F_5$) and asymmetric (C_6F_5XeCN) organoxenon compounds, and have characterized C_6F_5XeCN with ^{19}F, ^{13}C, and ^{129}Xe nuclear magnetic resonance (NMR). These compounds have been shown to be stable at -78°C for up to a few weeks. As previous chapters have shown, what is synthetically possible for xenon is at least *in silica* possible for radon. In order to better understand the link between radon and xenon chemistry, and to better understand these extant xenon-containing compounds, I have computed structures and properties for organic compounds of radon and xenon containing phenyl and perfluorophenyl groups and another small organic ligand. In this Chapter, molecules of the type C_6F_5RgA and C_6H_5RgA, where Rg is either radon or xenon and A is one of F, CN, CCH, or CCF, are analyzed using a variety of quantum chemical methods, beginning with the optimization of their structures and continuing with analysis of the Gibbs free energy change in

their formation reaction (ΔG), bond orders, harmonic vibrational frequencies, and concluding with Quantum Theory of Atoms in Molecules (QTAIM) analysis.

6.2 Computational Methods

C_6F_5RgA and C_6H_5RgA molecules are studied as the products of the following reactions, which are related to Reaction 5.1 in Chapter 5:

$$(CH_3)_3SiA + C_6H_5RgF \longrightarrow (CH_3)_3SiF + C_6H_5RgA \qquad \Delta G_1 \qquad (6.1)$$

$$(CH_3)_3SiA + C_6F_5RgF \longrightarrow (CH_3)_3SiF + C_6F_5RgA \qquad \Delta G_2 \qquad (6.2)$$

where A is one of the -CN, -CCH, or -CCF groups. The numbering scheme used for the atoms in these molecules is given in Figure 6.1.

Figure 6.1: *Numbering of atoms in C_6F_5RnCN.*

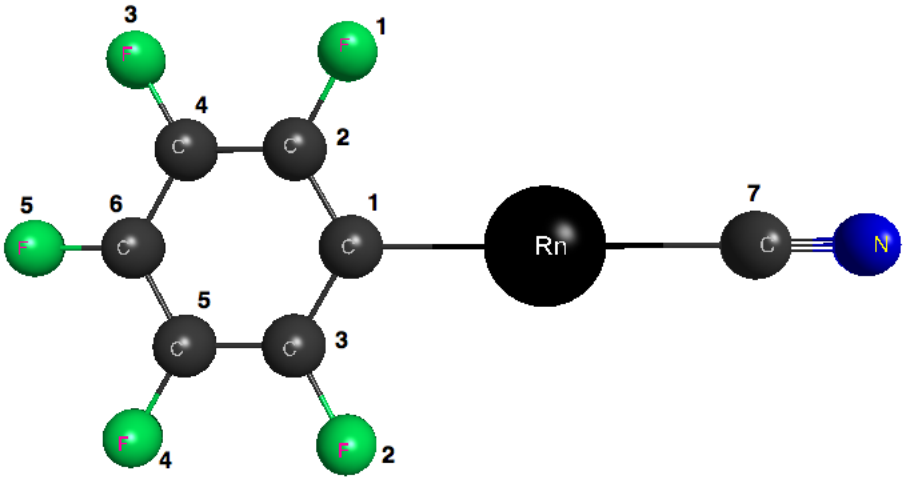

Properties of C_6F_5RgA and C_6H_5RgA molecules were computed at the MP2/MCP-TZP level of theory. The MCP-TZP basis set was chosen for its blend of computational efficiency and extensive polarization and correlation functions. The composition of this basis set, in [S/P/D/F] format, where each integer indicates the number of primitives composing each contracted basis function, is [311/11/1] for hydrogen; [211/211/21/2] for carbon, nitrogen, and fluorine; [5111/4111/611/2] for xenon; and

[6111/5111/721/3] for radon. The large molecules studied in this chapter necessitate a choice of an efficient basis set. The details of the theory behind the MCP basis sets have been discussed thoroughly in Chapter 1. As this basis set does not contain additional diffuse functions, it is more efficient than the aug-MCP-TZP basis set used in previous chapters. The MP2 method, which has also been described in the introductory Chapter, was chosen for this study as it both accounts for the effects of electron correlation and is efficient. Several properties were computed at the optimized geometries of C_6F_5RgA and C_6H_5RgA. Harmonic vibrational frequencies, bond orders, and Gibbs free energy change of formation for these molecules were computed using GAMESS-US.[278] The QTAIM analysis of the electron density of C_6F_5RgA and C_6H_5RgA molecules was carried out with the AIMStudio program.[250] Locally modified GAMESS-US code was used to generate extended wavefunction (.wfx) files (necessary when using pseudopotentials) as part of a single-point energy computation with the MP2 method for C_6F_5RgA and C_6H_5RgA molecules at the geometry corresponding to a local minimum on the potential energy surface. The basis set used in the generation of .wfx files was the MCP-TZP basis set with f-type polarization and correlating functions removed, based on the advice of the author of the AIMStudio program.[279] These functions have been observed to overlap in regions of space not near any nuclei in the molecule, leading the QTAIM algorithms to believe that there is a non-nuclear attractor critical point in these regions when in fact there is not. Removal of these long-tailed functions effectively solves this. In Chapter 5, the basis functions used were compact enough that they did not have this problem. Harmonic vibrational frequencies were visualized using the MacMolPlt program.[264] Results of computations involving GAMESS-US reported in this chapter were obtained on dual-quad core Apple Macintosh computers at the University of Alberta and the Westgrid Grex cluster at the University of Manitoba.

6.3 Results and Discussion

6.3.1 Structure of C_6H_5RgA and C_6F_5RgA

Optimized geometries of C_6H_5RgA and C_6F_5RgA molecules were confirmed to be minima on the potential energy surface of the molecule through analysis of the eigenvalues of the hessian matrix. Structural data for C_6H_5RgA may be found in Table 6.1. Inspection of the structures of C_6H_5RgA molecules reveals five major characteristics. For C_6H_5RgA molecules, neither of the bond lengths internal to the phenyl group (r(C-H) and r(C-C)) are altered when the rare gas is increased in size nor when the ligand A is changed. The angles within the phenyl group, $\Theta_{C_1\,C_3\,C_5}$ and $\Theta_{F_2\,C_1\,C_3}$ are similarly unaffected by substitutions of the ligand A or the rare gas. This indicates that in these molecules, the phenyl group is interacting with the other groups as one unit, as in purely organic molecules with functional groups. The bond between the rare gas and the primary carbon of the phenyl group is always 0.1 Å longer for molecules containing radon than for otherwise identical molecules containing xenon; this is consistent with structural data presented in Chapter 5 for smaller organic rare gas containing molecules. Similarly, the bond between the rare gas and the ligand is between 0.07 Å and 0.1 Å longer for radon-containing molecules than for related xenon containing molecules. Finally, internal bond lengths within the ligand (for the cases of the -CN, -CCH, and -CCF ligands) are unaffected by substitution of radon for xenon, indicating that as with the phenyl group, these ligands are likely interacting with the rare gas as a single unit rather than as individual atoms. This will be examined in more detail through QTAIM analysis of atomic charges.

For C_6F_5RgA molecules, whose structural parameters may be found in Table 6.2, the internal structure of the perfluorophenyl group is not significantly altered by increasing the size of the ligand from the -F and -CN groups to the larger -CCH and -CCF groups: the C-F bond length increases by a maximum of 0.002 Å for the larger two ligands. This is not large enough of an increase to have a recognizable effect upon the chemistry of the molecule as a whole, especially as the C-C bond length is unaffected by substitution of a larger ligand. For both of these bond lengths,

Table 6.1: *Structures of C_6H_5RgA molecules computed at the MP2/MCP-TZP level of theory*[a]

C_6H_5RnF	r(C-H)	r(C-C)	r(Rn-C_1)	r(Rn-F)	$\Theta_{Rn\,C_1\,C_3}$	$\Theta_{C_1\,C_3\,C_5}$	$\Theta_{F_2\,C_1\,C_3}$		
	1.0791	1.3866	2.2323	2.1595	119.5	119.4	119.8		
C_6H_5XeF	r(C-H)	r(C-C)	r(Xe-C_1)	r(Xe-F)	$\Theta_{Xe\,C_1\,C_3}$	$\Theta_{C_1\,C_3\,C_5}$	$\Theta_{F_2\,C_1\,C_3}$		
	1.0790	1.3868	2.1312	2.0846	119.3	119.1	120.1		
C_6H_5RnCN	r(C-H)	r(C-C)	r(Rn-C_1)	r(Rn-C_7)	r(C_7-N)	$\Theta_{Rn\,C_1\,C_3}$	$\Theta_{C_1\,C_3\,C_5}$	$\Theta_{F_2\,C_1\,C_3}$	
	1.0791	1.3867	2.2672	2.4298	1.1716	119.4	119.2	119.7	
C_6H_5XeCN	r(C-H)	r(C-C)	r(Xe-C_1)	r(Xe-C_7)	r(C_7-N)	$\Theta_{Xe\,C_1\,C_3}$	$\Theta_{C_1\,C_3\,C_5}$	$\Theta_{F_2\,C_1\,C_3}$	
	1.0790	1.3869	2.1735	2.3766	1.1717	119.1	118.9	120.1	
C_6H_5RnCCH	r(C-H)	r(C-C)	r(Rn-C_1)	r(Rn-C_7)	r(C_7-C_8)	r(C_8-H)	$\Theta_{Rn\,C_1\,C_3}$	$\Theta_{C_1\,C_3\,C_5}$	$\Theta_{F_2\,C_1\,C_3}$
	1.0794	1.3869	2.3044	2.3663	1.2217	1.0624	119.9	119.8	119.4
C_6H_5XeCCH	r(C-H)	r(C-C)	r(Xe-C_1)	r(Xe-C_7)	r(C_7-C_8)	r(C_8-H)	$\Theta_{Xe\,C_1\,C_3}$	$\Theta_{C_1\,C_3\,C_5}$	$\Theta_{F_2\,C_1\,C_3}$
	1.0793	1.3872	2.2187	2.2993	1.2216	1.0625	119.6	119.4	119.7
C_6H_5RnCCF	r(C-H)	r(C-C)	r(Rn-C_1)	r(Rn-C_7)	r(C_7-C_8)	r(C_8-F)	$\Theta_{Rn\,C_1\,C_3}$	$\Theta_{C_1\,C_3\,C_5}$	$\Theta_{F_2\,C_1\,C_3}$
	1.0793	1.3869	2.2940	2.3654	1.2198	1.2836	119.8	119.7	119.4
C_6H_5XeCCF	r(C-H)	r(C-C)	r(Xe-C_1)	r(Xe-C_7)	r(C_7-C_8)	r(C_8-F)	$\Theta_{Xe\,C_1\,C_3}$	$\Theta_{C_1\,C_3\,C_5}$	$\Theta_{F_2\,C_1\,C_3}$
	1.0792	1.3871	2.2060	2.3002	1.2196	1.2835	119.5	119.4	119.8

[a] Bond lengths are given in Å; angles are given in degrees.

Table 6.2: *Structures of C_6F_5RgA molecules computed at the MP2/MCP-TZP level of theory*[a]

C_6H_5RnF	r(C-F)	r(C-C)	r(Rn-C_1)	r(Rn-F)	$\Theta_{Rn\,C_1\,C_3}$	$\Theta_{C_1\,C_3\,C_5}$	$\Theta_{F_2\,C_1\,C_3}$		
	1.3207	1.3847	2.2430	2.1196	120.6	121.2	118.4		
C_6H_5XeF	r(C-F)	r(C-C)	r(Xe-C_1)	r(Xe-F)	$\Theta_{Xe\,C_1\,C_3}$	$\Theta_{C_1\,C_3\,C_5}$	$\Theta_{F_2\,C_1\,C_3}$		
	1.3203	1.3848	2.1459	2.0448	120.4	121.0	118.6		
C_6H_5RnCN	r(C-F)	r(C-C)	r(Rn-C_1)	r(Rn-C_7)	r(C_7-N)	$\Theta_{Rn\,C_1\,C_3}$	$\Theta_{C_1\,C_3\,C_5}$	$\Theta_{F_2\,C_1\,C_3}$	
	1.3206	1.3854	2.2961	2.3437	1.1708	120.5	121.3	118.5	
C_6H_5XeCN	r(C-F)	r(C-C)	r(Xe-C_1)	r(Xe-C_7)	r(C_7-N)	$\Theta_{Xe\,C_1\,C_3}$	$\Theta_{C_1\,C_3\,C_5}$	$\Theta_{F_2\,C_1\,C_3}$	
	1.3204	1.3856	2.2165	2.2791	1.1710	120.3	121.0	118.7	
C_6H_5RnCCH	r(C-F)	r(C-C)	r(Rn-C_1)	r(Rn-C_7)	r(C_7-C_8)	r(C_8-H)	$\Theta_{Rn\,C_1\,C_3}$	$\Theta_{C_1\,C_3\,C_5}$	$\Theta_{F_2\,C_1\,C_3}$
	1.3227	1.3851	2.3387	2.2865	1.2183	1.0621	120.9	121.8	118.1
C_6H_5XeCCH	r(C-F)	r(C-C)	r(Xe-C_1)	r(Xe-C_7)	r(C_7-C_8)	r(C_8-H)	$\Theta_{Xe\,C_1\,C_3}$	$\Theta_{C_1\,C_3\,C_5}$	$\Theta_{F_2\,C_1\,C_3}$
	1.3226	1.3853	2.2666	2.2118	1.2179	1.0623	120.7	121.5	118.2
C_6H_5RnCCF	r(C-F)	r(C-C)	r(Rn-C_1)	r(Rn-C_7)	r(C_7-C_8)	r(C_8-F)	$\Theta_{Rn\,C_1\,C_3}$	$\Theta_{C_1\,C_3\,C_5}$	$\Theta_{F_2\,C_1\,C_3}$
	1.3224	1.3851	2.3277	2.2847	1.2152	1.2771	120.8	121.7	118.1
C_6H_5XeCCF	r(C-F)	r(C-C)	r(Xe-C_1)	r(Xe-C_7)	r(C_7-C_8)	r(C_8-F)	$\Theta_{Xe\,C_1\,C_3}$	$\Theta_{C_1\,C_3\,C_5}$	$\Theta_{F_2\,C_1\,C_3}$
	1.3223	1.3853	2.2535	2.2109	1.2147	1.2765	120.6	121.4	118.3

[a] Bond lengths are given in Å; angles are given in degrees.

increasing the size of the rare gas from xenon to radon has no effect. As with the C_6H_5RgA molecules, increasing the size of the ligand or the size of the rare gas has no effect upon the internal angles of the perfluorophenyl group. This further supports the interpretation that the phenyl and perfluorophenyl groups in these molecules interact with the rare gas and ligand as a rigid group. As with the phenyl-containing molecules, the C_6F_5RgA molecules have a longer bond between the rare gas and the primary carbon of the perfluorophenyl group by 0.1 Å for radon-containing compounds than for similar xenon-containing compounds. This is both consistent with results discussed in the previous paragraph of this Chapter and with results in previous Chapters for related molecules. Likewise, the bond between the rare gas and the first atom of the ligand is 0.1 Å longer for radon-containing molecules than for similar xenon compounds. The consistency between these rare gas to ligand bond lengths across several organic, rare-gas containing compounds indicate that 0.1 Å may be a standard difference between xenon-organic group bond lengths and radon-organic group bond lengths, and may be useful in designing novel radon-containing analogs of existing xenon-containing compounds.

Backbonding also contributes to the strengthening of the bond between the rare gas and the primary carbon, and consequently the shortening of the bond length between the two atoms as well. Backbonding is defined by the International Union of Pure and Applied Chemistry (IUPAC) as

"*a synergic process with donation of electrons from the filled π-orbital or lone electron pair orbital of a ligand into an empty orbital of the metal together with the release of electrons from an nd-orbital of π symmetry with respect to the metal-ligand axis of the metal into the empty π^*-antibonding orbital of the ligand.*" [280]

While the word "metal" is used in the definition, backbonding is not unique to metal-ligand interactions and has in fact been reported in many systems. All that is required to meet the IUPAC definition is an availability of electron density that is symmetrically compatible with the bond between the heavy atom and the ligand, and a selection of *d*-type orbitals on the heavy atom to contribute to the symmetrically compatible antibonding molecular orbital which accepts the π-electron density. For

example, Dorsey et al. demonstrated in 2014 that backbonding occurs in the diamidocarbene coordinated stibinidene molecule between the antimony(I) and the carbene ligand.[281] For the molecules in which I am interested in the present Chapter, there are two molecular orbitals which have this effect. The strongest is in the π molecular orbital in which electron density is shared between the radon and the perfluorophenyl group. Through this, the bond between the primary carbon and radon is strengthened and shortened by the effect of back bonding. Another example is the σ molecular orbital, composed of contributions from the cyan carbon, the perflurophenyl group, and the radon, which has shared electron density centred along the primary axis of the molecule.This is clearly demonstrated in Figure 6.2.

Finally, the internal bond lengths and angles of the ligand are unaffected by an increase in size of the rare gas, suggesting that as with the phenyl compounds, ligands in perfluorophenyl rare gas compounds are also interacting as a single entity rather than as a collection of atoms. This idea will be examined more thoroughly as part of the discussion of QTAIM results for each molecule.

6.3.2 Bond Order Analysis

Bond orders computed with the Mayer method[246] as described in Chapter 5, of C_6H_5RgA and C_6F_5RgA compounds computed at the MP2/MCP-TZP level of theory are tabulated in Tables 6.3 and 6.4. Bond orders of bonds within the phenyl group are unaffected by a change in the size of the rare gas or the ligand, supporting the hypothesis above that the phenyl group is interacting with the rest of the C_6H_5RgA molecule as a single entity. This is also true of the perfluorophenyl compounds. Bond orders for the phenyl-rare gas bond are up to 10% lower for radon-containing C_6H_5RnA than for the corresponding xenon-containing C_6H_5XeA. For perfluorophenyl compounds, the radon-perfluorophenyl group bond order is up to 12% lower than the xenon-prefluorophenyl group bond order for the corresponding xenon compound. Similarly, bond orders between the rare gas and the first atom in the ligand are 1 to 10% lower for radon-containing phenyl compounds and 3 to 10% lower for radon-containing perfluorophenyl compounds than they are in similar xenon-containing compounds, further

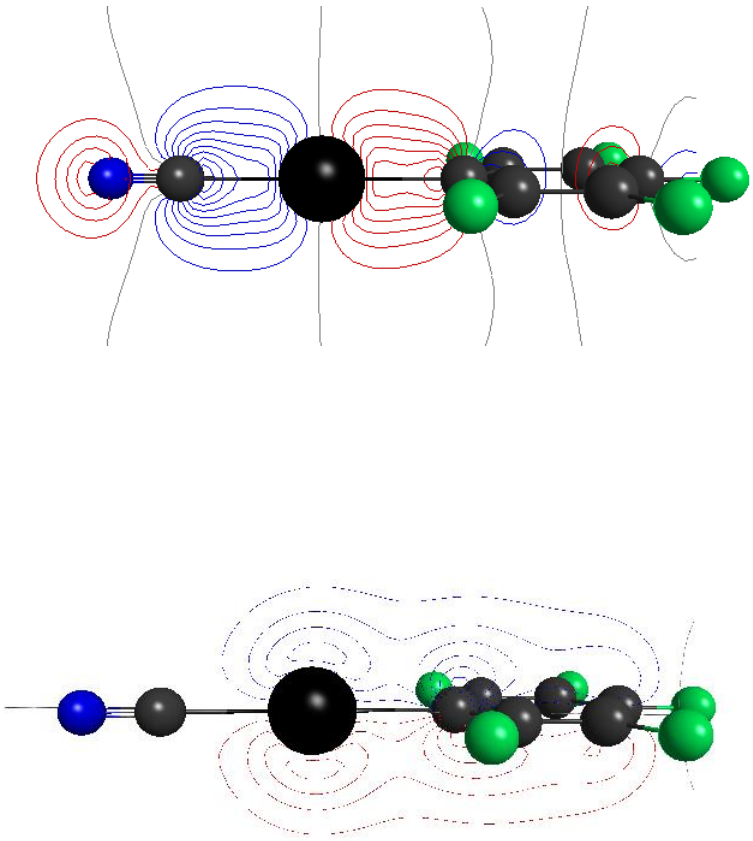

Figure 6.2: *Backbonding in C_6F_5RnCN. Top: shared σ molecular orbital between all carbon atoms in the molecule and the Rn; Lower: shared π molecular orbital between the C_6F_5 group and Rn.*

supporting the idea that like the phenyl and perfluorophenyl groups, the ligands are interacting with the rare gas as a functional group rather than as individual atoms. Finally, in both phenyl and perfluorophenyl rare gas compounds, the bond orders for bonds within the ligand are only 3 to 6% smaller for radon than for xenon, indicating that the bonding within the molecule as a whole and the ligands in particular remains the same regardless of which rare gas is involved. The slight decrease in bond order for rare gas to ligand bonds in the radon-containing species studied in this Chapter

is consistent with results for other molecules, such as the HRgF species studied in Chapter 2, and may be a result of the slightly (up to 0.1 Å) longer rare gas to ligand bond lengths found in the radon-containing compounds.

Table 6.3: *Bond orders of C_6H_5RgA, computed at the MP2/MCP-TZP level of theory*

C_6H_5RnF	o(C-H)	o(C-C)	o(Rn-C_1)	o(Rn-F)		
	0.92	1.25	0.63	0.48		
C_6H_5XeF	o(C-H)	o(C-C)	o(Xe-C_1)	o(Xe-F)		
	0.92	1.25	0.70	0.49		
C_6H_5RnCN	o(C-H)	o(C-C)	o(Rn-C_1)	o(Rn-C_7)	o(C_7-N)	
	0.92	1.25	0.57	0.38	2.73	
C_6H_5XeCN	o(C-H)	o(C-C)	o(Xe-C_1)	o(Xe-C_7)	o(C_7-N)	
	0.92	1.25	0.62	0.41	2.73	
C_6H_5RnCCH	o(C-H)	o(C-C)	o(Rn-C_1)	o(Rn-C_7)	o(C_7-C_8)	o(C_8-H)
	0.92	1.25	0.49	0.31	2.45	0.95
C_6H_5XeCCH	o(C-H)	o(C-C)	o(Xe-C_1)	o(Xe-C_7)	o(C_7-C_8)	o(C_8-H)
	0.92	1.25	0.54	0.38	2.42	0.95
C_6H_5RnCCF	o(C-H)	o(C-C)	o(Rn-C_1)	o(Rn-C_7)	o(C_7-C_8)	o(C_8-F)
	0.92	1.25	0.51	0.35	2.39	1.17
C_6H_5XeCCF	o(C-H)	o(C-C)	o(Xe-C_1)	o(Xe-C_7)	o(C_7-C_8)	o(C_8-F)
	0.92	1.25	0.56	0.40	2.35	1.17

6.3.3 Harmonic Vibrational Frequencies of C_6H_5RgA and C_6F_5RgA

The harmonic vibrational spectra of C_6H_5RnCN, C_6H_5XeCN, C_6F_5RnCN, and C_6F_5XeCN will be discussed in detail, with the harmonic vibrational frequencies and their corresponding intensities for all other molecules listed in the Appendix to this Chapter. Results for the phenyl-containing compounds will be discussed first, followed by the results for the perfluorophenyl-containing compounds and a summary of the effects of substitution of fluorine for hydrogen in the aromatic ring.

There are three dominant peaks in the harmonic vibrational spectra of C_6H_5RnCN and C_6H_5XeCN. For C_6H_5RnCN, whose spectrum is presented in Figure 6.4, the first of these occurs at 297.98 cm^{-1} and corresponds to a symmetric stretch of the C-N bond towards the direction of the phenyl ring and the rare gas. This is the highest-intensity peak of the three major peaks. The next occurs at 750.52 cm^{-1} and arises from the

Table 6.4: *Bond orders of C_6F_5RgA, computed at the MP2/MCP-TZP level of theory*

C_6F_5RnF	o(C-F)	o(C-C)	o(Rn-C_1)	o(Rn-F)		
	1.09	1.23	0.60	0.54		
C_6F_5XeF	o(C-F)	o(C-C)	o(Xe-C_1)	o(Xe-F)		
	1.09	1.23	0.69	0.54		
C_6F_5RnCN	o(C-F)	o(C-C)	o(Rn-C_1)	o(Rn-C_7)	o(C_7-N)	
	1.09	1.23	0.54	0.46	2.74	
C_6F_5XeCN	o(C-F)	o(C-C)	o(Xe-C_1)	o(Xe-C_7)	o(C_7-N)	
	1.09	1.23	0.59	0.48	2.75	
C_6F_5RnCCH	o(C-F)	o(C-C)	o(Rn-C_1)	o(Rn-C_7)	o(C_7-C_8)	o(C_8-H)
	1.08	1.23	0.46	0.39	2.44	0.96
C_6F_5XeCCH	o(C-F)	o(C-C)	o(Xe-C_1)	o(Xe-C_7)	o(C_7-C_8)	o(C_8-H)
	1.08	1.23	0.52	0.46	2.40	0.96
C_6F_5RnCCF	o(C-F)	o(C-C)	o(Rn-C_1)	o(Rn-$C_7$7)	o(C_7-C_8)	o(C_8-F)
	1.08	1.23	0.48	0.43	3.40	1.18
C_6F_5XeCCF	o(C-F)	o(C-C)	o(Xe-C_1)	o(Xe-C_7)	o(C_7-C_8)	o(C_8-F)
	1.08	1.23	0.54	0.48	2.37	1.20

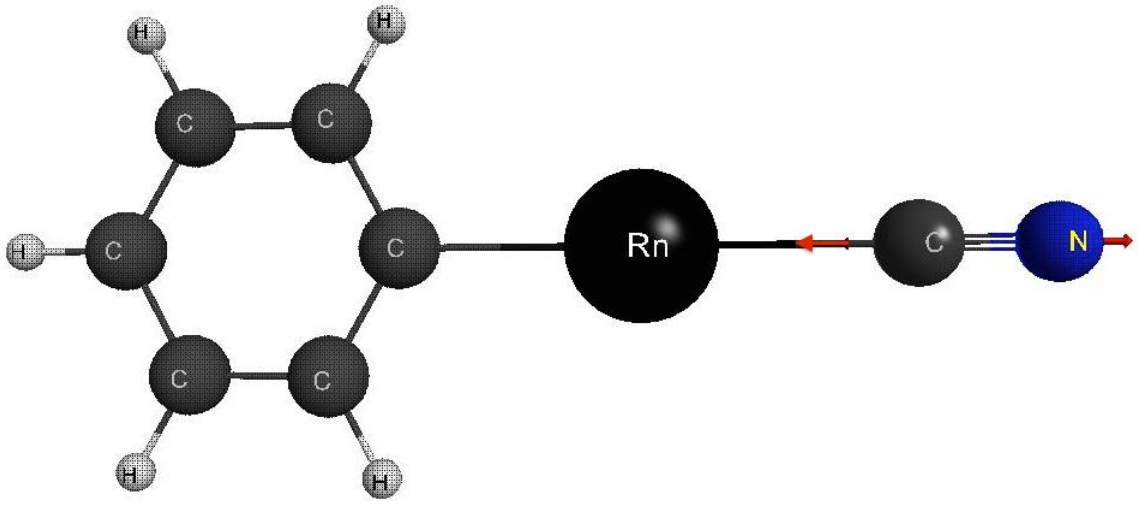

Figure 6.3: *Asymmetric stretch of C-N bond of C_6H_5RnCN, computed at the MP2/MCP-TZP level of theory.*

stretches of the C-H bonds in the phenyl group and is the lowest intensity peak of the three. The last, which occurs at 2075.66 cm^{-1}, corresponds to the asymmetric stretching of the C-N bond. This stretching is illustrated in Figure 6.3 by red arrows. As expected from compounds which have already been demonstrated to share many

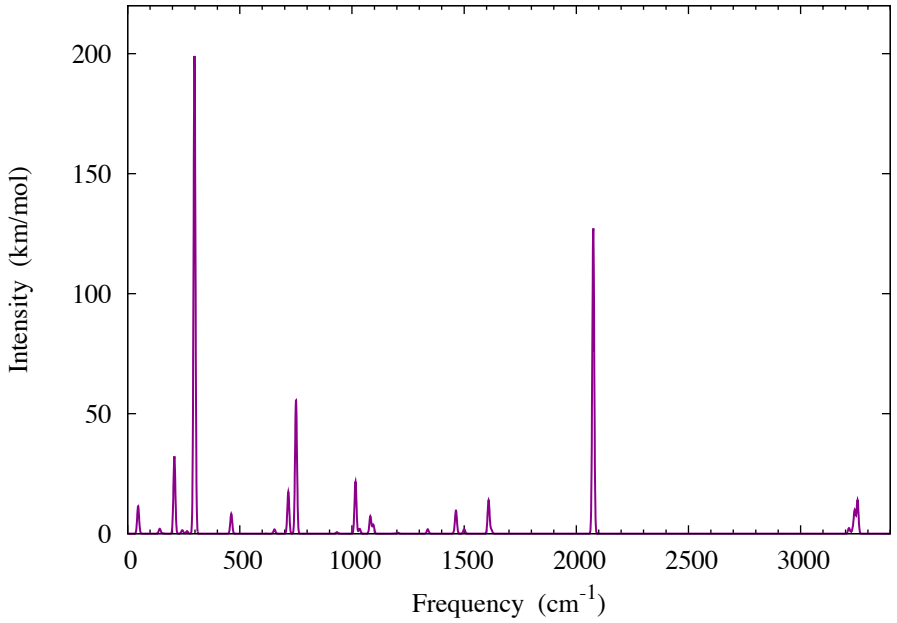

Figure 6.4: *Vibrational spectrum of* C_6H_5RnCN[(a)]

[(a)] Spectrum generated using Gaussian line types and 1 half-width at half-height, with a scaling factor of 1. All spectra presented in this chapter used the same parameters.

characteristics of geometry and bond orders, C_6H_5XeCN has a very similar harmonic vibrational spectrum to C_6H_5RnCN. The highest intensity peak is located at 288.15 cm^{-1}, and as with the spectrum of C_6H_5RnCN, arises from the stretch of the C-N bond towards the radon and phenyl groups. The peak corresponding to the asymmetric stretching of the C-H bonds within the phenyl group occurs at 754.31 cm^{-1} and is the lowest-intensity of the three most intense peaks in the spectrum. Finally, the peak at 2071.02 cm^{-1} is produced by the asymmetric stretch of the C-N bond. The harmonic vibrational spectrum of C_6H_5XeCN may be found in Figure 6.6.

The four highest-intensity peaks in the harmonic vibrational spectra of C_6F_5RnCN, which may be found in Figure 6.7, result from stretching of the C-N bond and internal motions within the perfluorophenyl group. The peak at 327.75 cm^{-1} is produced by

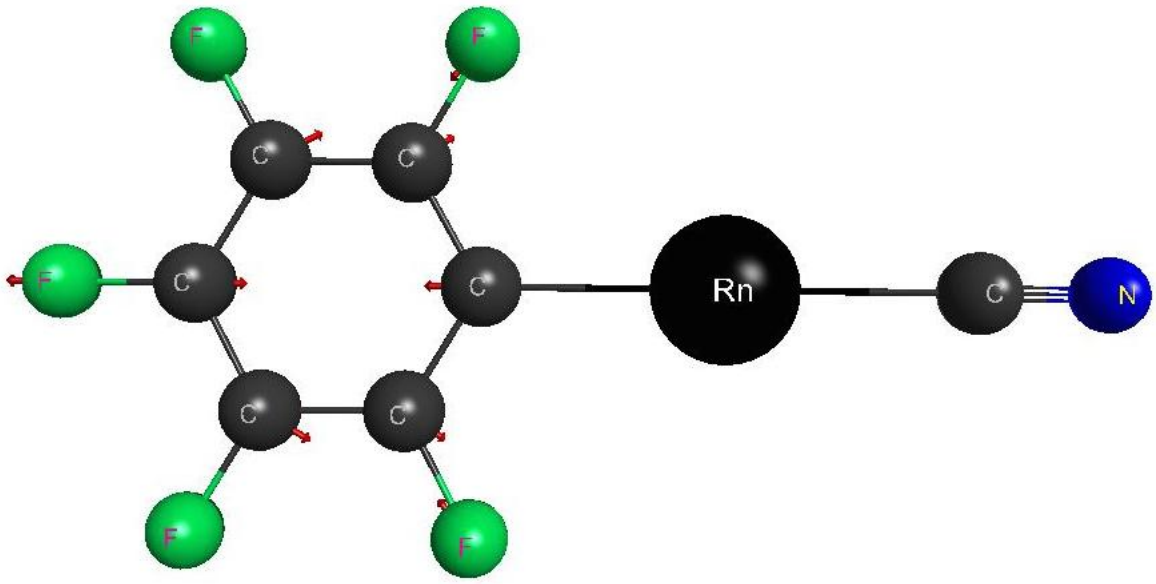

Figure 6.5: *Asymmetric stretch/ring twisting mode of C_6F_5RnCN, computed at the MP2/MCP-TZP level of theory.*

a symmetric stretch of the C-N bond towards the direction of the radon and perfluorophenyl group. The next significant peak occurs at 1101.47 cm^{-1} and is caused by a combination of asymmetric stretches of the C-F bonds and twisting of the C-C bonds away from the ring centre, both within the phenyl group. This normal mode is shown in Figure 6.5.

The third significant peak is located at 1532.82 cm^{-1}, and results from the C-C bonds within the phenyl group twisting towards the ring centre. The last high-intensity peak occurs at 1554.81 cm^{-1} and corresponds to a wag of the C-C bonds inside the perfluorophenyl group. The spectrum of C_6F_5XeCN, located in Figure 6.8, contains the same major features as the spectrum of C_6F_5RnCN. The peak at 321.97 cm^{-1} represents the symmetric C-N bond stretching towards the rest of the molecule. At 1101.33 cm^{-1}, the combined asymmetric C-F stretches away from the centre of the ring and the C-C bond twists may be found. The C-C bonds twisting towards the ring centre cause the peak at 1536.50 cm^{-1}, and finally the C-C bonds' wag occurs at 1554.59 cm.

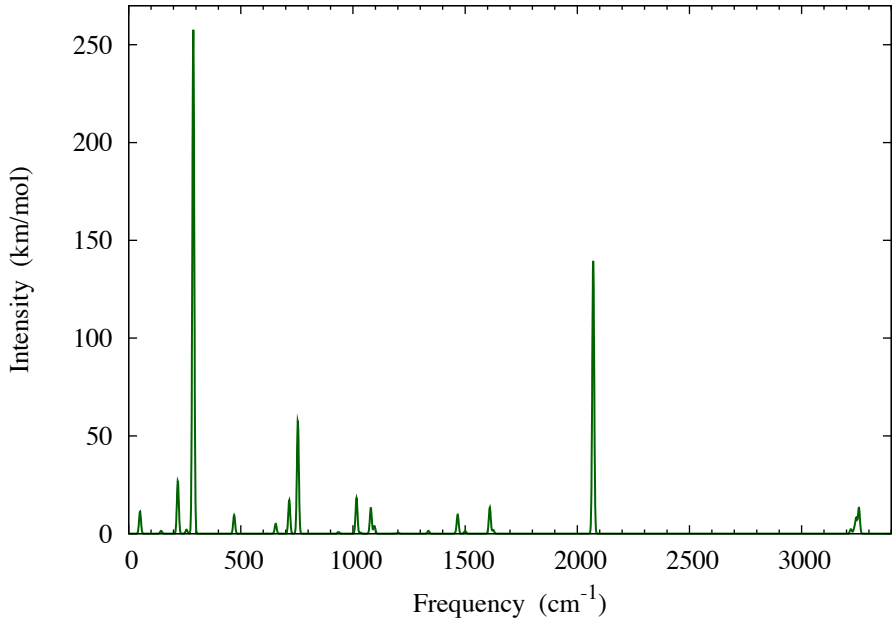

Figure 6.6: *Vibrational spectrum of* C_6H_5XeCN

In all four spectra, a stretch of the C-Rg bond, with the nitrogen following the carbon, occurs in the 288 and 321 cm^{-1} region. For radon-containing compounds, the frequency at which the peak occurs is 2 to 3% higher than for xenon-containing compounds. The second significant peak in the perfluorophenyl compounds' spectra has no equivalent peak of significant intensity in the spectra of the phenyl-containing compounds. The third peak in the spectra of perfluoromethyl compounds corresponds to the second significant peak in the spectra of the phenyl-containing compounds. The last peak of significant intensity in the phenyl-containing compounds is the asymmetric stretch of the C-N bond, while in the spectra of the perfluorophenyl-containing compounds it is the wag of the C-C bonds within the ring. Both normal modes necessarily occur within both types of molecules.

Whenever low-frequency vibrational modes are present in a molecule, the question of the role of anharmonicity in the vibrational spectra should be raised. In the

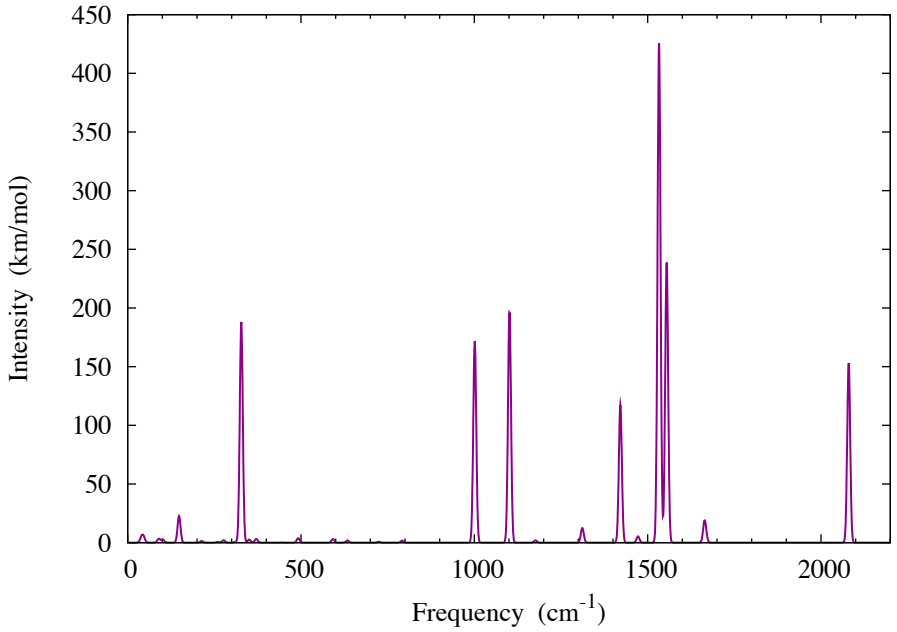

Figure 6.7: *Vibrational spectrum of C_6F_5RnCN*

present cases, I have deemed it unnecessary to compute such effects. This decision rests on the following: first, the heavy atom does not account for an overwhelming proportion of the mass of these molecules. For some of the smaller molecules studied in previous Chapters, such as HRnF from Chapter 2, the rare gas contributes over 90% of the total mass of the molecule. In these cases, it is natural to expect a strongly anharmonic vibrational spectrum. In the case of C_6F_5RnCN, the radon contributes approximately half (53.5%) of the total mass of the molecule. The phenyl groups and other organic ligands in this chapter are not typically strongly anharmonic, and therefore do not increase the anharmonicity of the molecule. Contributions to the centre of mass of the molecule are more equally weighted between the rare gas, the perfluorophenyl group, and the ligand than is the case in smaller rare gas containing molecules. Second, a prime contributor to the anharmonicity of any molecule is the floppiness of all phenyl-rare gas bonds. Some bonds in the molecules studied in this

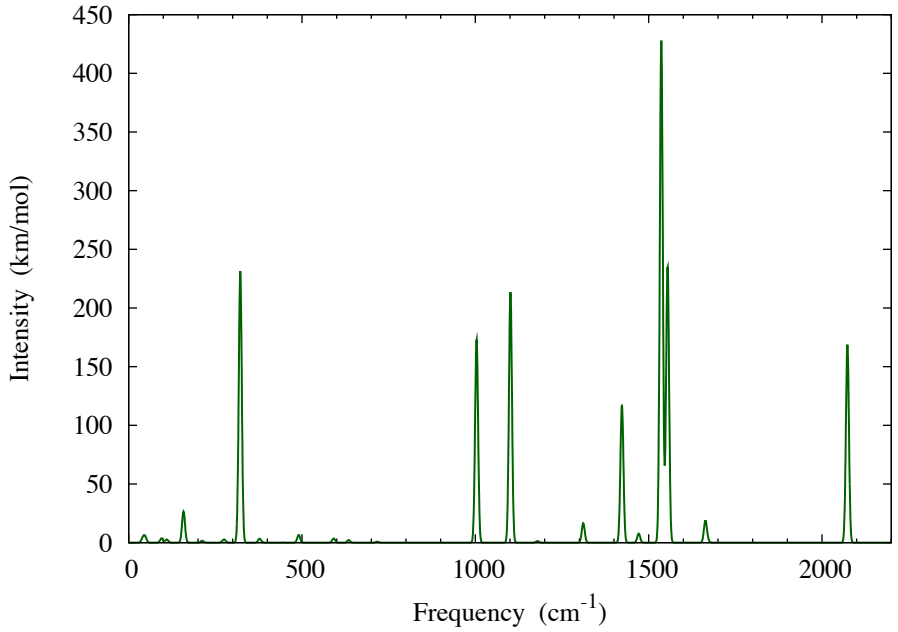

Figure 6.8: *Vibrational spectrum of C_6F_5XeCN*

Chapter are much more rigid than bonds in some other rare gas containing compounds (CH_3RnCH_3, for example), and thus anharmonic contributions from this source are likely low.

6.3.4 Gibbs free energy of formation

I computed Gibbs free energy changes for the formation (ΔG_1) of C_6H_5RgA and C_6F_5RgA molecules based on the results of geometry optimizations and hessian computations. These ΔG are listed in Table 6.5. As can be seen in this table, the compounds with the largest (most negative) ΔG are those which include radon rather than xenon, have a perfluorophenyl group rather than a phenyl group, and have a cyano group as the ligand rather than one of the bulkier groups. These data are useful for identifying prime candidate compounds for experimental study; rather than focus attention on attempting to synthesize C_6H_5RnCCF, which has a ΔG of only -66.6

kJ·mol^{-1}, a much more rewarding use of time may be to work towards synthesizing C_6F_5RnCN, which has a 40.5% larger ΔG.

Table 6.5: *Free energy change of formation (ΔG) for C_6H_5RgA and C_6F_5RgA*[(a)]

C_6H_5RgA	ΔG_1	C_6F_5RgA	ΔG_2
C_6H_5RnCN	-90.2	C_6F_5RnCN	-93.6
C_6H_5XeCN	-81.8	C_6F_5XeCN	-84.9
C_6H_5RnCCH	-67.6	C_6F_5RnCCH	-87.1
C_6H_5XeCCH	-59.6	C_6F_5XeCCH	-80.4
C_6H_5RnCCF	-66.6	C_6F_5RnCCF	-83.1
C_6H_5XeCCF	-58.1	C_6F_5XeCCF	-75.7

[(a)] ΔG given in units of kJ·mol^{-1}.

6.3.5 QTAIM Analysis of C_6H_5RgA and C_6F_5RgA

Bonding was further analyzed in C_6H_5RgA and C_6F_5RgA through the QTAIM method. Results for the C_6H_5RnCN and C_6F_5RnCN molecules will be analyzed in detail. These molecules have 11 bond critical points within the phenyl or perfluorophenyl group and an additional three in the rest of the molecule, with one each between the aromatic group and the radon, another between the radon and the cyano carbon, and the last between the cyano carbon and the nitrogen. In the contour plots of the electron density of these compounds shown in Figures 6.9 and 6.10, yellow represents less density, cyan some, and blue the greatest concentration of electron density. The highest-density regions are of course the immediate vicinity of the nuclei, with shared electron density of lesser magnitude throughout the rest of the molecule.

Several interesting features of these molecules can be seen in the contour maps of the C_6H_5RnCN and C_6F_5RnCN. First, the aromatic natures of the phenyl and perfluorophenyl groups are clearly reflected in the concentric ringed contour lines located inside the phenyl or perfluorophenyl ring. The triple bond between the cyano carbon and nitrogen is indicated by a region of higher electron density immediately around and between the two nuclei than is seen between any other pairs of nuclei, and is also apparent in the contour plot for C_6F_5RnCN.

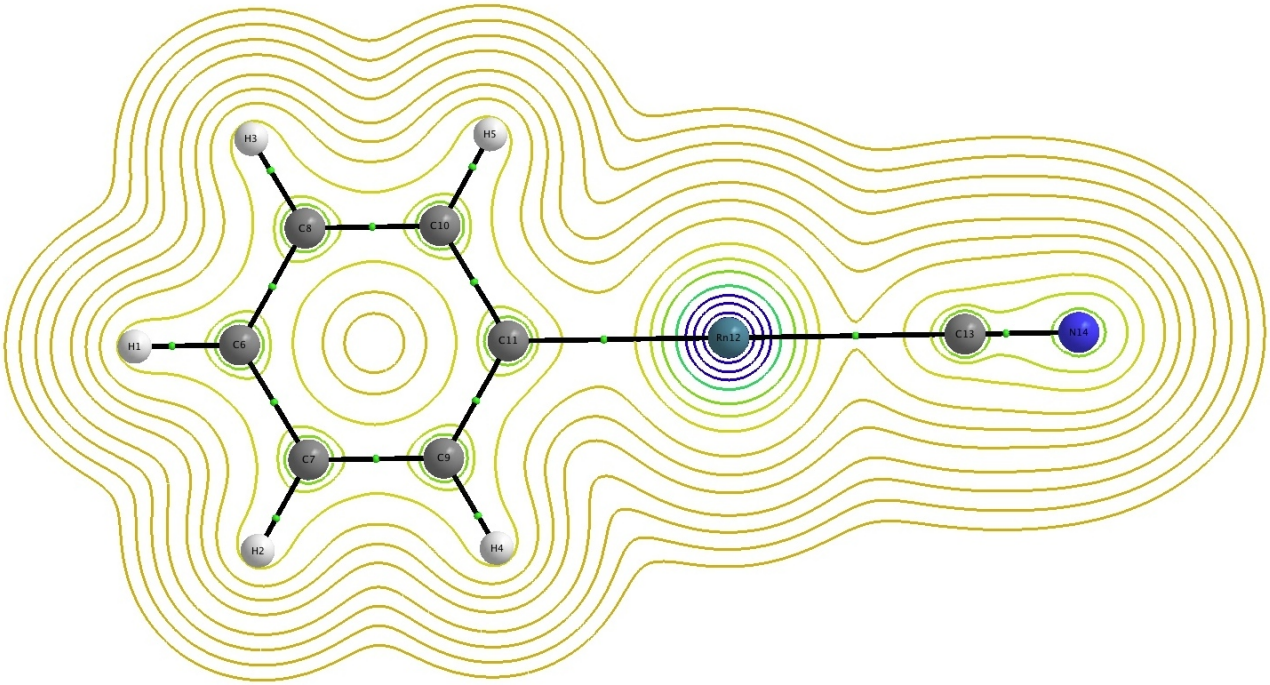

Figure 6.9: *Contour plot of ρ(r) for C_6H_5RnCN, MP2/MCP-TZP-f level of theory.*

Second, the shape of the contours around the radon and phenyl group makes it clear that there is some sharing of π-electron density from the phenyl group to the phenyl-radon bond. This sharing is stronger for C_6H_5RnCN than for C_6F_5RnCN, and contributes to shortening the Rn-C_1 bond, as seen in Tables 6.1 and 6.2. The π-electron sharing does occur in C_6F_5RnC to a lesser degree; Rn-C_1 bond lengths in these molecules are up to 0.3 Å shorter than the Rn-C_1 bond lengths seen for the molecules studied in Chapter 5.

The contour maps of the C_6H_5XeCN and C_6F_5XeCN molecules, shown in Figures 6.11 and 6.12, clearly show the aromatic nature of the phenyl or perfluorophenyl group through the concentric contour lines inside the ring. As with the radon-containing compounds the triple C-N bond is reflected in the region of shared electron density between the carbon and nitrogen. Additionally, the donation of electron density from the aromatic ring to the bond between the primary carbon and the xenon is evident from the contour lines in the region around this bond in both Figures 6.11 and 6.12.

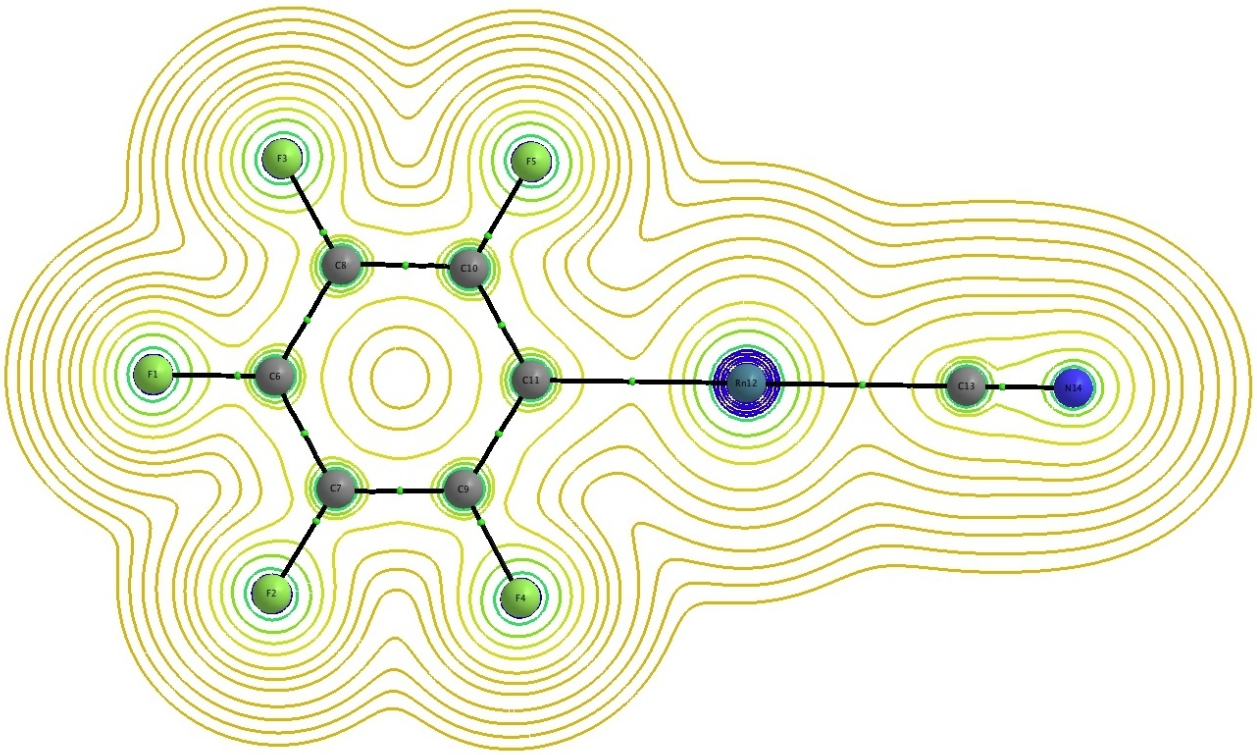

Figure 6.10: *Contour plot of ρ(r) for C_6F_5RnCN, MP2/MCP-TZP-f level of theory.*

Charges on atoms and functional groups in C_6H_5RnCN and C_6F_5RnCN are tabulated in Table 6.6. For all four molecules, the rare gas atom has a strong partial positive charge and interacts with two negatively charged organic groups of varying strength. In the case of C_6H_5RgCN molecules, the phenyl group has a very weak negative charge, and the cyano group takes on the role of the more electron-withdrawing moiety in the molecule. The opposite is true of the C_6F_5RgCN compounds; the fluorine atoms in the aromatic ring turn it into a much more nucleophilic group with a negative charge four to ten times that of the phenyl group's charge in C_6H_5RgCN molecules. In this case, the strength of the partial positive charge on the rare gas increases as well, and the cyano group becomes more neutral.

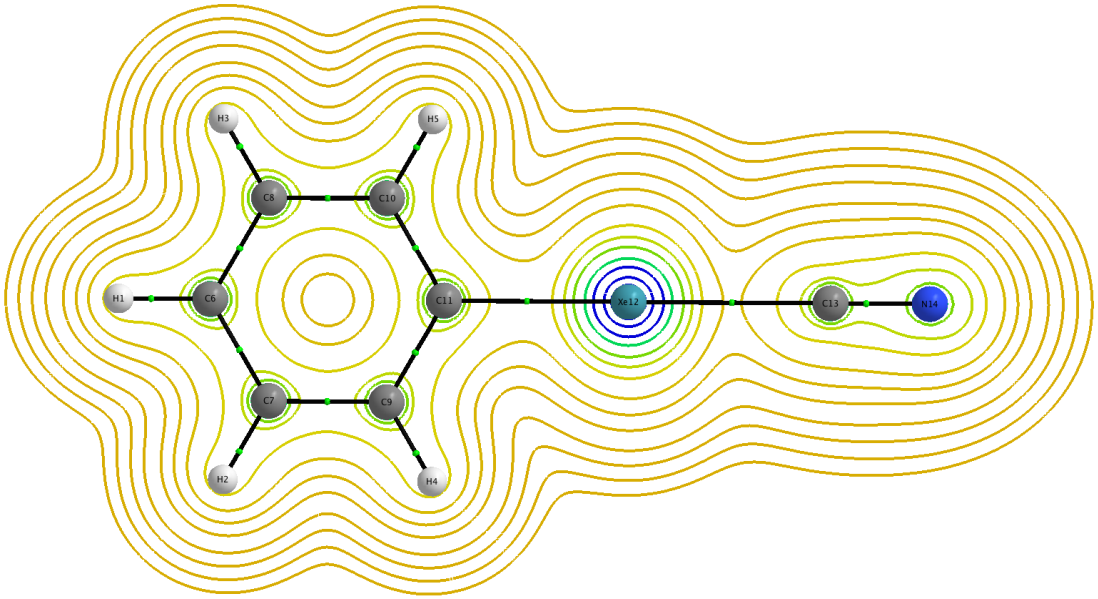

Figure 6.11: *Contour plot of $\rho(r)$ for C_6H_5XeCN, MP2/MCP-TZP-f level of theory.*

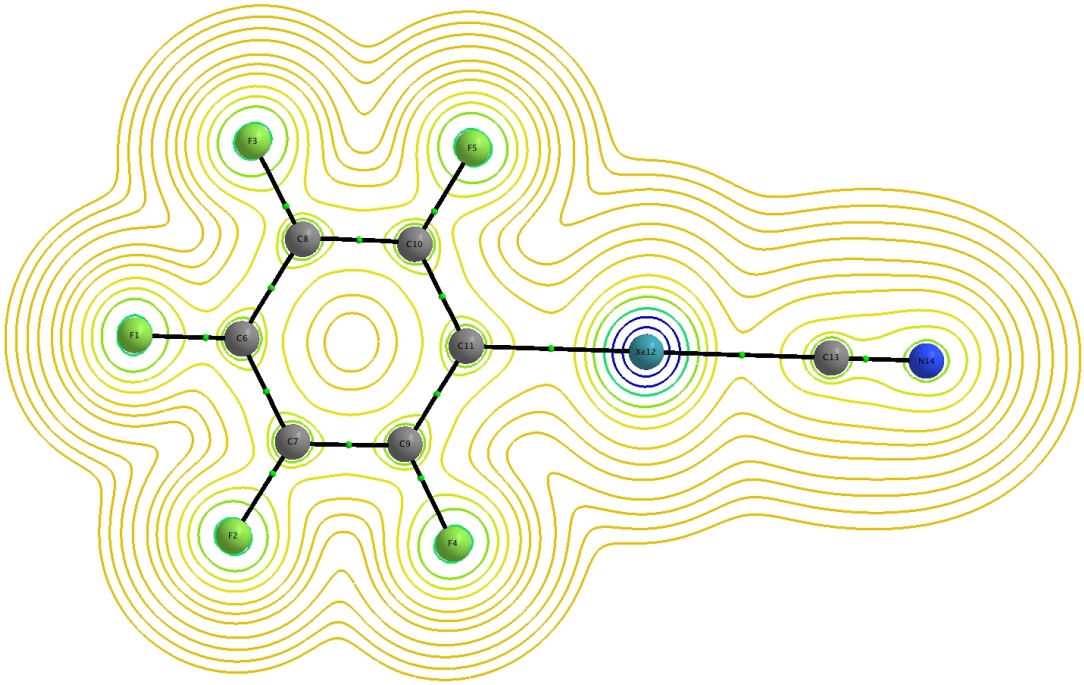

Figure 6.12: *Contour plot of $\rho(r)$ for C_6F_5XeCN, MP2/MCP-TZP-f level of theory.*

Table 6.6: *QTAIM atomic and group charges on C_6X_5RnCN and C_6X_5XeCN*[(a)]

molecule	q(Ph)	q(Rg)	q(CN)
C_6H_5RnCN	-0.11	0.85	-0.74
C_6H_5XeCN	-0.05	0.80	-0.75
C_6F_5RnCN	-0.46	0.94	-0.58
C_6F_5XeCN	-0.98	0.96	-0.64

[(a)] Computed at the MP2/MCP-TZP-f level of theory and given in units of e.

6.4 Conclusion

In this Chapter, I have presented computed structures and properties of molecules of the type C_6H_5RgA and C_6F_5RgA, where Rg is either radon or xenon and A is one of F, CN, CCH, or CCF. These molecules were analyzed using a variety of quantum chemical methods, beginning with the optimization of their structures and continuing with analysis of the Gibbs free energy change of reaction (ΔG), bond orders, harmonic vibrational frequencies, and Quantum Theory of Atoms in Molecules (QTAIM) analysis. Some of these compounds, like C_6F_5XeCN, have been studied experimentally;[27] others are related to those compounds and are demonstrated to be ideal candidates for experimental study. The bond lengths and angles within the phenyl, perfluorophenyl, and ligands are unaffected by variation in the rare gas, confirming that they are interacting as a unit rather than as individual atoms. Bonds between the ligand and the rare gas and the phenyl or perfluorophenyl and the rare gas are 0.1 Å longer for all radon-containing compounds than for the corresponding xenon-containing compounds: this increase in bond length is a standard relationship between the two rare gases and reflects their difference in atomic radii. All of the compounds studied in this chapter have shorter rare gas to organic group bond lengths than compounds involving organic groups studied in previous chapters, indicating that the C_6H_5RgA and C_6F_5RgA molecules are more rigid than the related organic rare gas compounds studied in Chapter 5. Bond orders for radon-containing compounds are nearly 10% smaller than the bond orders for the corresponding xenon-containing compounds, and these are unaffected by a change in the size of the ligand, indicating that while the bonds in radon-containing compounds may be slightly weaker than the bonds

in xenon-containing compounds, they are still definitively bonded species. The computed harmonic vibrational spectra of C_6H_5RgA and C_6F_5RgA display a high degree of similarity between radon and xenon-containing compounds, indicating that spectra for previously-characterized xenon-containing compounds may be useful as a general guide to aid in the identification of related radon-containing compounds. The dramatically larger ΔG for radon-containing C_6H_5RgA and C_6F_5RgA indicate that these may be more thermodynamically stable than the related xenon compounds, which is promising. Finally, QTAIM analysis reveals that the shared π-electron density from the aromatic ring to the bond between the rare gas and the aromatic group serves to further stabilize the compounds and shorten the aromatic-rare gas bond. Additionally, the atomic charges indicate a degree of electron transfer between the rare gases and the organic groups that is consistent with previous results for the compounds studied in Chapter 5.

Chapter 7

Effect of Harmonic Confinement on the Properties and Reactions of HRgX

7.1 Introduction

The surge of interest in rare gas chemistry following Bartlett's discovery of a stable xenon-containing compound[2] resulted in the discovery of over 500 rare gas containing molecules that exist today.[22,72,147,161] These molecules are not merely chemical curiosities, but have found many uses in several branches of chemistry.[22,29,126] Recent work on the rare gas hydrides[158,163,176] has demonstrated that many of these metastable molecules are good candidates for synthesis in the lab, due to the indications of kinetic stability found in high activation energies to the decomposition reaction.[160,258,259,274]. Some of these compounds have even been predicted to be stable in the gas phase at near-room temperatures![137,158] Many of the current theoretical studies of radon chemistry begin with exploring related compounds containing the lighter rare gases. Argon-, krypton-, and xenon-containing halohydrides have been synthesized via photodissociation of a halide, such as HF, inside of an argon- or krypton-doped rare gas matrix.[37,282] Organic, xenon-containing compounds[24] and HXeOH[43] have been synthesized under similar conditions. The kinetic stability of HRgX(Rg=Xe, Rn; X=F, Cl) molecules, then, is best understood in the context of the surrounding rare gas matrix.

In the present work, in order to better understand the behaviour of motions of electrons and solutions of the quantum mechanical equations in such environments, I used an analytical potential which acts on the electrons in the system. The use of such confinements in quantum-chemical calculations has a long history. In 1996, Jaskólski reviewed extant methods for confining molecules, focusing on the effect of confinement upon the electronic structure of a molecule.[283] Electronic spectra of two electron systems confined in harmonic oscillator potentials were studied in 2001 by Diercksen et al.[284,285] In 2004, Manson et al. studied atoms confined in a potential designed to mimic a C_{60} cage.[286]. Several studies have been carried out for the Be_2 molecule confined within a cylindrical harmonic potential.[287–289] Cylindrical harmonic potentials have also been applied to studies of excited states of the hydrogen molecule[290], potential energy curves of the Rydberg molecules NeH[291], HeH[292] and noble metal hydrides[293]. Bielińska-Wąż et al. applied perturbation theory to computations of potential energy surfaces and properties of Rydberg molecules in 2006.[294] Sako and Diercksen computed excitation spectra for a two-electron system inside a one-dimensional potential confinement with the configuration interaction method and an anisotropic Gaussian basis set in 2007[295], and in 2008 extended this to a three-electron system[296].

This Chapter reports results of studies of the HRgX molecules in such confinements. Two types of studies were carried out. First, I did computations of the two-body decomposition pathway of HRgX systems inside a harmonic confinement. Then, I analyzed the effect of various types of analytical confinement on the excited and ionized states of HRgX. The two-body decomposition pathway was chosen because it has been shown to be the more likely channel through which the metastable HRgX will dissociate into HX + Rg.[37] The following reactions are relevant to the formation and decomposition of the rare gas halohydrides:

$$\mathrm{H}_{(g)} + \mathrm{X}_{(g)} + \mathrm{Rg}_{(g)} \rightarrow \mathrm{HRgX}_{(g)}, \qquad \Delta E_1, \tag{7.1}$$

$$\mathrm{HRgX}_{(g)} \rightarrow \mathrm{HX}_{(g)} + \mathrm{Rg}_{(g)}, \qquad \Delta E_2, \tag{7.2}$$

$$\mathrm{HRgX}_{(g)} \rightarrow \mathrm{HRgX}^{\mathrm{TS}}_{(g)}, \qquad \Delta E^{\mathrm{TS}}. \tag{7.3}$$

The HRgX found in Reaction (1) proceeds through the transition state barrier (Reaction 3) and decomposes to produce a free rare gas atom and an HX molecule (Reaction 2).

7.2 Computational Methods

The decomposition reaction for an HRgX species rearranging and decomposing into HX + Rg was studied inside a planar harmonic confinement at two levels of theory with three Model Core Potentials (MCP) basis sets. The first round of computations used the Restricted Hartree-Fock (RHF) method with an improved Model Core Potential (iMCP) basis set. The iMCP basis sets were chosen because they combine the high-quality description of the core region, which is characteristic of Model Core Potentials (MCPs), with improved efficiency in integral and gradient evaluation due to the inclusion of an L-shell in the basis set.[83,195,196]. The second round of computations were done with the Møller-Plesset second order (MP2) perturbation theory[31] in conjunction with the augmented triple-zeta MCP basis set aug-MCP-TZP. The third series of computations, in which I computed the effect of confinement upon the excited electronic states and ionized states of HRgX, used the coupled clusters method with singles, doubles, and non-iterative triples (CCSD(T))[33,219], and the completely renormalized CCSD(T) equation-of-motion (CR-EOMCCSD(T))[297–299] method, again with the aug-MCP-TZP basis set.

The MCP basis sets I used included both a relativistic basis set and a non-relativistic basis set, whose compositions are described in Table 7.1. Details of this format for basis set description are given in the Computational Methods section of Chapter 5.

Both the model core potential and the harmonic confinement potential used in this work require the addition of extra terms to the Hamiltonian for the system. The additional terms required by the Model Core Potentials basis sets have already been described in detail in Chapter 1, in Equations 1.18 to 1.34.

Two different types of confining potentials were used in this study: a planar po-

Table 7.1: *Composition of MCP basis sets*[a]

Atom	iMCP-NR2	iMCP-SR2	aug-MCP-TZP
H	[311/11/1]	[311/11/1]	[411/211/21]
F	[311/311/2/1]	[311/311/2/1]	[2111/2111/211/21]
Cl	[311/311/2/1]	[311/311/2/1]	[2111/2111/311/21]
Xe	[511/511/62/1]	[511/511/62/1]	[51111/41111/6111/21]
Rn	[611/611/62/1]	[611/611/62/1]	[61111/51111/7211/31]

[a] Basis set composition given in [S/P/D/F] format.

tential and a cylindrical potential. For the planar potential, the term that represents harmonic potential confinement contains parameters whose values are chosen based on the symmetry of the confined molecule. An ideal potential is defined so that it conforms to the symmetry of the molecule and any effect of the confinement experienced by the nuclei will be completely uniform throughout the entire molecule. In the present case, the cylindrical potential will produce a uniform confinement for the molecule when it is linear, and the planar potential will produce a uniform confinement for the molecule when it is in its transition state and other angles along the decomposition pathway. For an atom, the ideal potential shape would be spherical. For a molecule in C_s symmetry in planar confinement, the harmonic potential extends above and below the plane of the molecule. For each electron present in a molecule located in the xy-plane, such as the HRgX transition state, this potential takes the following form:

$$W(r_i) = \omega[z_i - z_0]^2 \tag{7.4}$$

where z_i is the Cartesian coordinate of the potential, z_0 is the origin of the potential, ω is an adjustable parameter representing the strength of the potential. Potential strengths of $\omega = 0.00, 0.10, 0.20, 0.30$, and 0.40 a.u. were used in this study.

Combining these terms results in a molecular Hamiltonian of the following form for the planar potential:

$$H_{MCP,W}(1, 2, ..., N_v) = \sum_{i=1}^{N_v} \hat{h}_{MCP}(r_i) + \sum_{i>j}^{N_v} \frac{1}{r_{ij}} + \omega \sum_{i}^{N_v} [z_i - z_o]^2. \tag{7.5}$$

For the cylindrical potential, the principal axis of the potential is chosen to coincide with the z-axis of the molecule. As with the planar potential, the confinement exerted by the cylindrical potential is uniform in nature so that all nuclei of the HRgX molecule experience the same confining effect:[293]

$$W(r_i) = \frac{\omega^2}{2}\sum_i[(x_i - x_0)^2 + (y_i - y_0)^2] = \sum_i \frac{\omega^2}{2}(x_i^2 + y_i^2) \tag{7.6}$$

The cylindrical potential is added into the molecular Hamiltonian in the same way as the planar potential:

$$H_{MCP,W}(1, 2, ..., N_v) = \sum_{i=1}^{N_v} \hat{h}_{MCP}(r_i) + \sum_{i>j}^{N_v} \frac{1}{r_{ij}} + \frac{\omega^2}{2}\sum_i (x_i^2 + y_i^2). \tag{7.7}$$

The orientation of the transition state and of linear HRgX in these potentials are shown in Figure 7.1.

The effects of confinement within a harmonic potential on the stability of the transition state and the decomposition reaction of HRgX were examined by optimizing the geometry of the HRgX species at fixed increments of the angle H-Rg-X along the decomposition pathway. This was accomplished with the non-gradient total energy minimization routine TRUDGE in GAMESS-US[278], with coordinates defined in terms of Hilderbrandt internal coordinates[300].

In addition to the analysis of quantum confinement effects on the dissociation energy barrier, the two lowest-lying excited states of each HRgX of each irreducible representation within the C_{2v} point group were identified with the completely renormalized CCSD(T) equation-of-motion (CR-EOMCCSD(T))[297–299] method. This method was chosen over the more efficient CCSD-EOM (EOMCC) method due to the inability of EOMCC to describe states with significant contributions from two-electron transitions[301] and bond-breaking. The CR-EOMCCSD(T) excitation energies – those generated by correcting EOMCC excitation energies with perturbative triples – were chosen for analysis as suggested in the GAMESS Coupled Clusters documentation.

To what degree is the singlet, closed-shell ground state wavefunction of each HRgX multi-reference, and if so, what effect does the increase in strength of a planar, con-

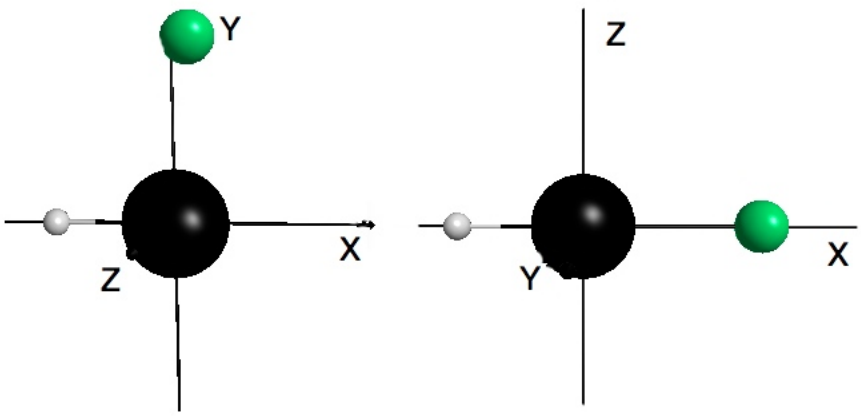

Figure 7.1: *Orientation of transition state and linear HRgX within the harmonic potential*

fining potential alter this multi-reference character? Without any confinement, the absolute values of T1 amplitudes for HRgX are 0.03 and of the T2 amplitudes are at a maximum 0.05, indicating that the unconfined, ground-state wave function is essentially single-reference. The T1 and T2 amplitudes of HRnF increase by at most 3% when the confinement is increased from ω=0 to ω=0.4 and up to 5% for HRnCl. For HXeF and HXeCl, these amplitudes increase by a maximum of 1.5% and a maximum of 5%, respectively. Therefore, the ground states of HRgX do not receive significant contributions from any singly or doubly excited configurations. It is thus clear that any multi-reference character of the ground state wave function is minimal. Consequently, further energy computations on the decomposition pathway are done with the single-reference MP2 method.

By analyzing the effect of confinement on the energies and ordering of the lowest

excited states of HRgX, I hope to understand which molecular orbitals and electrons are affected most strongly by confinement. Further calculations with the CCSD(T) ionization process (IP-EOM3A)[302,303] method identified the molecular orbitals out of which an electron may be most easily ionized in a confined HRgX, providing a more detailed picture of confinement effects on HRgX.

MacMolPlt[264] was used to visualize electron density distributions. All computations were carried out on dual-core or dual-quad core Apple Macintosh computers at the University of Alberta.

7.3 Results and Discussion

Results for relativistic and non-relativistic basis sets with the RHF method are compared first, followed by individual sections where structural and energetic results computed at the MP2/aug-MCP-TZP level of theory for each HRgX are discussed in detail. Next, results of CR-EOM and IP-EOM3A computations for excited states of HRgX are discussed.

HRgX are small molecules, 78 to 92% of whose mass comes from the nucleus of the rare gas. Consequently, relativity will play a significant role in determining the structure of the molecule. Table 7.1 shows that iMCP-NR2 and iMCP-SR2 basis sets differ only in the way relativity is treated; the number of contracted functions for each atom is identical. This provides an optimum situation for illustrating the effect that relativity plays in the structure of HRgX. Figure 7.2 illustrates this in detail for the $80^\circ \leq \Theta_{H\,Rg\,X} \leq 120^\circ$ region of the decomposition pathway. Both for HRgF and HRgCl, the relativistic basis set produces a transition state with a smaller H-Rg-X angle and a smaller energy barrier than does the non-relativistic basis set. For HRnF, the transition state occurs at approximately $\Theta_{H\,Rg\,X} = 100^\circ$ when computed with non-relativistic iMCPs, but narrows to $\Theta_{H\,Rg\,X} = 95^\circ$ when computed with the relativistic iMCP. The relativistic basis sets and core potentials significantly change the shape of the decomposition pathway curve, as can be seen from the change in the angle at which the transition state occurs.

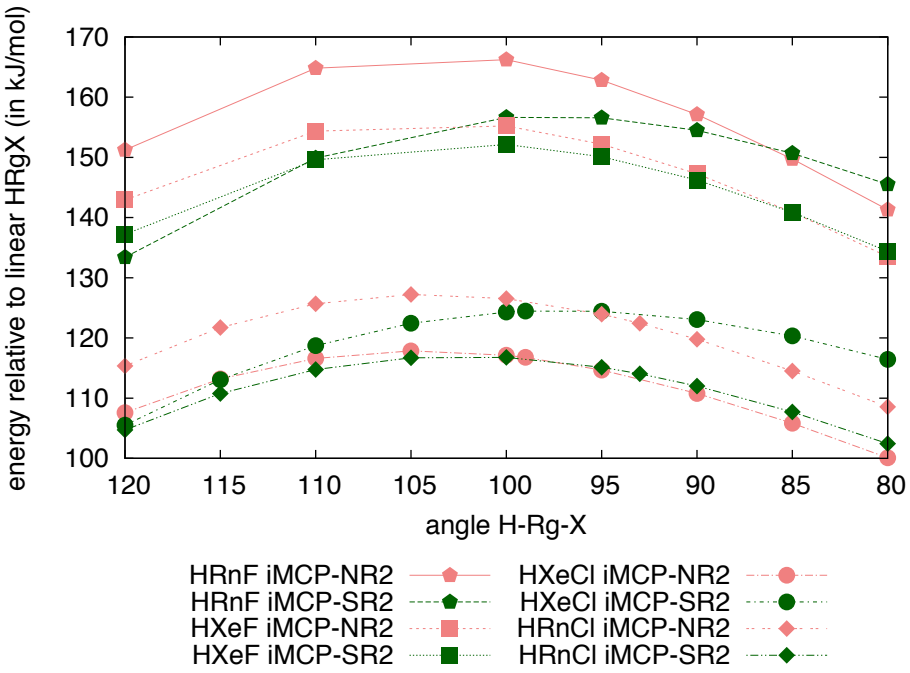

Figure 7.2: *Profile of decomposition pathways of HRgX near the transition state without confinement at the RHF/iMCP-NR2 and RHF/iMCP-SR2 levels*

7.3.1 MP2 Decomposition Pathways in Confinement

In this section, I intend to explore how the confinement affects HRgX species through analysis of the geometry of HRgX, of the geometry of the transition state, and through analysis of the molecular orbitals of HRgX. Discussion of specific results for each molecule is given below. The region of interest on the decomposition pathway for HRnF is shown in Figure 7.3 for ω=0, 0.10, 0.20, and 0.30 a.u. A few features of this graph are immediately apparent. First, the difference in ΔE at the transition state between the strongest confining potential (ω = 0.30 a.u.) and the weakest (ω = 0.0 a.u.) is 5 kJ·mol^{-1}. The points for the first few weakest potentials are very close to the points for the unconfined species, indicating that a confinement strength of at least ω = 0.20 a.u. is needed to produce a qualitative difference in ΔE_{TS} values. Second, all six arcs for the various confinement strengths peak in approximately the same location along the x-axis as does the arc for the unconfined HRnF, indicating that this harmonic potential does not alter the angle $\Theta_{H\,Rn\,F}$ of approximately 95°

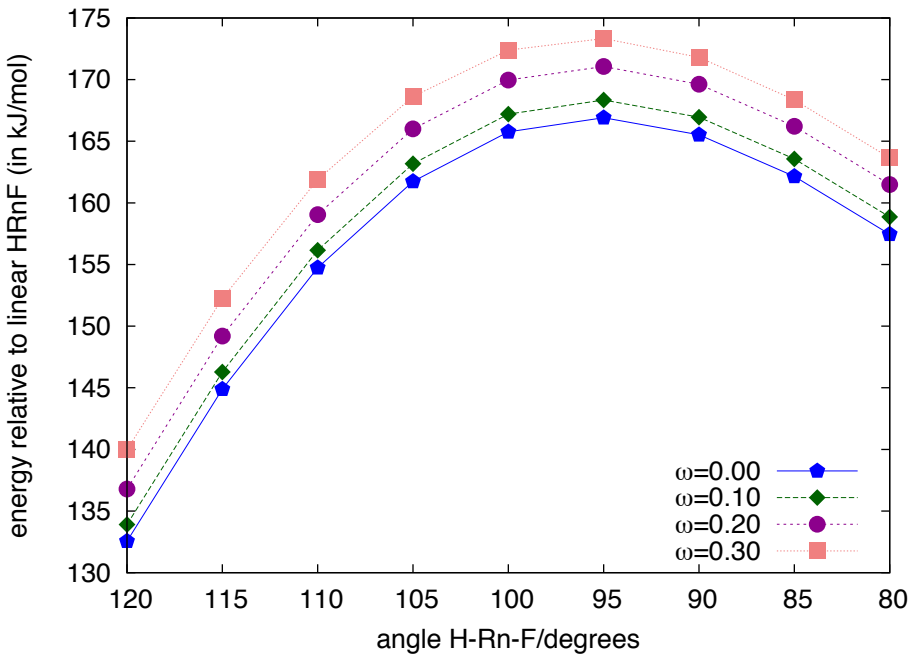

Figure 7.3: *Expanded region of HRnF decomposition pathway in confinement at the MP2/aug-MCP-TZP level*

at which the transition state occurs. Confinement in a harmonic potential stabilizes the HRnF species by increasing the energy barrier to the transition state. For HXeF (Figure 7.4), increasing the strength of the confinement does not alter the angle of about 100.0° at which the transition state occurs. Similarly the energy barrier to the transition state is increased as the confining potential becomes stronger, kinetically stabilizing the triatomic species. The harmonic confinement produces the same effects upon HRnCl (Figure 7.5) as it does upon HRnF. Absence of confinement leads to the lowest barrier to the transition state, followed by the weakest confinement; the highest energy barrier to formation of the transition state results from the strongest ($\omega = 0.30$ a.u.) confinement. The strongest confinement increases the energy barrier by 10.5 kJ·mol^{-1}. Increasing confinement strength has no effect upon the angle $\Theta_{H\,Rn\,Cl}$ of about 94 ° at which the transition state occurs. Results are shown in Figure 7.6 for HXeCl and illustrate that increasing the strength of the confinement raises the energy barrier to the transition state.

The angle at which the transition state occurs (approximately 100° for HXeCl) is

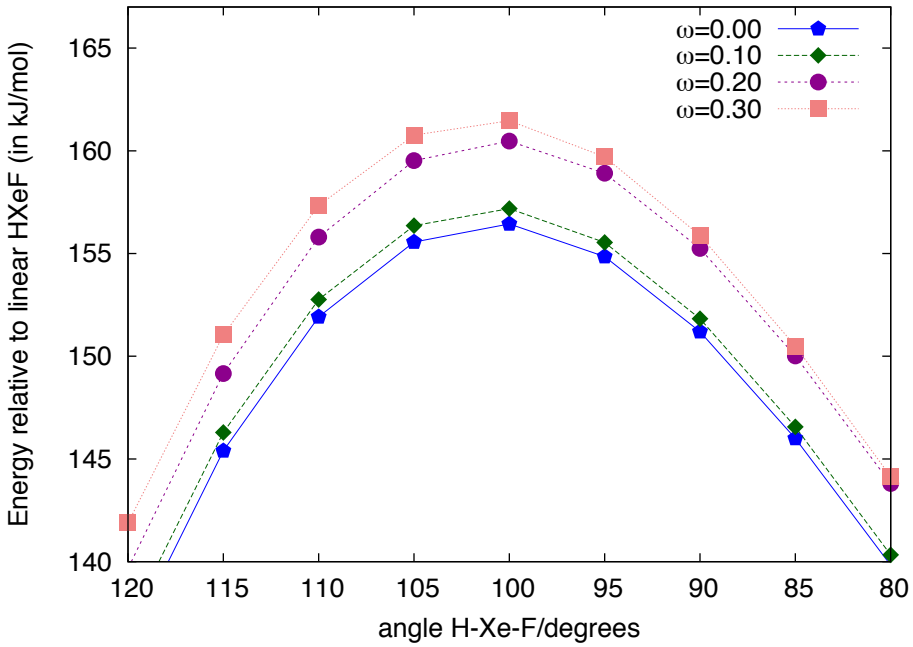

Figure 7.4: *Expanded region of HXeF decomposition pathway in confinement at the MP2/aug-MCP-TZP level*

unaltered by an increase in confinement strength. It is clear that geometry optimizations at fixed angle increments along the HRgX decomposition pathway in the planar confinement shows that neither the presence nor the change in strength of the confining potential alters the angle at which the transition state occurs, indicating that the electrons most involved in the decomposition are not in those molecular orbitals that are affected by the confinement.

7.3.2 Excited States in Linear HRgX Systems

The excitation energies of the lowest two excited states of each irreducible representation in the C_{2v} point group were computed in both types of confinement for confinement strengths of ω=0, 0.1, 0.2, 0.3, and 0.4 a.u. with the CCSD(T)/aug-MCP-TZP level of theory.

The energy difference between the unconfined ground electronic states and the confined ground electronic states in cylindrical confinement for each HRgX molecule at each confinement strength are shown in Figure 7.7. As expected, as the strength

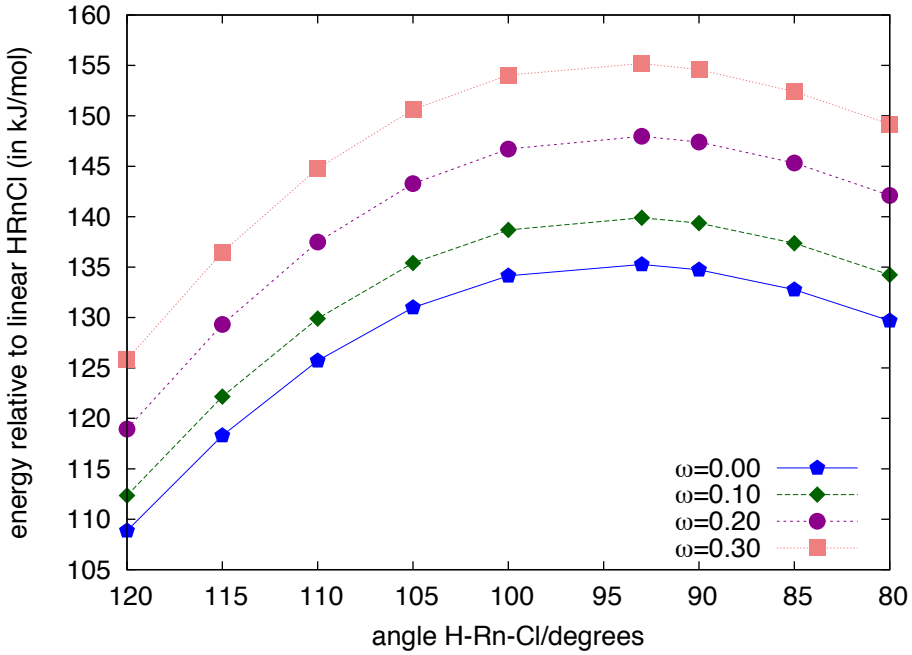

Figure 7.5: *Expanded region of HRnCl decomposition pathway in confinement at the MP2/aug-MCP-TZP level*

of the confinement increases, the energy of the ground state does as well.

Planar Confinement: C_{2v} Symmetry

The HRgX molecules belong the the $C_{\infty v}$ point group. This point group transforms as follows to the C_{2v} point group which was used for computations in GAMESS-US: Σ^+ becomes A_1; Σ^- becomes A_2; Π becomes B_1 and B_2. Consequently, the X^1B_1 and A^1B_2 states are degenerate. As the confinement strength increases, this degeneracy breaks. The full C_{2v} symmetry was used for both cylindrical confinements and for planar confinements, with the confining potential extending parallel to the z-axis.

In the absence of any confining potential, several states are degenerate. The lowest-lying $A\ ^1B_1$ and $B\ ^1B_2$ states are degenerate with each other, as are the next $E\ ^1B_1$ and $D\ ^1B_2$ states. The $G\ ^1A_2$ and $H\ ^1A_2$ states are also degenerate. A confinement of only 0.1 a.u. is needed to break the degeneracy in both sets of $^1B_1$ and $^1B_2$ states and in the $G\ ^1A_2$ and $H\ ^1A_2$ states for HRgF, but for HRgCl a confinement of at least 0.2 a.u. is necessary to break the degeneracy in the $G\ ^1A_2$ and $H\ ^1A_2$ states.

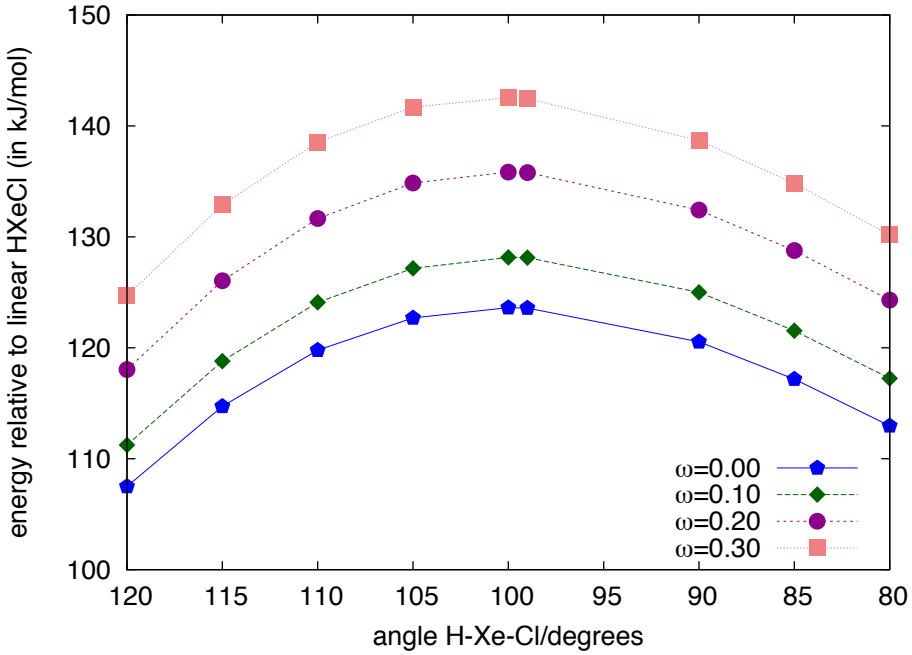

Figure 7.6: *Expanded region of HXeCl decomposition pathway in confinement at the MP2/aug-MCP-TZP level*

For all confinement strengths, the lowest-lying $A\ ^1B_1$ (or the $A\ ^1B_1/B\ ^1B_2$ degenerate state for ω=0) has the lowest excitation energy and is therefore the most accessible. Additionally, it is the only state to steadily decrease in excitation energy as the confinement strength is increased, hinting that the molecular orbitals containing the bulk of the electron density are orthogonal to the principal axis of the confinement, and are not experiencing the full strength of the potential. Conversely, once the degeneracy of the $G\ ^1A_2$ and $H\ ^1A_2$ states is broken, the $G\ ^1A_2$ state increases dramatically in excitation energy, as does the $C\ ^1A_1$ state. Clearly, these states hold electrons in molecular orbitals that are strongly affected by the confining potential.

Both the rare gas and the halogen are responsible for the ordering of the excitation energies of the excited states of HRgX: this can be seen through inspection of Figures 7.8, 7.9, 7.10 and 7.11. The trends exhibited by the excitation energies eight lowest-lying excited states of HRnF and HRnCl resemble one another closely. At the highest confinement strength, the most accessible states are the $A\ ^1B_1$ and either $E\ ^1B_1$ or the $B\ ^1B_2$ state. For HRnF, the $E\ ^1B_1$ becomes degenerate with the

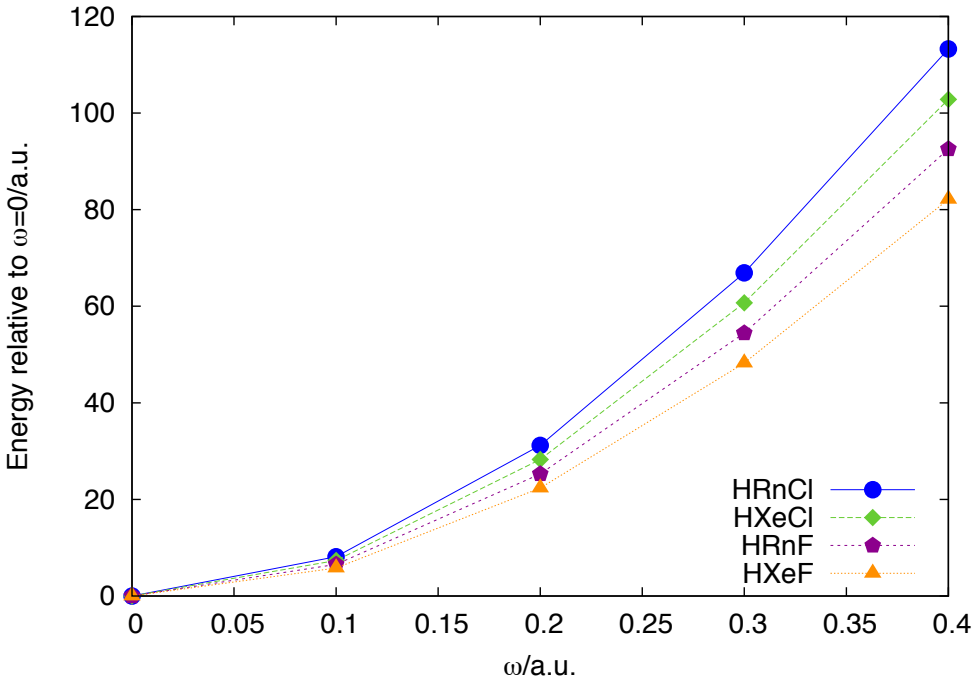

Figure 7.7: *Effect of cylindrical confinement on the energy of the ground electronic state of HRgX; CCSD/aug-MCP-TZP*

$G\ ^1A_2$ state at ω=0.4 and has the median excitation energy. The three most accessible states for HRnF, then, are $A\ ^1B_1$, $B\ ^1B_2$, and $G\ ^1A_2$. For HRnCl, all degeneracies are broken by ω=0.2 and the three lowest-lying states are $A\ ^1B_1$, $E\ ^1B_1$, and $B\ ^1B_2$.

For HXeF and HXeCl, the three most inaccessible states at the highest confinement strength are $H\ ^1A_2$, $F\ ^1A_1$, and $G\ ^1B_2$. In the case of HXeF, the $D\ ^1B_2$ state is degenerate with the $G\ ^1A_2$ state. For both molecules, the $A\ ^1B_1$, $E\ ^1B_1$, and $B\ ^1B_2$ states are the three lowest-lying, with the latter two being degenerate and the $C\ ^1A_1$ state being the next lowest state.

Cylindrical Confinement: C_{2v} Symmetry

It is important to note that unlike in the planar confinement, in cylindrical confinement the B_1 and B_2 states are degenerate – therefore the two lowest-lying excited states of each of the three unique symmetry labels are discussed. The actual symmetry of HRgX in cylindrical confinement is $C_{\infty v}$, but the Abelian point group C_{2v} was

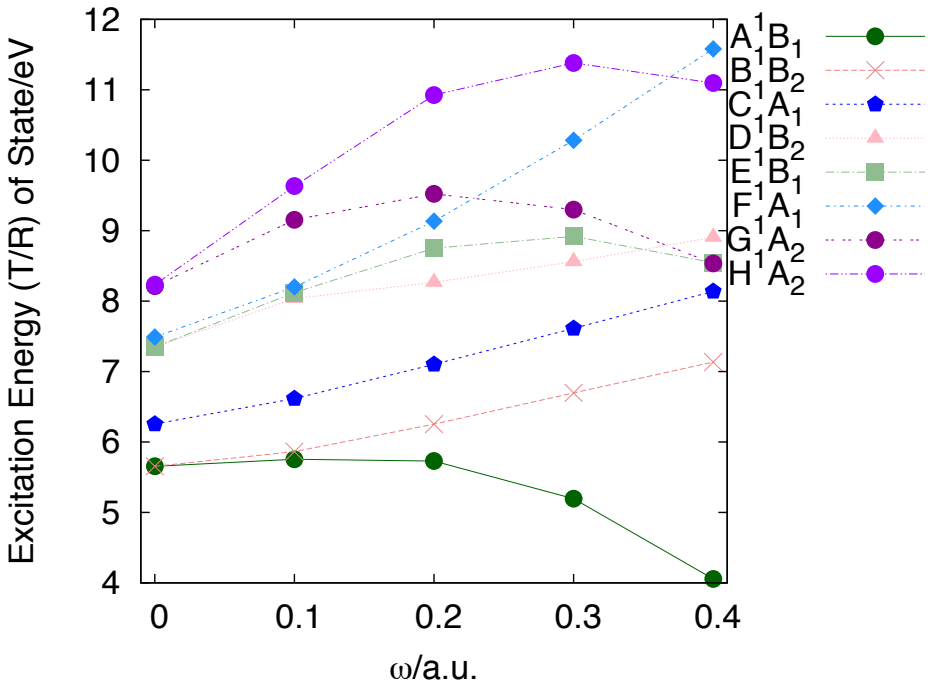

Figure 7.8: *Effect of planar confinement on the excitation energy of HRnF, CR-EOM/aug-MCP-TZP*

chosen for use in MP2 computations as it is a subgroup of $C_{\infty v}$. With the exception of the $A\ ^1B_1$ state, all excited states ultimately increase in excitation energy when the strength of the confining potential is maximized. When unconfined, the excited states of HRgX are in the following order, from the lowest-lying to highest: $A\ ^1B_1$, $B\ ^1A_1$, $C\ ^1B_1$, $D\ ^1A_1$, followed by the $E\ ^1A_2$ and $F\ ^1A_2$ states, which are degenerate in energy. As the strength of the confining potential increases, the states retain the same order with an increase in the excitation energy between each state. For HRnF, HXeF, and HXeCl, at ω=0.20 a.u. the $D\ ^1A_1$ state becomes degenerate with the $E\ ^1A_2$ and $F\ ^1A_2$ states. For HRnCl, the $C\ ^1A_1$ state does not become degenerate but at ω=0.2 a.u. decreases in excitation energy to 9.6 eV. Plots of the excitation energies to these states as a function of increasing potential strength are given in Figures 7.12 through 7.15.

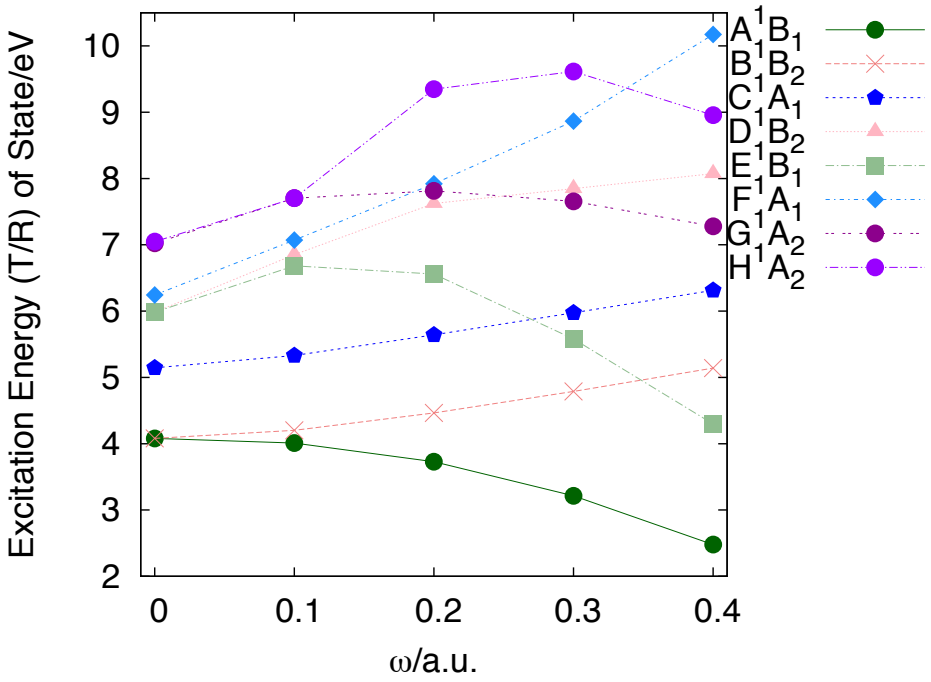

Figure 7.9: *Effect of planar confinement on the excitation energy of HRnCl, CR-EOM/aug-MCP-TZP*

7.3.3 Analysis of Ionization Potentials for HRgX

Vertical ionization potentials from the singlet, closed-shell ground state of HRgX (X $^1A_1$ in C_{2v} or X $^1A'$ in C_s) were computed with the IP-EOM CCSD(T)[302,303] method in order to evaluate the effect of an increase in strength of a confining potential on the accessibility of various excited states. These ionization potentials were computed for each linear HRgX in both planar and cylindrical confined environments at the same range of potential strengths as were the excitation energies: ω=0, 0.1, 0.2, 0.3, and 0.4 a.u. The lowest-lying vertically ionized states for all $HRgX^+$ ion is the $A\ ^2B_1$ state, and for chlorides the $B\ ^2B_2$ is equally accessible. The shape of the potential does not alter which state is the most accessible; only the strength of the potential is relevant. For all HRgF, the $^2A_1$ state is the lowest-lying when unconfined or weakly confined, but as potential strength increases the ionization potentials of all excited states decrease, with the ionization potential of the $A\ ^2B_1$ state decreasing

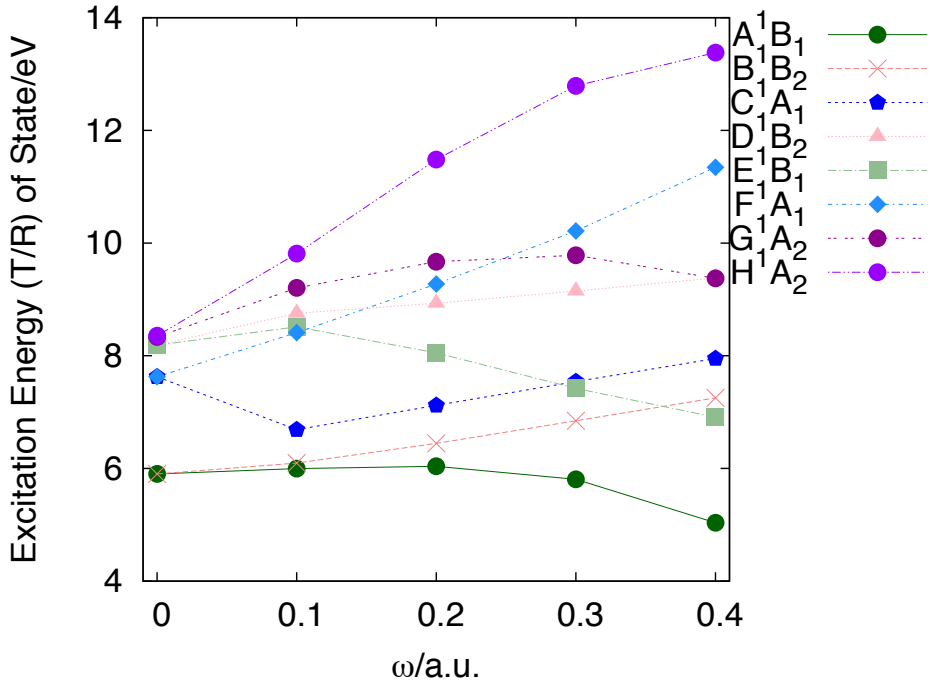

Figure 7.10: *Effect of planar confinement on the excitation energy of HXeF, CR-EOM/aug-MCP-TZP*

most rapidly, causing it to become the most accessible state by the time the potential strength is 0.2 a.u. HRgCl are most easily ionized to the $A\ ^2B_1$ state regardless of the strength of the potential; it is relevant here to note that in the case of the cylindrical potential, the $A\ ^2B_1$ state has a degenerate $A\ ^2B_2$ companion due to the symmetry imposed on the molecule: in the $C_{\infty v}$ representation, these states would together comprise the Π irreducible representation. In all cases where the $A\ ^2B_1$ state is the lowest-lying, there is an accompanying $^2B_2$ state of slightly higher ionization potential. In the planar confinement, the $^2B_1$ and $^2B_2$ states are degenerate when the molecule is unconfined, but as the confinement strength increases, the $^2B_1$ state decrease in ionization energyl more sharply than all other state, becoming the most accessible. For HXeCl at a potential strength of 0.20 a.u., the accompanying $^2B_2$ state passes the $^2B_1$ state in ionization potential and is the most accessible state. However, as the confining potential strength continues to increase the $^2B_1$ state again becomes

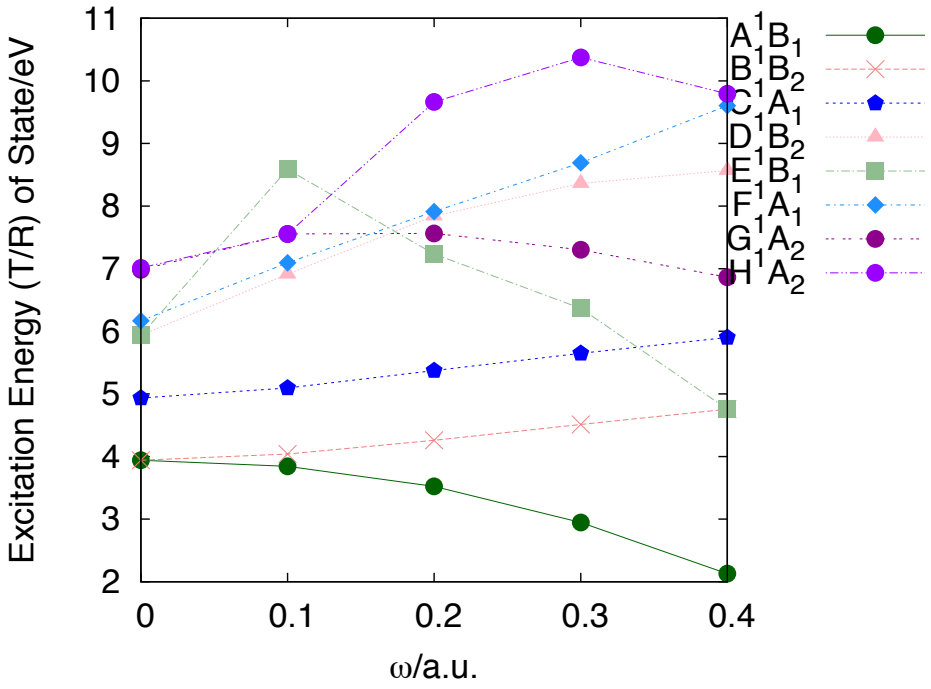

Figure 7.11: *Effect of planar confinement on the excitation energy of HXeCl, CR-EOM/aug-MCP-TZP*

dominant.

7.3.4 Molecular Orbitals and Ionization by Pressure in Planar Confinement

Molecular orbitals of HRgX in C_{2v} symmetry fall into two categories in relation to the confining potential: those which are in the plane of the confining potential and are thus relatively unaffected by it, and those that are perpendicular to the plane of the potential, and experience the largest effect. For unconfined HRnF, the highest occupied molecular orbital (HOMO) is of a_1 symmetry and is composed of the s valence atomic orbital from all three atoms in the molecule, with about $\frac{1}{3}$ of its character originating from each. The (HOMO-1) molecular orbital is an equal combination of the p_y atomic orbital of radon and fluorine, and the (HOMO-2) is a combination of p_x atomic orbitals of radon and fluorine. When HRnF experiences confinement

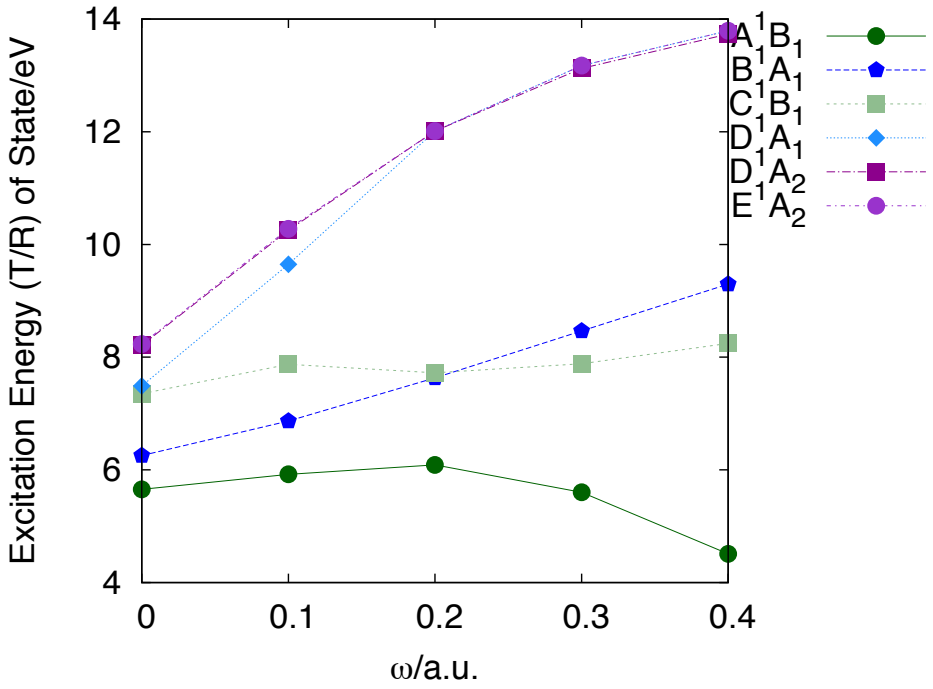

Figure 7.12: *Effect of cylindrical confinement on the excitation energy of HRnF in a cylindrical confinement, CR-EOM/aug-MCP-TZP*

by a planar potential that is oriented parallel to the z-axis, the (HOMO-1) is most strongly affected due to being perpendicular to the plane of the confining potential. Conversely, the (HOMO-2) is barely affected at all, as it lies parallel to the potential. The B_2 (HOMO-1) is so strongly affected by the confinement that its orbital energy increases until it replaces the original A_1 HOMO as the highest energy occupied MO at a potential strength of ω=0.2 a.u. This effect can be seen in Figure 7.16. Pressure ionization, or the removal of an electron through quantum confinement of sufficient strength to ionize it, has been recently reviewed[304] and is relevant to the present studies of HRgX molecules in confinement. While ionization energies reported here have been computed with the CC-IPEOM method, ionization by pressure have also been related to Koopman's theorem: the reduced binding energy, calculated as a ratio of the binding energy for a confined ion and the binding energy of the free ion, is typically determined using orbital energies obtained through Koopmans theorem.[304]

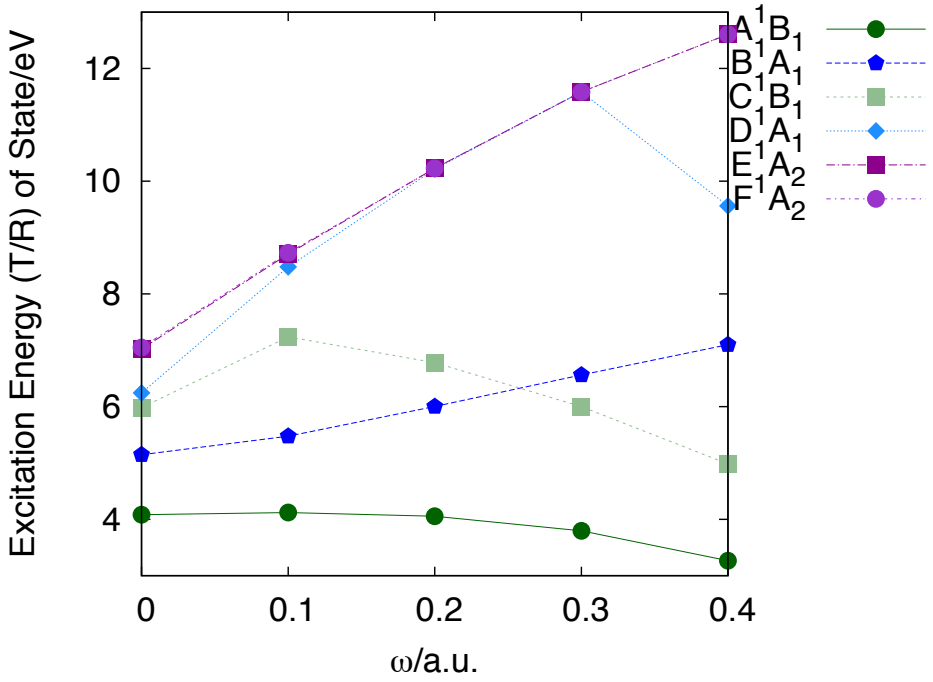

Figure 7.13: *Effect of cylindrical confinement on the excitation energy of HRnCl in a cylindrical confinement, CR-EOM/aug-MCP-TZP*

When the strength of the confining potential increases by 0.1 a.u., the energy of the B_1 molecular orbital (HOMO-1 at ω=0.1 a.u.; HOMO at ω=0.2 a.u.) also increases by about 0.1 E_h. (Figure 7.16.) Extrapolating from this, HRnF would then require a confining potential of 0.6 a.u. in order to force an electron out of this B_1 molecular orbital.

7.4 Conclusion

Computed decomposition pathways of HRgX in confinement demonstrate that in harmonic confinement radon halohydrides have greater kinetic stability than similar xenon halohydrides. The effect of a relativistic basis set on the location of the transition state (Figure 7.2) is to both decrease the angle at which the transition state occurs and to lower the ΔE_{TS} for the molecule. The relativistic basis set decreased the ΔE_{TS} by 4% for HRnF and by 10% for HRnCl. Single-point wave functions and

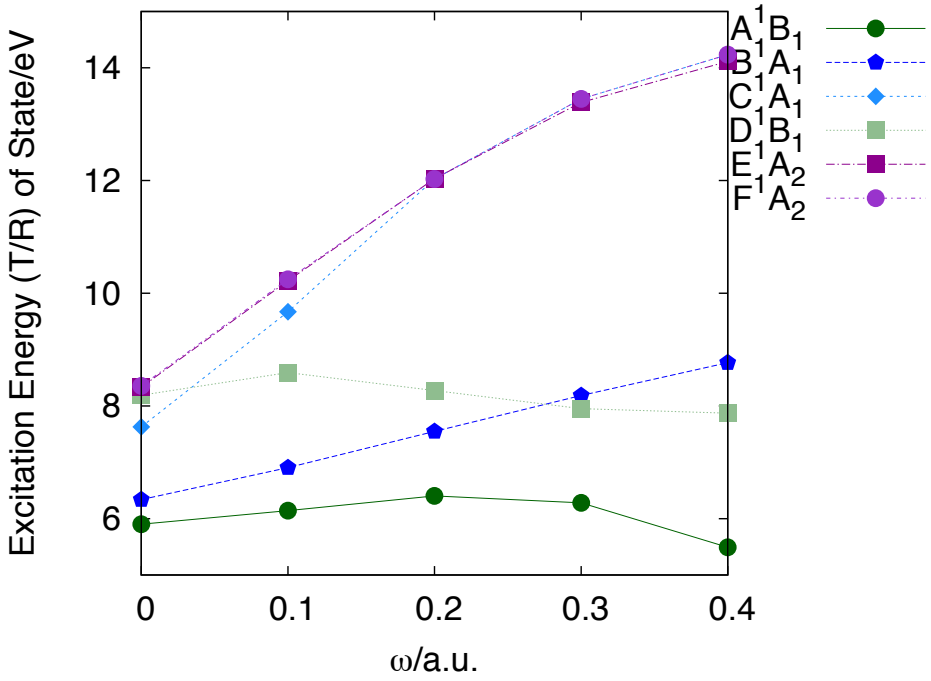

Figure 7.14: *Effect of cylindrical confinement on the excitation energy of HXeF in a cylindrical confinement, CR-EOM/aug-MCP-TZP*

energies computed at the CCSD(T)/aug-MCP-TZP level of theory reveal that the ground state wavefunction of HRgX is primarily single-reference in character, and that this character is independent of the presence or strength of a confining potential. Decomposition pathways for HRgX were computed inside harmonic confining potentials to examine two effects: (1) the effect of confinement on the angle H-Rg-X at which the transition state occurs; (2) the effect of confinement on kinetic stabilization of the HRgX species, as measured by the height of the energy barrier at the transition state. My results have demonstrated that for all four HRgX molecules the harmonic potential does not significantly affect the angle at which the transition state occurs. For all HRgX, the potential has a stabilizing, if small, effect on the molecule, increasing the energy barrier to the transition state by 9.9 kJ·mol^{-1} for HRnF and by 10.5 kJ·mol^{-1} for HRnCl. For HXeF, the energy barrier is only 4 kJ·mol^{-1} higher in the strongest confinement, whereas HXeCl is gains an additional 25 kJ·mol^{-1} to its energy barrier.

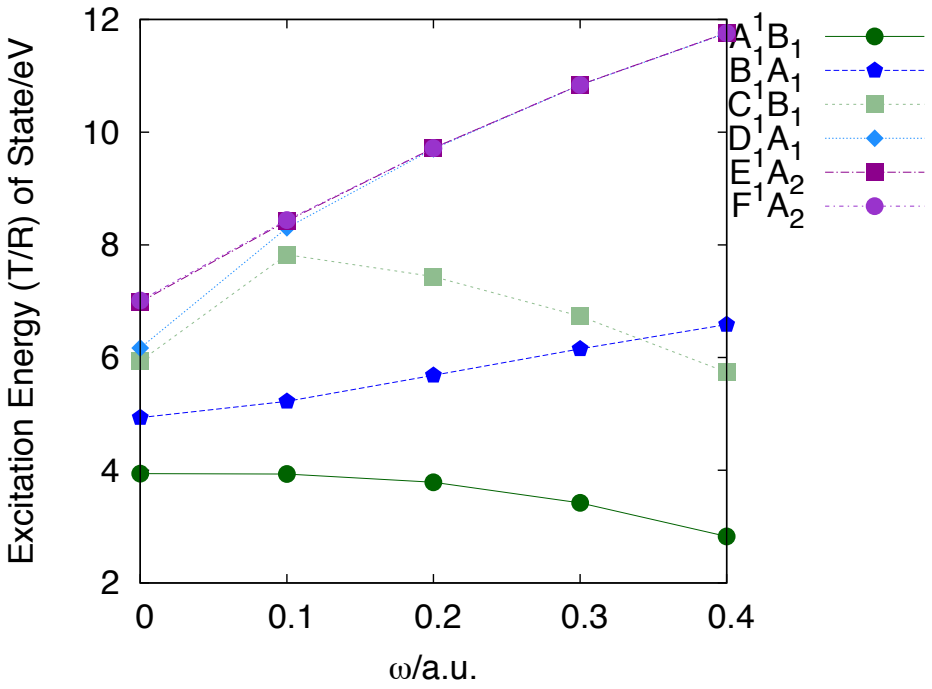

Figure 7.15: *Effect of cylindrical confinement on the excitation energy of HXeCl in a cylindrical confinement, CR-EOM/aug-MCP-TZP*

The symmetry of the lowest-lying excited states of HRgX does, however, depend strongly on the strength of the confining potential. The most straightforward situations are the HRgX confined in the cylindrical potential, where the states of A_1 and A_2 symmetry become degenerate as the strength of the confining potential increases, and the excitation energy of the $^1B_1$ state decreases uniformly while all other states ultimately increase excitation energy with respect to their values at ω=0.00 a.u. The $^1B_1$ state dominates as the most accessible in the planar confinement as well, and in reference to excitation energies at ω=0.00 a.u., only the $^1B_1$ state also decreases in energy with respect to the ground state. Other states increase in excitation energy, creating a larger excitation energy between the states at ω=0.40 a.u. Results of vertical ionization potentials computations confirm that the $^1B_1$ state is the most accessible of the excited states of HRgX in all cases except for unconfined or weakly confined HRgF.

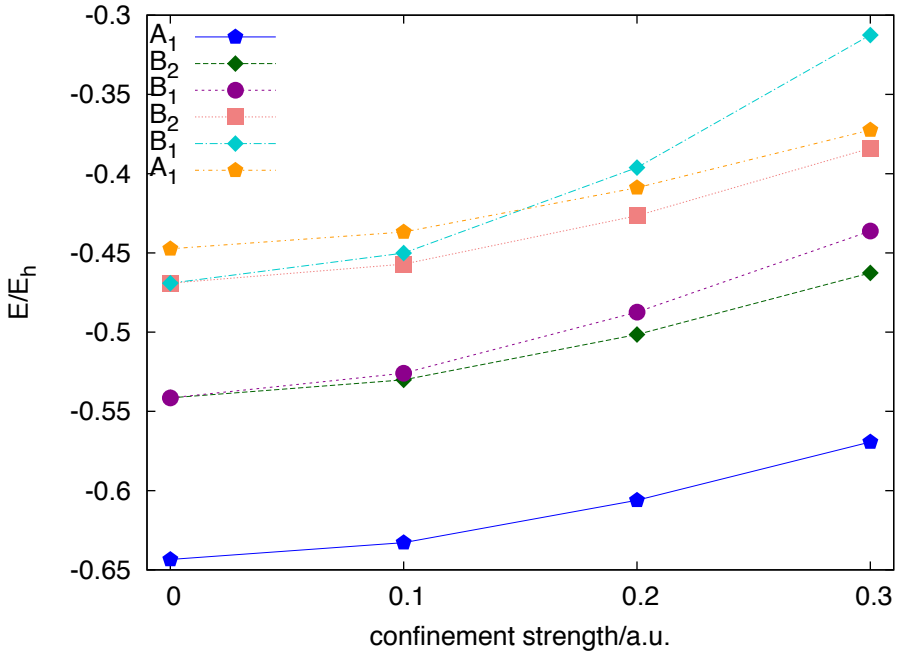

Figure 7.16: *Energies of the Six Highest Molecular Orbitals of HRnF, CCSD(T)/acp3*

Chapter 8

Effects of Discrete Confinement on the Properties and Reactions of HRgX

8.1 Introduction

In the previous Chapter, the effect of confinement within an analytical harmonic potential upon HRgX molecules was discussed. In this Chapter, I extend the idea of confining HRgX to a model rare gas matrix that is more representative of the experimental conditions under which HRgX molecules have been synthesized. As noted in Chapter 1, the first HRgX species to be synthesized were HXeCl, HXeBr, and HXeI, which Pettersson et al.[36] synthesized in 1995 through photodissociation of the HX molecule inside a low-temperature rare gas matrix. This would become the standard method for synthesizing all small (five atoms or less) rare gas containing compounds, and in the years since this group has applied this method to synthesize HXeCCH, HXeOH, HXeSH, HKrOH, and many other rare gas containing molecules. Indeed, no other method for synthesizing HRgX species has been proposed to date. Examples of this abound: In 2000, Pettersson et al. synthesized HXeNCO inside a solid xenon matrix;[67] Khriachtchev et al. synthesized HXeCCH and related compounds in a solid xenon matrix in 2003.[90] These and other developments in HRgX chemistry were reviewed by Gerber in 2005.[109] Computational studies have been a part of the chemistry of HRgX molecules from the beginning: it was with the aid of vi-

brational spectra computed with the MP2 method and effective core potentials that Pettersson et al. were able to confirm that the HXeX species they studied were new, triatomic compounds rather than simply van der Waals adducts of HX and Xe.[36] On the computational side of HRgX chemistry, the majority of the literature has focused on obtaining geometries, vibrational spectra, and properties of these species in the gas phase. Other early computational studies include the work of Johansson et al. in 1999, in which they located the four lowest-lying excited states of HXeCl,[45] and the work of Lundell et al. in 2000, who analyzed the role anharmonicity plays in the vibrational spectra of HXeI.[56]

While HRgX species have been shown to be thermodynamically metastable, and kinetic stability has been predicted[274] in Chapters 2 through 6, these questions have been previously addressed in the gas phase and in solvents described by the polarized continuum model. This is an important first step, but the investigation must not end there, as HRgX species are never synthesized in the gas phase, but are always synthesized as part of a low-temperature rare gas matrix.

Almost twenty-five years after the first HRgX compound was reported, much of their reactivity is understood. However, theoretical models of these species in the solid state have not yet been reported. For this reason, I have studied HRgX compounds within a helium matrix in order to create a theoretical model that goes toward the actual experimental conditions under which these molecules exist. In order to do this, I have designed a sheet of gas-phase helium atoms and placed the optimized HRgX structure between a pair of these sheets. In this environment, the well-known decomposition reaction of HRgX:

$$\mathrm{HRgX} \rightarrow \mathrm{HRgX}^{\mathrm{TS}}, \qquad \Delta E^{\mathrm{TS}} \tag{8.1}$$

$$\mathrm{HRgX} \rightarrow \mathrm{HX} + \mathrm{Rg}, \qquad \Delta E, \tag{8.2}$$

has been studied in detail. The effects of confinement within helium sheets on $\Delta \mathrm{E}_{TS}$ and ΔE are discussed. Additionally, I discuss the effect of altering the location of the HRgX molecule within the helium sheets upon the decomposition pathway and on the structure of the transition state. The effect of confinement upon the bonding

in HRgX is elucidated through analysis of the electron density of the molecule by Quantum Theory of Atoms in Molecules (QTAIM).[200]

8.2 Computational Methods

In previous Chapters, the majority of my reported results have come from second-order Møller-Plesset perturbation theory (MP2) computations. The helium sheets are large, composed of 64 helium nuclei each, and including them in an MP2 computation would add significant computational costs to the project. I have compared results from MP2 computations and Restricted Hartree-Fock (RHF)[305] computations in order to determine if the RHF method is sufficiently accurate for the properties in which I am interested in the present Chapter.

Comparison of computed decomposition pathways with the (RHF) method and the Møller-Plesset second order perturbation theory (MP2)[31] methods reveal that the main problem with RHF is in the values of ΔE_{TS}, while the RHF and MP2 structural parameters agree quite well. Bond lengths of HRgX at the transition state and energy barriers are compared in Table 8.1 and show identical values of r(Rg-H) for the two methods and differences of less than 0.08 Å for values of r(Rg-X), as well as identical angles at which the transition state occurs for the chlorides. For the fluorides HRnF and HXeF the structural parameters differ, with the RHF method overestimating this angle by 1-2°), indicating that the structure of HRgX is insignificantly affected by the change from MP2 to RHF method. However, the energy barrier at the transition state differs: the RHF method underestimates ΔE^{TS} by 12-13 kJ·mol^{-1} for HRgF and between 20-30 kJ·mol^{-1} for HRgCl.

As the underestimation is consistently small in magnitude, the RHF method is deemed to provide, for the purpose of the present study, qualitatively representative results for ΔE^{TS}. All electronic structure computations for confined systems were done using the RHF method in GAMESS-US.[278] MacMolPlt[264] was used to visualize electron density distributions. All computations were carried out on dual-core or dual-quad core Apple Macintosh computers at the University of Alberta.

Table 8.1: *Comparison of results obtained in the gas phase for the HRgX transition state with the MP2 and RHF methods with the iMCP-SR2 basis set*

Molecule/Method	r(Rg-X)$^{(a)}$	r(Rg-H)	$\Theta^{(b)}_{H\,Rg\,X}$	$\Delta E^{TS(c)}$
HRnF/RHF	2.54	1.67	98.6	154.2
HRnF/MP2	2.50	1.66	96.4	168.2
HXeF/RHF	2.48	1.57	102.8	149.2
HXeF/MP2	2.43	1.56	101.0	162.1
HRnCl/RHF	3.17	1.68	97.1	124.6
HRnCl/MP2	3.09	1.66	93.8	154.5
HXeCl/RHF	3.08	1.57	102.4	117.0
HXeCl/MP2	2.99	1.56	99.9	147.8

$^{(a)}$ In Å. $^{(b)}$ In degrees $^{(c)}$ In kJ·mol^{-1}.

The decomposition reaction for an HRgX species rearranging and decomposing into HX + Rg was studied inside confined environments with two Improved Model Core Potentials (iMCP) family basis sets. The iMCP basis sets were chosen because they combine the high-quality description of the core region, which is characteristic of Model Core Potentials (MCPs), with improved efficiency in integral and gradient evaluation due to the inclusion of an L-shell in the basis set.[83,195,196]. The iMCP basis sets we used included a relativistic basis set and a non-relativistic basis set, whose compositions are described in Table 7.1 of Chapter 7.

Confinement within the helium sheet is set up as follows. The HRgX molecule is placed in the xy-plane and aligned along the x-axis with a pair of planar sheets of helium atoms designed in C_s symmetry, with one sheet above the plane of the molecule, perpendicular to the z-axis, and its reflection below the xy-plane. These sheets contain eight helium atoms 2 Å apart in each dimension for a total of 64 helium atoms in each sheet, with a 2.5 Å space between the top sheet and the xy-plane. I also examined the effect that the placement of the HRgX molecule within the helium sheet has upon the structure of the transition state and the energy barrier to decomposition, as the strength of the confining effect experienced by the HRgX molecule depends on how the molecule is placed within the helium sheets. Three orientations of the HRgX molecule were examined. First, the HRgX molecule was centred with the

rare gas sitting directly underneath a helium atom, such that a plane parallel to the yz-plane could be defined by collinear He-Rg-He. This case will be referred to as configuration A in the discussion. Second, the rare gas was offset from the origin of the coordinate system by 1.0 Å, so that a vertical line extending through the rare gas would not pass through any helium atoms; this case was labelled configuration B. In

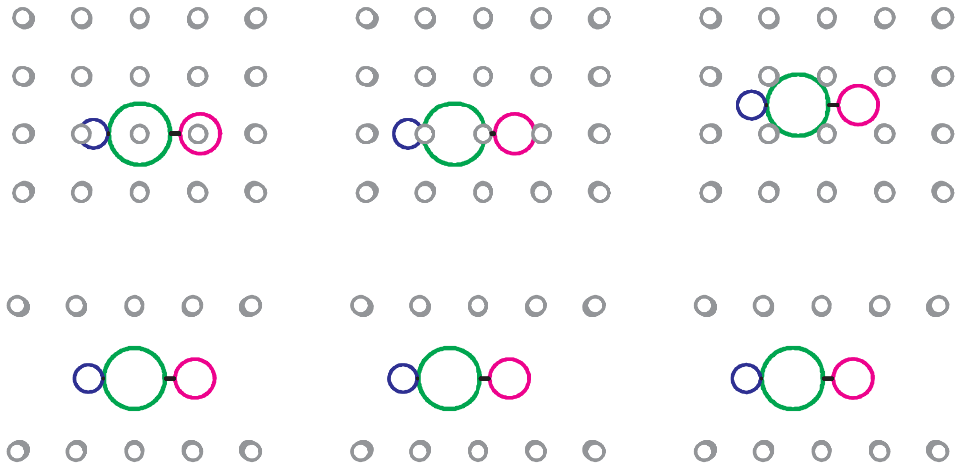

Figure 8.1: *Configurations of linear HRgX within helium sheets.*
Green: rare gas; pink: halogen; blue: hydrogen.
Left: configuration A; centre: configuration B; right: configuration C.
Top row: view from top in the xy-plane; bottom row: view from side in the xz-plane.
See text for details.

the third orientation the rare gas was positioned between four helium atoms, creating a body-centred tetragonal lattice which is referred to as configuration C. In all three cases, the HRgX molecule then extended in the xy-plane. These three configurations of HRgX in the helium sheets are shown in Figure 8.1. Planar sheets were chosen to model the rare gas matrix in which HRgX-type molecules are synthesized; when experimental research groups study reactions inside solid rare gas matrices, such as argon, these matrices are in the face-centred cubic configuration.

The effects of confinement on the stability of the transition state and the decomposition reaction of the HRgX species were examined by optimizing their geometries at

fixed increments of the angle HRgX ($\Theta_{H\,Rg\,X}$) along the decomposition pathway. This was accomplished with the non-gradient total energy minimization routine TRUDGE in GAMESS-US[278], with coordinates defined in terms of Hilderbrandt internal coordinates.[300] Two series of TRUDGE optimizations were carried out for each of the three orientations of the HRgX molecule described above. In the first series, the position of the rare gas was held fixed and only the bond lengths r(Rg-X) and r(Rg-H) were optimized for each HRgX angle. In the second series, the position of the rare gas was optimized in addition to the two bond lengths.

Results of geometry optimizations were analyzed using the AIMStudio program suite[250], which carries out Quantum Theory of Atoms in Molecules (QTAIM)[199,200] integrations and provides a graphical interface for designing figures. Because the MCP operators shift the core orbitals to virtual space, it was necessary to supplement the existing wavefunction file with additional electron density functions (EDFs)[252] for the QTAIM computations only. The EDFs appropriate for the MCP atoms were generated by scaling the EDFs produced by Gaussian09[253] for atomic calculations of fluorine, chlorine, xenon, and radon with the SBKJC[256,306] basis set.

8.3 Results and Discussion

The results for confinement in helium sheets will be presented in three parts: energy results for the first series of computations (with position of the rare gas atom fixed in TRUDGE optimization), energy results for the second series (with the rare gas allowed to move), and QTAIM analysis of the electron density.

8.3.1 Series 1: The Position of the Rare Gas is Fixed

The strength of confinement experienced by the HRgX molecule varies depending on the location of the molecule within the helium sheets. Varying the configuration with the position of the rare gas held fixed does not significantly alter the angle of the transition state, except in the case of HXeF, where the transition state occurs 5° earlier in configuration B than it does in configurations A or C. These angles are

tabulated in Table 8.2. Bond lengths between the rare gas and halogen for all HRgX increase from 0.01 Å to 0.05 Å when the configuration is changed from A to B to C. In configuration C, the rare gas is at its maximum distance from neighbouring helium atoms.

Table 8.2: *Approximate structure of HRgX transition state in configurations A, B, and C*[(a)]

Molecule-X	r(Rg-X)	r(Rg-H)	$\Theta_{H\,Rg\,X}$	$\Delta E^{TS(b)}$
HRnF-A	2.56	1.67	100	148.7
HRnF-B	2.55	1.67	100	160.5
HRnF-C	2.55	1.67	100	155.9
HXeF-A	2.50	1.57	105	143.8
HXeF-B	2.48	1.56	100	153.3
HXeF-C	2.48	1.57	105	150.2
HRnCl-A	3.15	1.67	95	123.6
HRnCl-B	3.20	1.67	95	135.0
HRnCl-C	3.20	1.67	95	130.2
HXeCl-A	3.08	1.57	100	114.2
HXeCl-B	3.09	1.57	100	126.2
HXeCl-C	3.09	1.57	100	122.6

[(a)] Bond lengths are given in Å; energies are given in kJ·mol^{-1}; angles are given in degrees. [(b)] As with the results given in Table 8.1, data here refers to the highest energy structure computed using five-degree increments along the decomposition pathway rather that the exact transition state of the molecule.

For all four HRgX species, the energy barrier is the lowest in the gas phase, as seen in Figure 8.2 for HRnX and in Figure 8.3 for HXeX, and highest in configuration B. These effects may be rationalized by considering the distances of the hydrogen and rare gas atoms from their nearest helium neighbours in each configuration. The greatest stabilizing effect is experienced by HRgX in configurations B and C, where the hydrogen, the atom that is displaced the most during the decomposition process, is situated either just in front of or just behind the line connecting the two helium atoms directly above the hydrogen, and as a result experiences the same strength of confinement in both configurations during the section of the pathway nearest the transition state, i.e. from 80° to 120°. The difference between the two is due to the location of the rare gas atom within the helium sheets. In configuration B, the heaviest

atom is located directly between the two nearest helium atoms while remaining in the same plane. This places it in greater proximity to the nearest neighbouring helium atoms than in configuration C, where the rare gas is in a body-centred tetragonal orientation, resulting in the maximum possible distance from the neighbouring helium atoms while remaining inside the helium sheets. Consequently, the confining effect experienced by the hydrogen is the same in both cases, while in configuration B the rare gas experiences a stronger confinement than it does in configuration C, resulting in a larger value of ΔE^{TS} by 3-5 kJ·mol^{-1}.

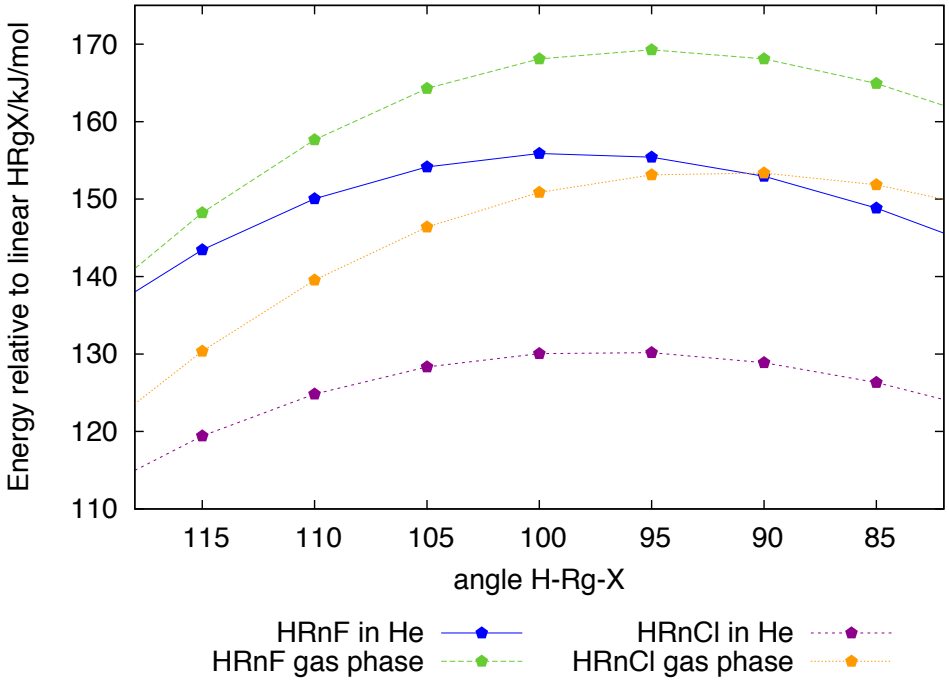

Figure 8.2: *Effect of confinement in a helium lattice in configuration A on the energy barrier of HRnX*

8.3.2 Series 2: The Position of the Rare Gas is Optimized

In the second series of computations the rare gas atom was allowed to move along the x-axis. The starting configurations A, B, and C described in the Methods section produced only two configurations after geometry optimization when the position of the rare gas was optimized. In configuration A the rare gas moved from its initial

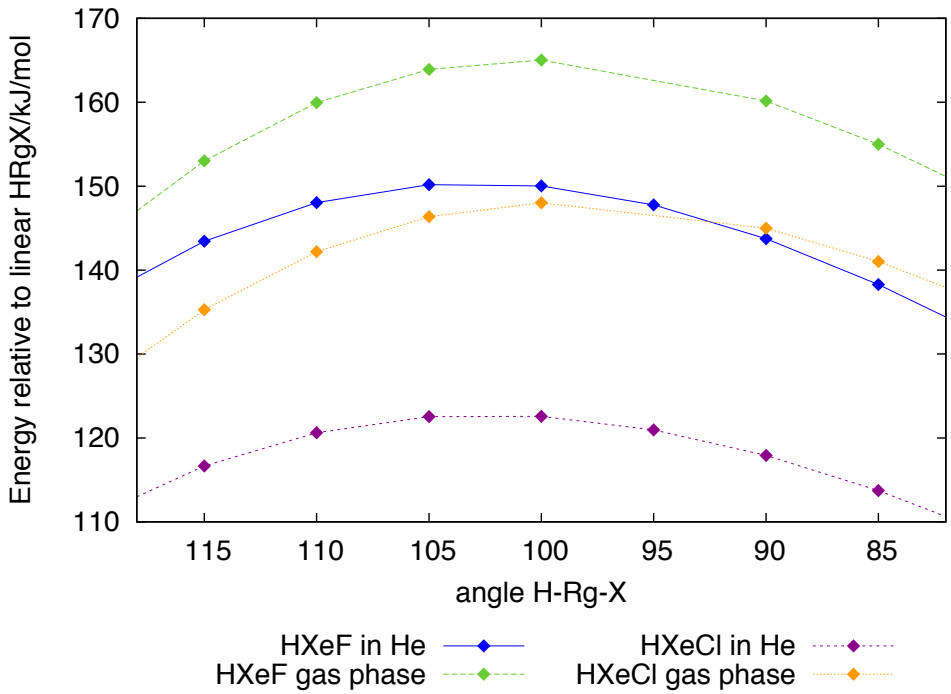

Figure 8.3: *Effect of confinement in a helium lattice in configuration A on the energy barrier of HXeX*

position either to the left or to the right towards the nearest helium neighbour, producing configuration B. When configuration B was optimized, the rare gas moved slightly back and forth to the left and right over the course of the optimization, ultimately settling in the same location as the rare gas in the optimized configuration A. Consequently, only results for configurations B and C will be discussed. During the optimizations of these configurations, the rare gas atom moves only slightly, responding to the movement of the hydrogen as it orbits the rare gas on its way towards the halogen. The movement of the rare gas is smaller in configuration C than in B, as any change in position of the rare gas in the former case results in an increase in the strength of the confinement experienced by the molecule, and is consequently energetically unfavourable.

The effect of allowing the rare gas to move during optimization on the bond distances within the HRnF molecule in configuration B is depicted in Figure 8.4, and

Figure 8.5 shows the same information for configuration C. Here and in subsequent tables, the notation "B-1" indicates configuration B, series 1, and "B-2" indicates configuration B series 2 results. While the two configurations produce slightly different geometries, especially in the 40°– 0° region of the decomposition process, the ability of the rare gas to move does not alter the optimized geometry. At 0°, the HRgX species has completely dissociated into a free rare gas and an HX.

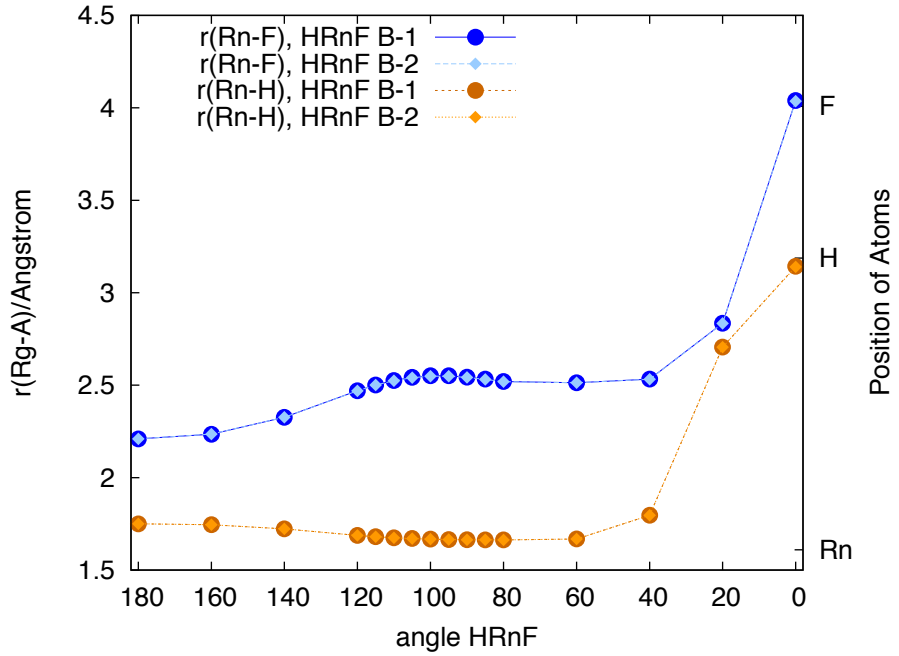

Figure 8.4: *Bond lengths for the HRnF molecule in configuration B*

In configuration B, HXeF has the same structure for both series 1 and series 2 computations, and closely resembles HRnF. This is shown in Figure 8.6. However in configuration C, the hydrogen from HXeF moves around to the opposite side of the xenon at the last angle computed (0°), so that the dissociated product is Xe + FH, rather than Xe + HF as is produced in configuration B, as shown in Figure 8.7.

The effects of optimizing the position of the rare gas upon the bond distances in the HRnCl molecule are given in Figure 8.8 for configuration B and in Figure 8.9 for configuration C. Throughout most of the decomposition pathway, the bond distance between the radon and the hydrogen (r(Rn-H) is unaltered from series 1 to series 2.

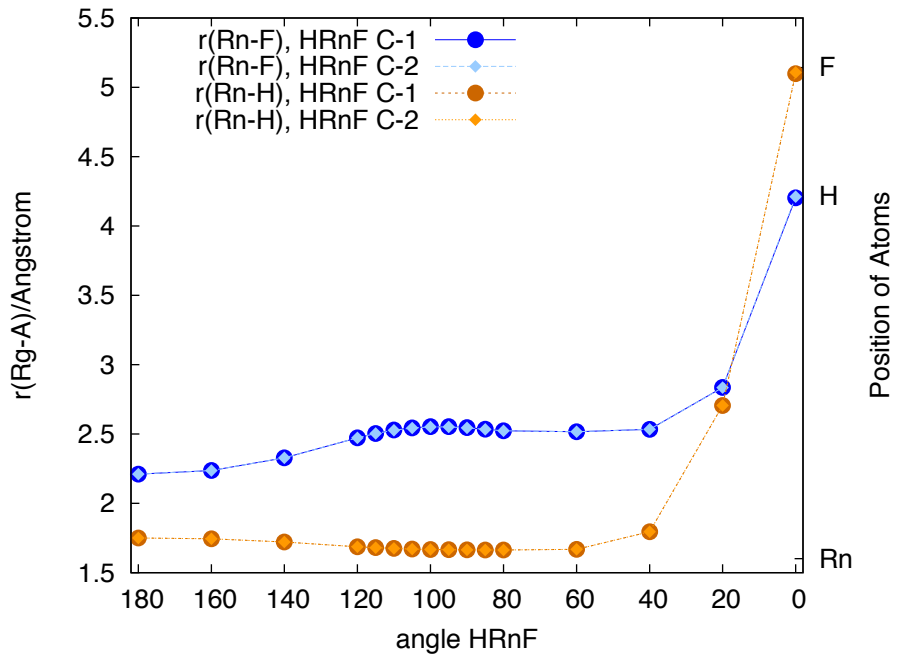

Figure 8.5: *Bond lengths for the HRnF molecule in configuration C*

The radon–chloride bond distance (r(Rn-Cl)) is always slightly longer in the series 2 computations than in series 1 for both configurations B and C. However, at the last angle for which I computed structures (0°), both bond distances r(Rn-H) and r(Rn-Cl) become slightly longer for the species in the series 2 computation. The lengthening of bond distances is caused by the constraints of the configurations: when the rare gas is allowed to relax and seek the lowest-energy position within its configuration, it has to move farther from the chloride in order to be at a maximum distance from the confining helium atoms.

In series 1 and 2 computations, the geometry of the HXeCl molecule is identical throughout the majority of the optimization process, unlike HRnCl. At the last step (0°), both bond distances become slightly longer for series 2 computations than the corresponding bond distance in series 1 computations, indicating that as the rare gas moves to minimize pressure from the helium sheet, the position of the other atoms in the molecule adjust as well. This can be clearly seen in Figure 8.10 for configuration B and in Figure 8.11 for configuration C.

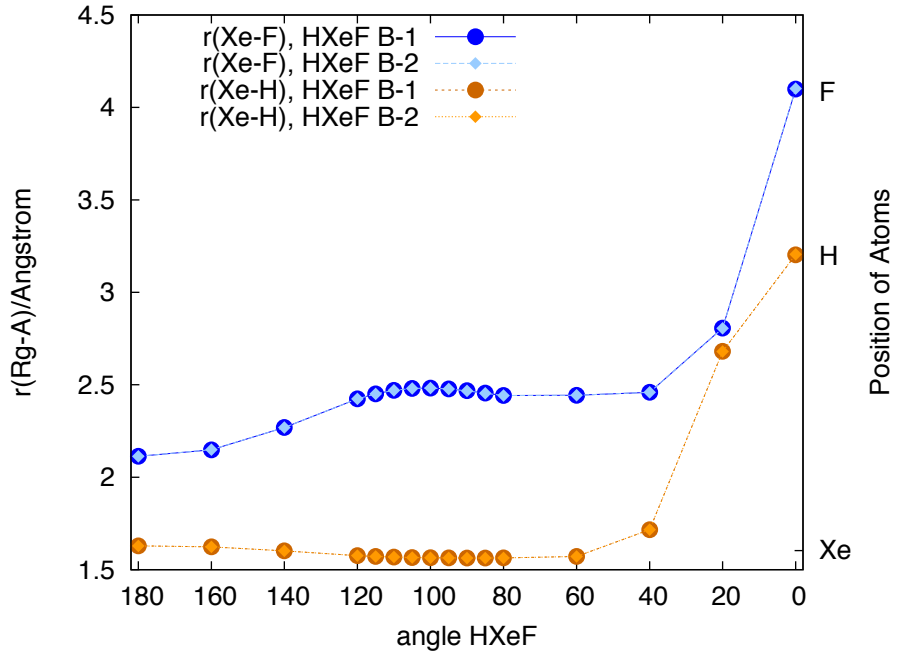

Figure 8.6: *Bond lengths for the HXeF molecule in configuration B*

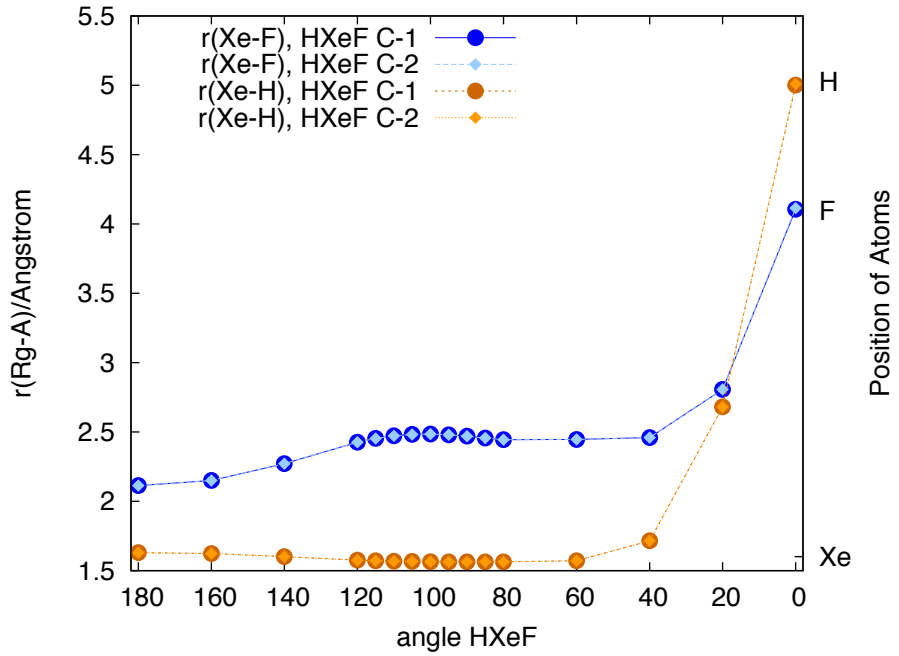

Figure 8.7: *Bond lengths for the HXeF molecule in configuration C*

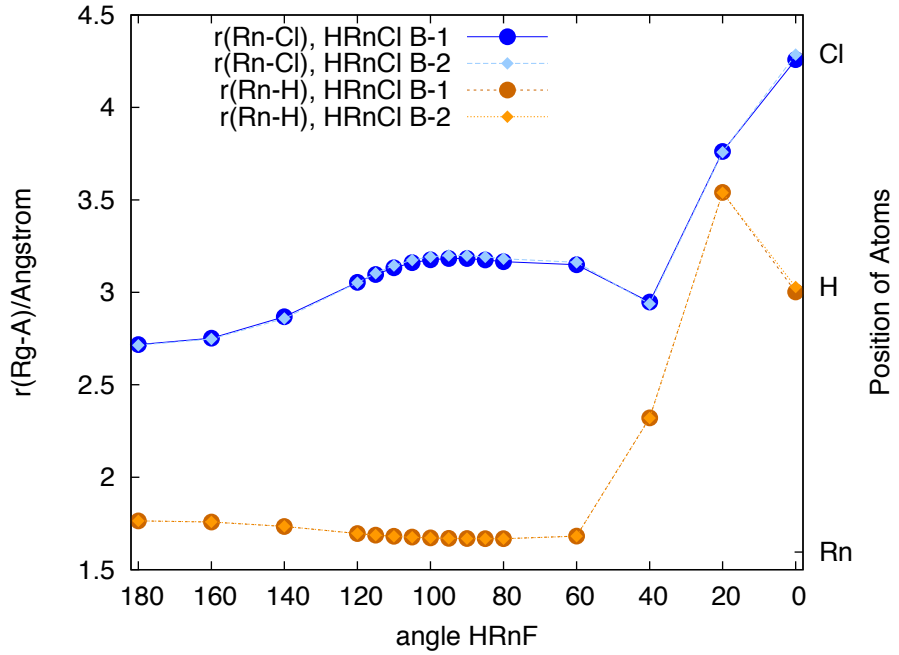

Figure 8.8: *Bond lengths of the HRnCl molecule in Configuration B*

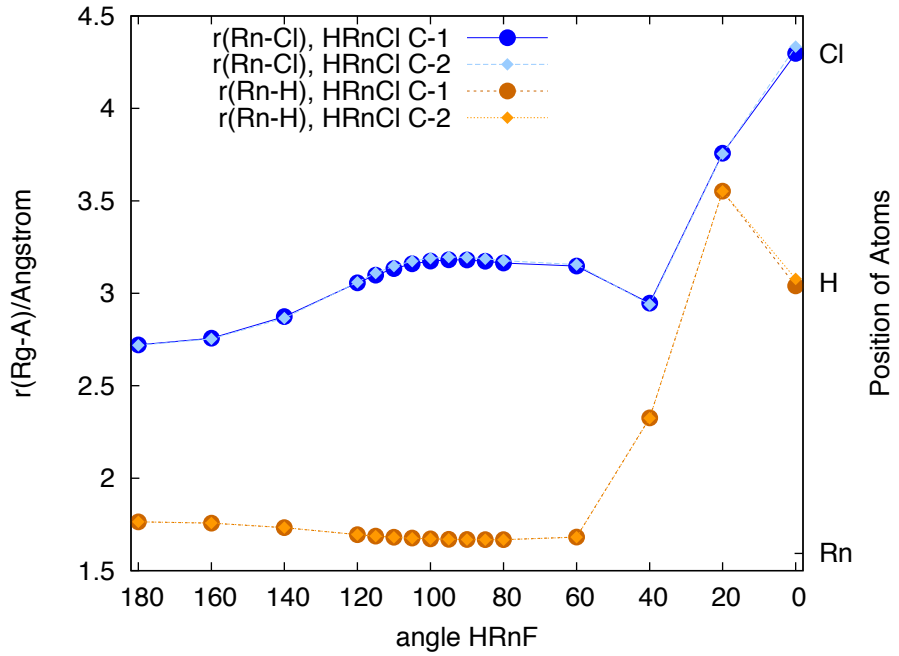

Figure 8.9: *Bond lengths of the HRnCl molecule in Configuration C*

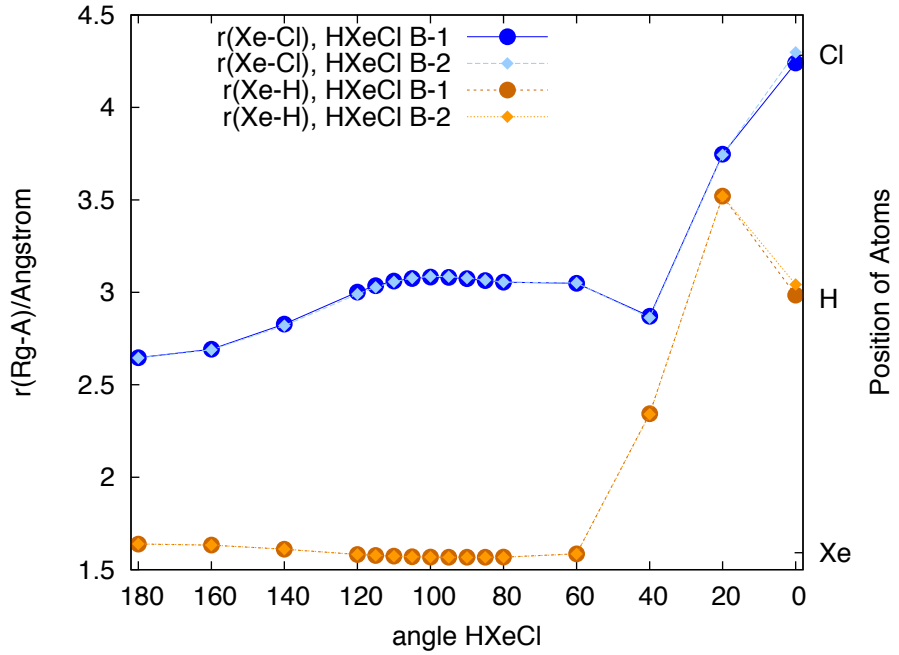

Figure 8.10: *Bond lengths for the HXeCl molecule in configuration B*

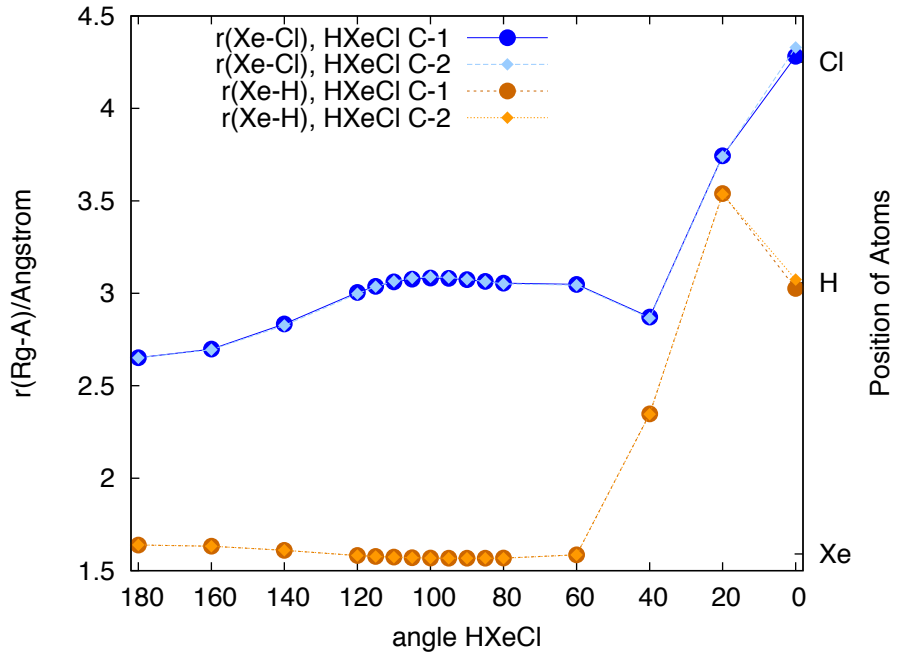

Figure 8.11: *Bond lengths for the HXeCl molecule in configuration C*

8.3.3 QTAIM Analysis of HRgX

Values of Laplacian of the electron density $\nabla^2(\rho)$ at bond critical points and the bond ellipticities computed for HRgX within configuration A illustrate several important features of the HRgX molecule in confinement. First, the changing values of $\nabla^2(\rho)$, shown in Table 8.3, illustrate the changing distribution of the electron density as the HRgX decomposes, with the Rg-H and Rg-X bonds dissociating and an H-X bond forming instead, and reflect the changing bonds between the atoms in the HRgX molecule. In all four cases, $\nabla^2(\rho)$ begins as a small, negative value when the HRgX molecule is linear, as expected for a pair of covalently bound atoms. The sign of

Table 8.3: *Laplacian of the electron density $\nabla^2(\rho)$ at the Rg-H bond critical points in configuration A*

Angle H-Rg-X				
Molecule	180°	TS	50°	0°
HRnF	-0.116	-0.304	-0.370	0.012
HRnCl	-0.131	-0.314	-0.318	0.006
HXeF	-0.180	-0.345	-0.419	0.008
HXeCl	-0.204	-0.357	-0.368	0.005

$\nabla^2(\rho)$ at a bond critical point reflects the nature of the interaction between the atoms involved: covalently bonded atoms will always produce a negative value of $\nabla^2(\rho)$. As the angle H-Rg-X decreases, the distance between the rare gas and the hydrogen shrinks as well and this increase in proximity is reflected in the increased magnitude of $\nabla^2(\rho)$ at the transition state angle as shown in the centre column of Table 8.3. As the decomposition continues to 50°, a slight increase in the magnitude of $\nabla^2(\rho)$ occurs in spite of an 0.03 Å increase in distance between the rare gas atom and the hydrogen for HRgF as the hydrogen prepares to dissociate completely and bond with the halogen. Finally, when the angle H-Rg-X of the HRgX complex reaches 0°, the distance between the hydrogen and the rare gas has increased to 3.3 Å for HRnF and to 3.4 Å for HXeF, producing no concentration at all of electron density between the two atoms, which are now outside of their respective van der Waals radii and bonded to the halogen atom.

Next, the bond ellipticities were computed as a measure of the bond order of the H-Rg and Rg-X bonds in the HRgX molecule when confined between helium sheets. Ellipticity is maximized for a π-bond, and a σ-bond or the σ-component of a triple bond will have ϵ=0, being perfectly cylindrically symmetrical about the internuclear axis.[200] Bond ellipticity values are collected in Table 8.4 and clearly show that both the Rg-H and the Rg-X bonds are wholly σ-bonds prior to dissociation. Ellipticities were computed in order to corroborate the findings of previous Natural

Table 8.4: *Bond ellipticity in linear HRgX in configuration A*

Molecule	H-Rg	Rg-X
HRnF	0.011	0.012
HRnCl	0.010	0.008
HXeF	0.010	0.011
HXeCl	0.009	0.004

Bond Orbitals (NBO) population analysis results, where the bonding in the HRgX molecule was shown to be $[H\text{-}Rg]^+$ X^-: an electrostatic interaction which would produce a σ-bonded compound[56,258,274]. The near-zero values of bond ellipticities indicate that interaction of the HRgX molecule with the helium sheets is not affecting the bond order of the confined molecule. Changes in $\nabla^2(\rho)$ and the values of the bond ellipticities demonstrate two important features of the HRgX molecule in confinement: first, that the changes in the values of $\nabla^2(\rho)$ which happen concurrently with the decomposition of the molecule indicate the points during the decomposition pathway at which electron density between the rare gas and the other atoms is reduced nearly to zero, indicating the dissolution of bonds. Second, the values of bond ellipticities confirm that the confinement is not deforming the geometry of the linear HRgX into an entirely new structure.

8.4 Conclusion

Computed decomposition pathways of HRgX in confinement demonstrate that in an environment which mimics experimental conditions radon halohydrides have greater

kinetic stability than analogous xenon halohydrides. Specifically, the energy barriers to decomposition of HRnX are larger in magnitude than the energy barriers to decomposition of similar HXeX. The QTAIM analysis of HRgX transition states confined between helium sheets in the example case of configuration A confirms the confining effect of the sheets and provides further insight into the decomposition process. Specifically, it pinpoints the angle along the decomposition pathway at which the rare gas is no longer bound to either the hydrogen or the halogen. In the case of HRgX species, that angle is less than 50°. Computed values of bond ellipticities indicate that confinement within a pair of helium sheets does not alter the order of either of the bonds within a linear HRgX species. Of the three configurations of the HRgX molecule within the helium sheet studied herein, confinement in configuration B produces the largest ΔE^{TS} and the greatest stabilizing effect on the HRgX molecule. When the position of the rare gas is optimized alongside the two bond lengths, no change in the bond lengths is observed, while in the case of configuration A, the molecule shifts into configuration B, thereby decreasing the strength of the confining effect experienced by the HRgX molecule. Due to this instability inherent in configuration A, experimentally one would expect to observe only configuration C: total energies for HRgX in configuration C are lower at 180°, the transition state, and 0° than the total energies of other configurations for every combination of rare gas and halogen, and the most energetically favourable case is C-2. Confinement within the helium sheets decreases the energy barrier to decomposition and therefore to stabilize the HRgX molecule, indicating that these metastable compounds should enjoy greater stability than has previously been predicted with gas phase computations.

Chapter 9

Anharmonic Effects in the Vibrational Spectra of Radon-Containing Small Molecules*

9.1 Introduction

For an element discovered over a century ago, little has been accomplished in the field of radon chemistry. Long thought to be completely inert even after Bartlett's discovery of xenon hexa-fluoroplatinate(V)[2], few radon-containing compounds were discovered. Part of this can be attributed to the very short half-life (3.8 days)[7] of radon, and its known carcinogenic properties. Highlights of research in this area include the work of Fields, Stein, and Zirin who created the first radon fluoride in 1962,[6] and in 1967 Haseltine and Moser successfully oxidized Rn-222 when it was produced through the decay of radium in a mixture of $RaBr_2$ inside ionic aqueous solutions.[9] In 1970, Stein synthesized radon difluoride[10], and Pitzer commented on properties and states of radon fluorides in his 1975 communication[12]. The state of radon chemistry in 1982 was reviewed by Avrorin et al.[16]. The year 1999 saw computations of the interaction energy of a radon-water complex[52] and an experimental study of the enthalpy of adsorption of ^{220}Rn, which has a short half-life of 55.6 s[51].

*A version of this chapter was published in *Chem. Phys. Lett.*, **2014**, *612*, 73.

The past three years have seen more interest in radon chemistry than the last decade. In 2000, Lundell et al. computed structures and anharmonic vibrational spectra for HRgF (Rg=He-Rn) molecules, finding that HRnF ought not to exist due to an extremely large Rn-F distance[59]. However, this result turned out to be an artifact of a particular basis set, and HRnF was indeed later shown to be stable *in silica*[258]. Interest in the other radon halohydrides lead to studies of HRnX (X=F, Cl, Br, I) molecules[160,307]. HRnCCH and HRnOH were predicted to be stable at room temperature[158]. Unstable compounds of radon and hypohalous acids were studied in 2012[308]. HRnCCH was studied along with HRnCCF, HRnCN, $HRnCF_3$ and $HRnCH_3$ and found to have a large energy barrier to their transition states along their two-bond dissociation pathway, indicating probable kinetic stability[274].

Frequencies of the vibrationally active modes of radon-containing molecules are some of the most useful data that theoretical chemists can provide to our experimental colleagues in order to assist in the identification of newly discovered molecules. Although no experimental vibrational spectra exist for the molecules studied herein, it is reasonable to expect that anharmonicity will play a large role in the spectra of HRnX, HRnAH, and $HRnBH_2$ for several reasons. First, xenon halohydrides, which are known to have very similar chemistry to radon halohydrides, have been shown to have vibrational modes with large anharmonic contributions[56,59]. Second, the vibrational modes of xenon halohydrides and HXeOH have been shown to be strongly coupled[57], a condition which cannot be accurately modelled with the simple harmonic approximation. Finally, anharmonic vibrational frequencies have been computed for several other small compounds of rare gases,[80,139,143,201,309–311] and a meaningful comparison between related compounds of rare gases requires that anharmonic effects be accounted for in radon-containing compounds.

In this Chapter, I present computed kinetics and anharmonic vibrational frequencies for the molecules HRnAH and HRnAF (A=O, S), $HRnZH_2$ and $HRnZF_2$ (Z=N, P). These compounds are interesting for their similarity to the familiar radon halohydrides, and provide a new perspective on radon chemistry.

9.2 Computational Methods

All geometries were optimized at the Møller-Plesset second-order perturbation theory (MP2)[31], which was described in detail in the Introduction, using aug-MCP-TZP[191] basis sets in the C_s point group. This level of theory, MP2/aug-MCP-TZP, was chosen based on the established reliability of the MCP-family basis sets[189], which are known for their many polarization, correlation, and diffuse functions as well as accurate reproduction of the core orbitals' nodal structure, and have been described in previous Chapters. The triple-zeta MCP basis set was chosen because triple-zeta valence basis sets are recommended for anharmonic frequency calculations as they produce frequencies accurate to about 50 cm^{-1}[312]. The aug-MCP-TZP basis set incorporates small core sizes ([He] for the first row atoms, [Ne] for the second row atoms, and [Xe] for radon) and extensive basis sets for the valence region of each atom: [411/211/21] for hydrogen, [2111/2222/211/21] for fluorine, [2111/2111/211/21] for oxygen, [2111/2111/311/21] for sulfur, [2111/2111/211/21] for nitrogen, [2111/2111/311/21] for phosphorus, and [61111/51111/7211/31] for radon. This basis set notation was described in detail in the Computational Methods section of Chapter 5. The basis set for hydrogen was different from the standard MCP-ATZP basis set provided with GAMESS-US distribution: the s-portion of the basis set was taken from the work of Yamamoto and Matsuoka[313] and polarization/correlating functions were designed by Noro et al.[207]. The shorthand notation for contracted basis sets, $(n_1^s\, n_2^s\, \ldots\, n_K^s \,/\, n_1^p\, n_2^p\, \ldots\, n_L^p \,/\, n_1^d\, n_2^d\, \ldots\, n_M^d \,/\, n_1^f\, n_2^f\, \ldots\, n_N^f)$, indicates that there are $K, L, M,$ and N contracted functions in $s, p, d,$ and f symmetries, respectively, with the number of primitive functions in each contracted function being, taking as an example the s symmetry, n_1^s, n_2^s, ..., n_K^s[314].

ΔG for the transition state (ΔG^{TS}) ΔG of decomposition (ΔG_2) were computed from these structures, according to the following reactions:

$$HRnAX_n \longrightarrow HRnAX_n^{TS}, \qquad \Delta G^{TS} \tag{9.1}$$

$$HRnAX_n \longrightarrow Rn + HAX_n, \qquad \Delta G_2 \tag{9.2}$$

Harmonic vibrational frequencies in the ground electronic state for each molecule

were computed to confirm that the optimized structures were minima on their potential energy surfaces. Anharmonic vibrational frequencies of the ground electronic state for each molecule were computed with the correlation-corrected Vibrational Self-Consistent Field (cc-VSCF) method, an application of perturbation theory to the computation of anharmonic vibrational excitations. In this approach, the assumption is made that "correlation effects for [low-lying vibrational excited states] are relatively small, and can be treated by perturbation theory"[315]. Correlation effects are included as a component of the perturbation operator, and as with the MP2 method, high-order correlation corrections are assumed to be negligible compared to the the second order correction. Properties (the vibrational states) and the second-order energy correction are obtained from the first-order corrected wavefunction.

Anharmonic vibrational frequencies of the fundamentals, the first and second overtones, and the combination bands associated with the fundamentals and first two overtones were computed. The implementation of the cc-VSCF method in GAMESS-US[278] by Chaban et al.[316] includes two different levels of accuracy for computing anharmonic vibrational frequencies: the quartic force field (QFF) approximation[317], which approximates the potential energy surface of a molecule with a fourth-degree polynomial, and the direct method, which directly computes the potential energy surface of the molecule. In each case, pairs of energy and dipole values are computed using the MP2 density matrix for the molecule of interest. This code currently does not treat symmetry, causing a small splitting in normally degenerate frequencies as described by Chaban and Gerber.[310] Visualization of results was accomplished with the MacMolPlt program.[264] All cc-VSCF computations used the May 2013 version of the GAMESS-US program suite on the Grex cluster of Westgrid and on dual-core 2.66 GHz Intel Apple Macintosh computers at the University of Alberta.

9.3 Results and Discussion

First, optimized geometries of all molecules will be discussed, followed by a discussion of Reactions 9.1 and 9.2. Next, timing information for cc-VSCF computations with

the direct and QFF methods will be compared, and then results for the representative molecules HRnSH and $HRnPH_2$ will be discussed in detail. Complete harmonic vibrational data, optimized structures, and energies of the decomposition reaction for all of the $HRnAX_n$ studied in this Chapter, together with all similar data for the transition state of each $HRnAX_n$ are available in the Appendix to this Chapter.

Geometries of HRnOH, HRnOF, HRnSH, HRnSF, $HRnNH_2$, $HRnNF_2$, $HRnPH_2$, and $HRnPF_2$ were first optimized with a smaller MCP basis set, iMCP-SR2[195,196] and the optimized structures from this computation were then used to start calculations at the level MP2/aug-MCP-TZP. Optimized structural parameters of all molecules considered in this study are presented in Tables 9.1 and 9.2. For HRnOH, the bond lengths reported in Table 9.1 are within 0.03 Å of the values reported by Tsivion and Gerber.[158]

Table 9.1: *Optimized Structures of HRnAX (A=O,S; X=H,F) in C_s Symmetry, MP2/aug-MCP-TZP*[(a)]

Molecule	r(Rn-H)	r(Rn-A)	r(A-X)	$\Theta_{Rn\,A\,X}$
HRnOH	1.782	2.234	0.9634	112.3
HRnOF	1.758	2.268	1.436	99.17
HRnSH	1.824	2.746	1.335	90.47
HRnSF	1.816	2.743	1.664	87.23

[(a)] Bond lengths in Å; bond angles in degrees

Table 9.2: *Optimized structures of $HRnBX_2$ (B=N,P; X=H,F) in C_s symmetry, MP2/aug-MCP-TZP in Å*[(a)]

Molecule	r(Rn-H)	r(Rn-B)	r(B-X)	$\Theta_{Rn\,B\,X}$	$\Theta_{X\,B\,X}$
$HRnNH_2$	1.850	2.323	1.018	107.2	104.4
$HRnNF_2$	1.807	2.377	1.409	99.37	101.7
$HRnPH_2$	1.931	2.866	1.414	87.89	92.05
$HRnPF_2$	2.001	2.902	1.597	91.99	97.38

[(a)] Bond lengths in Å; bond angles in degrees

In monohydrides, substitution of hydrogen by fluorine in the AH group has a very

small effect upon the Rn-H bond length, decreasing it by a maximum of 0.03 Å, increases all other bond lengths, and decreases the Rn-A-X angle by 3°. This is expected, considering the much larger atomic radius of fluorine compared to hydrogen (0.64 Å vs 0.32 Å)[266]. Upon substitution of fluorine for hydrogen in the dihydrides, all bond lengths increase and all angles decrease for $HRnNX_2$, while all bond lengths and all angles increase for $HRnPX_2$. This incongruity in structures may be a consequence of the difference in characteristics between nitrogen and phosphorus: "beyond the stoichiometries of some of the simpler compounds [...] there is little resemblance between the characteristics of these elements and nitrogen", as states by Cotton and Wilkinson on page 367 in Reference[318]). The $-PH_2$ group has a much more rigid structure than the $-NH_2$ group (its barrier to inversion is approximately six times as high),[318] and this also may contribute to the differences in the two structures.

Gibbs free energy changes of formation of the transition state and decomposition into atomic Rn and HAX or HBX_2 according to Reactions 9.1 and 9.2 were computed at the MP2/aug-MCP-TZP level of theory. All molecules studied herein have a positive value of ΔG^{TS}. These values range from 47.73 kJ·mol^{-1} for $HRnPF_2$, the least stable of the molecules studied, to 183.77 kJ·mol^{-1} for HRnSF, the most stable. These values are tabulated for all molecules in Table 9.3.

Table 9.3: ΔG^{TS} *and* $\Delta G_2{}^{(a)}$ *for all molecules, MP2/aug-MCP-TZP level of theory*

Molecule	ΔG_2	ΔG^{TS}
HRnOH	-395.70	162.46
HRnOF	-356.40	138.06
HRnSH	-355.36	162.11
HRnSF	-350.73	183.77
$HRnNH_2$	-432.44	133.18
$HRnNF_2$	-378.46	139.85
$HRnPH_2$	-376.10	89.21
$HRnPF_2$	-390.23	47.73

$^{(a)}$ All ΔG are in units of kJ·mol^{-1}.

It is clear that all of these molecules will have some kinetic stability, as demonstrated by their positive values of ΔG^{TS}. As their decomposition into a free radon

atom and an HAX or HBX_2 molecule is spontaneous at room temperature, kinetic stability will be determined by the height of the energy barrier to the transition state. For some of these molecules, it is considerable. HRnOH has already been shown to be kinetically stable by Tsivion and Gerber;[158] and as HRnSF has a larger value of ΔG^{TS} than HRnOH does, HRnSF should be more stable than HRnOH at room temperature. HRnSH has a value of ΔG^{TS} almost equal to that of HRnOH, and should be stable as well. HRnOF, $HRnNH_2$, and $HRnNF_2$ also have values of ΔG^{TS} that are large enough to predict kinetic stability at room conditions. However, $HRnPH_2$ and $HRnPF_2$ have very low values of ΔG^{TS} compared with the other molecules, and are the least likely to be stable at room temperature based on the heights of their energy barriers to the transition state.

Anharmonic vibrational frequencies were computed with both the quartic force field and direct methods. Direct computations took from 12 to 17 times as long as QFF computations for the same molecule due to the computation of a significantly larger number of points on the potential energy surface. For HRnSH, a QFF cc-VSCF calculation required computation of 216 (energy, dipole) points, whereas a direct mode cc-VSCF calculation involves 3936 such points. For $HRnPH_2$, the QFF computes 486 (energy, dipole) points and the direct mode computes 9360 points. The cc-VSCF method has been employed to study large, biological systems, with the use of empirical force fields. Gerber and Sebek caution against their use, saying that empirical force fields typically produce sub-par spectroscopic results to those produced by *ab initio* force fields, such as MP2, while acknowledging that empirical force fields are one of the computational biologist's main tools at present.[319] Results discussed in the following sections will primarily be those of direct cc-VSCF computations.

9.3.1 Results for HRnSH

Fundamentals, overtones, and combination bands obtained at the MP2/aug-MCP-TZP cc-VSCF direct level of theory will be discussed as well as the effect of substituting a halogen for the hydrogen attached to sulfur. Anharmonic computations of vibrational modes are essential for floppy molecules containing heavy atoms such as

HRnSH. This is clear in a comparison of the six fundamentals computed with the cc-VSCF direct and harmonic methods. The harmonic approximation results in a blue shift of the majority of the fundamentals with respect to their locations computed with the cc-VSCF direct method. The fundamentals of HRnSH computed at all three levels of theory are listed in Table 9.4. Quantitatively, the harmonic approximation is between 0.2 to 5.9 % in error with respect to the QFF approximation, which in turn differs by 0.1 to 2.0 % from the direct method.

Of the fundamentals of HRnSH, the second mode has by far the highest intensity, with the next highest in descending order being the sixth and fifth. Therefore, the experimentalist interested in characterizing HRnSH should look first to the second fundamental mode as a key way to identify the molecule. Computation of the first and second overtones of HRnSH reveals that some of those have very high intensity, and would consequently also be of great use in identifying HRnSH. These overtones are numbered from highest to lowest frequency as described in Table 9.5. The overtones computed in this study are listed in Table 9.5. In particular, the 4_0^2 and 2_0^2 overtones are of higher intensity than some of the fundamentals. Accuracy of the QFF approximation is much poorer for overtones than for fundamentals: overtones of HRnSH computed with the QFF approximation differ by up to 38.8 % with respect to the direct method.

Computation of combination bands involving the fundamentals and the first and second overtones reveals several combination bands which are of high enough intensity to be relevant to experiment, indicating significant coupling of vibrational modes in the HRnSH molecule. There are 28 combination bands of HRnSH which may be formed from the fundamentals and first two overtones, and of these only the $(2_0^1\,5_0^2)$ combination band found at 2288.1 cm^{-1} has an intensity large enough to be of interest to experimentalists. The predicted anharmonic vibrational spectrum of HRnSH, including fundamentals, first and second overtones, and combination bands of highest intensity is presented in Figure 9.1.

Substitution of a fluorine atom for the hydrogen attached to sulfur in HRnSH has four notable effects upon the vibrational spectrum of the molecule. First, the 1_0^1 fun-

Table 9.4: *Fundamental Vibrational Modes of HRnSH in C_s Symmetry*[a]

Mode	Label[b]	Harmonic	Intensity[e]	Δ_{h-q}[c]	QFF	Intensity	Δ_{q-d}[d]	Direct	Intensity	Symmetry
1	υ_s RnS	2773.5	1.25	117.8	2655.7	3.68	-7.4	2663.1	3.69	A’
2	δ_s H(RnS)H	1620.1	0.12	96.7	1523.4	1911.08	-11.2	1534.6	1937.77	A’
3	ω HRnS	606.2	0.02	-33.2	639.4	0.57	13.0	626.4	0.57	A’
4	ρ H(RnS)H	488.0	0.01	17.9	470.1	0.89	-0.5	470.6	0.85	A”
5	υ_s RnH	437.1	50.76	14.5	422.6	5.09	10.1	412.5	5.11	A’
6	υ_s SH	254.6	0.09	4.4	250.2	51.94	-0.1	250.3	51.93	A’

[a] in cm^{-1}; [b] υ_s AB: symmetric stretch; δ_s ABC: in-plane bend (scissor); ω ABC: out-of-plane bend (wag); ρ ABC: in-plane bend (rock); [c] Δ_{h-q} = Harmonic – QFF; [d] Δ_{q-d} = QFF – Direct; $\Delta_{h-d} = \Delta_{h-q} + \Delta_{q-d}$. [e] Intensities are given in units of km·mol^{-1}.

Table 9.5: *First and Second Overtones of HRnSH in C_s Symmetry*[a]

Overtone	QFF	Intensity[b]	Δ_{q-d}[c]	Direct	Intensity	Label
1	7705.1	0.01	-20.2	7725.3	0.02	1_0^3
2	5216.3	0.28	-20.4	5236.7	0.29	1_0^2
3	4404.0	0.71	-10.2	4414.2	0.96	2_0^3
4	2980.1	94.05	-23.7	3003.8	94.10	2_0^2
5	1587.4	0.03	-615.4	2022.8	0.02	$3\,{}_0^3$
6	1321.5	0.00	-57.6	1379.1	0.01	4_0^3
7	1505.1	0.22	196.4	1308.7	0.22	3_0^2
8	1092.8	0.35	2.5	1090.3	0.24	5_0^3
9	919.9	16.36	-10.2	930.1	16.62	4_0^2
10	794.3	4.76	18.4	775.9	4.89	5_0^2
11	746.7	0.01	0.1	746.6	0.01	6_0^3
12	499.0	0.37	-0.2	499.2	0.37	6_0^2

[a] in cm^{-1}; [b] Intensities are given in units of km·mol^{-1}. [c] Δ_{q-d} = QFF – Direct.

damental, rather than the 2_0^1, has the highest intensity and dominates the spectrum. As with HRnSH, it is located at approximately 1500 cm^{-1}. Second, there are two additional small peaks, one on either side of the 1_0^1 fundamental which correspond to the $(1_0^1\,6_0^1)$ combination band at 1614 cm^{-1} and the 2_0^2 overtone at 1439 cm^{-1}. Third, there is an additional peak at 723 cm^{-1} corresponding to the 2_0^1 fundamental. Finally, all other vibrational excitations are red-shifted by approximately 50 cm^{-1} compared to their locations on the HRnSH spectrum.

9.3.2 Results for $HRnPH_2$

Results for $HRnPH_2$ will be discussed in the same order as those of HRnSH: first the fundamentals will be discussed, with an analysis of the overtones and combination bands to follow. Finally, the effect of fluorine substitution in the $–PH_2$ group will be considered. It is tempting to discount the necessity of performing anharmonic vibrational computations for a $HRnPH_2$ based on the rigidity of the $–PH_2$ group in comparison to $–NH_2$, however, the 5-16% blue shift present in six of the nine fundamentals by the harmonic approximation in comparison to the QFF approximation

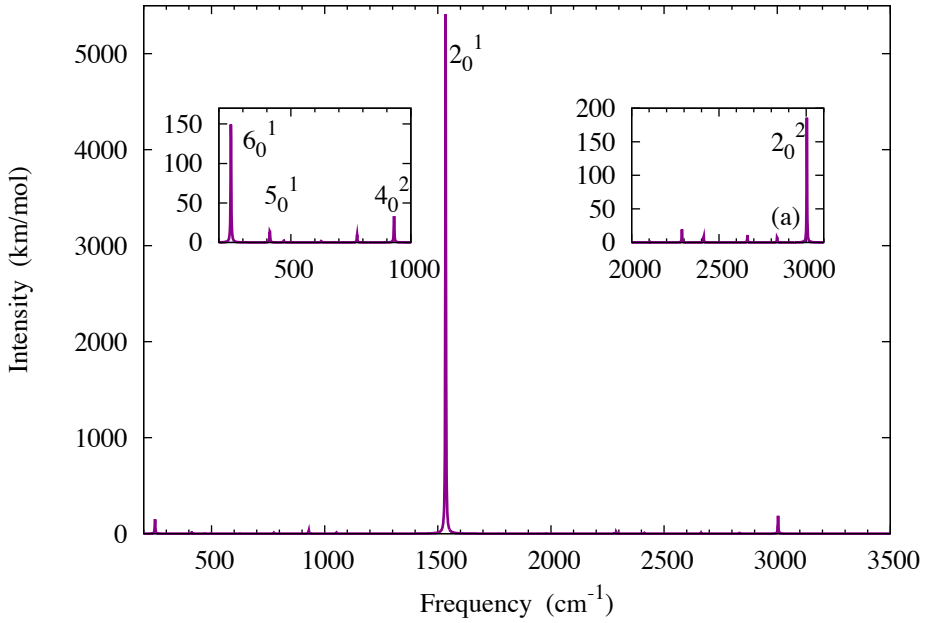

Figure 9.1: *Anharmonic Vibrational Spectrum of HRnSH, at the MP2/aug-MCP-TZP Direct level of theory. (a) The (2_0^1 5_0^2) combination band.*

emphasizes that even in computation of the fundamentals, anharmonic effects are present and strong in $HRnPH_2$. These fundamentals are collected in Table 9.6.

Errors in fundamentals computed with the harmonic approximation range from 0.9% to 5.0% with respect to values computed with the QFF approximation, which itself differs by up to 1.4% with respect to results of the direct method. Of these fundamentals, the first, second, and third dominate the spectrum, and the weaker fundamentals may be detected with a more powerful instrument.

Computed overtones of highest intensity are 3_0^2, 3_0^3, 8_0^2, and 7_0^2. As with the overtones of HRnSH, these overtones are numbered from highest to lowest frequency as described in Table 9.7. The overtones of the third fundamental in particular have higher intensity than some fundamentals, and should provide assistance in identifying $HRnPH_2$ from a vibrational spectrum. All computed overtones on $HRnPH_2$ are

Table 9.6: *Fundamental Vibrational Modes of $HRnPH_2$ in C_s Symmetry*[a]

Mode	Label[b]	Harmonic	Intensity[e]	Δ_{h-q}[c]	QFF	Intensity	Δ_{q-d}[d]	Direct	Intensity	Symmetry
1	υ_s RnP	2456.9	9.39	122.1	2334.8	43.06	-4.6	2339.4	43.11	A”
2	τ HPH	2444.5	13.05	103.0	2341.5	50.39	19.7	2321.8	50.30	A’
3	ω HPH + δ_s HRnP	1359.2	10.17	81.6	1277.6	1717.55	-7.5	1285.1	1743.05	A’
4	ω HPH + δ_s HRnP	1127.0	4.80	45.6	1081.4	15.72	-0.2	1081.6	15.95	A’
5	τ HPH	581.0	0.00	-10.9	591.9	0.00	4.9	587.0	0.00	A”
6	δ_s HPH	562.1	17.37	-14.7	576.8	5.22	5.1	571.7	5.15	A’
7	υ_s RnH	392.1	2009.35	-3.7	395.8	10.30	5.7	390.1	10.23	A”
8	υ_s HPH	386.2	42.73	-3.3	389.5	13.22	5.5	384.0	13.13	A”
9	υ_{as} HPH	221.4	52.05	7.6	213.8	8.39	0.0	213.8	8.38	A’

[a] in cm^{-1}; [b] υ_{as} AB: asymmetric stretch; τ ABC: out-of-plane bend (twist); for description of remaining labels see Table 9.4; [c] Δ_{h-q} = Harmonic – QFF; [d] Δ_{q-d} = QFF – Direct ; $\Delta_{h-d} = \Delta_{h-q} + \Delta_{q-d}$. [e] Intensities are given in units of km·mol^{-1}

Table 9.7: *First and Second Overtones of HRnPH$_2$ in C_s Symmetry*[a]

Overtone	QFF	Intensity[e]	Δ_{q-d}[b]	Direct	Intensity	Label
1	6884.6	0.89	51.0	6833.6	0.01	2_0^3
2	6874.4	0.01	124.3	6750.1	1.55	1_0^3
3	4619.5	0.17	16.4	4603.1	0.17	2_0^2
4	4622.0	0.27	53.4	4568.6	0.27	1_0^2
5	3741.8	8.87	28.5	3713.3	11.67	3_0^3
6	3200.5	0.07	-3.4	3203.9	0.07	4_0^3
7	2513.9	227.71	-7.9	2521.8	228.48	3_0^2
8	2149.5	0.10	-0.5	2150.0	0.10	4_0^2
9	1824.6	0.01	47.9	1776.7	0.00	6_0^3
10	1823.8	0.00	31.7	1792.1	0.00	5_0^3
11	1195.1	0.23	12.9	1182.2	0.23	5_0^2
12	1180.8	0.36	20.8	1166.0	0.28	6_0^2
13	1126.2	0.09	12.4	1113.8	0.80	7_0^3
14	1109.2	0.14	9.4	1099.8	0.12	8_0^3
15	773.7	7.24	12.3	761.4	7.40	7_0^2
16	762.0	7.67	11.6	750.4	7.83	8_0^2
17	637.0	0.01	273.8	636.2	0.01	9_0^3
18	426.2	0.33	0.3	425.9	0.33	9_0^2

[a] in cm^{-1}; [b] Δ_{q-d} = QFF – Direct.

listed in Table 9.7. As with the HRnSH molecule, the QFF approximation produces significant errors for computed overtones, sometimes as large as 43.0%.

In contrast to HRnSH, the anharmonic spectrum of HRnPH$_2$ contains several high-intensity combination bands, further underscoring the large contribution that coupling of vibrational modes makes the the spectra of such molecules. Combination bands of HRnPH$_2$ are of uniformly low intensity, but the highest of these are the ($3_0^1\,8_0^2$) and ($3_0^1\,7_0^2$) bands, which are close in intensity, followed by the ($3_0^1\,9_0^1$), ($1_0^1\,3_0^1$), ($6_0^1\,7_0^1$), and ($5_0^1\,8_0^1$) bands. These combination bands have higher intensity only than the weakest fundamentals, and are likely to be useful for identifying HRnPH$_2$ from high-resolution spectra. The vibrational spectra of HRNPH$_2$ including all high-intensity excitations is given in Figure 9.2.

When the phosphoryl hydrogens are substituted with fluorine atoms, all vibra-

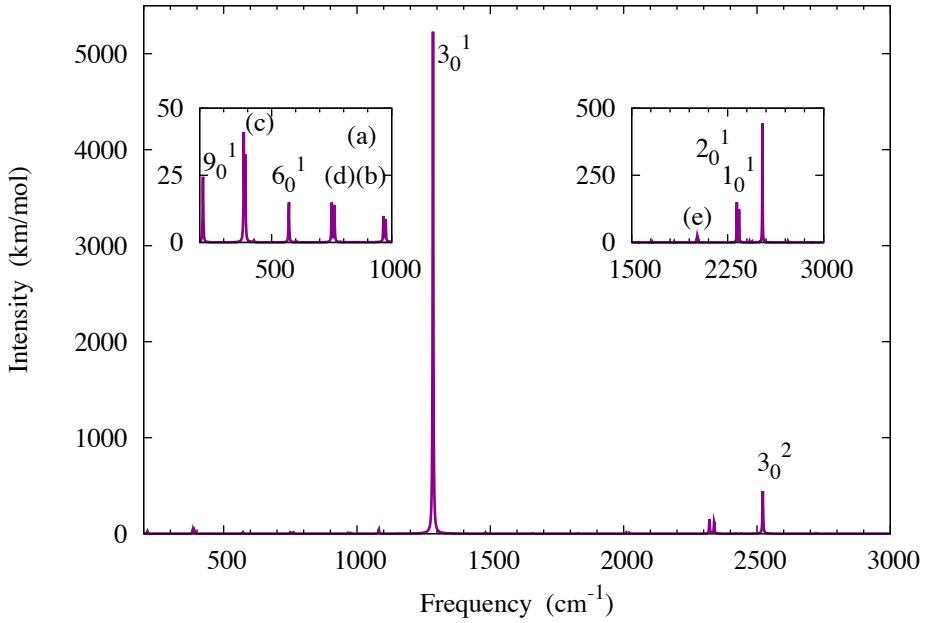

Figure 9.2: *Anharmonic vibrational spectrum of $HRnPH_2$ at the MP2/aug-MCP-TZP direct level of theory. (a) The (6_0^1 7_0^1) combination band at 965 cm^{-1}; (b) the (5_0^1 8_0^1) combination band at 974 cm^{-1}; (c) the 8_0^1 fundamental at 383 cm^{-1} and the 7_0^1 fundamental at 390 cm^{-1}; (d) the 8_0^2 overtone at 750 cm^{-1} and the 7_0^2 overtone at 761 cm^{-1}; (e) the (3_0^1 8_0^2) combination band at 2008 cm^{-1}.*

tional excitations in the spectrum become significantly red-shifted. A few peaks of low intensity for $HRnPH_2$ between 1000-2500 cm^{-1} gain larger intensity with the substitution of fluorine.

9.4 Conclusions

In this Chapter, I have analyzed the effect of anharmonicity upon the vibrational spectra of small molecules containing radon. Two different methods were used to compute anharmonic vibrational excitations, and results are generally consistent between these methods with respect to peak location and peak intensity. In some cases,

a peak will have extremely low intensity (0.01 km·mol^{-1}) with the direct method, and zero intensity with the QFF approximation. One example of this is the the 3_0^3 overtone of HRnSH. In other cases, a mode will have near-zero intensity (0.02 km·mol^{-1}) in the harmonic approximation, and zero intensity in both the direct and QFF calculations. I attribute the first case to the difference in completeness of computation of the potential energy surface of the electronic state of the molecule, and defer to the result of the direct mode calculation as authoritative. In the second case, the potential energy surface was computed only with the direct mode, and we again recognize that result as definitive.

The vibrational spectrum of HRnSH is dominated by the 2_0^1 fundamental, the 4_0^2 and 2_0^2 overtones, and the $(2_0^1\,5_0^2)$ combination band. While substitution of fluorine for the sulfuric hydrogen causes significant changes in which specific fundamentals, overtones, and combination bands contribute most strongly to the vibrational spectrum, the overall appearance of the spectrum remains the same.

In the case of $HRnPH_2$, the first three fundamentals are of high intensity and will be the most easily detected experimentally. There are also several high-intensity overtones and six combination bands intense enough to be detectable by sensitive instruments.

Fundamentals of both molecules are computed by the QFF approximation with a high degree of accuracy, with the largest error being only 2.0%. However, the errors of up to 43.0% in overtones computed with the QFF approximation indicate that computations with the direct method are necessary to obtain reliable results.

Chapter 10

Conclusions

10.1 Conclusions

Throughout the work presented herein it has been my goal to demonstrate that *in silica*, radon is at least as reactive as xenon, and in some cases more reactive, and that compounds of radon and various organic ligands are excellent candidates for experimental study. In the first several Chapters, I have studied radon-containing compounds in tandem with xenon-containing compounds, and this is intentional. Much more is known both experimentally and computationally about the chemistry of xenon than about the chemistry of radon, and given the periodic relationship between the two atoms, chemical intuition suggests that the existing compounds involving xenon are a good starting point for investigating hypothetical radon compounds.

In the second Chapter, I demonstrated that HRnF is indeed chemically bound, and supported this with evidence from several types of computations. *Ab initio* computations with correlated methods (MP2, CCSD, CCSD(T), and CR-CC(2,3)) and large Model Core Potentials basis sets produced optimized structures of HRnF that were consistent with the structure of HXeF. In addition to being a bound species, HRnF was shown to bind more strongly than fluorides of all of the lighter rare gases. This was established through comparison of the computed dissociation energies for HArF, HKrF, HXeF, and HRnF. While HRnF is the most thermodynamically stable of the four compounds, it is important to note that all of them are only metastable: the dissociation into a free rare gas and hydrogen fluoride is lowest in energy on the

potential energy surface of the molecule. These results open up possibilities of other radon-containing compounds which I have begun to explore in later Chapters.

In the third Chapter, I expanded upon the premise of Chapter 2 and studied halohydrides of xenon and radon with perturbation theory, density functional theory, and a series of extensive Model Core Potentials basis sets. Results of geometry optimizations and energy of formation and dissociation computations indicated that like HRnF, radon halohydrides of the heavier halogens should be bound, thermodynamically metastable species. Results of QTAIM population analysis and analysis of the electron density in radon halohydrides also confirmed this.

In the fourth Chapter, I examined structure and energies of formation and decomposition for small, organic compounds of xenon and radon. These compounds are formed through reactions with functionalized perfluoromethyl silanes and either XeF_2 or RnF_2. I determined that the slightly lower stability of the radon compounds is a result of the higher stability enjoyed by RnF_2 over XeF_2. I further analyzed the strength of binding in these compounds through computed core electron binding energies, where the energy necessary to ionize a core electron from any of the organic elements was computed.

In the fifth Chapter, I studied compounds of methyl and perfluoromethyl groups with xenon or radon, and found that for each of the symmetric compounds, there are two distinct minima on the potential energy surface, corresponding to equilibrium structures in both the D_{3h} and D_{3d} symmetries when these structures are studied with density functional theory.

In the sixth Chapter, I presented computed structures and properties of molecules of the type C_6H_5RgA and C_6F_5RgA, where Rg is either radon or xenon and A is one of F, CN, CCH, or CCF. As with the molecules studied in previous Chapters, I computed optimized structures and energy barriers to dissociation in order to evaluate the kinetic stability of these molecules. I found that radon-containing large organic compounds are equally stable as their xenon-containing cousins, and have similar properties such as bond properties and atomic charges. The compounds studied in this Chapter are unique in that they are the only molecules I studied that contain

aromatic groups. These groups stabilize the bond between themselves and the rare gas through donation of π-electron density back into an antibonding molecular orbital of the rare gas which is collinear with the bond.

In the seventh Chapter, I investigated the effect of confining the HRgX molecule inside of a cylindrical or planar harmonic potential upon the structure of the HRgX species, the shape of the decomposition pathway, and upon the molecular orbitals of the molecule and the accessibility of the excited electronic states. Through analysis of the vertical ionization potentials for confined HRgX, I have determined that the most accessible excited electronic state is the $^1B_1$ state.

In the eighth Chapter, I extended the studies of the previous Chapter to include discrete confinement comprised of a pair of 8x8 helium atom sheets which are located above and below the plane of the HRgX molecule, and again studied the effect of confinement upon the decomposition pathway for HRgX species. The discrete confinement also presented the opportunity to evaluate the optimal location within the sheets for the HRgX molecule to most increase the stability of the molecule against the two-body dissociation.

Finally, in the ninth Chapter I determined the extent to which anharmonicity affects the vibrational spectrum of several radon-containing small molecules. I established that all of these molecules are at least metastable, with many having large enough Gibbs free energy barriers to dissociation to make stability at room temperature and pressure extremely likely. The vibrational spectra of these molecules are strongly anharmonic, and contain many overtones and combination bands of high intensity.

The overall goal of the work presented in this thesis has been to demonstrate that many types of radon-containing compounds are kinetically stable and have properties similar to those of existing xenon-containing compounds which make them ideal candidates for synthesis. I have also shown that the presence of a harmonic confining environment kinetically stabilizes the HRgX species. As most small xenon-containing molecules that have already been synthesized have been created inside of low-temperature rare gas matrices, it is useful to know that similar radon-containing

compounds should be synthesizable under the same conditions.

10.2 Future Work

There are many possibilities for continuing computational investigations into radon chemistry. Most of the molecules that I have studied have received little previous attention. Consequently, there are several types of studies that would be useful in order to better understand radon chemistry.

In Chapter 8, I analyzed the effect that discrete confinement within a pair of helium sheets had upon the structure and properties of HRgX molecules. When HXeX (X=F, Cl, Br, OH, SH) molecules are synthesized experimentally, they are synthesized inside of a low-temperature rare gas matrix composed of either krypton or xenon. It may therefore be interesting to replace the helium sheets with a pair of krypton or xenon sheets in order to have a model that more accurately reflects experimental conditions.

In my final results Chapter, I addressed the role that anharmonicity plays in the vibrational spectra of some radon-containing small molecules. Another useful step would be to compute anharmonic vibrational spectra for all of the other groups of radon-containing molecules that I have described in the preceding Chapters. While time consuming, these computations would be worthwhile as they would provide an accurate standard of comparison for experimental chemists looking to characterize newly synthesized radon-containing compounds.

In addition to infrared spectra, microwave spectra are also commonly used to identify new molecules. Recently published work by Cassam-Chenaï and Liévin describes a method for computing rotational spectra of small molecules in their vibrational ground state using potential energy surfaces generated from *ab initio* computations.[320] Their method involves using a modified harmonic oscillator and rigid rotor Hamiltonian, and is available as part of the MOLPRO program.[321] This method could be applied to compute the rotational spectrum of small radon-containing molecules such as HRnF, CNRnF, and HRnOF.

In Chapter 7 I analyzed some of the low-lying excited electronic states for the HRgX (Rg=Xe, Rn;X=F, Cl) molecules. It would also be useful to compute these states for the molecules studied in Chapters 3, 4, 5 and 9, as well as for the heavier halohydrides HRgBr and HRgI.

An investigation into the effect of radon's decay into polonium by emission of an α-particle on the radon-containing compounds studied in this thesis is also warranted. There are two interesting questions here: first, would the energy released in the decay process be sufficient to destroy any of these molecules? Second, would the polonium-containing version of these radon-containing compounds be a minimum-energy structure on the potential energy surface of that system?

To my knowledge, as of the summer of 2014 there have not been any molecular dynamics studies of radon-containing molecules. While my research has been strictly focused on quantum mechanical studies, there are several pieces of information that could be obtained from molecular dynamics simulations that would help to complete the understanding of radon chemistry. For example, xenon-containing molecules of the type Ph-Xe-A, where A is some small organic group such as any of those studied in Chapters 4-6, are commonly synthesized in bulk at low temperatures. Through molecular dynamics simulations, information on bulk phase properties of radon-containing analogs of these compounds could be obtained.

Bibliography

[1] Ramsay, W.; Whytlaw-Gray, R. *Aca. Sci.* **1910**, 126–.

[2] Bartlett, N. *Proc. Chem. Soc.* **1962**, 218.

[3] Christe, K. O. *Chem. Commun.* **2013**, *49*, 4588.

[4] Claassen, H. H.; Selig, H.; Malm, J. G. *J. Am. Chem. Soc.* **1962**, *84*, 3593.

[5] Chernick, C. L. In *Noble-Gas Compounds*; Hyman, H. H., Ed.; The University of Chicago Press, 1963; Chapter Fluorides of Xenon, Preparation and Properties: An Introduction and Review, pp 35–58.

[6] Fields, P. R.; Stein, L.; Zirin, M. H. *J. Am. Chem. Soc.* **1962**, *84*, 4164–4165.

[7] Emsley, J. *The Elements, p.171*; Oxford University Press, 1989.

[8] Hyman, H. H., Ed. *Noble-Gas Compounds*; The University of Chicago Press, 1963.

[9] Haseltine, M. W.; Moser, H. C. *J. Am. Chem. Soc.* **1967**, *89*, 2497–2498.

[10] Stein, L. *Science* **1970**, *168*, 362–364.

[11] Carroll, T. X.; Shaw, R. W.; Thomas, T. D.; Kindle, C.; Bartlett, N. *J. Am. Chem. Soc.* **1974**, *96*, 1989–1996.

[12] Pitzer, K. S. *J. Chem. Soc. Chem. Comm.* **1975**, 760–761.

[13] Seppelt, K. *Chem. Elec. Elem.* **1979**, *12*, 211–216.

[14] Seppelt, K. *Angew. Chem. Int. Ed.* **1979**, *18*, 186–202.

[15] Turbini, L. J.; Aikman, R. E.; Lagow, R. J. *J. Am. Chem. Soc.* **1979**, *101*, 5833–5834.

[16] Avrorin, V. V.; Krasikova, R. N.; Nefedov, V. D.; Toropova, M. A. *Russ. Chem. Rev.* **1982**, *51*, 12–20.

[17] Stein, L. *Radiochimica Acta* **1983**, *32*, 163–171.

[18] Frohn, H.-J.; Jakobs, S. *J. Chem. Soc. Chem. Comm.* **1989**, *10*, 625–627.

[19] Naumann, D.; Tyrra, W. *J. Chem. Soc. Chem. Comm.* **1989**, 47–50.

[20] Turowsky, L.; Seppelt, K. *Inorg. Chem.* **1990**, *29*, 3226–3228.

[21] Wells, J. R.; Weitz, E. *J. Am. Chem. Soc.* **1992**, *114*, 2783–2787.

[22] Zhdankin, V. V. *Russ. Chem. Bull.* **1993**, *42*, 1849–1857.

[23] Frohn, H.-J.; Klose, A.; Schroer, T.; Henkel, G.; Buss, V.; Opitz, D.; Vahrenhorst, R. *Inorg. Chem.* **1998**, *37*, 4884–4890.

[24] Kotting, C.; Sander, W.; Breidung, J.; Thiel, W.; Senzlober, M.; Burger, H. *J. Am. Chem. Soc.* **1998**, *120*, 219–220.

[25] Naumann, D.; Butler, H.; Gnann, R.; Tyrra, W. *Inorg. Chem.* **1993**, *32*, 861–863.

[26] Frohn, H.-J.; Schroer, T.; Henkel, G. *Angew. Chem. Int. Ed.* **1999**, *38*, 2554–2556.

[27] Frohn, H.-J.; Theissen, M. *Angew. Chem. Int. Ed.* **2000**, *39*, 4591–4593.

[28] Maggiarosa, N.; Naumann, D.; Tyrra, W. *Angew. Chem. Int. Ed.* **2000**, *39*, 4588–4591.

[29] Brel, V. K.; Pirkuliev, N. S.; Zefirov, N. S. *Russ. Chem. Rev.* **2001**, *70*, 231.

[30] Pettersson, M.; Lundell, J.; Räsänen, M. *J. Chem. Phys.* **1995**, *103*, 205–210.

[31] Møller, C.; Plesset, M. S. *Phys. Rev.* **1934**, *46*, 618–622.

[32] 2014; `https://bse.pnl.gov/bse/portal`.

[33] Piecuch, P.; Kucharski, S. A.; Kowalski, K.; Musial, M. *Comput. Phys. Commun.* **2002**, *149*, 71.

[34] Runeberg, N.; Seth, M.; Pyykkö, P. *Chem. Phys. Lett.* **1995**, *246*, 239–244.

[35] Pyykkö, P. *J. Am. Chem. Soc.* **1995**, *117*, 2067.

[36] Pettersson, M.; Lundell, J.; Räsänen, M. *J. Chem. Phys.* **1995**, *102*, 6423–6431.

[37] Pettersson, M.; Nieminen, J.; Khriachtchev, L.; Räsänen, M. *J. Chem. Phys.* **1997**, *107*, 8432–8431.

[38] Pettersson, M.; Lundell, J.; Khriachtchev, L.; Isoniemi, E.; Räsänen, M. *J. Am. Chem. Soc.* **1998**, *120*, 7979–7980.

[39] Pettersson, M.; Lundell, J.; Khriachtchev, L.; Räsänen, M. *J. Chem. Phys.* **1998**, *109*.

[40] Burda, J. V.; Runeberg, N.; Pyykkö, P. *Chem. Phys. Lett.* **1998**, *288*, 635–641.

[41] Schroder, D.; Harvey, J. N.; Aschi, M.; Schwarz, H. *J. Chem. Phys.* **1998**, *108*, 8446–8455.

[42] Isoniemi, E.; Pettersson, M.; Khriachtchev, L.; Lundell, J.; Räsänen, M. *J. Phys. Chem.* **1999**, *103*, 679–685.

[43] Pettersson, M.; Khriachtchev, L.; Lundell, J.; Räsänen, M. *J. Am. Chem. Soc.* **1999**, *121*, 11904–11905.

[44] Pettersson, M.; Lundell, J.; Räsänen, M. *Eur. J. Inorg. Chem.* **1999**, 729–737.

[45] Johansson, M.; Hotokka, M.; Pettersson, M.; Räsänen, M. *Chem. Phy.s* **1999**, *224*, 25–34.

[46] Koskinen, J. T.; Cooks, R. G. *J. Phys. Chem. A* **1999**, *103*, 9565–9569.

[47] Crépin-Gilbert, C.; Tramer, A. *Int. Rev. Phys. Chem.* **1999**, *18*, 485–556.

[48] Runeberg, N.; Pyykkö, P. *Int. J. Quantum Chem* **1998**, *66*, 131–140.

[49] Liao, M.-S.; Zhang, Q.-E. *J. Phys. Chem. A* **1998**, *102*, 10647–10654.

[50] Han, Y. K.; Lee, Y. S. *J. Phys. Chem. A* **1999**, *103*, 1104–1108.

[51] Eichler, B.; Zimmermann, H. P.; Gäggeler, H. W. *J. Phys. Chem. A* **1999**, *104*, 3126–3131.

[52] Lee, E. P. F.; Wright, T. G. *J. Phys. Chem. A* **1999**, *103*, 7843–7847.

[53] Holloway, J. H.; Hop, E. G. In *Advances in Inorganic Chemistry*; Sykes, A. G., Ed.; Advances in Inorganic Chemistry; Academic Press, 1999; Vol. 46; Chapter Recent Advances in Noble-Gas Chemistry, pp 51–100.

[54] Seidel, S.; Seppelt, K. *Science* **2000**, *290*, 117.

[55] Grills, D. C.; Sun, X. Z.; Childs, G. I.; George, M. W. *J. Phys. Chem. A* **2000**, *104*, 4300–4307.

[56] Lundell, J.; Pettersson, M.; Khriachtchev, L.; Räsänen, M.; Chaban, G. M.; Gerber, R. B. *Chem. Phys. Lett.* **2000**, *322*, 389–394.

[57] Lundell, J.; Chaban, G. M.; Gerber, R. B. *J. Phys. Chem. A* **2000**, *104*, 7944–7949.

[58] Ahokas, J.; Vaskonen, K.; Eloranta, J.; Kunttu, H. *J. Phys. Chem. A* **2000**, *104*, 9506–9511.

[59] Lundell, J.; Chaban, G. M.; Gerber, R. B. *Chem. Phys. Lett.* **2000**, *331*, 308–316.

[60] Lee, E. P. F.; Gamblin, S. D.; Wright, T. G. *Chem. Phys. Lett.* **2000**, *322*, 377–381.

[61] Ball, D. W. *J. Mol. Struct. (Theochem)* **2000**, *532*, 239–244.

[62] Eloranta, J.; Kunttu, H. *J. Chem. Phys.* **2000**, *113*, 7446–7452.

[63] Faas, S.; van Lenthe, J. H.; Snijders, J. G. *Mol. Phys.* **2000**, *98*, 1467–1472.

[64] Graham, L.; Graudejus, O.; Jha, N. K.; Bartlett, N. *Coordination Chemistry Reviews* **2000**, *197*, 321–334.

[65] Lundell, J.; Pettersson, M.; Räsänen, M. *Computers and Chemistry* **2000**, *24*, 325–330.

[66] Lundell, J.; Khriachtchev, L.; Pettersson, M.; Räsänen, M. *Low Temperature Physics* **2000**, *26*, 923–936.

[67] Pettersson, M.; Khriachtchev, L.; Lundell, J.; Jolkkonen, S.; Räsänen, M. *J. Phys. Chem. A* **2000**, *104*, 3579–3583.

[68] Pyykkö, P. *Science* **2000**, *290*, 64.

[69] Gerkin, M.; Schrobilgen, G. J. *Coordination Chemistry Reviews* **2000**, *197*, 335–395.

[70] Malli, G. L. *J. Mol. Struct. (Theochem)* **2001**, *537*, 71–77.

[71] Yu, D.; Chen, Z. *J. Mol. Struct. (Theochem)* **2001**, *540*, 29–33.

[72] Frohn, H.-J.; Bardin, V. V. *Organometallics* **2001**, *20*, 4750–4762.

[73] Christe, K. O. *Angew. Chem. Int. Ed.* **2001**, *40*, 1419–1421.

[74] Childs, G. I.; Grills, D. C.; Sun, X. Z.; George, M. W. *Pure & Applied Chemistry* **2001**, *73*, 443–447.

[75] Cohen, A.; Niv, M. Y.; Gerber, R. B. *Faraday Discuss.* **2001**, *118*, 269–280.

[76] Machado, F. B. C.; Ghanty, T. K.; Chakravorty, S.; Davidson, E. R. *Int. J. Quantum Chem.* **2001**, *81*, 238–245.

[77] Cunje, A.; Baranov, V. I.; Ling, Y.; Hopkinson, A. C.; Bohme, D. K. *J. Phys. Chem. A* **2001**, *105*, 11073–11079.

[78] Tyrra, W.; Naumann, D. In *Inorganic Chemistry Highlights*; Meyer, G., Naumann, D., Wesemann, L., Eds.; Wiley-VCH, Weinheim, 2002; Chapter 19: Organoxenon Compounds, pp 297–316.

[79] Panek, J.; Latajka, Z.; Lundell, J. *Phys. Chem. Chem. Phys.* **2002**, *4*, 2504–2510.

[80] Bihary, Z.; Chaban, G. M.; Gerber, R. B. *J. Chem. Phys.* **2002**, *116*, 5521–5529.

[81] Nemukhin, A. V.; Grigorenko, B. L.; Khriachtchev, L.; Tanskanen, H.; Pettersson, M.; Räsänen, M. *J. Am. Chem. Soc.* **2002**, *124*, 10706–10711.

[82] Himmel, H.-J.; Downs, A. J.; Greene, T. M. *Chem. Rev.* **2002**, *102*, 4191–4241.

[83] Lovallo, C. C.; Klobukowski, M. *Int. J. Quantum Chem.* **2002**, *90*, 1099–1107.

[84] Lundell, J.; Cohen, A.; Gerber, R. B. *J. Phys. Chem. A* **2002**, *106*, 11950–11955.

[85] Drews, T.; Seidel, S.; Seppelt, K. *Angew. Chem. Int. Ed.* **2002**, *41*, 454.

[86] Malli, G. L. *Int. J. Quantum Chem.* **2002**, *90*, 611–615.

[87] Khriachtchev, L.; Pettersson, M.; Lundell, J.; Tanskanen, H.; Kiviniemi, T.; Runeberg, N.; Räsänen, M. *J. Am. Chem. Soc.* **2003**, *125*, 1454–1455.

[88] Tanskanen, H.; Khriachtchev, L.; Kiljunen, H.; Räsänen, M. *J. Am. Chem. Soc.* **2003**, *125*, 16361–16366.

[89] Tsvetkov, A. V.; Bobrov, M. F.; Tsirelson, V. G. *J. Mol. Struct. (Theochem)* **2003**, *624*, 145–152.

[90] Khriachtchev, L.; Tanskanen, H.; Lundell, J.; Pettersson, M.; Kiljunen, H.; Räsänen, M. *J. Am. Chem. Soc.* **2003**, *125*, 4696–4697.

[91] Feldman, V. I.; Sukhov, F. F.; Orlov, A. Y.; Tyulpina, I. V. *J. Am. Chem. Soc.* **2003**, *125*, 4698–4699.

[92] Slavicek, P.; Kalus, R.; Paska, P.; Odvarkova, I.; Hobza, P.; Maljevsky, A. *J. Chem. Phys.* **2003**, *119*, 2102–2119.

[93] Buth, C.; Santra, R.; Cederbaum, L. S. *J. Chem. Phys.* **2003**, *119*, 7763–7771.

[94] Lein, M.; Frenking, G. *Aust. J. Chem.* **2004**, *57*, 1191–1195.

[95] Gerken, M.; Hazendonk, P.; Nieboer, J.; Schrobilgen, G. J. *J. Fluor. Chem.* **2004**, *125*, 1163–1168.

[96] Cooke, S. A.; Gerry, M. C. L. *J. Am. Chem. Soc.* **2004**, *123*, 17000.

[97] Ginter, M. L.; Eden, J. G. *Can. J. Chem.* **2004**, *82*, 762–778.

[98] Yen, S.-Y.; Mou, C.-H.; Hu, W.-P. *Chem. Phys. Lett.* **2004**, *383*, 606–611.

[99] Tanskanen, H.; Khriachtchev, L.; Lundell, J.; Räsänen, M. *J. Chem. Phys.* **2004**, *121*, 8291–8298.

[100] Gerber, R. B. *Annu. Rev. Phys. Chem.* **2004**, *55*, 55–78.

[101] Semenov, S. G.; Sigolaev, Y. F. *Russ. J. Org. Chem.* **2004**, *40*, 1825–1837.

[102] Semenov, S. G.; Sigolaev, Y. F. *Russ. J. Org. Chem.* **2004**, *40*, 1757–1759.

[103] Frohn, H.-J.; Theissen, M. *J. Fluor. Chem.* **2004**, *125*, 981–988.

[104] Forgeron, M. A. M.; Wasylishen, R. E.; Penner, G. H. *J. Phys. Chem. A* **2004**, *108*, 4751–4758.

[105] Chaban, G. M. *Chem. Phys. Lett.* **2005**, *401*, 318–322.

[106] Brown, E. C.; Cohen, A.; Gerber, R. B. *J. Chem. Phys.* **2005**, *122*, 171101.

[107] Ghanty, T. K. *J. Chem. Phys.* **2005**, *123*, 074323.

[108] Khriachtchev, L.; Lignell, A.; Juselius, J.; Räsänen, M.; Savchenko, E. *J. Chem. Phys.* **2005**, *122*, 014510.

[109] Gerber, R. B. *Bull. Israel Chem. Soc.* **2005**, 7–14.

[110] Ball, G. E.; Darwish, T. A.; Geftakis, S.; George, M. W.; Lawes, D. J.; Portius, P.; Rourke, J. P. *Proc. Nat. Acad. Sci.* **2005**, *120*, 1853–1858.

[111] McMaster, J.; Portius, P.; Ball, G. E.; Rourke, J. P.; George, M. W. *Organometallics* **2006**, *25*, 5242–5248.

[112] Ghanty, T. K. *J. Chem. Phys.* **20206**, *124*, 124304.

[113] Buck, U.; Farnik, M. *Int. Rev. Phys. Chem.* **2006**, *25*, 583–612.

[114] Khriachtchev, L.; Lignell, A.; Tanskanen, H.; Lundell, J.; Kiljunen, H.; Räsänen, M. *J. Phys. Chem. A* **2006**, *110*, 11876–11885.

[115] Tanskanen, H.; Khriachtchev, L.; Lundell, J.; Räsänen, M. *J. Chem. Phys.* **2006**, *125*, 074501.

[116] Lignell, A.; Khriachtchev, L.; Lundell, J.; Tanskanen, H.; Räsänen, M. *J. Chem. Phys* **2006**, *125*, 184514.

[117] Ansbacher, A.; Gerber, R. B. *Phys. Chem. Chem. Phys.* **2006**, *2006*, 4175–4181.

[118] Semenov, S. G.; Sigolaev, Y. F. *Russ. J. Org. Chem.* **2006**, *42*, 1789–1971.

[119] Tramsek, M.; Zemva, B. *Acta. Chim. Slov.* **2006**, *53*, 105–116.

[120] Krouse, I. H.; Hao, C.; Check, C. E.; Lobring, K. C.; Sunderlin, L. S.; Wenthold, P. G. *J. Am. Chem. Soc.* **2007**, *129*, 846–852.

[121] Straka, M.; Lantto, P.; Räsänen, M.; Vaara, J. *J. Chem. Phys.* **2007**, *127*, 234314.

[122] Takayanagi, T.; Asakura, T.; Takahashi, K.; Taketsugu, Y.; Taketsugu, T.; Noro, T. *Chem. Phys. Lett.* **2007**, *446*, 14–19.

[123] Brock, D. S.; Bilir, V.; Mercier, H. P. A.; Schrobilgen, G. J. *J. Am. Chem. Soc.* **2007**, *129*, 3598–3611.

[124] Sheng, L.; Gerber, R. B. *J. Chem. Phys.* **2007**, *126*, 021108.

[125] Antoniotti, P.; Borocci, S.; Bronzolino, N.; Cecchi, P.; Grandinetti, F. *J. Phys. Chem. A* **2007**, *111*, 10144–10151.

[126] Grochala, W. *Chem. Soc. Rev.* **2007**, *36*, 1632–1655.

[127] Kurzydlowski, D.; Grochala, W. *Z. Anorg. Allg. Chem.* **2008**, *634*, 1082–1086.

[128] Belpassi, L.; Infante, I.; Tarantelli, F.; Visscher, L. *J. Am. Chem. Soc.* **2008**, *130*, 1048–1–6–.

[129] Mou, C.-H.; Witek, H. A. *J. Chem. Phys.* **2008**, *129*, 244310.

[130] Breckenridge, W. H.; Ayles, V. L.; Wright, T. G. *J. Phys. Chem. A* **2008**, *112*, 4209–4214.

[131] Poterya, V.; Votava, O.; Farnik, M.; Oncak, M.; Slavicek, P.; Buck, U.; Friederich, B. *J. Chem. Phys.* **2008**, *128*, 104313.

[132] Khriachtchev, L.; Isokoski, K.; Cohen, A.; Räsänen, M.; Gerber, R. B. *J. Am. Chem. Soc.* **2008**, *130*, 6114–6118.

[133] Huang, Z.; Yang, E.; Xie, D. *J. Mol. Struct. (Theochem)* **2008**, *867*, 95–100.

[134] Fang, H.; Zhang, Z.-G. *Theor. Chem. Acc.* **2009**, *123*, 443–453.

[135] Lignell, A.; Lundell, J.; Khriachtchev, L.; Räsänen, M. *J. Phys. Chem. A* **2008**, *112*, 5486–5494.

[136] Tanskanen, H.; Johansson, S.; Lignell, A.; Khriachtchev, L.; Räsänen, M. *J. Chem. Phys.* **2007**, *127*, 154313.

[137] Tsivion, E.; Zilberg, S.; Gerber, R. B. *Chem. Phys. Lett.* **2008**, *460*, 23–36.

[138] Jayasekharan, T.; Ghanty, T. K. *J. Chem. Phys.* **2008**, *129*, 124302.

[139] Feldman, V. I.; Kobzarenko, A. V.; Baranova, I. A.; Danchenko, A. V.; Sukhov, F. F.; Tsivion, E.; Gerber, R. B. *J. Chem. Phys.* **2009**, *131*, 151101.

[140] Tsivion, E.; Gerber, R. B. *Chem. Phys. Lett.* **2009**, *482*, 30–33.

[141] Domanskaya, A.; Kobzarenko, A. V.; Tsivion, E.; Khriachtchev, L.; Feldman, V. I.; Gerber, R. B.; Räsänen, M. *Chem. Phys. Lett.* **2009**, *481*, 83–87.

[142] Muck, L. A.; Timoshkin, A. Y.; von Hopffgarten, M.; Frenking, G. *J. Am. Chem. Soc.* **2009**, *131*, 3942–3949.

[143] Jimenez-Halla, C. O. C.; Fernandez, I.; Frenking, G. *Angew. Chem. Int. Ed.* **2009**, *48*, 366–369.

[144] Huang, Z.-G.; Yang, E.-C.; Xie, D.-Q. *Chin. J. Struct. Chem.* **2009**, *28*, 569–576.

[145] Perez-Peralta, N.; Juarez, R.; Cerpa, E.; Bickelhaupt, F. M.; Merino, G. *J. Phys. Chem. A* **2009**, *113*, 9700–9706.

[146] Misochko, E. Y.; Akimov, A. V.; Belov, V. A.; Tyurin, D. A. *Inorg. Chem.* **2009**, *48*, 8723–8728.

[147] Khriachtchev, L.; Räsänen, M.; Gerber, R. B. *Acc. Chem. Res.* **2009**, *42*, 183–191.

[148] Gardner, A. M.; Plowright, R. J.; Watkins, M. J.; Wright, T. G.; Breckenridge, W. H. *J. Chem. Phys.* **2010**, *132*, 184301.

[149] Torigoe, H.; Mori, T.; Fujie, K.; Ohkubo, T.; Itadani, A.; Gotoh, K.; Ishida, H.; Yamashita, H.; Yumura, T.; Kobayashi, H.; Kuroda, Y. *J. Phys. Chem. Lett.* **2010**, *1*, 2642–2650.

[150] Maroulis, G. *Theor. Chem. Acc.* **2011**, *129*, 437–445.

[151] Khriachtchev, L.; Domanskaya, A.; Lundell, J.; Akimov, A.; Räsänen, M.; Misochko, E. *J. Phys. Chem. A* **2010**, *114*, 4181–4187.

[152] Grant, D. J.; Wang, T.-H.; Dixon, D. A. *Inorg. Chem.* **2010**, *49*, 261–270.

[153] Borocci, S.; Bronzolino, N.; Giordani, M.; Grandinetti, F. *J. Phys. Chem. A* **2010**, *114*, 7382–7390.

[154] Liu, G.; Yang, Y.; Zhang, W. *Struct. Chem.* **2010**, *21*, 197–202.

[155] Rodigues, E. F. F.; de Sa, E. L.; Haiduke, R. L. A. *J. Phys. Chem. A* **2010**, *114*, 5222–5229.

[156] Sun, Y.-L.; Hong, J.-T.; Hu, W.-P. *J. Phys. Chem. A* **2010**, *114*, 9359–9367.

[157] Kobayashi, T.; Seki, K.; Takayanagi, T. *Chem. Phys. Lett.* **2010**, *498*, 235–239.

[158] Tsivion, E.; Gerber, R. B. *Phys. Chem. Chem. Phys.* **2010**, *12*, 11791–11794.

[159] Jacobson, D. R.; Khan, N. S.; Collé, R.; Fitzgerald, R.; Laureano-Pérez, L.; Bai, Y.; Dmochowski, I. J. *Proc. Nat. Acad. Sci.* **2011**, *108*, 10969–10973.

[160] Juarez, R.; Zavala-Oseguera, C.; Oscar, J.; Jimenez-Halla, C.; Bickelhaupt, F. M.; Merino, G. *Phys. Chem. Chem. Phys.* **2011**, *13*, 2222–2227.

[161] Grochala, W.; Khriachtchev, L.; Räsänen, M. In *Physics and Chemistry at Low Temperatures*; Khriachtchev, L., Ed.; Pan Stanford, 2011; Chapter 13: Noble-Gas Chemistry, pp 419–446.

[162] Khriachtchev, L.; Tapio, S.; Domanskaya, A. V.; Räsänen, M.; Isokoski, K.; Lundell, J. *J. Chem. Phys.* **2011**, *134*, 124307.

[163] Tsivion, E.; Gerber, R. B. *Phys. Chem. Chem. Phys.* **2011**, *13*, 19061–19606.

[164] Borocci, S.; Giordani, M.; Grandinetti, F. *Computational and Theoretical Chemistry* **2011**, *964*, 318–323.

[165] Zins, E.-L.; Milko, P.; Schroder, D.; Aysina, J.; Ascenzi, D.; Zabka, J.; Alcaraz, C.; Price, S. D.; Roithova, J. *Chem. Eur. J.* **2011**, *17*, 4012–4020.

[166] Zins, E.-L.; Schroder, D. *Int. J. Mass. Spec.* **2011**, *299*, 53–58.

[167] Tonner, R.; Frenking, G.; Lein, M.; Schwerdtfeger, P. *Chem. Phys. Chem.* **2011**, *12*, 2081–2084.

[168] Liu, G.; Li, H.; Zhang, X.; Zhang, W. *Compt. Theo. Chem.* **2011**, *963*, 394–402.

[169] Lai, T.-Y.; Yang, C.-Y.; Lin, H.-J.; Yang, C.-Y.; Hu, W.-P. *J. Chem. Phys.* **2011**, *134*, 244110.

[170] Schrobilgen, G. J.; Brock, D. S. *Annu. Rep. Prog. Chem., Sect. A* **2011**, *107*, 135–141.

[171] Schrobilgen, G. J.; Brock, D. S. *Annu. Rep. Prog. Chem., Sect. A* **2012**, *108*, 138–145.

[172] Brock, D. S.; Schrobilgen, G. J. *Annu. Rep. Prog. Chem., Sect. A* **2013**, *109*, 101–107.

[173] Peterson, K. A.; Dixon, D. A.; Stoll, H. *J. Phys. Chem. A* **2012**, *116*, 9777–9782.

[174] Zhang, M.; Sheng, L. *J. Chem. Phys.* **2013**, *138*, 114301.

[175] Ma, L.; Huang, Z.; Niu, X.; Shen, T.; Guo, L. *Comput. Theo. Chem.* **2013**, *1017*, 14–21.

[176] Cohen, A.; Tsuge, M.; Khriachtchev, L.; Räsänen, M.; Gerber, R. B. *Chem. Phys. Lett.* **2014**, *UPDATE*, UPDATE.

[177] Szabo, A.; Ostlund, N. S. *Modern Quantum Chemistry: Introduction to Advanced Electronic Structure Theory*; Dover, 1996.

[178] Pople, J. A.; Nesbet, R. K. *J. Chem. Phys.* **1954**, *22*, 571.

[179] Piecuch, P.; Włoch, M. *J. Chem. Phys.* **2005**, *123*, 224105/1–10.

[180] Jorgensen, P.; Simons, J. *Second Quantization-Based Methods in Quantum Chemistry*; Academic Press, 1981.

[181] Chéron, N.; Jacquemin, D.; Fleurat-Lessard, P. *Phys. Chem. Chem. Phys.* **2012**, *14*, 7170–7175.

[182] Burke, K. *The ABC of DFT*; Department of Chemistry, University of California Irvine: http://chem.ps.uci.edu/ kieron/dft/book, 2007.

[183] Perdew, J. P.; Burke, K.; Ernzerhof, M. *Phys. Rev. Lett* **1996**, *77*, 3865.

[184] Adamo, C.; Barone, V. *J. Chem. Phys.* **1999**, *110*, 6158.

[185] Miyoshi, E.; Mori, H.; Hirayama, R.; Osanai, Y.; Noro, T.; Honda, H.; Klobukowski, M. *J. Chem. Phys.* **2005**, *122*, 074101/1–8.

[186] Osanai, Y.; Mon, M. S.; Noro, T.; Mori, H.; Nakashima, H.; Klobukowski, M.; Miyoshi, E. *Chem. Phys. Lett.* **2008**, *452*, 210–214.

[187] Osanai, Y.; Soejima, E.; Noro, T.; Mori, H.; Mon, M. S.; Klobukowski, M.; Miyoshi, E. *Chem. Phys. Lett.* **2008**, *463*, 230–234.

[188] Mori, H.; Ueno-Noto, K.; Osanai, Y.; Noro, T.; Fujiwara, T.; Klobukowski, M.; Miyoshi, E. *Chem. Phys. Lett.* **2009**, *476*, 317–322.

[189] Klobukowski, M.; Huzinaga, S.; Sakai, Y. In *Computational Chemistry: Reviews of Current Trends*; Leszczynski, J., Ed.; World Scientific, Singapore, 1999; Vol. 3; Chapter 2: Model Core Potentials: Theory and Applications.

[190] Höjer, G.; Chung, J. *Int. J. Quantum Chem.* **1978**, *14*, 1978.

[191] Miyoshi, E.; Mori, H.; Hirayama, R.; Osanai, Y.; Noro, T.; Honda, H.; Klobukowski, M. *J. Chem. Phys.* **2005**, *122*, 074104/1–8.

[192] Miyoshi, E.; Mori, H.; Hirayama, R.; Osanai, Y.; Noro, T.; Honda, H.; Klobukowski, M. *J. Chem. Phys.* **2005**, *122*, 074104.

[193] Sekiya, M.; Noro, T.; Osanai, Y.; Koga, T. *Theor. Chim. Acta* **2001**, *106*, 297–300.

[194] Noro, T.; Sekiya, M.; Osanai, Y.; Miyoshi, E.; Koga, T. *J. Chem. Phys.* **2003**, *119*, 5142–5148.

[195] Lovallo, C. C.; Klobukowski, M. *J. Comput. Chem.* **2003**, *24*, 1009.

[196] Lovallo, C.; Klobukowski, M. *J. Comp. Chem.* **2004**, *25*, 1206–1213.

[197] Zeng, T.; Mori, H.; Miyoshi, E.; Klobukowski, M. *Int. J. Quantum Chem.* **2009**, *109*, 3235–3245.

[198] Zeng, T.; Klobukowski, M. *J. Chem. Phys.* **2010**, *133*, 114107.

[199] Bader, R. F. W. *Acc. Chem. Res.* **1985**, *18*, 9–15.

[200] Matta, C. F.; Boyd, R. J. In *The Quantum Theory of Atoms in Molecules: From Solid State to DNA and Drug Design*; Matta, C. F., Boyd, R. J., Eds.; Wiley-VCH, Weinheim, 2007; Chapter 1, pp 1–34.

[201] Khriachtchev, L.; Pettersson, M.; Runeberg, N.; Lundell, J.; Räsänen, M. *Nature* **2000**, *406*, 874–876.

[202] Runeberg, N.; Pettersson, M.; Khriachtchev, L.; Lundell, J.; Räsänen, M. *J. Chem. Phys.* **2001**, *114*, 836–841.

[203] Cohen, A.; Lundell, J.; Gerber, R. B. *J. Chem. Phys.* **2003**, *119*, 6415–6417.

[204] Liebman, J. F. *Inorg. Nucl. Chem. Lett.* **1975**, *11*, 687–690.

[205] Frenking, G. *Nature* **2000**, *406*, 836–837.

[206] Yamamoto, H.; Matsuoka, O. *Bull. Univ. Electro-Comm.* **1992**, *5*, 23.

[207] Noro, T.; Sekiya, M.; Koga, T. *Theor. Chem. Acc.* **2003**, *109*, 85–90.

[208] Dunning Jr., T. H. *J. Chem. Phys.* **1989**, *90*, 1007–1023.

[209] Woon, D. E.; T. H. Dunning, J. *J. Chem. Phys* **1993**, *98*, 1358–1371.

[210] Wilson, A. K.; Woon, D. E.; Peterson, K. A.; Dunning, T. H. *J. Chem. Phys.* **1999**, *110*, 7667–7676.

[211] Tatewaki, H.; Koga, T. *J. Chem. Phys.* **1996**, *104*, 8493–8499.

[212] Koga, T.; Tatewaki, H.; Shimazaki, T. *Chem. Phys. Lett.* **2000**, *328*, 473–482.

[213] Noro, T.; Sekiya, M.; Koga, T. *Theor. Chem. Acc.* **1997**, *98*, 25–32.

[214] Sekiya, M.; Noro, T.; Koga, T.; Matsuyama, H. *J. Mol. Struct. (Theochem)* **1998**, *451*, 51–60.

[215] Koga, T.; Tatewaki, H.; Matsuyama, H.; Satoh, Y. *Theor. Chem. Acc.* **1999**, *102*, 105–111.

[216] Koga, T.; Yamamoto, S.; Shimazaki, T.; Tatewaki, H. *Theor. Chem. Acc.* **2002**, *108*, 41–45.

[217] Nakajima, T.; Hirao, K. *J. Chem. Phys.* **2002**, *116*, 8270–8275.

[218] `http://setani.sci.hokudai.ac.jp/sapporo/Welcome.do`.

[219] Piecuch, P.; Kucharski, S. A.; Kowalski, K.; Musiał, M. *Comput. Phys. Comm.* **2002**, *149*, 71–96.

[220] Knowles, P. J.; Andrews, J. S.; Amos, R. D.; Handy, N. C.; Pople, J. A. *Chem. Phys. Lett.* **1991**, *186*, 130–136.

[221] Lauderdale, W. J.; Stanton, J. F.; Gauss, J.; Watts, J. D.; Bartlett, R. J. *Chem. Phys. Lett.* **1991**, *187*, 21–28.

[222] Wong, M. W. *J. Am. Chem. Soc.* **2000**, *122*, 6289–6290.

[223] Lein, M.; Frunzke, J.; Frenking, G. *Struct. Bond.* **2004**, *106*, 181–191.

[224] McWeeny, R.; Diercksen, G. H. F. *J. Chem. Phys.* **1968**, *49*, 4852–4856.

[225] Guest, M. F.; Saunders, V. R. *Mol. Phys.* **1974**, *28*, 819–828.

[226] Hsu, H.; Davidson, E. R.; Pitzer, R. M. *J. Chem. Phys.* **1976**, *65*, 609–613.

[227] Moore, C. E. *Atomic Energy Levels*; National Bureau of Standards: Washington, D.C., 1949; Vol. 1.

[228] Moore, C. E. *Atomic Energy Levels*; National Bureau of Standards: Washington, D.C., 1952; Vol. 2.

[229] Moore, C. E. *Atomic Energy Levels*; National Bureau of Standards: Washington, D.C., 1957; Vol. 3.

[230] van Duijneveldt, F. B.; van Duijneveldt-van de Rijdt, J. G. C. M.; van Lenthe, J. H. *Chem. Rev.* **1994**, *94*, 1873–1885.

[231] Chałasinski, G.; Szczęśniak, M. M. *Chem. Rev.* **2000**, *100*, 4227–4252.

[232] Boys, S. F.; Bernardi, F. *Mol. Phys.* **1970**, *19*, 553–566.

[233] Grev, R. S.; Schaefer III, H. F. *J. Chem. Phys.* **1989**, *91*, 7305–7306.

[234] Li, H.; Xie, D.; Guo, H. *J. Chem. Phys.* **2004**, *120*, 4273–4280.

[235] Li, T. H.; Liu, Y. L.; Lin, R. J.; Yeh, T. Y.; Hu, W. P. *Chem. Phys. Lett.* **2007**, *434*, 38–41.

[236] Hurley, M. M.; Pacios, L. F.; Christiansen, P. A.; Ross, R. B.; Ermler, W. C. *J. Chem. Phys.* **1986**, *84*, 6840–6853.

[237] LaJohn, L. A.; Christiansen, P. A.; Ross, R. B.; Atashroo, T.; Ermler, W. C. *J. Chem. Phys.* **1987**, *87*, 2812–2824.

[238] Ross, R. B.; Powers, J. M.; Atashroo, T.; Ermler, W. C.; LaJohn, L. A.; Christiansen, P. A. *J. Chem. Phys.* **1990**, *93*, 6654–6670.

[239] Martin, J. M. L.; de Oliveira, G. *J. Chem. Phys.* **1999**, *111*, 1843–1856.

[240] Mulliken, R. S. *J. Chem. Phys.* **1955**, *23*, 1833–1840.

[241] Levine, I. N. *Quantum Chemistry, p.432-434*, 3rd ed.; The Allyn and Bacon Chemistry Series; Allyn and Bacon, 1983.

[242] Löwdin, P.-O. *J. Chem. Phys.* **1950**, *18*, 365–375.

[243] Read, A. E.; Weinhold, F. *J. Chem. Phys.* **1983**, *78*, 4066–4073.

[244] Read, A. E.; Weinstock, R. B.; Weinhold, F. *J. Chem. Phys.* **1985**, *83*, 735–746.

[245] Giambagi, M.; Giambagi, M.; Grempel, D. R.; Heymann, C. D. *J. Chim. Phys.* **1975**, *72*, 15–22.

[246] Mayer, I. *Chem. Phys. Lett.* **1983**, *97*, 270–274.

[247] Møller, Chr.; Plesset, M. S. *Phys. Rev. A* **1934**, *46*, 618–622.

[248] MacDougall, P. J.; Schrobilgen, G. J.; Bader, R. F. W. *Inorg. Chem.* **1989**, *28*, 763–769.

[249] Schmidt, M. W.; Baldridge, K. K.; Boatz, J. A.; Elbert, S. T.; Gordon, M. S.; Jensen, J. H.; Koseki, S.; Matsunaga, N.; Nguyen, K. A.; Su, S.; Windus, T. L.; Dupuis, M.; Montgomery, J. A. *J. Comput. Chem.* **1993**, *14*, 1347–1363.

[250] Keith, T. A. AIMAll (Version 12.06.03). TK Gristmill Software, Overland Park KS, USA, 2012 (aim.tkgristmill.com).

[251] Cioslowski, J.; Piskorz, P. *Chem. Phys. Lett.* **1996**, *255*, 315–319.

[252] Keith, T. A.; Frisch, M. J. *J. Phys. Chem. A* **2011**, *115*, 12879–1294.

[253] Frisch, M. J. et al. Gaussian, Inc, Wallingford CT.

[254] Binkley, J. S.; Pople, J. A.; Hehre, W. J. *J. Am. Chem. Soc.* **1980**, *102*, 939.

[255] Stevens, W. J.; Basch, H.; Krauss, M. *J .Chem. Phys.* **1984**, *81*, 6026.

[256] Stevens, W. J.; Krauss, M.; Basch, H.; Jasien, P. G. *Can. J. Chem.* **1992**, *70*, 612–630.

[257] Glendening, E. D.; Badenhoop, J. K.; Reed, A. E.; Carpenter, J. E.; Bohmann, J. A.; Morales, C. M.; Weinhold, F. NBO 5.G. Theoretical Chemistry Institute, University of Wisconsin, Madison, WI, U.S.A., 2004.

[258] Fitzsimmons, A.; Mori, H.; Miyoshi, E.; Klobukowski, M. *J. Phys. Chem. A* **2010**, *114*, 8786.

[259] Chaban, G. M.; Lundell, J.; Gerber, R. B. *Chem. Phys. Lett.* **2002**, *364*, 628–633.

[260] Cowan, R. D.; Griffin, D. C. *J. Opt. Soc. Am.* **1976**, *66*, 1010.

[261] Douglas, M.; Kroll, N. M. *Ann. Phys.* **1974**, *82*, 89–115.

[262] Hess, B. A. *Phys. Rev. A* **1986**, *33*, 3742.

[263] Shim, J.; Klobukowski, M.; Barysz, M.; Leszczynski, J. *Phys. Chem. Chem. Phys.* **2011**, *13*, 5703–5711.

[264] Bode, B. M.; Gordon, M. S. *J. Mol. Graphics Modell.* **1998**, *16*, 133–138.

[265] Pyykkö, P.; Atsumi, M. *Chem. Eur. J.* **2009**, *15*, 12770–12779.

[266] Pyykkö, P.; Atsumi, M. *Chem. Eur. J.* **2009**, *15*, 186–197.

[267] Pyykkö, P.; Riedel, S.; Patzschke, M. *Chem. Eur. J.* **2005**, *11*, 3511–3520.

[268] Weinhold, F. *Encyclopedia of Computational Chemistry* **1998**, *3*, 1792.

[269] Miertus, S.; Scrocco, E.; Tomasi, J. *Chem. Phys.* **1981**, *55*, 117–129.

[270] Tomasi, J.; Persico, M. *Chem. Rev.* **1994**, *94*, 2027–2094.

[271] Tomasi, J.; Mennucci, B.; Cammi, R. *Chem. Rev.* **2005**, *105*, 2999–3093.

[272] Bancroft, G. M.; Malmqvist, P.-Å.; Svensson, S.; Basilier, E.; Gelius, U.; Siegbahn, K. *Inorg. Chem.* **1978**, *17*, 1595–1599.

[273] Schmeisser, V. M.; Walter, R.; Naumann, D. *Z. Anorg. Allg. Chem.* **1980**, *464*, 233–239.

[274] Fitzsimmons, A.; Klobukowski, M. *Theor. Chem. Acc.* **2013**, *132*, 1314.

[275] Chai, J.-D.; Head-Gordon, M. *J. Chem. Phys.* **2008**, *128*, 084106.

[276] Koch, W.; Holthausen, M. C. *A Chemist's guide to density functional theory*, 2nd ed.; WILEY-VCH, New York, 2008.

[277] Fitzsimmons, A.; Klobukowski, M. The source code for this local modification of GAMESS-US is available from the authors upon request.

[278] Schmidt, M. W.; Baldridge, K. K.; Boatz, J. A.; Elbert, S. T.; Gordon, M. S.; Jensen, J. H.; Koseki, S.; Matsunaga, N.; Nguyen, K. A.; Su, S.; Windus, T. L.; Dupuis, M.; Montgomery, J. A. *J. Comput. Chem.* **1993**, *14*, 1347–1363.

[279] Keith, T. A.

[280] McNaught, A. D.; Wilkinson, A. *IUPAC Compendium of Chemical Terminology*, 2nd ed.; Blackwell Scientific Publications: Oxford, 1997.

[281] Dorsey, C. L.; Mushinski, R. M.; Hudnall, T. W. *Chem. Eur. J.* **2014**, *(Early View) DOI: 10.1002/chem.201403578*.

[282] Bihary, Z.; Chaban, G. M.; Gerber, R. B. *J. Chem. Phys.* **2003**, *119*, 11278–11284.

[283] Jaskólski, W. *Phys. Rep.* **1996**, *217*, 1–66.

[284] Bielińska-Wąż, D.; Karwowski, J.; Diercksen, G. H. F. *J. Phys. B* **2001**, *34*, 1987–2000.

[285] Bielińska-Wąż, D.; Diercksen, G. H. F.; Klobukowski, M. *Chem. Phys. Lett.* **2001**, *349*, 215–219.

[286] Dolmatov, V. K.; Baltenkov, A. S.; Connerade, J.-P.; Manson, S. T. *Rad. Phys. Chem.* **2004**, *70*, 417–433.

[287] Lo, J. M. H.; Klobukowski, M. *Mol. Phys.* **2004**, *102*, 2511–2519.

[288] Lo, J. M. H.; Klobukowski, M. *Mol. Phys.* **2005**, *103*, 2599–2612.

[289] Kadosh, J. S.; Lo, J. M. H.; Klobukowski, M. *Lecture Series on Computer and Computational Sciences*; Brill Academic Publishers, 2006; Vol. 1; pp 1–3.

[290] Lo, J. M. H.; Klobukowski, M.; Diercksen, G. H. F. *Adv. Quantum Chem.* **2005**, *48*, 59–89.

[291] Lo, J. M. H.; Klobukowski, M.; Bielińska-Wąż, D.; Diercksen, G. H. F. *J. Phys. B: At. Mol. Phys.* **2005**, *38*, 1143–1159.

[292] Lo, J. M. H.; Klobukowski, M.; Bielińska-Wąż, D.; Schreiner, E. W. S.; Diercksen, G. H. F. *J. Phys. B: At. Mol. Phys.* **2006**, *39*, 2385–2402.

[293] Lo, J. M. H.; Klobukowski, M. *Theor. Chim. Acta* **2007**, *118*, 607.

[294] Bielińska-Wąż, D.; Lo, J. M. H.; Klobukowski, M.; Schreiner, E. W. S.; Diercksen, G. H. F. *Chem. Phys. Lett.* **2006**, *422*, 391–396.

[295] Sako, T.; Diercksen, G. H. F. *Phys. Rev. B* **2007**, *75*, 115413.

[296] Sako, T.; Diercksen, G. H. F. *J. Phys.: Condens. Matter* **2008**, *20*, 155202.

[297] Piecuch, P.; Kucharski, S. A.; Kowalski, K.; Musiał, M. *Comput. Phys. Commun.* **2002**, *149*, 71–96.

[298] Kowalski, K.; Piecuch, P. *J. Chem. Phys.* **2004**, *120*, 1715–1738.

[299] Włoch, M.; Gour, J. R.; Kowalski, K.; Piecuch, P. *J. Chem. Phys.* **2005**, *122*, 214107.

[300] Hilderbrandt, R. L. *J. Chem. Phys.* **1969**, *51*, 1654–1659.

[301] GAMESS-US Reference Manual, section 4: Further Information. Quote is from the Coupled Clusters section, "available computations (excited states)".

[302] Gour, J. R.; Piecuch, P.; Włoch, M. *J. Chem. Phys.* **2005**, *123*, 134113.

[303] Gour, J. R.; Piecuch, P. *J. Chem. Phys.* **2006**, *125*, 234107.

[304] Connerade, J. P. *AIP Conference Proceedings* **2009**, *1197*, 1–33.

[305] Levine, I. N. *Quantum Chemistry, Chapter 11*, 3rd ed.; The Allyn and Bacon Chemistry Series; Allyn and Bacon, 1983.

[306] Stevens, W. J.; Basch, H.; Krauss, M. *J. Chem. Phys.* **1984**, *81*, 6026.

[307] Fitzsimmons, A.; Klobukowski, M. *Can. J. Chem.* **2013**, *91*, 894–901.

[308] Shen, T.; Huang, Z.; Guo, L.; Wang, H. *Inorg. Chim. Acta* **2012**, *386*, 68–72.

[309] Haiduke, R. L. A.; Filho, H. D. P. M.; da Silva, A. B. F. *Chem. Phys.* **2008**, *348*, 89–96.

[310] Chaban, G. M.; Gerber, R. B. *Theor. Chem. Acc.* **2008**, *120*, 273–279.

[311] Huang, Z.; Guo, L.; Shen, T.; Ma, L.; Niu, X. *Phys. Chem. Chem. Phys.* **2012**, *14*, 8083–8089.

[312] GAMESS-US Reference Manual, Section 2. Quote is from the $VSCF input group description.

[313] Yamamoto, H.; Matsuoka, O. *Bull. University Elec.-Commun.* **1992**, *5*, 23–34.

[314] Huzinaga, S. *Comp. Phys. Rep.* **1985**, *2*, 279–340.

[315] Gerber, R. B.; Jung, J. O. In *Computational Molecular Spectroscopy*; Jensen, P., Bunker, P. R., Eds.; Wiley & Sons Ltd., 2000; Chapter 11: The Vibrational Self-Consistent Field Approach and Extensions: Method and Applications to Spectroscopy of Large Molecules and Clusters, pp 365–390.

[316] Chaban, G. M.; Jung, J. O.; Gerber, R. B. *J. Chem. Phys.* **1999**, *111*, 1823.

[317] Yagi, K.; Hirao, K.; Taketsugu, T.; Schmidt, M. W.; Gordon, M. S. *J. Chem. Phys.* **2004**, *121*, 1383–1389.

[318] Cotton, F. A.; Wilkinson, G. *Advanced Inorganic Chemistry: A Comprehensive Text*, 3rd ed.; Interscience Publishers, 1972.

[319] Gerber, R. B.; Sebek, J. In *Physics and Chemistry at Low Temperatures*; Khriachtchev, L., Ed.; Pan Stanford, 2011; Chapter 15: Spectroscopy of Biological Molecules at Very Low Temperatures: Theoretical Studies, pp 469–496.

[320] Cassam-Chenaï, P.; Liévin, J. *J. Chem. Phys.* **2012**, *136*, 174309.

[321] Werner, H.-J.; Knowles, P. J.; Lindh, R.; Manby, F. R.; Schütz, M. MOLPRO program version 2009.

Appendix to Chapter 4

All results were obtained at the MP2/aug-MCP-TZP level of theory. The numbering system for atoms in the molecules described in this paper counts from the left of the molecule (following the chemical formula as written in the chapter), with the first incidence of any repeated atoms being X_1 and subsequent appearances being numbered X_2, X_n, etc.

Table A1: *Structural parameters of AXeF systems (Å and degrees).*

CNXeF	r(N-C)	r(C-Xe)	r(Xe-F)	
	1.169	2.080	2.021	
CCFXeF	r(F_1-C_1)	r(C_1-C_2)	r(C_2-Xe)	r(Xe-F_2)
	1.270	1.206	2.053	2.045
CCHXeF	r(H-C_1)	r(C_1-C_2)	r(C_2-Xe)	r(Xe-F)
	1.053	1.212	2.053	2.051
CF_3XeF	r(F_1-C)	r(C-Xe)	r(Xe-F_4)	∠(F_1-C-Xe)
	1.322	2.187	2.072	110.07
CH_3XeF	r(H-C)	r(C-Xe)	r(Xe-F)	∠(H-C-Xe)
	1.063	2.158	2.116	111.54

Table A2: *Structural parameters of ARnF systems (Å and degrees).*

CNRnF	r(C-N)	r(C-Rn)	r(Rn-F)	
	1.169	2.181	2.098	
CCFRnF	r(F_1-C_1)	r(C_1-C_2)	r(C_2-Rn)	r(Rn-F_2)
	1.271	1.208	2.154	2.120
CCHRnF	r(H-C_1)	r(C_1-C_2)	r(C_1-Rn)	r(Rn-F)
	1.053	1.214	2.155	2.125
CF_3RnF	r(F_1-C)	r(C-Rn)	r(Rn-F_2)	$\angle$(F_1-C-Rn)
	1.326	2.278	2.147	110.14
CH_3RnF	r(H-C)	r(C-Rn)	r(Rn-F)	$\angle$(H-C-Rn)
	1.063	2.250	2.184	111.54

Table A3: ΔG *(in kJ/mol) for Reaction (2)*

A-Rg-B	ΔG_2	reactant 1	reactant 2	ΔG_1
CNXeCN	-68			
CCFXeCN	-69	$(CH_3)_3$Si-CCF	CN-Xe-F	-116
CCFXeCCF	-53			
CCHXeCN	-77	$(CH_3)_3$Si-CCH	CN-Xe-F	-116
CCHXeCCF	-61	$(CH_3)_3$Si-CCH	CCF-Xe-F	-120
CCHXeCCH	-55			
CF_3XeCN	-124	$(CH_3)_3$Si-CF_3	CN-Xe-F	-116
CF_3XeCCF	-105	$(CH_3)_3$Si-CF_3	CCF-Xe-F	-120
CF_3XeCCH	-100	$(CH_3)_3$Si-CF_3	CCH-Xe-F	-131
CH_3XeCN	-146	$(CH_3)_3$Si-CH_3	CN-Xe-F	-116
CH_3XeCCF	-114	$(CH_3)_3$Si-CH_3	CCF-Xe-F	-120
CH_3XeCCH	-107	$(CH_3)_3$Si-CH_3	CCH-Xe-F	-131
CNRnCN	-71			
CCFRnCN	-72	$(CH_3)_3$Si-CCF	CN-Rn-F	-112
CCFRnCCF	-58			
CCHRnCN	-79	$(CH_3)_3$Si-CCH	CN-Rn-F	-112
CCHRnCCF	-65	$(CH_3)_3$Si-CCH	CCF-Rn-F	-114
CCHRnCCH	-60			
CF_3RnCN	-116	$(CH_3)_3$Si-CF_3	CN-Rn-F	-112
CF_3RnCCF	-100	$(CH_3)_3$Si-CF_3	CCF-Rn-F	-114
CF_3RnCCH	-95	$(CH_3)_3$Si-CF_3	CCH-Rn-F	-124
CH_3RnCN	-136	$(CH_3)_3$Si-CH_3	CN-Rn-F	-112
CH_3RnCF	-108	$(CH_3)_3$Si-CH_3	CCF-Rn-F	-114
CH_3RnCCH	-100	$(CH_3)_3$Si-CH_3	CCH-Rn-F	-124

Table A4: *ΔG (in kJ/mol) for Reaction (5)*

A-Rg-B	ΔG_3	reactant 1	reactant 2	ΔG_1
CNXeCN	-68			
CCFXeCN	-65	$(CH_3)_3$Si-CN	CCF-Xe-F	-120
CCFXeCCF	-53			
CCHXeCN	-62	$(CH_3)_3$Si-CN	CCH-Xe-F	-131
CCHXeCCF	-50	$(CH_3)_3$Si-CCF	CCH-Xe-F	-131
CCHXeCCH	-55			
CF_3XeCN	-61	$(CH_3)_3$Si-CN	CF_3-Xe-F	-179
CF_3XeCCF	-46	$(CH_3)_3$Si-CCF	CF_3-Xe-F	-179
CF_3XeCCH	-51	$(CH_3)_3$Si-CCH	CF_3-Xe-F	-179
CH_3XeCN	-60	$(CH_3)_3$Si-CN	CH_3-Xe-F	-202
CH_3XeCCF	-33	$(CH_3)_3$Si-CCF	CH_3-Xe-F	-202
CH_3XeCCH	-35	$(CH_3)_3$Si-CCH	CH_3-Xe-F	-202
CNRnCN	-71			
CCFRnCN	-70	$(CH_3)_3$Si-CN	CCF-Rn-F	-114
CCFRnCCF	-58			
CCHRnCN	-67	$(CH_3)_3$Si-CN	CCH-Rn-F	-124
CCHRnCCF	-56	$(CH_3)_3$Si-CCF	CCH-Rn-F	-124
CCHRnCCH	-60			
CF_3RnCN	-64	$(CH_3)_3$Si-CN	CF_3-Rn-F	-164
CF_3RnCCF	-50	$(CH_3)_3$Si-CCF	CF_3-Rn-F	-164
CF_3RnCCH	-55	$(CH_3)_3$Si-CCH	CF_3-Rn-F	-164
CH_3RnCN	-63	$(CH_3)_3$Si-CN	CH_3-Rn-F	-185
CH_3RnCF	-37	$(CH_3)_3$Si-CCF	CH_3-Rn-F	-185
CH_3RnCCH	-38	$(CH_3)_3$Si-CCH	CH_3-Rn-F	-185

Table A5: *Structural parameters of AXeB systems (Å and degrees).*

CNXeCN	r(N-C)	r(C-Xe)				
	1.171	2.192				
CCFXeCN	r(F_1-C_1)	r(C_1-C_2)	r(C_2-Xe)	r(Xe-C_3)	r(C_3-C_4)	
	1.271	1.211	2.135	2.238	1.171	
CCFXeCCF	r(F-$C_{1,4}$)	r($C_{1,3}$-$C_{2,4}$)	r($C_{2,3}$-Xe)			
	1.276	1.214	2.178			
CCHXeCN	r(H-C_1)	r(C_1-C_2)	r(C_2-Xe)	r(Xe-C_3)	r(C_3-N)	
	1.054	1.216	2.133	2.252	1.172	
CCHXeCCF	r(H-C_1)	r(C_1-C_2)	r(C_2-Xe)	r(Xe-C_3)	r(C_3-C_4)	r(C_4-F)
	1.054	1.218	2.176	2.193	1.215	1.276
CCHXeCCH	r(H-$C_{1,4}$)	r($C_{1,3}$-$C_{2,4}$)	r($C_{2,3}$-Xe)			
	1.054	1.219	2.190			
CF_3XeCN	r(F-C_1)	r(C_1-Xe)	r(Xe-C_2)	r(C_2-N)	∠(F_1-C_1-Xe)	
	1.324	2.260	2.315	1.172	109.84	
CF_3XeCCF	r(F-C_1)	r(C_1-Xe)	r(Xe-C_2)	r(C_2-C_3)	r(C_3-F)	∠(F_1-C_1-Xe)
	1.330	2.277	2.249	1.217	1.278	109.55
CF_3XeCCH	r(F-C_1)	r(C_1-Xe)	r(Xe-C_2)	r(C_2-C_3)	r(H-C_3)	∠(F_1-C_1-Xe)
	1.331	2.287	2.251	1.221	1.062	110.65
CH_3XeCN	r(H-C_1)	r(C_1-Xe)	r(Xe-C_2)	r(C_2-N)	∠(H-C_1-Xe)	
	1.063	2.204	2.390	1.173	111.54	
CH_3XeCCF	r(H-C_1)	r(C_1-Xe)	r(Xe-C_2)	r(C_2-C_3)	r(C_3-F)	∠(H-C_1-Xe)
	1.063	2.239	2.318	1.221	1.284	111.54
CH_3XeCCH	r(H_1-C_1)	r(C_1-Xe)	r(Xe-C_2)	r(C_2-C_3)	r(C_3-H_4)	∠(H_1-C_1-Xe)
	1.083	2.251	2.318	1.224	1.062	107.34

Table A6: *Structural parameters of ARnB systems (Å and degrees).*

CNRnCN	r(C-N)	r(C-Rn)				
	1.171	2.268				
CCFRnCN	r(F-C_1)	r(C_1-C_2)	r(C_2-Rn)	r(Rn-C_3)	r(C_3-N)	
	1.272	1.213	2.222	2.305	1.171	
CCFRnCCF	r($C_{1,4}$-F)	r($C_{1,3}$-$C_{2,4}$)	r($C_{2,3}$-Rn)			
	1.276	1.215	2.257			
CCHRnCN	r(H-C_1)	r(C_1-C_2)	r(C_2-Rn)	r(Rn-C_3)	r(C_3-N)	
	1.054	1.217	2.222	2.317	1.171	
CCHRnCCF	r(H-C_1)	r(C_1-C_2)	r(C_2-Rn)	r(Rn-C_3)	r(C_3-F)	
	1.219	2.257	2.269	1.216	1.277	
CCHRnCCH	r(H-C_1)	r($C_{1,3}$-$C_{2,4}$)	r($C_{2,3}$-Rn)			
	1.053	1.220	2.269			
CF_3RnCN	r(F-C_1)	r(C_1-Rn)	r(Rn-C_2)	r(C_2-N)	∠(F$_1$-C$_1$-Rn)	
	1.329	2.334	2.371	1.173	110.14	
CF_3RnCCF	r($F_{1,2,3}$-C_1)	r(C_1-Rn)	r(Rn-C_2)	r(C_2-C_3)	r(C_3-F)	∠(F$_1$-C$_1$-Rn)
	1.335	2.350	2.316	1.218	1.278	110.07
CF_3RnCCH	r(F-C_1)	r(C_1-Rn)	r(Rn-C_2)	r(C_2-C_3)	∠(F$_1$-C$_1$-Rn)	
	1.336	2.359	2.318	1.221	111.20	
CH_3RnCN	r(H$_1$-C$_1$)	r(C_1-Rn)	r(Rn-C_2)	r(C_2-N)	∠(H$_1$-C$_1$-Rn)	
	1.063	2.288	2.436	1.173	111.54	
CH_3RnCCF	r(H$_1$-C$_1$)	r(C_1-Rn)	r(Rn-C_2)	r(C_2-C_3)	r(C_3-F)	∠(H-C$_1$-Rn)
	1.063	2.316	2.378	1.222	1.284	111.54
CH_3RnCCH	r(H$_1$-C$_1$)	r(C_1-Rn)	r(Rn-C_2)	r(C_2-C_3)	r(C_3-H$_4$)	∠(H$_1$-C$_1$-Rn)
	1.083	2.327	2.379	1.224	1.062	107.34

Table A7: *CEBE for molecules with two distinct light atoms (in eV)*

Molecule	CEBE 1	CEBE 2
CNXeCN	N 405.52	C 291.65
CNRnCN	N 405.36	C 291.50
CCHXeCCH	C_1 290.02	C_2 289.60
CCHRnCCH	C_1 289.92	C_2 289.49
CH_3XeF	C 291.44	F 687.50
CH_3RnF	C 291.21	F 688.10
CCHXeCCH	$C_{1,2}$ 290.03	$C_{3,4}$ 289.60
CCHRnCCH	$C_{1,2}$ 289.92	$C_{3,4}$ 289.49

Table A8: *CEBE for molecules with three distinct light atoms (in eV)*

Molecule	CEBE 1	CEBE 2	CEBE 3
CNXeF	C 292.60	N 406.17	F 689.86
CNRnF	C 292.32	N 406.06	F 690.29
CCHXeF	C_1 291.22	C_2 291.17	F 688.80
CCHRnF	C_1 290.95	C_2 290.82	F 688.70
CCFXeCCF	$C_{1,2}$ 292.68	$C_{3,4}$ 289.84	F 694.67
CCFRnCCF	$C_{1,2}$ 292.57	$C_{3,4}$ 289.74	F 694.59
CF_3XeF	C 298.85	$F_{1,2,3}$ 694.95	F_4 688.65
CF_3RnF	C 298.48	$F_{1,2,3}$ 694.68	F_4 688.53
CH_3XeCCH	C_1 290.14	C_2 288.40	C_3 288.98
CH_3RnCCH	C_1 289.94	C_2 288.41	C_3 288.98
CH_3XeCN	C_1 291.17	C_2 289.38	N 403.41
CH_3RnCN	C_1 290.87	C_2 289.50	N 403.50

Table A9: *CEBE for molecules with four distinct light atoms (in eV)*

Molecule	CEBE 1	CEBE 2	CEBE 3	CEBE 4
CCFXeF	C_1 293.81	C_2 291.27	F_1 695.53	F_2 688.93
CCFRnF	C_1 293.53	C_2 290.93	F_1 695.34	F_2 688.83
CCHXeCN	C_1 290.89	C_2 290.57	C_3 290.63	N 404.56
CCHRnCN	C_1 290.69	C_2 290.33	C_3 290.61	N 404.53
CF_3XeCCH	F 693.88	C_1 297.20	C_2 289.85	C_3 289.34
CF_3RnCCH	F 693.67	C_1 297.01	C_2 289.80	C_3 289.30
CH_3XeCCF	C_1 290.33	C_2 291.49	C_3 288.54	F 693.70
CH_3RnCCF	C_1 290.11	C_2 291.50	C_3 288.57	F 693.71
CF_3XeCN	C_1 298.24	F 694.73	C_2 290.35	N 404.36
CF_3RnCN	C_1 297.96	F 694.47	C_2 290.38	N 404.36

Table A10: *CEBE for molecules with five distinct light atoms (in eV)*

Molecule	CEBE 1	CEBE 2	CEBE 3	CEBE 4	CEBE 5
CCFXeCN	F 695.28	C_1 293.44	C_2 290.64	C_3 290.78	N 404.70
CCFRnCN	F 695.14	C_1 293.24	C_2 290.43	C_3 290.75	N 404.64
CCHXeCCF	C_1 290.16	C_2 289.76	C_3 289.69	C_4 292.55	F 694.56
CCHRnCCF	C_1 290.03	C_2 289.63	C_3 289.60	C_4 292.45	F 694.50
CF_3XeCCF	$F_{1,2,3}$ 694.01	C_1 297.37	C_2 292.38	C_3 289.46	F_4 694.43
CF_3RnCCF	$F_{1,2,3}$ 693.79	C_1 297.17	C_2 292.33	C_3 289.43	F_4 694.40

Table A11: *NPA atomic charges in AXeF systems.*

CNXeF	C	N	Xe	F			
	-0.10	-0.27	1.06	-0.68			
CNXeCN	C	N	Xe				
	-0.05	-0.37	0.84				
CCFXeF	F_1	C_1	C_2	Xe	F_2		
	-0.24	0.40	-0.50	1.05	-0.71		
CCFXeCN	F	C_1	C_2	Xe	C_3	N	
	-0.25	0.37	-0.50	0.90	-0.17	-0.34	
CCFXeCCF	F	$C_{1,4}$	$C_{2,3}$	Xe			
	-0.26	0.34	-0.52	0.88			
CCHXeF	H	C_1	C_2	Xe	F		
	0.23	-0.16	-0.39	1.04	-0.72		
CCHXeCN	H	C_1	C_2	Xe	C_3	N	
	0.22	-0.16	-0.43	0.87	-0.09	-0.41	
CCHXeCCF	H	C_1	C_2	Xe	C_3	C_4	F
	0.22	-0.20	-0.44	0.88	-0.53	0.33	-0.26
CCHXeCCH	H	$C_{1,4}$	$C_{2,3}$	Xe			
	0.20	-0.23	-0.36	0.78			
CF_3XeF	$F_{1,2,3}$	C	Xe	F_4			
	-0.31	0.78	0.88	-0.71			
CF_3XeCN	$F_{1,2,3}$	C_1	Xe	C_2	N		
	-0.32	0.76	0.75	-0.18	-0.37		
CF_3XeCCF	$F_{1,2,3}$	C_1	Xe	C_2	C_3	F_4	
	-0.33	0.73	0.76	0.34	-0.43	-0.26	
CF_3XeCCH	$F_{1,2,3}$	C_1	Xe	C_2	C_3	H	
	-0.33	0.72	0.75	-0.22	-0.46	0.21	
CH_3XeF	$H_{1,2,3}$	C	Xe	F			
	0.22	-0.80	0.88	-0.76			
CH_3XeCN	$H_{1,2,3}$	C_1	Xe	C_2	N		
	0.22	-0.82	0.79	-0.22	-0.42		
CH_3XeCCF	$H_{1,2,3}$	C_1	Xe	C_2	C_3	F	
	0.22	-0.85	0.78	0.31	-0.61	-0.27	
CH_3XeCCH	$H_{1,2,3}$	C_1	Xe	C_2	C_3	H_4	
	0.21	-0.86	0.76	-0.48	-0.26	0.20	

Table A12: *NPA atomic charges in ARnF systems.*

CNRnF	C	N	Rn	F			
	-0.13	-0.29	1.12	-0.70			
CNRnCN	C	N	Rn				
	-0.20	-0.29	0.98				
CCFRnF	F_1	C_1	C_2	Rn	F_2		
	-0.25	0.41	-0.56	1.12	-0.73		
CCFRnCN	F	C_1	C_2	Rn	C_3	N	
	-0.25	0.41	-0.61	0.99	-0.19	-0.35	
CCFRnCCF	F	$C_{1,4}$	$C_{2,3}$	Rn			
	-0.26	0.38	-0.61	0.99			
CCHRnF	H	C_1	C_2	Rn	F		
	0.21	-0.14	-0.45	1.11	-0.74		
CCHRnCN	H	C_1	C_2	Rn	C_3	N	
	0.21	-0.14	-0.48	0.96	-0.20	-0.35	
CCHRnCCF	H	C_1	C_2	Rn	C_3	C_4	F
	0.20	-0.17	-0.49	0.98	-0.63	0.38	-0.26
CCHRnCCH	H	$C_{1,4}$	$C_{2,3}$	Rn			
	0.20	-0.18	-0.50	0.95			
CF_3RNF	$F_{1,2,3}$	C	Rn	F_4			
	-0.32	0.76	0.94	-0.74			
CF_3RnCN	$F_{1,2,3}$	C_1	Rn	C_2	N		
	-0.33	0.74	0.82	-0.21	-0.37		
CF_3RnCCF	$F_{1,2,3}$	C_1	Rn	C_2	C_3	F_4	
	-0.34	0.71	0.84	0.37	-0.64	-0.26	
CF_3RnCCH	$F_{1,2,3}$	C_1	Rn	C_2	C_3	H	
	-0.34	0.70	0.83	-0.23	-0.49	0.21	
CH_3RnF	$H_{1,2,3}$	C	Rn	F			
	0.22	-0.84	0.95	-0.78			
CH_3RnCN	$H_{1,2,3}$	C_1	Rn	C_2	N		
	0.22	-0.87	0.86	-0.24	-0.41		
CH_3RnCCF	$H_{1,2,3}$	C_1	Rn	C_2	C_3	F	
	0.21	-0.90	0.86	0.33	-0.66	-0.28	
CH_3RnCCH	$H_{1,2,3}$	C_1	Rn	C_2	C_3	H_4	
	0.21	-0.90	0.84	-0.51	-0.27	0.20	

Table A13: *Optimized coordinates of AXeF systems (in Å).*

```
CNXeF mp2 acp3    ( cnxef_mp2_acp3_gh.out )

N           7.0  -0.0000000000   0.0000000000   3.3572908630
C           6.0   0.0000000000   0.0000000000   2.1886231846
XE         54.0   0.0000000000   0.0000000000   0.1087633542
F           9.0  -0.0000000000   0.0000000000  -1.9123609155

CCFXeF mp2 acp3    ( ccfxef_mp2_acp3_gh.out )

F           9.0   0.0000000000   0.0000000000   4.5416521990
C           6.0   0.0000000000   0.0000000000   3.2721391725
C           6.0  -0.0000000000   0.0000000000   2.0660433187
XE         54.0  -0.0000000000   0.0000000000   0.0133880739
F           9.0   0.0000000000   0.0000000000  -2.0320194655

CCHXeF mp2 acp3    ( cchxef_mp2_acp3_gh.out )

H           1.0   0.0000000000   0.0000000000   4.3784549899
C           6.0   0.0000000000   0.0000000000   3.3183987496
C           6.0   0.0000000000   0.0000000000   2.1066864390
XE         54.0   0.0000000000   0.0000000000   0.0541360688
F           9.0   0.0000000000   0.0000000000  -1.9964729486

CF3XeF mp2 acp3    ( cf3xef_mp2_acp3_gh.out )

F           9.0  -0.6205925424   1.0748978142   2.6461762051
F           9.0  -0.6205925424  -1.0748978142   2.6461762051
F           9.0   1.2411850847   0.0000000000   2.6461762051
C           6.0  -0.0000000000  -0.0000000000   2.1920589455
XE         54.0  -0.0000000000   0.0000000000   0.0046513928
F           9.0   0.0000000000   0.0000000000  -2.0672092953

CH3XeF mp2 acp3    ( ch3xef_mp2_acp3_gh.out )

H           1.0  -0.5159777132   0.8936996148   2.6144164970
H           1.0  -0.5159777132  -0.8936996148   2.6144164970
H           1.0   1.0319554263   0.0000000000   2.6144164970
C           6.0  -0.0000000000  -0.0000000000   2.2919905540
XE         54.0  -0.0000000000  -0.0000000000   0.1341012098
F           9.0   0.0000000000   0.0000000000  -1.9817492090
```

Table A14: *Optimized coordinates of ARnF systems (in Å).*

```
CNRnF mp2 acp3    ( cnrnf_mp2_acp3_gh.out )

N           7.0   0.0000000000   0.0000000000   3.4275062282
C           6.0   0.0000000000   0.0000000000   2.2580563473
RN         86.0  -0.0000000000   0.0000000000   0.0774676044
F           9.0   0.0000000000   0.0000000000  -2.0207136937

CCFRnF mp2 acp3    ( ccfrnf_mp2_acp3_gh.out )

F           9.0   0.0000000000   0.0000000000   4.5997267561
C           6.0  -0.0000000000   0.0000000000   3.3287256655
C           6.0  -0.0000000000   0.0000000000   2.1203636219
RN         86.0  -0.0000000000   0.0000000000  -0.0339588182
F           9.0   0.0000000000   0.0000000000  -2.1536539265

CCHRnF mp2 acp3    ( cchrnf_mp2_acp3_gh.out )

H           1.0   0.0000000000   0.0000000000   4.4360651052
C           6.0   0.0000000000   0.0000000000   3.3754941794
C           6.0   0.0000000000   0.0000000000   2.1617343760
RN         86.0   0.0000000000   0.0000000000   0.0065388347
F           9.0   0.0000000000   0.0000000000  -2.1186291967

CF3RnF mp2 acp3    ( cf3rnf_mp2_acp3_gh.out )

F           9.0  -0.6203777367   1.0745257599   2.6953301295
F           9.0  -0.6203777367  -1.0745257599   2.6953301295
F           9.0   1.2407554734   0.0000000000   2.6953301295
C           6.0  -0.0000000000  -0.0000000000   2.2280354268
RN         86.0  -0.0000000000   0.0000000000  -0.0497702040
F           9.0   0.0000000000  -0.0000000000  -2.1962259530

CH3RnF mp2 acp3    ( ch3rnf_mp2_acp3_gh.out )

H           1.0  -0.5155796835   0.8930102072   2.6575690329
H           1.0  -0.5155796835  -0.8930102072   2.6575690329
H           1.0   1.0311593670   0.0000000000   2.6575690329
C           6.0  -0.0000000000  -0.0000000000   2.3327221113
RN         86.0  -0.0000000000   0.0000000000   0.0831668758
F           9.0   0.0000000000  -0.0000000000  -2.1010040401
```

Table A15: *Optimized coordinates of AXeB systems (in Å).*

```
CNXeCN mp2 acp3    ( cnxecn_mp2_acp3_gh.out )

N           7.0  -0.0000000000   0.0000000000  -3.3629272023
N           7.0   0.0000000000   0.0000000000   3.3629272023
C           6.0   0.0000000000  -0.0000000000  -2.1919061518
C           6.0  -0.0000000000   0.0000000000   2.1919061518
XE         54.0  -0.0000000000   0.0000000000   0.0000000000

CCFXeCN mp2 acp3    ( ccfxecn_mp2_acp3_gh.out )

F           9.0   0.0000000000   0.0000000000   4.6143470667
C           6.0  -0.0000000000   0.0000000000   3.3434900980
C           6.0  -0.0000000000   0.0000000000   2.1321572142
XE         54.0  -0.0000000000   0.0000000000  -0.0031186452
C           6.0  -0.0000000000   0.0000000000  -2.2414374896
N           7.0   0.0000000000   0.0000000000  -3.4127590823

CCFXeCCF mp2 acp3    ( ccfxeccf_mp2_acp3_gh.out )

F           9.0   0.0000000000  -0.0000000000  -4.6680349731
F           9.0  -0.0000000000   0.0000000000   4.6680349731
C           6.0   0.0000000000  -0.0000000000  -3.3924690486
C           6.0  -0.0000000000   0.0000000000   3.3924690486
C           6.0  -0.0000000000   0.0000000000  -2.1784064496
C           6.0   0.0000000000   0.0000000000   2.1784064496
XE         54.0   0.0000000000   0.0000000000   0.0000000000

CCHXeCN mp2 acp3    ( cchxecn_mp2_acp3_gh.out )

H           1.0  -0.0000000000   0.0000000000   4.4125943493
C           6.0  -0.0000000000   0.0000000000   3.3517078931
C           6.0   0.0000000000   0.0000000000   2.1359238055
XE         54.0   0.0000000000   0.0000000000   0.0026392460
C           6.0  -0.0000000000   0.0000000000  -2.2493446418
N           7.0  -0.0000000000   0.0000000000  -3.4208414903

CCHXeCCF mp2 acp3    ( cchxeccf_mp2_acp3_gh.out )

H           1.0  -0.0000000000   0.0000000000   4.4825293804
C           6.0  -0.0000000000   0.0000000000   3.4216606321
C           6.0   0.0000000000   0.0000000000   2.2034990264
XE         54.0   0.0000000000   0.0000000000   0.0273636122
C           6.0   0.0000000000   0.0000000000  -2.1653961357
C           6.0  -0.0000000000   0.0000000000  -3.3803656813
F           9.0  -0.0000000000   0.0000000000  -4.6567517837

CCHXeCCH mp2 acp3    ( cchxecch_mp2_acp3_gh.out )
```

```
H           1.0   0.0000000000  -0.0000000000  -4.4695516365
H           1.0  -0.0000000000   0.0000000000   4.4695516365
C           6.0   0.0000000000  -0.0000000000  -3.4085905872
C           6.0  -0.0000000000   0.0000000000   3.4085905872
C           6.0  -0.0000000000   0.0000000000  -2.1897297579
C           6.0   0.0000000000   0.0000000000   2.1897297579
XE         54.0   0.0000000000   0.0000000000   0.0000000000

CF3XeCN mp2 acp3    ( cf3xecn_mp2_acp3_gh.out )

F           9.0  -0.6219718269   1.0772868050   2.7546893943
F           9.0  -0.6219718269  -1.0772868050   2.7546893943
F           9.0   1.2439436537   0.0000000000   2.7546893943
C           6.0  -0.0000000000  -0.0000000000   2.3019880486
XE         54.0  -0.0000000000  -0.0000000000   0.0417393228
C           6.0  -0.0000000000   0.0000000000  -2.2734606268
N           7.0   0.0000000000  -0.0000000000  -3.4461195499

CF3XeCCF mp2 acp3    ( cf3xeccf_mp2_acp3_gh.out )

F           9.0  -0.6221508037   1.0775968020   2.7366923905
F           9.0  -0.6221508037  -1.0775968020   2.7366923905
F           9.0   1.2443016074   0.0000000000   2.7366923905
C           6.0  -0.0000000000  -0.0000000000   2.2667020056
XE         54.0   0.0000000000   0.0000000000  -0.0100670259
C           6.0  -0.0000000000  -0.0000000000  -3.4762129623
C           6.0   0.0000000000  -0.0000000000  -2.2590507986
F           9.0  -0.0000000000   0.0000000000  -4.7539173775

CF3XeCCH mp2 acp3    ( cf3xecch_mp2_acp3_gh.out )

F           9.0  -0.6222626194   1.0777904725   2.7518715897
F           9.0  -0.6222626194  -1.0777904725   2.7518715897
F           9.0   1.2445252389   0.0000000000   2.7518715897
C           6.0   0.0000000000  -0.0000000000   2.2792685776
XE         54.0   0.0000000000   0.0000000000  -0.0078064705
C           6.0  -0.0000000000  -0.0000000000  -3.4796147748
C           6.0   0.0000000000  -0.0000000000  -2.2589092477
H           1.0  -0.0000000000  -0.0000000000  -4.5410218409

CH3XeCN mp2 acp3    ( ch3xecn_mp2_acp3_gh.out )

H           1.0  -0.5177308317   0.8967361052   2.6331206948
H           1.0  -0.5177308317  -0.8967361052   2.6331206948
H           1.0   1.0354616635   0.0000000000   2.6331206948
C           6.0  -0.0000000000   0.0000000000   2.3192451350
XE         54.0   0.0000000000  -0.0000000000   0.1157731387
C           6.0   0.0000000000   0.0000000000  -2.2743177811
N           7.0  -0.0000000000  -0.0000000000  -3.4474147121
```

CH3XeCCF mp2 acp3   (ch3xeccf_mp2_acp3_gh.out)

H	1.0	-0.5174366329	0.8962265379	2.6343241294
H	1.0	-0.5174366329	-0.8962265379	2.6343241294
H	1.0	1.0348732659	0.0000000000	2.6343241294
C	6.0	-0.0000000000	0.0000000000	2.3157586076
XE	54.0	0.0000000000	-0.0000000000	0.0771642002
C	6.0	-0.0000000000	0.0000000000	-3.4623596972
C	6.0	0.0000000000	-0.0000000000	-2.2411985985
F	9.0	-0.0000000000	-0.0000000000	-4.7463420051

CH3XeCCH mp2 acp3   (ch3xecch_mp2_acp3_gh.out)

H	1.0	-0.5175433369	0.8964113547	2.6341323586
H	1.0	-0.5175433369	-0.8964113547	2.6341323586
H	1.0	1.0350866739	0.0000000000	2.6341323586
C	6.0	-0.0000000000	0.0000000000	2.3154274670
XE	54.0	0.0000000000	0.0000000000	0.0642720064
C	6.0	-0.0000000000	-0.0000000000	-2.2535579718
C	6.0	0.0000000000	0.0000000000	-3.4772516406
H	1.0	-0.0000000000	0.0000000000	-4.5391267296

Table A16: *Optimized coordinates of ARnB systems (in Å).*

```
CNRnCN mp2 acp3    ( cnrncn_mp2_acp3_gh.out )

N           7.0   0.0000000000  -0.0000000000  -3.4392934791
N           7.0  -0.0000000000   0.0000000000   3.4392934791
C           6.0   0.0000000000   0.0000000000  -2.2683138752
C           6.0  -0.0000000000   0.0000000000   2.2683138752
RN         86.0   0.0000000000   0.0000000000   0.0000000000

CCFRnCN mp2 acp3    ( ccfrncn_mp2_acp3_gh.out )

F           9.0   0.0000000000   0.0000000000   4.6851288650
C           6.0   0.0000000000   0.0000000000   3.4128400857
C           6.0  -0.0000000000   0.0000000000   2.1999631526
RN         86.0  -0.0000000000   0.0000000000  -0.0224643795
C           6.0  -0.0000000000   0.0000000000  -2.3275036531
N           7.0   0.0000000000   0.0000000000  -3.4987687643

CCFRnCCF mp2 acp3    ( ccfrnccf_mp2_acp3_gh.out )

F           9.0  -0.0000000000   0.0000000000  -4.7488193306
F           9.0   0.0000000000   0.0000000000   4.7488193306
C           6.0  -0.0000000000   0.0000000000  -3.4723583516
C           6.0   0.0000000000   0.0000000000   3.4723583516
C           6.0   0.0000000000  -0.0000000000  -2.2571902528
C           6.0  -0.0000000000   0.0000000000   2.2571902528
RN         86.0  -0.0000000000   0.0000000000   0.0000000000

CCHRnCN mp2 acp3    ( cchrncn_mp2_acp3_gh.out )

H           1.0  -0.0000000000   0.0000000000   4.4826440111
C           6.0  -0.0000000000   0.0000000000   3.4214966107
C           6.0   0.0000000000   0.0000000000   2.2043145208
RN         86.0   0.0000000000   0.0000000000  -0.0181066776
C           6.0   0.0000000000   0.0000000000  -2.3348496685
N           7.0  -0.0000000000   0.0000000000  -3.5063034902

CCHRnCCF mp2 acp3    ( cchrnccf_mp2_acp3_gh.out )

H           1.0   0.0000000000   0.0000000000   4.4984727866
C           6.0   0.0000000000   0.0000000000   3.4374162485
C           6.0  -0.0000000000   0.0000000000   2.2182276778
RN         86.0  -0.0000000000   0.0000000000  -0.0392416905
C           6.0  -0.0000000000   0.0000000000  -2.3084978493
C           6.0  -0.0000000000   0.0000000000  -3.5243913134
F           9.0   0.0000000000   0.0000000000  -4.8015832643

CCHRnCCH mp2 acp3    ( cchrncch_mp2_acp3_gh.out )
```

```
H           1.0   0.0000000000  -0.0000000000  -4.5502134338
H           1.0  -0.0000000000   0.0000000000   4.5502134338
C           6.0   0.0000000000  -0.0000000000  -3.4890272954
C           6.0  -0.0000000000   0.0000000000   3.4890272954
C           6.0  -0.0000000000   0.0000000000  -2.2692697462
C           6.0   0.0000000000   0.0000000000   2.2692697462
RN         86.0   0.0000000000   0.0000000000   0.0000000000

CF3RnCN mp2 acp3    ( cf3rncn_mp2_acp3_gh.out )

F           9.0  -0.6214879173   1.0764486491   2.7672709910
F           9.0  -0.6214879173  -1.0764486491   2.7672709910
F           9.0   1.2429758347   0.0000000000   2.7672709910
C           6.0  -0.0000000000  -0.0000000000   2.2982653562
RN         86.0   0.0000000000  -0.0000000000  -0.0357929947
C           6.0   0.0000000000   0.0000000000  -2.4068978752
N           7.0  -0.0000000000   0.0000000000  -3.5794190892

CF3RnCCF mp2 acp3    ( cf3rnccf_mp2_acp3_gh.out )

F           9.0  -0.6216406695   1.0767132236   2.7499944689
F           9.0  -0.6216406695  -1.0767132236   2.7499944689
F           9.0   1.2432813389   0.0000000000   2.7499944689
C           6.0  -0.0000000000  -0.0000000000   2.2652129893
RN         86.0   0.0000000000  -0.0000000000  -0.0844279338
C           6.0  -0.0000000000  -0.0000000000  -3.6177635276
C           6.0   0.0000000000  -0.0000000000  -2.3999733287
F           9.0  -0.0000000000  -0.0000000000  -4.8958714709

CF3RnCCH mp2 acp3    ( cf3rncch_mp2_acp3_gh.out )

F           9.0  -0.6217313617   1.0768703071   2.7651990722
F           9.0  -0.6217313617  -1.0768703071   2.7651990722
F           9.0   1.2434627234   0.0000000000   2.7651990722
C           6.0   0.0000000000   0.0000000000   2.2777810152
RN         86.0  -0.0000000000   0.0000000000  -0.0808548334
C           6.0   0.0000000000  -0.0000000000  -3.6198948750
C           6.0  -0.0000000000  -0.0000000000  -2.3986544363
H           1.0   0.0000000000  -0.0000000000  -4.6813762680

CH3RnCN mp2 acp3    ( ch3rncn_mp2_acp3_gh.out )

H           1.0  -0.5165434230   0.8946794529   2.6868913327
H           1.0  -0.5165434230  -0.8946794529   2.6868913327
H           1.0   1.0330868460   0.0000000000   2.6868913327
C           6.0  -0.0000000000  -0.0000000000   2.3653683746
RN         86.0   0.0000000000   0.0000000000   0.0768784712
C           6.0   0.0000000000   0.0000000000  -2.3587109240
N           7.0  -0.0000000000  -0.0000000000  -3.5315620551
```

CH3RnCCF mp2 acp3   (ch3rnccf_mp2_acp3_gh.out)

H	1.0	-0.5160684009	0.8938566906	2.7009190791
H	1.0	-0.5160684009	-0.8938566906	2.7009190791
H	1.0	1.0321368018	0.0000000000	2.7009190791
C	6.0	-0.0000000000	-0.0000000000	2.3740504342
RN	86.0	0.0000000000	0.0000000000	0.0576607049
C	6.0	-0.0000000000	-0.0000000000	-3.5420347695
C	6.0	0.0000000000	-0.0000000000	-2.3203925378
F	9.0	-0.0000000000	0.0000000000	-4.8260461741

CH3RnCCH mp2 acp3   (ch3rncch_mp2_acp3_gh.out)

H	1.0	-0.5160778786	0.8938731063	2.7004865296
H	1.0	-0.5160778786	-0.8938731063	2.7004865296
H	1.0	1.0321557571	0.0000000000	2.7004865296
C	6.0	-0.0000000000	0.0000000000	2.3728241407
RN	86.0	0.0000000000	-0.0000000000	0.0460286596
C	6.0	0.0000000000	-0.0000000000	-2.3326505944
C	6.0	0.0000000000	-0.0000000000	-3.5568025969
H	1.0	-0.0000000000	0.0000000000	-4.6186989906

Table A17: *Optimized coordinates of ARgF transition states (in Å) in the gas phase.*

```
CNXeF MP2 ACP3 (cnxef-ts_mp2_acp3_gh.out)
 N           7.0  -0.1444142351   3.3583330545   0.0000000000
 C           6.0  -0.0429299561   2.1927799013   0.0000000000
 Xe         54.0   0.1232961379   0.2618117157   0.0000000000
 F           9.0   2.4131530532   0.1111883286   0.0000000000

CNRNF MP2 ACP3 (cnrnf-ts_mp2_acp3_gh.out)
 N           7.0  -0.1169227524   3.3794073668   0.0000000000
 C           6.0  -0.0383013065   2.2113419514   0.0000000000
 Rn         86.0   0.0784064061   0.1798790810   0.0000000000
 F           9.0   2.4259226528   0.1534846009   0.0000000000

CCFXeF MP2 ACP3 (ccfxef-ts_mp2_acp3_gh.out)
 F           9.0  -0.0145018449   4.6566642342   0.0000000000
 C           6.0  -0.0539806152   3.3967206860   0.0000000000
 C           6.0  -0.1094857461   2.1999636182   0.0000000000
 Xe         54.0  -0.0555202278   0.2709777897   0.0000000000
 F           9.0   2.2703904338  -0.0451083282   0.0000000000

CCFRnF MP2 ACP3 (ccfrnf-ts_mp2_acp3_gh.out)
 F           9.0  -0.0159512121   4.6706346286   0.0000000000
 C           6.0  -0.0393446751   3.4087339312   0.0000000000
 C           6.0  -0.0766588550   2.2096335020   0.0000000000
 Rn         86.0   0.0004662282   0.1854975626   0.0000000000
 F           9.0   2.3884351089   0.1108551308   0.0000000000

CCHXeF MP2 ACP3 (cchxef-ts_mp2_acp3_gh.out)
 H           1.0  -0.0282966620   4.4037272976   0.0000000000
 C           6.0  -0.0561412845   3.3443366227   0.0000000000
 C           6.0  -0.0857802172   2.1393337481   0.0000000000
 Xe         54.0  -0.0528355949   0.2077183743   0.0000000000
 F           9.0   2.2670227587  -0.1088310427   0.0000000000

CCHRnF MP2 ACP3 (cchrnf-ts_mp2_acp3_gh.out)
 H           1.0   0.0039574365   4.4106253202   0.0000000000
 C           6.0  -0.0432870062   3.3516555587   0.0000000000
 C           6.0  -0.0905499799   2.1455083622   0.0000000000
 Rn         86.0  -0.1028964120   0.1168473513   0.0000000000
 F           9.0   2.2767449618  -0.0383515924   0.0000000000
```

Table A18: *Optimized coordinates of ARgF transition states (in Å) in CH_2Cl_2.*

```
CNXeF MP2 ACP3 (cnxef-ts-s1_mp2_acp3_gh.out)
 N           7.0  -0.1340455859   3.3689854857   0.0033418634
 C           6.0  -0.0840475328   2.2023474706  -0.0053600188
 XE         54.0   0.0332784310   0.2673359623   0.0020327119
 F           9.0   2.5339196876   0.0854440816  -0.0000145564

CCFXeF MP2 ACP3 (ccfxef-ts-s1_mp2_acp3_gh.out)
 F           9.0  -0.0277411194   4.6723004076   0.0042952687
 C           6.0  -0.0732781469   3.4185150674  -0.0021248825
 C           6.0  -0.1275334421   2.2227681047  -0.0063219851
 XE         54.0  -0.1449531609   0.2937428182   0.0042432996
 F           9.0   2.4104078690  -0.1281083980  -0.0000917008

CCHXeF MP2 ACP3 (cchxef-ts-s1_mp2_acp3_gh.out)
 H           1.0  -0.0355678914   4.4305760013   0.0051539224
 C           6.0  -0.0708117669   3.3608870786  -0.0019954364
 C           6.0  -0.1173116792   2.1571768984  -0.0079649079
 XE         54.0  -0.1441638599   0.2235407842   0.0048259572
 F           9.0   2.4118241975  -0.1858957624  -0.0000195352

CNRNF MP2 ACP3 (cnrnf-ts-s1_mp2_acp3_gh.out)
 N           7.0  -0.1261620369   3.3964279037  -0.0020940186
 C           6.0  -0.0875667648   2.2285166880   0.0033004762
 RN         86.0   0.0074899835   0.1976992312  -0.0011939182
 F           9.0   2.5553438182   0.1014691772  -0.0000125394

CCFRnF MP2 ACP3 (ccfrnf-ts-s1_mp2_acp3_gh.out)
 F           9.0  -0.0386276861   4.6919492035   0.0033223939
 C           6.0  -0.0676232468   3.4346443345  -0.0014216197
 C           6.0  -0.0989425018   2.2361682727  -0.0050856370
 RN         86.0  -0.0789732634   0.2114061543   0.0030845051
 F           9.0   2.5411132931   0.0111867902   0.0001003577

 CCHRnF MP2 ACP3 (cchrnf-ts-s1_mp2_acp3_gh.out)
 H           1.0  -0.0110242198   4.4405304404   0.0069808880
 C           6.0  -0.0628995849   3.3719070897  -0.0024111572
 C           6.0  -0.1263737030   2.1668663368  -0.0109613836
 RN         86.0  -0.1829438682   0.1378920980   0.0063207393
 F           9.0   2.4272103761  -0.1309109649   0.0000709136
```

Table A19: *Optimized coordinates of ARgF transition states (in Å) in acetonitrile.*

```
CNXeF MP2 ACP3 (cnxef-ts-s2_mp2_acp3_gh.out)
 N           7.0  -0.1376961667   3.3736539531   0.0038277912
 C           6.0  -0.0941127570   2.2069626463  -0.0061371177
 Xe         54.0   0.0228368937   0.2712881670   0.0023063053
 F           9.0   2.5580770300   0.0722082337   0.0000030212

 CNRnF MP2 ACP3 (cnrnf-ts-s2_mp2_acp3_gh.out)
 N           7.0  -0.1340627950   3.4025103802  -0.0026608763
 C           6.0  -0.0984260536   2.2347079446   0.0041947391
 Rn         86.0   0.0020291020   0.2037630532  -0.0015249242
 F           9.0   2.5795647466   0.0831316221  -0.0000089387

 CCFXeF MP2 ACP3 (ccfxef-ts-s2_mp2_acp3_gh.out)
 F           9.0  -0.0334721568   4.6794942019   0.0038070256
 C           6.0  -0.0806631625   3.4264184984  -0.0021452262
 C           6.0  -0.1373214005   2.2307837009  -0.0051605395
 Xe         54.0  -0.1481039348   0.3011960865   0.0035189281
 F           9.0   2.4364626544  -0.1586744877  -0.0000201880

 CCFRnF MP2 ACP3 (ccfrnf-ts-s2_mp2_acp3_gh.out)
 F           9.0  -0.0437484321   4.6950008962   0.0028138557
 C           6.0  -0.0712041177   3.4381619848  -0.0012246084
 C           6.0  -0.0988851633   2.2396586446  -0.0042850816
 Rn         86.0  -0.0918032740   0.2148039227   0.0028010429
 F           9.0   2.5625875820  -0.0022706932  -0.0001052086

 CCHXeF MP2 ACP3 (ccfxef-ts-s2_mp2_acp3_gh.out)
 F           9.0  -0.0334721568   4.6794942019   0.0038070256
 C           6.0  -0.0806631625   3.4264184984  -0.0021452262
 C           6.0  -0.1373214005   2.2307837009  -0.0051605395
 Xe         54.0  -0.1481039348   0.3011960865   0.0035189281
 F           9.0   2.4364626544  -0.1586744877  -0.0000201880

 CCHRnF MP2 ACP3 (ccfrnf-ts-s2_mp2_acp3_gh.out)
 F           9.0  -0.0437484321   4.6950008962   0.0028138557
 C           6.0  -0.0712041177   3.4381619848  -0.0012246084
 C           6.0  -0.0988851633   2.2396586446  -0.0042850816
 Rn         86.0  -0.0918032740   0.2148039227   0.0028010429
 F           9.0   2.5625875820  -0.0022706932  -0.0001052086




 H           1.0  -0.6043466674   2.6598935446  -0.9007692106
 H           1.0  -0.6043466674   2.6598935446   0.9007692106
 H           1.0   0.9621666745   2.6485577404   0.0000000000
 C           6.0  -0.0835301442   2.3763825898   0.0000000000
```

Table A20: *Optimized coordinates of CH_3RgF transition states (in Å) in the gas phase*

Xe	54.0	-0.0045798127	0.2727085948	0.0000000000
F	9.0	2.3329564022	-0.3315241836	0.0000000000
H	1.0	-0.5818875645	2.6946920538	-0.9001253426
H	1.0	-0.5818875645	2.6946920538	0.9001253426
H	1.0	0.9844395191	2.6600829658	0.0000000000
C	6.0	-0.0652306753	2.4022711042	0.0000000000
Rn	86.0	-0.0050729914	0.2145983915	0.0000000000
F	9.0	2.4000828786	-0.2283009214	0.0000000000

Table A21: *Optimized coordinates of CF_3RgF rotamer transition states (in Å) in the gas phase.*

F	9.0	2.5999870387	-0.4734189203	0.0000000000
Xe	54.0	0.3728850563	0.2124269889	0.0000000000
C	6.0	1.5009794678	2.1246567068	0.0000000000
F	9.0	2.7530639263	1.9434465573	0.0000000000
F	9.0	1.0821262555	2.7353928337	-1.0737421395
F	9.0	1.0821262555	2.7353928337	1.0737421395
F	9.0	2.6104266657	-0.4789970820	0.0000000000
Rn	86.0	0.3317464409	0.1594832892	0.0000000000
C	6.0	1.5029301631	2.1271170304	0.0000000000
F	9.0	2.7627321892	1.9624379865	0.0000000000
F	9.0	1.0916662706	2.7539278879	-1.0740824661
F	9.0	1.0916662706	2.7539278879	1.0740824661

Table A22: *Optimized coordinates of CF_3RgF rotamer (in Å) in the gas phase.*

F	9.0	2.5925729011	-0.1854660963	0.0000000000
XE	54.0	0.2720627150	0.2089117353	0.0000000000
C	6.0	1.5171649422	2.0522517206	0.0000000000
F	9.0	0.6065687806	2.9994809237	0.0000000000
F	9.0	2.2029948306	2.0852813584	-1.0785574605
F	9.0	2.2029948306	2.0852813584	1.0785574605
F	9.0	2.5928939173	-0.1999497741	0.0000000000
RN	86.0	0.2405351521	0.1546256640	0.0000000000
C	6.0	1.5171408839	2.0570168247	0.0000000000
F	9.0	0.6139200317	3.0188280724	0.0000000000
F	9.0	2.2149345075	2.1076101065	-1.0777707458
F	9.0	2.2149345075	2.1076101065	1.0777707458

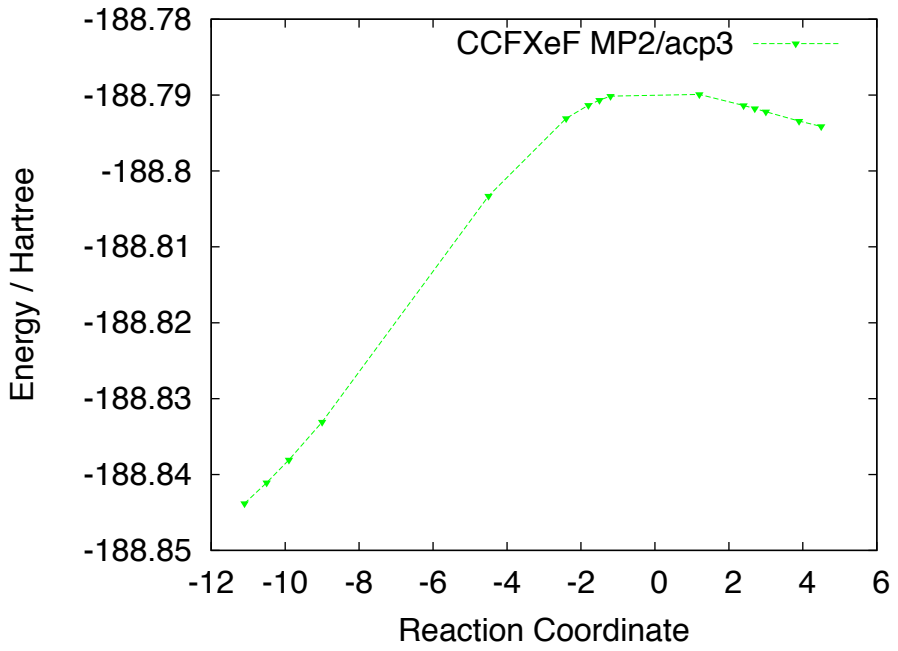

Figure 1: *Energy change along the intrinsic reaction coordinate for CCFXeF*

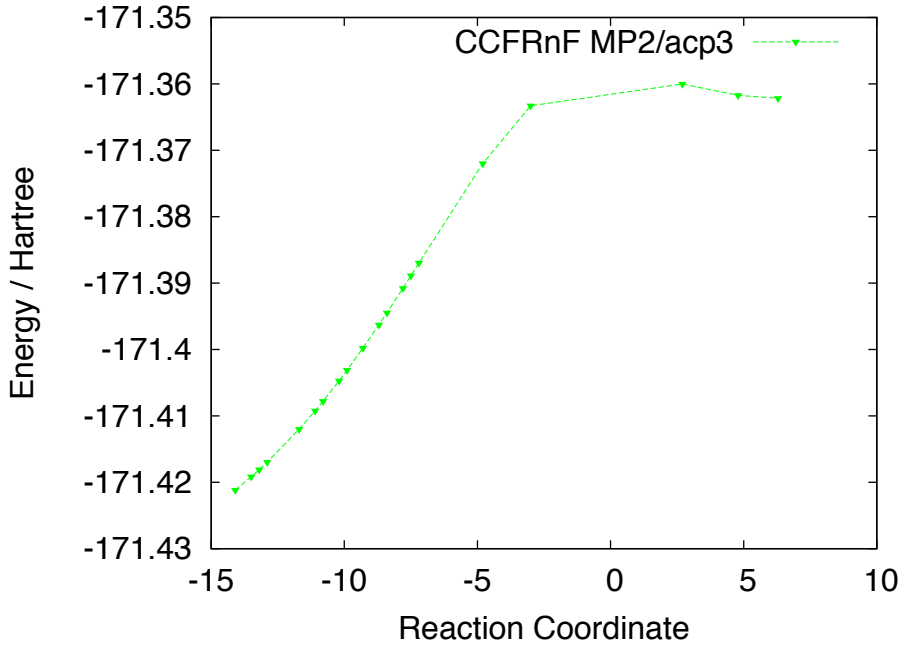

Figure 2: *Energy change along the intrinsic reaction coordinate for CCFRnF*

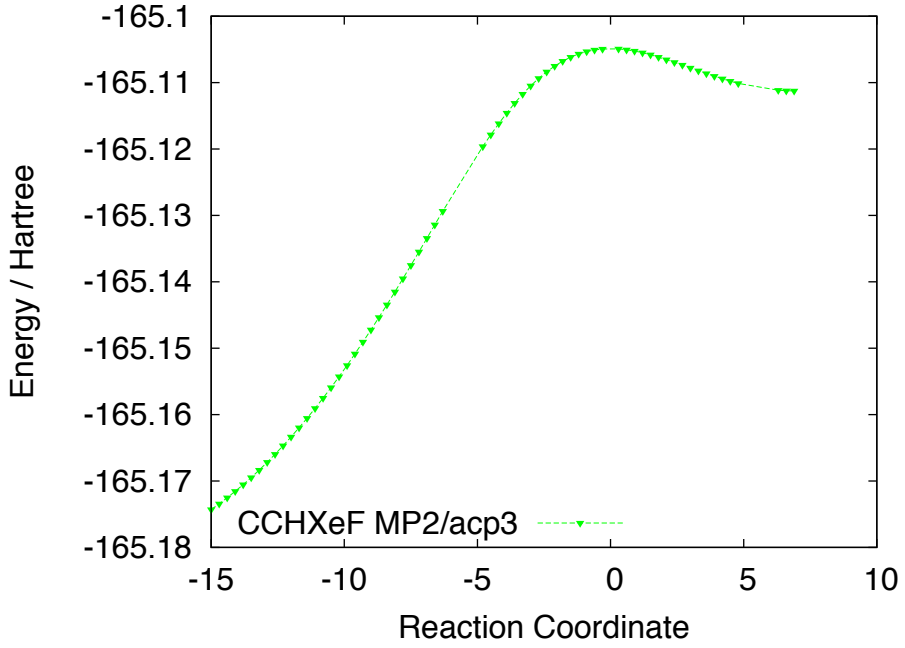

Figure 3: *Energy change along the intrinsic reaction coordinate for CCHXeF*

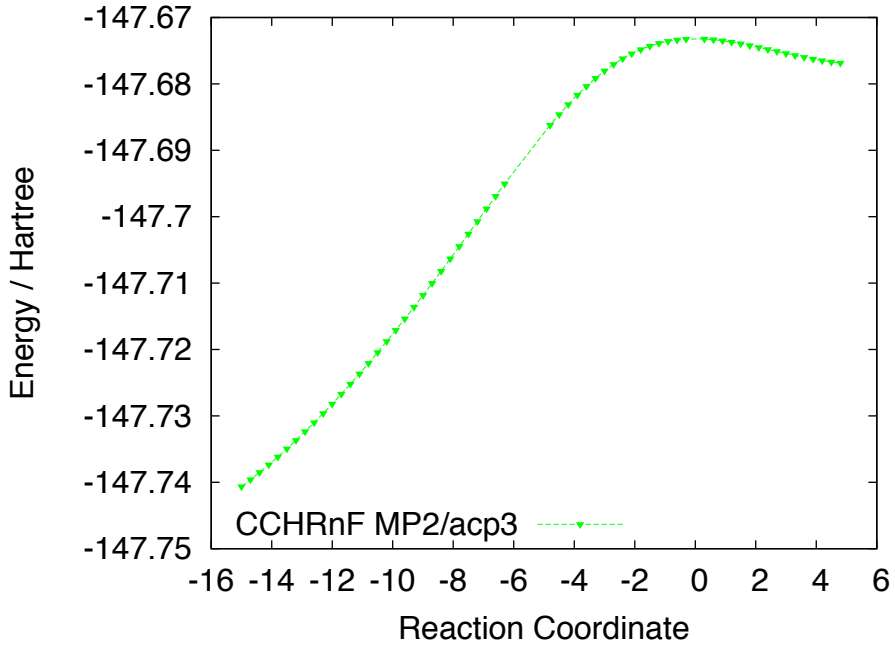

Figure 4: *Energy change along the intrinsic reaction coordinate for CCHRnF*

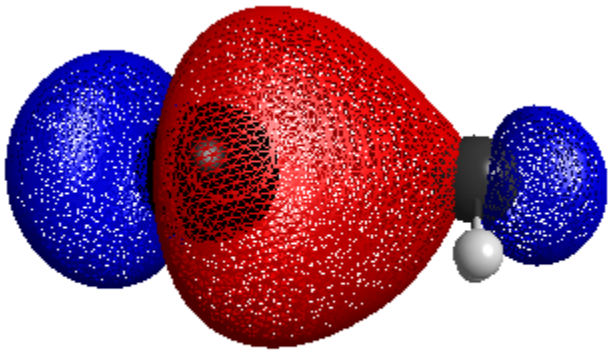

Figure 5: *A_1 σ NBO of CH_2Xe*

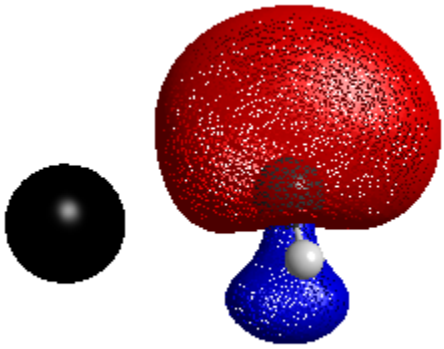

Figure 6: *Lone pair on carbon NBO of CH_2Xe*

Appendix to Chapter 6

All results were obtained at the MP2/MCP-TZP level of theory. This Appendix contains harmonic vibrational frequencies for all molecules studied in Chapter 6, as well as contour plots of C_6H_5XeCN and C_6F_5XeCN.

Table A23: *Harmonic vibrational frequencies of C_6H_5RgA molecules. Intensities are given in units of km·mol^{-1} and vibrational frequencies are given in units of cm^{-1}. All frequencies are unscaled.*

C_6H_5RnF

Frequency	Intensity
81.57	5.18
84.44	8.08
188.69	7.25
224.34	9.83
227.93	3.55
406.68	0.00
460.79	257.68
466.45	9.90
619.26	0.05
661.25	0.58
719.90	22.66
755.31	48.92
867.89	0.00
938.35	0.74
992.61	0.00
1012.66	0.10
1017.81	11.58
1038.47	4.56
1089.47	1.94
1095.31	3.45
1185.87	0.06
1205.59	0.03
1337.26	2.16
1456.24	1.15
1465.52	9.72
1503.27	4.94
1613.56	10.78
1621.97	1.29
3219.84	0.07
3222.33	0.50
3234.33	0.32
3243.03	10.48
3254.64	12.35

C_6H_5XeF

Frequency	Intensity
91.15	4.48
95.92	7.79
210.44	7.70
242.29	6.37
257.75	3.95
408.70	0.00
470.11	295.79
474.67	11.47
619.66	0.07
665.70	3.18
721.22	23.06
759.84	49.94
870.58	0.00
942.32	1.15
998.68	0.00
1015.85	0.16
1019.21	8.03
1039.84	3.16
1090.99	4.18
1096.27	3.59
1185.41	0.09
1203.19	0.05
1335.60	1.64
1460.20	0.31
1468.22	10.45
1504.72	4.80
1616.88	9.01
1626.36	1.30
3224.29	0.10
3227.71	0.09
3237.66	0.36
3245.87	8.88
3256.62	11.44

C_6H_5RnCN

Frequency	Intensity
46.35	5.15
46.90	6.37
143.00	2.06
157.76	0.12
208.25	32.26
243.55	1.46
264.66	1.05
297.98	199.05
403.53	0.00
461.88	8.26
617.34	0.03
654.42	1.78
716.17	17.47
750.52	55.89
864.64	0.00
933.51	0.63
987.17	0.00
1009.05	0.09
1015.69	21.72
1034.15	2.02
1081.87	7.26
1094.99	3.76
1186.71	0.06
1205.35	0.37
1337.75	1.82
1457.31	0.51
1463.65	9.49
1500.21	1.83
1609.01	13.99
1620.86	1.70
2075.66	127.55
3214.70	1.26
3216.89	1.18
3232.24	1.67
3241.22	9.67
3253.92	13.93

C_6H_5XeCN

Frequency	Intensity
50.42	5.03
50.80	6.31
144.56	1.43
159.41	0.01
219.19	26.92
257.87	2.06
286.94	1.42
288.15	256.44
405.16	0.00
470.27	9.58
616.62	0.05
655.41	5.08
715.89	17.18
754.31	57.64
864.89	0.00
935.41	0.93
990.88	0.00
1010.58	0.12
1015.87	18.17
1033.79	0.54
1079.50	13.17
1095.67	3.91
1186.70	0.09
1202.49	0.45
1336.30	1.43
1460.80	0.45
1466.88	9.63
1500.03	1.40
1609.94	13.44
1625.13	1.86
2071.02	139.53
3219.38	1.94
3222.26	0.38
3234.97	2.44
3243.60	7.78
3255.64	13.14

C_6H_5RnCCH

Frequency	Intensity
45.04	0.00
45.68	0.06
133.06	1.31
143.97	5.80
199.42	32.30
237.11	20.01
259.19	15.83
331.34	210.02
400.72	0.00
459.78	10.02
619.00	0.02
649.16	2.87
674.82	35.25
676.07	33.70
718.01	22.78
748.03	47.28
867.98	0.00
931.34	0.43
983.27	0.00
1003.97	0.08
1016.39	20.03
1032.72	2.14
1079.11	9.75
1091.81	3.44
1184.19	0.02
1204.19	0.68
1336.13	1.88
1452.50	2.39
1461.54	6.94
1498.97	0.60
1608.16	10.21
1617.72	0.82
1977.03	12.97
3204.34	1.23
3206.06	4.49
3226.09	2.54
3235.14	16.51
3249.76	20.96
3483.53	36.27

C_6H_5XeCCH

Frequency	Intensity
48.35	0.06
48.70	0.00
132.51	2.21
142.23	7.06
204.85	30.38
253.76	17.68
284.24	14.10
326.01	253.81
401.90	0.00
467.01	11.49
617.99	0.03
648.12	7.71
669.99	36.44
672.08	34.23
716.98	21.40
750.15	49.95
867.73	0.00
931.13	0.61
985.23	0.00
1003.90	0.10
1016.15	16.19
1031.53	0.26
1075.38	17.21
1092.07	3.58
1183.90	0.05
1200.68	0.71
1333.82	1.53
1457.91	0.64
1462.47	8.76
1497.98	0.29
1608.28	9.32
1621.08	0.84
1974.37	15.44
3207.22	1.92
3209.34	3.32
3227.49	3.17
3236.31	15.15
3250.76	20.25
3481.27	35.69

C_6H_5RnCCF

Frequency	Intensity
27.61	0.04
27.67	0.01
108.61	2.36
114.11	5.93
201.46	24.31
204.13	10.16
231.06	5.80
250.17	161.64
389.51	2.36
390.48	3.05
401.45	0.00
460.09	9.54
618.83	0.03
650.48	2.13
717.83	21.06
748.80	50.15
867.50	0.00
932.07	0.51
984.29	0.00
1005.13	0.08
1016.13	19.28
1033.15	1.82
1079.57	14.10
1092.46	3.59
1096.77	20.04
1184.59	0.03
1204.48	0.57
1336.47	1.80
1453.27	2.00
1462.07	7.26
1499.44	1.00
1608.67	11.64
1618.34	0.99
2203.22	248.75
3206.87	1.09
3208.74	3.56
3227.35	2.26
3236.38	15.28
3250.56	19.66

C_6H_5XeCCF

Frequency	Intensity
28.96	0.08
29.22	0.17
109.90	2.44
116.45	6.09
204.44	7.21
226.27	9.73
253.08	223.66
258.73	5.66
388.92	2.59
391.09	3.57
402.80	0.00
467.80	11.27
617.93	0.04
649.90	6.20
717.12	19.85
751.52	52.59
867.48	0.00
932.48	0.72
986.70	0.00
1005.42	0.11
1016.01	15.52
1032.14	0.17
1075.97	22.62
1092.82	3.75
1094.66	14.38
1184.41	0.05
1201.09	0.64
1334.39	1.45
1458.52	0.33
1463.32	8.96
1498.68	0.62
1609.08	10.82
1621.91	1.03
2202.13	254.51
3210.21	1.73
3212.51	2.41
3229.08	2.90
3237.85	13.81
3251.77	18.87

Table A24: *Harmonic vibrational frequencies of C_6F_5RgA molecules. Intensities are given in units of km·mol^{-1} and vibrational frequencies are given in units of cm^{-1}. All frequencies are unscaled.*

C_6F_5RnF

Frequency	Intensity
58.21	2.38
73.55	2.76
129.59	7.40
132.73	0.00
154.20	8.03
160.23	10.90
175.80	1.02
223.82	0.65
277.73	0.02
278.49	0.70
311.69	0.73
352.75	0.34
371.03	3.94
409.30	0.00
446.62	0.10
492.60	163.55
495.43	79.90
592.95	1.02
639.88	2.24
678.65	0.00
730.67	0.94
758.41	0.02
805.84	6.29
1005.07	167.64
1107.08	171.54
1180.54	2.15
1315.98	8.74
1433.60	45.64
1468.43	2.77
1536.79	428.48
1557.11	220.88
1667.88	18.60
1670.41	2.05

C_6F_5XeF

Frequency	Intensity
60.55	2.25
79.10	2.81
133.21	0.00
143.61	6.41
177.22	11.10
181.89	2.68
184.33	8.51
228.49	0.24
277.51	0.02
278.49	0.79
311.39	0.62
353.12	0.23
376.80	4.35
406.71	0.00
446.17	0.06
492.95	29.48
505.43	249.96
592.93	1.31
641.49	2.47
676.12	0.00
721.89	1.05
761.30	0.06
807.23	1.91
1008.27	170.15
1108.89	181.82
1183.95	1.61
1317.74	11.58
1438.11	39.20
1466.99	3.69
1541.42	433.28
1557.75	215.66
1669.19	20.20
1672.37	1.22

C_6F_5RnCN

Frequency	Intensity
39.75	4.22
45.73	4.69
89.68	3.34
101.34	2.66
131.31	0.00
148.24	22.80
167.58	0.01
213.29	1.38
258.94	0.27
260.51	0.30
276.65	2.00
277.61	0.02
311.25	0.68
327.75	188.45
350.48	2.61
370.98	3.15
411.40	0.00
445.89	0.15
491.84	3.71
591.90	3.04
633.99	1.91
677.50	0.00
724.32	0.75
755.28	0.00
791.55	1.67
1001.24	171.84
1101.47	197.37
1176.50	1.91
1311.47	12.45
1421.24	117.42
1472.13	5.34
1532.82	425.81
1554.81	238.96
1664.13	18.15
1669.22	2.29
2079.92	152.99

C_6F_5XeCN

Frequency	Intensity
41.02	3.93
47.55	4.64
95.05	3.73
110.04	2.67
131.52	0.00
158.20	26.61
167.22	0.01
212.15	1.61
268.13	0.20
272.73	0.81
276.22	2.04
277.73	0.00
311.17	0.51
321.97	231.45
348.61	0.04
377.82	3.36
408.57	0.00
445.02	0.10
490.57	6.51
591.50	3.52
634.61	2.17
674.76	0.00
717.09	0.84
756.83	0.00
785.43	0.00
1003.62	173.81
1101.33	214.21
1179.14	1.35
1311.33	16.62
1422.87	117.54
1471.29	7.77
1536.50	430.25
1554.59	236.03
1663.64	18.73
1670.76	1.42
2073.34	169.29

C_6F_5RnCCH

Frequency	Intensity
38.39	0.02
44.12	0.00
85.75	0.05
94.75	0.11
129.58	0.00
143.53	24.83
166.41	0.89
210.63	8.81
246.37	17.71
247.18	6.45
276.22	1.79
277.60	0.00
311.34	0.31
347.52	50.11
358.39	161.97
368.34	6.14
415.58	0.00
446.52	0.16
490.16	4.53
591.40	2.53
631.52	1.88
678.18	0.00
682.53	32.84
682.83	33.79
724.02	1.38
752.33	0.00
785.06	1.69
995.81	176.50
1095.79	202.61
1168.16	1.72
1304.19	13.83
1409.58	138.58
1473.28	5.17
1524.14	430.91
1551.98	230.17
1662.38	21.54
1667.65	2.14
2002.05	27.20
3488.36	56.19

C_6F_5XeCCH

Frequency	Intensity
39.18	0.00
45.38	0.02
90.04	0.24
100.91	0.48
129.60	0.00
153.53	26.52
165.84	1.04
210.27	7.64
258.39	5.55
262.05	16.79
275.65	1.62
277.51	0.03
311.05	0.11
346.44	161.32
349.47	90.58
374.05	7.16
413.27	0.00
445.61	0.11
488.82	7.64
590.96	2.84
630.89	1.87
675.33	0.00
678.36	34.78
678.94	33.34
716.09	1.76
753.24	0.04
778.82	0.15
997.51	178.60
1095.00	213.63
1169.94	1.17
1303.27	16.89
1410.43	132.99
1472.86	8.30
1527.08	435.53
1551.31	227.51
1661.39	21.82
1668.78	1.33
2000.10	34.41
3486.65	56.24

C_6F_5RnCCF

Frequency	Intensity
24.80	0.05
26.33	0.02
70.56	0.21
81.13	0.24
129.96	0.00
143.58	21.32
157.57	3.71
186.13	5.58
191.86	8.81
226.08	0.07
269.65	163.79
276.42	0.82
277.57	0.02
311.24	0.56
349.76	0.44
365.81	2.75
390.48	3.49
392.22	4.88
414.83	0.00
446.50	0.15
490.58	4.63
591.51	3.02
632.04	2.20
678.00	0.00
723.75	0.98
752.92	0.01
787.02	2.04
996.86	176.32
1096.74	209.43
1123.29	7.24
1169.69	1.76
1305.63	12.59
1412.10	135.44
1472.89	4.82
1525.61	428.25
1552.56	233.64
1662.93	20.34
1667.89	2.28
2239.37	309.16

C_6F_5XeCCF

Frequency	Intensity
25.84	0.02
26.96	0.00
70.93	0.34
84.22	0.47
130.03	0.00
151.20	18.51
159.75	2.36
195.17	6.45
216.02	8.71
234.38	0.08
270.57	188.84
276.17	22.06
277.42	0.02
310.74	0.44
348.39	2.03
369.74	2.32
390.48	3.94
392.59	6.30
412.48	0.00
445.60	0.11
489.26	7.01
591.08	3.37
632.00	2.54
675.26	0.00
716.28	1.12
753.97	0.00
780.81	0.24
998.71	178.51
1095.86	222.27
1121.96	2.83
1171.62	1.21
1304.89	15.62
1413.13	130.28
1472.43	7.72
1528.69	432.72
1551.99	231.04
1662.06	20.69
1669.10	1.45
2240.45	325.41

Harmonic Approximation

Harmonic approximation data for all molecules, computed at the MP2/aug-MCP-TZP level of theory.

HRnOH

MODE n	FREQ(CM**-1) w/cm-1	SYMMETRY	IR INTENS. I/(km.mol-1)
1	456.040	A’	3.74
2	526.505	A’	0.14
3	570.617	A’’	0.04
4	738.853	A’	0.17
5	1849.645	A’	22.42
6	3823.936	A’	1.37

HRnOF

MODE n	FREQ(CM**-1) w/cm-1	SYMMETRY	IR INTENS. I/(km.mol-1)
1	152.649	A’	0.05
2	433.095	A’	3.41
3	562.035	A’’	0.05
4	591.674	A’	0.40
5	992.281	A’	0.21
6	1920.629	A’	18.96

HRnSH

MODE n	FREQ(CM**-1) w/cm-1	SYMMETRY	IR INTENS. I/(km.mol-1)
1	254.552	A’	1.25
2	437.081	A’	0.12
3	488.040	A’’	0.02
4	606.208	A’	0.01
5	1620.062	A’	50.76

6	2773.502	A’	0.09

HRnSF

MODE n	FREQ(CM**-1) w/cm-1	SYMMETRY	IR INTENS. I/(km.mol-1)
1	103.530	A’	0.01
2	264.926	A’	1.26
3	484.525	A’’	0.01
4	514.164	A’	0.06
5	729.038	A’	3.21
6	1625.836	A’	52.47

$HRnNH_2$

MODE n	FREQ(CM**-1) w/cm-1	SYMMETRY	IR INTENS. I/(km.mol-1)
1	415.29	A’	77.33
2	497.02	A’’	11.28
3	515.73	A’	0.19
4	669.92	A’	61.56
5	797.50	A’’	0.93
6	1514.32	A’	125.28
7	1637.76	A’	1345.41
8	3454.14	A’	12.74
9	3562.00	A’’	0.43

$HRnNF_2$

MODE n	FREQ(CM**-1) w/cm-1	SYMMETRY	IR INTENS. I/(km.mol-1)
1	153.87	A’’	0.05
2	159.58	A’	2.42
3	408.07	A’	50.81
4	502.26	A’	33.08
5	561.71	A’’	9.57
6	610.21	A’	10.58
7	888.70	A’’	111.12
8	971.50	A’	243.22
9	1681.75	A’	1751.93

HRnPH$_2$

MODE n	FREQ(CM**-1) w/cm-1	SYMMETRY	IR INTENS. I/(km.mol-1)
1	221.38	A’	9.39
2	386.16	A’’	13.05
3	392.10	A’	10.17
4	562.05	A’	4.80
5	580.95	A’’	0.00
6	1127.00	A’	17.37
7	1359.20	A’	2009.35
8	2444.50	A’	42.73
9	2456.87	A’’	52.05

HRnPF$_2$

MODE n	FREQ(CM**-1) w/cm-1	SYMMETRY	IR INTENS. I/(km.mol-1)
1	97.75	A’	1.13
2	102.15	A’’	2.12
3	239.75	A’	5.35
4	350.45	A’	14.96
5	410.01	A’’	23.37
6	435.79	A’	13.87
7	802.18	A’	434.13
8	808.11	A’’	142.23
9	1212.89	A’	1613.57

Quartic Force Field Approximation

cc-VSCF QFF approximation data for all molecules, computed at the MP2/aug-MCP-TZP level of theory.

HRnOH

Frequency (cm-1)	Intensity (km.mol-1)	Vibrational quanta
10616.88	0.02	3 0 0 0 0 0

8817.55	0.00	2 1 0 0 0 0
8359.75	0.00	1 0 2 0 0 0
7581.16	0.00	2 0 0 1 0 0
7517.43	0.00	2 0 1 0 0 0
7486.55	0.00	2 0 0 0 0 1
7443.41	0.00	2 0 0 0 1 0
7045.45	1.40	2 0 0 0 0 0
7045.45	1.40	2 0 0 0 0 0
6998.22	0.00	1 2 0 0 0 0
5660.35	0.00	0 1 2 0 0 0
5296.21	0.00	1 1 0 0 0 0
5173.13	0.12	0 3 0 0 0 0
4657.81	0.00	1 0 0 2 0 0
4467.86	0.00	1 0 0 0 2 0
4456.68	0.00	1 0 0 0 0 2
4307.74	0.00	1 0 1 0 0 0
4173.12	0.00	0 2 1 0 0 0
4143.84	0.00	0 0 2 1 0 0
4109.49	0.00	1 0 0 1 0 0
4067.85	0.00	1 0 0 0 1 0
4010.63	0.00	1 0 0 0 0 1
3999.38	0.00	0 0 2 0 0 1
3944.19	0.00	0 2 0 0 1 0
3935.38	0.00	0 2 0 1 0 0
3893.56	0.00	0 2 0 0 0 1
3614.58	55.29	1 0 0 0 0 0
3609.30	55.33	1 0 0 0 0 0
3609.30	55.33	1 0 0 0 0 0
3452.46	23.31	0 2 0 0 0 0
3452.46	23.31	0 2 0 0 0 0
2979.85	0.00	0 0 2 0 1 0
2842.99	0.00	0 1 0 2 0 0
2816.05	0.24	0 0 3 0 0 0
2710.50	0.00	0 1 0 0 2 0
2633.46	0.00	0 1 0 0 0 2
2432.69	0.00	0 1 1 0 0 0
2289.56	0.00	0 1 0 1 0 0
2273.16	0.00	0 1 0 0 1 0
2190.93	0.00	0 1 0 0 0 1
1807.45	0.00	0 0 1 0 2 0
1801.21	0.00	0 0 1 2 0 0
1754.78	889.02	0 1 0 0 0 0

1751.78	889.33	0 1 0 0 0 0
1751.78	889.33	0 1 0 0 0 0
1698.22	0.00	0 0 0 3 0 0
1631.78	0.00	0 0 0 2 1 0
1619.53	0.13	0 0 0 0 3 0
1598.15	0.00	0 0 1 0 0 2
1550.16	0.00	0 0 0 2 0 1
1506.36	0.00	0 0 0 1 2 0
1439.99	0.00	0 0 0 1 0 2
1437.52	0.00	0 0 0 0 2 1
1425.81	0.00	0 0 0 0 1 2
1372.00	0.00	0 0 1 0 1 0
1337.71	0.03	0 0 0 0 0 3
1250.71	0.00	0 0 1 1 0 0
1150.07	0.00	0 0 1 0 0 1
1142.77	0.08	0 0 2 0 0 0
1142.77	0.08	0 0 2 0 0 0
1083.72	5.68	0 0 0 2 0 0
1083.72	5.68	0 0 0 2 0 0
1077.83	0.00	0 0 0 1 1 0
996.77	0.00	0 0 0 1 0 1
980.19	0.00	0 0 0 0 1 1
962.83	6.85	0 0 1 0 0 0
962.83	6.85	0 0 1 0 0 0
944.95	2.86	0 0 0 0 2 0
944.95	2.86	0 0 0 0 2 0
894.97	6.90	0 0 1 0 0 0
894.10	1.81	0 0 0 0 0 2
894.10	1.81	0 0 0 0 0 2
552.95	1.63	0 0 0 1 0 0
550.47	1.63	0 0 0 1 0 0
550.47	1.63	0 0 0 1 0 0
509.43	5.39	0 0 0 0 1 0
500.76	5.37	0 0 0 0 1 0
500.76	5.37	0 0 0 0 1 0
448.58	154.16	0 0 0 0 0 1
448.53	154.15	0 0 0 0 0 1
448.53	154.15	0 0 0 0 0 1

HRnOF

Frequency (cm-1)	Intensity (km.mol-1)	Vibrational quanta
5275.45	0.51	3 0 0 0 0 0
4549.76	0.00	2 1 0 0 0 0
4085.19	0.00	2 0 1 0 0 0
4046.16	0.00	2 0 0 1 0 0
3993.79	0.00	2 0 0 0 1 0
3762.68	0.00	1 2 0 0 0 0
3721.80	0.00	2 0 0 0 0 1
3574.18	9.18	2 0 0 0 0 0
3574.18	9.18	2 0 0 0 0 0
2962.85	0.00	1 0 2 0 0 0
2927.91	0.07	0 3 0 0 0 0
2900.05	0.00	1 0 0 2 0 0
2786.01	0.00	1 1 0 0 0 0
2655.95	0.00	1 0 0 0 2 0
2534.23	0.00	0 2 1 0 0 0
2500.79	0.00	0 2 0 1 0 0
2388.06	0.00	0 2 0 0 1 0
2380.19	0.00	1 0 1 0 0 0
2349.90	0.00	1 0 0 1 0 0
2233.40	0.00	1 0 0 0 1 0
2134.02	0.00	0 1 2 0 0 0
2112.36	0.00	1 0 0 0 0 2
2106.35	0.00	0 2 0 0 0 1
2060.82	0.00	0 1 0 2 0 0
1958.87	0.00	1 0 0 0 0 1
1958.54	1.22	0 2 0 0 0 0
1958.54	1.22	0 2 0 0 0 0
1835.45	0.00	0 1 0 0 2 0
1826.68	775.12	1 0 0 0 0 0
1826.68	775.12	1 0 0 0 0 0
1826.68	775.12	1 0 0 0 0 0
1671.05	0.00	0 0 2 1 0 0
1666.85	0.08	0 0 3 0 0 0
1627.08	0.00	0 0 1 2 0 0
1576.35	0.00	0 0 2 0 1 0
1557.35	0.00	0 1 1 0 0 0
1523.39	0.00	0 1 0 1 0 0
1516.07	0.05	0 0 0 3 0 0
1500.38	0.00	0 0 0 2 1 0

1427.21	0.00	0	0	1	0	2	0
1411.93	0.00	0	1	0	0	1	0
1388.30	0.00	0	0	0	1	2	0
1306.27	0.00	0	0	2	0	0	1
1284.10	0.00	0	1	0	0	0	2
1270.86	0.00	0	0	0	0	3	0
1225.54	0.00	0	0	0	2	0	1
1138.51	3.43	0	0	2	0	0	0
1138.51	3.43	0	0	2	0	0	0
1132.70	0.00	0	1	0	0	0	1
1110.30	0.00	0	0	1	1	0	0
1057.84	4.83	0	0	0	2	0	0
1057.84	4.83	0	0	0	2	0	0
1007.13	0.00	0	0	0	0	2	1
1004.09	0.00	0	0	1	0	1	0
983.04	8.87	0	1	0	0	0	0
983.04	8.87	0	1	0	0	0	0
983.04	8.87	0	1	0	0	0	0
967.73	0.00	0	0	0	1	1	0
884.66	0.00	0	0	1	0	0	2
851.83	0.98	0	0	0	0	2	0
851.83	0.98	0	0	0	0	2	0
843.36	0.00	0	0	0	1	0	2
735.82	0.00	0	0	0	0	1	2
730.68	0.00	0	0	1	0	0	1
692.79	0.00	0	0	0	1	0	1
582.40	0.00	0	0	0	0	1	1
577.50	16.08	0	0	1	0	0	0
577.50	16.08	0	0	1	0	0	0
577.50	16.08	0	0	1	0	0	0
542.19	2.19	0	0	0	1	0	0
542.19	2.19	0	0	0	1	0	0
542.19	2.19	0	0	0	1	0	0
458.45	0.00	0	0	0	0	0	3
428.19	142.17	0	0	0	0	1	0
428.19	142.17	0	0	0	0	1	0
428.19	142.17	0	0	0	0	1	0
305.49	0.01	0	0	0	0	0	2
305.49	0.01	0	0	0	0	0	2
152.68	2.48	0	0	0	0	0	1
152.68	2.48	0	0	0	0	0	1
152.68	2.48	0	0	0	0	0	1

HRnSH

Frequency (cm-1)	Intensity (km.mol-1)	Vibrational quanta
7705.14	0.01	3 0 0 0 0 0
6712.63	0.00	2 1 0 0 0 0
5742.26	0.00	2 0 1 0 0 0
5682.45	0.00	2 0 0 1 0 0
5600.86	0.00	1 2 0 0 0 0
5580.33	0.00	2 0 0 0 1 0
5463.42	0.00	2 0 0 0 0 1
5216.31	0.28	2 0 0 0 0 0
5216.31	0.28	2 0 0 0 0 0
4404.01	0.71	0 3 0 0 0 0
4367.12	0.00	1 0 2 0 0 0
4139.10	0.00	1 1 0 0 0 0
3571.18	0.00	1 0 0 2 0 0
3532.80	0.00	0 2 1 0 0 0
3430.40	0.00	1 0 0 0 2 0
3357.96	0.00	0 2 0 0 1 0
3346.10	0.00	0 2 0 1 0 0
3227.91	0.00	1 0 1 0 0 0
3219.28	0.00	0 2 0 0 0 1
3133.49	0.00	1 0 0 0 0 2
3104.54	0.00	1 0 0 1 0 0
3062.66	0.00	0 1 2 0 0 0
3062.64	0.00	1 0 0 0 1 0
2980.08	94.05	0 2 0 0 0 0
2980.08	94.05	0 2 0 0 0 0
2885.04	0.00	1 0 0 0 0 1
2655.71	3.68	1 0 0 0 0 0
2655.71	3.68	1 0 0 0 0 0
2655.71	3.68	1 0 0 0 0 0
2440.07	0.00	0 1 0 2 0 0
2307.48	0.00	0 1 0 0 2 0
2094.84	0.00	0 1 1 0 0 0
2005.96	0.00	0 0 2 1 0 0
2000.92	0.00	0 1 0 0 0 2
1974.46	0.00	0 0 2 0 1 0
1966.16	0.00	0 1 0 1 0 0

1935.15	0.00	0 1 0 0 1 0
1783.30	0.00	0 0 2 0 0 1
1755.45	0.00	0 1 0 0 0 1
1587.38	0.03	0 0 3 0 0 0
1527.61	0.00	0 0 1 2 0 0
1523.36	1911.08	0 1 0 0 0 0
1523.36	1911.08	0 1 0 0 0 0
1523.36	1911.08	0 1 0 0 0 0
1505.12	0.22	0 0 2 0 0 0
1505.12	0.22	0 0 2 0 0 0
1503.24	0.00	0 0 1 0 2 0
1357.63	0.00	0 0 0 2 1 0
1321.51	0.00	0 0 0 3 0 0
1273.02	0.00	0 0 0 1 2 0
1185.36	0.00	0 0 0 2 0 1
1095.09	0.00	0 0 1 0 0 2
1094.62	0.00	0 0 1 0 1 0
1092.82	0.35	0 0 0 0 3 0
1066.99	0.00	0 0 0 0 2 1
1065.84	0.00	0 0 1 1 0 0
966.39	0.00	0 0 0 1 0 2
933.94	0.00	0 0 0 0 1 2
919.91	16.36	0 0 0 2 0 0
919.91	16.36	0 0 0 2 0 0
902.20	0.00	0 0 0 1 1 0
847.79	0.00	0 0 1 0 0 1
794.28	4.76	0 0 0 0 2 0
794.28	4.76	0 0 0 0 2 0
746.67	0.01	0 0 0 0 0 3
719.03	0.00	0 0 0 1 0 1
686.06	0.00	0 0 0 0 1 1
639.37	0.57	0 0 1 0 0 0
639.37	0.57	0 0 1 0 0 0
639.37	0.57	0 0 1 0 0 0
499.02	0.37	0 0 0 0 0 2
499.02	0.37	0 0 0 0 0 2
470.12	0.89	0 0 0 1 0 0
470.12	0.89	0 0 0 1 0 0
470.12	0.89	0 0 0 1 0 0
422.61	5.09	0 0 0 0 1 0
422.61	5.09	0 0 0 0 1 0
422.61	5.09	0 0 0 0 1 0

250.15	51.94	0 0 0 0 0 1
250.15	51.94	0 0 0 0 0 1
250.15	51.94	0 0 0 0 0 1

HRnSF

Frequency (cm-1)	Intensity (km.mol-1)	Vibrational quanta
4344.24	12.06	3 0 0 0 0 0
3680.92	0.00	2 1 0 0 0 0
3340.27	0.00	2 0 1 0 0 0
3310.27	0.00	2 0 0 1 0 0
3211.26	0.00	2 0 0 0 1 0
3055.18	0.00	2 0 0 0 0 1
2960.71	70.60	2 0 0 0 0 0
2960.71	70.60	2 0 0 0 0 0
2950.65	0.00	1 2 0 0 0 0
2479.04	0.00	1 0 2 0 0 0
2428.79	0.00	1 0 0 2 0 0
2229.43	0.00	1 1 0 0 0 0
2150.41	0.06	0 3 0 0 0 0
2021.21	0.00	1 0 0 0 2 0
1982.59	0.00	1 0 1 0 0 0
1956.78	0.00	1 0 0 1 0 0
1936.93	0.00	0 2 1 0 0 0
1906.88	0.00	0 2 0 1 0 0
1762.97	0.00	1 0 0 0 1 0
1716.83	0.00	0 1 2 0 0 0
1708.15	0.00	1 0 0 0 0 2
1699.93	0.00	0 2 0 0 1 0
1653.40	0.00	0 1 0 2 0 0
1606.06	0.00	1 0 0 0 0 1
1542.24	0.00	0 2 0 0 0 1
1520.72	1999.19	1 0 0 0 0 0
1520.72	1999.19	1 0 0 0 0 0
1520.72	1999.19	1 0 0 0 0 0
1439.36	2.63	0 2 0 0 0 0
1439.36	2.63	0 2 0 0 0 0
1438.45	0.00	0 0 2 1 0 0
1423.08	0.01	0 0 3 0 0 0
1401.68	0.00	0 0 1 2 0 0
1300.45	0.00	0 0 0 3 0 0

1253.48	0.00	0	0	2	0	1	0
1242.82	0.00	0	1	0	0	2	0
1219.89	0.00	0	1	1	0	0	0
1189.20	0.00	0	1	0	1	0	0
1187.78	0.00	0	0	0	2	1	0
1098.60	0.00	0	0	2	0	0	1
1028.84	0.00	0	0	0	2	0	1
1017.45	0.00	0	0	1	0	2	0
985.28	0.00	0	0	0	1	2	0
983.66	0.00	0	1	0	0	1	0
979.63	15.53	0	0	2	0	0	0
979.63	15.53	0	0	2	0	0	0
957.29	0.00	0	0	1	1	0	0
930.35	0.00	0	1	0	0	0	2
910.68	17.68	0	0	0	2	0	0
910.68	17.68	0	0	0	2	0	0
826.71	0.00	0	1	0	0	0	1
780.50	0.00	0	0	0	0	3	0
758.40	0.00	0	0	1	0	1	0
726.70	0.00	0	0	0	1	1	0
723.03	133.56	0	1	0	0	0	0
723.03	133.56	0	1	0	0	0	0
723.03	133.56	0	1	0	0	0	0
707.81	0.00	0	0	1	0	0	2
671.17	0.00	0	0	0	1	0	2
627.55	0.00	0	0	0	0	2	1
603.17	0.00	0	0	1	0	0	1
569.26	0.00	0	0	0	1	0	1
521.91	0.14	0	0	0	0	2	0
521.91	0.14	0	0	0	0	2	0
498.00	2.75	0	0	1	0	0	0
498.00	2.75	0	0	1	0	0	0
498.00	2.75	0	0	1	0	0	0
471.22	0.00	0	0	0	0	1	2
466.47	0.62	0	0	0	1	0	0
466.47	0.62	0	0	0	1	0	0
466.47	0.62	0	0	0	1	0	0
366.80	0.00	0	0	0	0	1	1
310.14	0.00	0	0	0	0	0	3
261.73	53.29	0	0	0	0	1	0
261.73	53.29	0	0	0	0	1	0
261.73	53.29	0	0	0	0	1	0

207.52	0.01	0 0 0 0 0 2
207.52	0.01	0 0 0 0 0 2
103.96	0.41	0 0 0 0 0 1
103.96	0.41	0 0 0 0 0 1
103.96	0.41	0 0 0 0 0 1

$HRnNH_2$

Frequency (cm-1)	Intensity (km.mol-1)	Vibrational quanta
9737.92	0.00	3 0 0 0 0 0 0 0 0
9523.81	0.02	0 3 0 0 0 0 0 0 0
9469.36	0.00	2 1 0 0 0 0 0 0 0
9462.28	0.00	1 2 0 0 0 0 0 0 0
8016.62	0.00	2 0 1 0 0 0 0 0 0
7970.79	0.00	0 2 1 0 0 0 0 0 0
7830.35	0.00	0 2 0 1 0 0 0 0 0
7814.71	0.00	2 0 0 1 0 0 0 0 0
7211.48	0.00	0 2 0 0 1 0 0 0 0
7195.25	0.00	2 0 0 0 1 0 0 0 0
7086.88	0.00	0 2 0 0 0 1 0 0 0
7059.68	0.00	2 0 0 0 0 1 0 0 0
6971.06	0.00	2 0 0 0 0 0 1 0 0
6951.86	0.00	2 0 0 0 0 0 0 1 0
6933.12	0.00	0 2 0 0 0 0 1 0 0
6916.17	0.00	0 2 0 0 0 0 0 1 0
6891.37	0.00	2 0 0 0 0 0 0 0 1
6840.83	0.00	0 2 0 0 0 0 0 0 1
6516.87	0.17	2 0 0 0 0 0 0 0 0
6516.87	0.17	2 0 0 0 0 0 0 0 0
6424.19	0.00	1 1 0 0 0 0 0 0 0
6416.50	0.80	0 2 0 0 0 0 0 0 0
6416.50	0.80	0 2 0 0 0 0 0 0 0
6362.41	0.00	1 0 2 0 0 0 0 0 0
6310.67	0.00	0 1 2 0 0 0 0 0 0
6082.59	0.00	1 0 0 2 0 0 0 0 0
5815.98	0.00	0 1 0 2 0 0 0 0 0
5174.55	0.00	1 0 0 0 0 2 0 0 0
5093.18	0.00	0 1 0 0 0 2 0 0 0
4947.10	0.00	0 1 0 0 2 0 0 0 0
4922.03	0.00	1 0 0 0 2 0 0 0 0
4851.67	0.00	1 0 1 0 0 0 0 0 0

4797.62	0.00	0	1	1	0	0	0	0	0	0
4709.70	0.00	1	0	0	1	0	0	0	0	0
4701.21	0.00	0	1	0	1	0	0	0	0	0
4565.83	0.18	0	0	3	0	0	0	0	0	0
4522.22	0.00	0	0	2	1	0	0	0	0	0
4288.83	0.00	1	0	0	0	0	0	2	0	0
4268.75	0.00	1	0	0	0	0	0	0	2	0
4252.25	0.00	0	1	0	0	0	0	2	0	0
4230.93	0.00	0	0	1	2	0	0	0	0	0
4227.95	0.00	0	1	0	0	0	0	0	2	0
4227.29	0.06	0	0	0	3	0	0	0	0	0
4102.45	0.00	1	0	0	0	0	0	0	0	2
4086.88	0.00	1	0	0	0	1	0	0	0	0
4082.17	0.00	0	1	0	0	1	0	0	0	0
4048.79	0.00	0	1	0	0	0	0	0	0	2
3953.49	0.00	0	1	0	0	0	1	0	0	0
3946.51	0.00	1	0	0	0	0	1	0	0	0
3876.19	0.00	0	0	2	0	1	0	0	0	0
3822.17	0.00	1	0	0	0	0	0	1	0	0
3803.69	0.00	1	0	0	0	0	0	0	1	0
3776.80	0.00	0	1	0	0	0	0	1	0	0
3757.14	0.00	0	1	0	0	0	0	0	1	0
3718.10	0.00	1	0	0	0	0	0	0	0	1
3663.03	0.00	0	1	0	0	0	0	0	0	1
3662.51	0.00	0	0	2	0	0	1	0	0	0
3625.85	0.00	0	0	0	2	1	0	0	0	0
3557.14	0.00	0	0	2	0	0	0	1	0	0
3532.70	0.00	0	0	2	0	0	0	0	1	0
3453.42	0.00	0	0	2	0	0	0	0	0	1
3336.19	0.00	0	0	0	2	0	0	1	0	0
3315.37	0.48	1	0	0	0	0	0	0	0	0
3315.37	0.48	1	0	0	0	0	0	0	0	0
3315.37	0.48	1	0	0	0	0	0	0	0	0
3297.76	0.00	0	0	0	2	0	0	0	1	0
3262.78	12.06	0	1	0	0	0	0	0	0	0
3262.78	12.06	0	1	0	0	0	0	0	0	0
3262.78	12.06	0	1	0	0	0	0	0	0	0
3216.80	0.00	0	0	1	0	2	0	0	0	0
3157.90	0.00	0	0	1	0	0	2	0	0	0
3149.87	0.00	0	0	0	2	0	0	0	0	1
3127.93	0.00	0	0	0	1	2	0	0	0	0
3054.37	60.58	0	0	2	0	0	0	0	0	0

3054.37	60.58	0	0	2	0	0	0	0	0	0
2994.55	0.00	0	0	1	1	0	0	0	0	0
2762.49	0.00	0	0	0	2	0	1	0	0	0
2619.03	0.68	0	0	0	2	0	0	0	0	0
2619.03	0.68	0	0	0	2	0	0	0	0	0
2566.25	0.00	0	0	1	0	0	0	2	0	0
2533.60	0.00	0	0	1	0	0	0	0	2	0
2494.53	0.03	0	0	0	0	3	0	0	0	0
2460.10	0.00	0	0	0	1	0	0	0	2	0
2452.25	0.00	0	0	0	1	0	0	2	0	0
2445.91	0.00	0	0	0	0	1	2	0	0	0
2414.35	0.00	0	0	0	0	2	1	0	0	0
2362.56	0.00	0	0	1	0	1	0	0	0	0
2334.15	0.00	0	0	1	0	0	0	0	0	2
2258.26	0.00	0	0	0	1	1	0	0	0	0
2247.57	0.00	0	0	0	0	2	0	1	0	0
2240.81	0.00	0	0	0	1	0	0	0	0	2
2226.78	0.00	0	0	1	0	0	1	0	0	0
2202.88	0.00	0	0	0	0	0	2	0	1	0
2202.55	0.00	0	0	0	0	0	2	1	0	0
2188.57	0.00	0	0	0	0	2	0	0	1	0
2128.08	0.00	0	0	0	0	0	2	0	0	1
2089.13	0.00	0	0	0	0	2	0	0	0	1
2074.40	0.00	0	0	1	0	0	0	1	0	0
2052.14	0.00	0	0	1	0	0	0	0	1	0
1970.59	0.00	0	0	0	1	0	0	1	0	0
1967.18	0.00	0	0	0	1	0	0	0	1	0
1950.47	0.00	0	0	1	0	0	0	0	0	1
1949.79	0.00	0	0	0	1	0	1	0	0	0
1891.78	0.00	0	0	0	0	1	0	2	0	0
1853.82	0.00	0	0	0	1	0	0	0	0	1
1832.65	0.00	0	0	0	0	1	0	0	2	0
1733.76	0.00	0	0	0	0	0	1	2	0	0
1710.17	0.00	0	0	0	0	0	1	0	2	0
1683.54	0.05	0	0	0	0	0	2	0	0	0
1683.54	0.05	0	0	0	0	0	2	0	0	0
1645.17	1.01	0	0	0	0	2	0	0	0	0
1645.17	1.01	0	0	0	0	2	0	0	0	0
1627.44	0.00	0	0	0	0	1	0	0	0	2
1560.80	1230.38	0	0	1	0	0	0	0	0	0
1560.80	1230.38	0	0	1	0	0	0	0	0	0
1560.80	1230.38	0	0	1	0	0	0	0	0	0

1542.23	0.00	0	0	0	0	0	0	2	1	0
1540.84	0.00	0	0	0	0	0	0	1	2	0
1529.48	0.00	0	0	0	0	1	1	0	0	0
1506.88	4.31	0	0	0	0	0	3	0	0	0
1474.42	0.03	0	0	0	0	0	0	3	0	0
1472.93	0.00	0	0	0	0	0	1	0	0	2
1442.16	0.09	0	0	0	0	0	0	0	3	0
1436.20	0.00	0	0	0	0	0	0	2	0	1
1406.07	0.00	0	0	0	0	0	0	0	2	1
1388.55	123.98	0	0	0	1	0	0	0	0	0
1388.55	123.98	0	0	0	1	0	0	0	0	0
1388.55	123.98	0	0	0	1	0	0	0	0	0
1369.35	0.00	0	0	0	0	1	0	1	0	0
1336.64	0.00	0	0	0	0	0	0	1	0	2
1336.06	0.00	0	0	0	0	1	0	0	1	0
1313.23	0.00	0	0	0	0	0	0	0	1	2
1231.38	0.00	0	0	0	0	0	1	1	0	0
1227.91	0.00	0	0	0	0	1	0	0	0	1
1201.19	0.00	0	0	0	0	0	1	0	1	0
1191.02	0.05	0	0	0	0	0	0	0	0	3
1078.91	0.00	0	0	0	0	0	1	0	0	1
1047.44	0.00	0	0	0	0	0	0	1	1	0
1004.95	3.94	0	0	0	0	0	0	2	0	0
1004.95	3.94	0	0	0	0	0	0	2	0	0
980.95	5.05	0	0	0	0	0	0	0	2	0
980.95	5.05	0	0	0	0	0	0	0	2	0
939.60	0.00	0	0	0	0	0	0	1	0	1
917.97	0.00	0	0	0	0	0	0	0	1	1
824.42	0.84	0	0	0	0	1	0	0	0	0
824.42	0.84	0	0	0	0	1	0	0	0	0
824.42	0.84	0	0	0	0	1	0	0	0	0
802.65	3.48	0	0	0	0	0	0	0	0	2
802.65	3.48	0	0	0	0	0	0	0	0	2
713.19	62.47	0	0	0	0	0	1	0	0	0
713.19	62.47	0	0	0	0	0	1	0	0	0
713.19	62.47	0	0	0	0	0	1	0	0	0
666.46	0.00	0	0	0	1	0	2	0	0	0
516.42	0.21	0	0	0	0	0	0	1	0	0
516.42	0.21	0	0	0	0	0	0	1	0	0
516.42	0.21	0	0	0	0	0	0	1	0	0
502.07	11.18	0	0	0	0	0	0	0	1	0
502.07	11.18	0	0	0	0	0	0	0	1	0

502.07	11.18	0 0 0 0 0 0 0 1 0
405.47	70.20	0 0 0 0 0 0 0 0 1
405.47	70.20	0 0 0 0 0 0 0 0 1
405.47	70.20	0 0 0 0 0 0 0 0 1

$HRnNF_2$

Frequency (cm-1)	Intensity (km.mol-1)	Vibrational quanta
4504.48	3.87	3 0 0 0 0 0 0 0 0
3999.10	0.00	2 1 0 0 0 0 0 0 0
3928.39	0.00	2 0 1 0 0 0 0 0 0
3566.87	0.00	2 0 0 1 0 0 0 0 0
3557.09	0.00	2 0 0 0 0 1 0 0 0
3478.46	0.00	2 0 0 0 1 0 0 0 0
3447.96	0.00	1 2 0 0 0 0 0 0 0
3419.57	0.00	2 0 0 0 0 0 1 0 0
3296.52	0.00	1 0 2 0 0 0 0 0 0
3209.67	0.00	2 0 0 0 0 0 0 1 0
3205.15	0.00	2 0 0 0 0 0 0 0 1
3056.87	36.37	2 0 0 0 0 0 0 0 0
3056.87	36.37	2 0 0 0 0 0 0 0 0
2851.94	0.05	0 3 0 0 0 0 0 0 0
2768.52	0.00	0 2 1 0 0 0 0 0 0
2709.64	0.00	1 0 0 2 0 0 0 0 0
2681.98	0.00	0 1 2 0 0 0 0 0 0
2611.21	0.00	1 0 0 0 2 0 0 0 0
2606.64	0.28	0 0 3 0 0 0 0 0 0
2556.00	0.00	1 0 0 0 0 2 0 0 0
2507.37	0.00	1 1 0 0 0 0 0 0 0
2493.83	0.00	0 2 0 1 0 0 0 0 0
2442.94	0.00	0 2 0 0 1 0 0 0 0
2432.13	0.00	1 0 1 0 0 0 0 0 0
2392.03	0.00	0 2 0 0 0 1 0 0 0
2339.79	0.00	1 0 0 0 0 0 2 0 0
2331.28	0.00	0 0 2 1 0 0 0 0 0
2308.69	0.00	0 2 0 0 0 0 1 0 0
2281.08	0.00	0 0 2 0 1 0 0 0 0
2219.00	0.00	0 0 2 0 0 1 0 0 0
2142.48	0.00	0 1 0 2 0 0 0 0 0
2138.79	0.00	0 0 2 0 0 0 1 0 0
2131.05	0.00	1 0 0 1 0 0 0 0 0

2077.62	0.00	1	0	0	0	1	0	0	0	0
2062.50	0.00	0	0	1	2	0	0	0	0	0
2061.59	0.00	0	2	0	0	0	0	0	1	0
2058.06	0.00	0	2	0	0	0	0	0	0	1
2057.60	0.00	1	0	0	0	0	1	0	0	0
2037.76	0.00	0	1	0	0	2	0	0	0	0
1957.83	0.00	0	0	1	0	2	0	0	0	0
1949.76	0.00	1	0	0	0	0	0	1	0	0
1940.73	0.00	0	1	0	0	0	2	0	0	0
1905.43	6.14	0	2	0	0	0	0	0	0	0
1905.43	6.14	0	2	0	0	0	0	0	0	0
1896.42	0.00	0	0	2	0	0	0	0	1	0
1888.83	0.00	0	0	2	0	0	0	0	0	1
1875.73	0.00	1	0	0	0	0	0	0	2	0
1867.67	0.00	1	0	0	0	0	0	0	0	2
1850.39	0.00	0	0	1	0	0	2	0	0	0
1820.96	0.00	0	1	1	0	0	0	0	0	0
1762.85	0.00	0	1	0	0	0	0	2	0	0
1758.40	0.01	0	0	0	3	0	0	0	0	0
1742.93	0.61	0	0	2	0	0	0	0	0	0
1742.93	0.61	0	0	2	0	0	0	0	0	0
1721.38	0.00	0	0	0	2	1	0	0	0	0
1716.91	0.00	1	0	0	0	0	0	0	1	0
1712.35	0.00	1	0	0	0	0	0	0	0	1
1685.34	0.00	0	0	0	2	0	1	0	0	0
1674.72	0.00	0	0	1	0	0	0	2	0	0
1664.49	0.00	0	0	0	1	2	0	0	0	0
1592.91	0.00	0	0	0	2	0	0	1	0	0
1585.73	0.00	0	0	0	1	0	2	0	0	0
1578.25	0.00	0	0	0	0	2	1	0	0	0
1568.50	1643.84	1	0	0	0	0	0	0	0	0
1568.50	1643.84	1	0	0	0	0	0	0	0	0
1568.50	1643.84	1	0	0	0	0	0	0	0	0
1557.15	0.04	0	0	0	0	3	0	0	0	0
1550.22	0.00	0	1	0	1	0	0	0	0	0
1533.32	0.00	0	0	0	0	1	2	0	0	0
1498.59	0.00	0	1	0	0	1	0	0	0	0
1485.64	0.00	0	0	0	0	0	3	0	0	0
1472.76	0.00	0	0	0	0	2	0	1	0	0
1468.55	0.00	0	0	1	1	0	0	0	0	0
1449.83	0.00	0	1	0	0	0	1	0	0	0
1416.97	0.00	0	0	1	0	1	0	0	0	0

1397.59	0.00	0	0	0	1	0	0	2	0	0
1394.28	0.00	0	0	0	0	0	2	1	0	0
1363.90	0.00	0	1	0	0	0	0	1	0	0
1363.37	0.00	0	0	1	0	0	1	0	0	0
1347.27	0.00	0	0	0	2	0	0	0	1	0
1341.20	0.00	0	0	0	2	0	0	0	0	1
1332.73	0.00	0	0	0	0	1	0	2	0	0
1298.59	0.00	0	0	0	0	0	1	2	0	0
1276.05	0.00	0	0	1	0	0	0	1	0	0
1275.34	0.00	0	1	0	0	0	0	0	2	0
1267.94	0.00	0	1	0	0	0	0	0	0	2
1238.02	0.00	0	0	0	0	2	0	0	0	1
1237.82	0.00	0	0	0	0	2	0	0	1	0
1192.87	0.00	0	0	1	0	0	0	0	2	0
1183.19	3.63	0	0	0	2	0	0	0	0	0
1183.19	3.63	0	0	0	2	0	0	0	0	0
1182.13	0.13	0	0	0	0	0	0	3	0	0
1180.77	0.00	0	0	1	0	0	0	0	0	2
1152.82	0.00	0	0	0	0	0	2	0	1	0
1146.13	0.00	0	0	0	0	0	2	0	0	1
1132.69	0.00	0	0	0	1	1	0	0	0	0
1117.28	0.00	0	1	0	0	0	0	0	1	0
1112.92	0.00	0	1	0	0	0	0	0	0	1
1091.35	0.00	0	0	0	1	0	1	0	0	0
1067.82	13.24	0	0	0	0	2	0	0	0	0
1067.82	13.24	0	0	0	0	2	0	0	0	0
1038.76	0.00	0	0	0	0	1	1	0	0	0
1034.13	0.00	0	0	1	0	0	0	0	1	0
1027.51	0.00	0	0	1	0	0	0	0	0	1
998.49	0.00	0	0	0	1	0	0	1	0	0
991.96	0.04	0	0	0	0	0	2	0	0	0
991.96	0.04	0	0	0	0	0	2	0	0	0
964.77	0.00	0	0	0	0	0	0	2	1	0
955.06	241.42	0	1	0	0	0	0	0	0	0
955.06	241.42	0	1	0	0	0	0	0	0	0
955.06	241.42	0	1	0	0	0	0	0	0	0
953.98	0.00	0	0	0	0	0	0	2	0	1
939.92	0.00	0	0	0	0	1	0	1	0	0
912.96	0.00	0	0	0	1	0	0	0	2	0
902.58	0.00	0	0	0	1	0	0	0	0	2
899.16	0.00	0	0	0	0	0	1	1	0	0
874.38	112.11	0	0	1	0	0	0	0	0	0

874.38	112.11	0	0	1	0	0	0	0	0	0
874.38	112.11	0	0	1	0	0	0	0	0	0
858.57	0.00	0	0	0	0	1	0	0	2	0
855.70	0.00	0	0	0	0	1	0	0	0	2
817.94	0.00	0	0	0	0	0	1	0	2	0
806.94	0.00	0	0	0	0	0	1	0	0	2
796.60	1.57	0	0	0	0	0	0	2	0	0
796.60	1.57	0	0	0	0	0	0	2	0	0
754.53	0.00	0	0	0	1	0	0	0	1	0
748.78	0.00	0	0	0	1	0	0	0	0	1
726.25	0.00	0	0	0	0	0	0	1	2	0
710.81	0.00	0	0	0	0	0	0	1	0	2
700.94	0.00	0	0	0	0	1	0	0	1	0
698.84	0.00	0	0	0	0	1	0	0	0	1
657.99	0.00	0	0	0	0	0	1	0	1	0
652.18	0.00	0	0	0	0	0	1	0	0	1
595.16	9.63	0	0	0	1	0	0	0	0	0
595.16	9.63	0	0	0	1	0	0	0	0	0
595.16	9.63	0	0	0	1	0	0	0	0	0
564.84	0.00	0	0	0	0	0	0	1	1	0
556.43	0.00	0	0	0	0	0	0	1	0	1
542.22	9.83	0	0	0	0	1	0	0	0	0
542.22	9.83	0	0	0	0	1	0	0	0	0
542.22	9.83	0	0	0	0	1	0	0	0	0
496.75	34.07	0	0	0	0	0	1	0	0	0
496.75	34.07	0	0	0	0	0	1	0	0	0
496.75	34.07	0	0	0	0	0	1	0	0	0
479.00	0.00	0	0	0	0	0	0	0	3	0
478.59	0.00	0	0	0	0	0	0	0	2	1
473.78	0.00	0	0	0	0	0	0	0	1	2
462.57	0.00	0	0	0	0	0	0	0	0	3
401.77	47.28	0	0	0	0	0	0	1	0	0
401.77	47.28	0	0	0	0	0	0	1	0	0
401.76	47.28	0	0	0	0	0	0	1	0	0
319.88	0.01	0	0	0	0	0	0	0	2	0
319.88	0.01	0	0	0	0	0	0	0	2	0
317.30	0.00	0	0	0	0	0	0	0	1	1
309.18	0.02	0	0	0	0	0	0	0	0	2
309.18	0.02	0	0	0	0	0	0	0	0	2
160.14	2.59	0	0	0	0	0	0	0	1	0
160.14	2.59	0	0	0	0	0	0	0	1	0
160.14	2.59	0	0	0	0	0	0	0	1	0

154.86	0.04	0 0 0 0 0 0 0 0 1
154.86	0.04	0 0 0 0 0 0 0 0 1
154.86	0.04	0 0 0 0 0 0 0 0 1

$HRnPH_2$

Frequency (cm-1)	Intensity (km.mol-1)	Vibrational quanta
6884.58	0.89	3 0 0 0 0 0 0 0 0
6874.41	0.01	0 3 0 0 0 0 0 0 0
6803.38	0.00	2 1 0 0 0 0 0 0 0
6751.89	0.00	1 2 0 0 0 0 0 0 0
5908.00	0.00	0 2 1 0 0 0 0 0 0
5873.97	0.00	2 0 1 0 0 0 0 0 0
5681.60	0.00	0 2 0 1 0 0 0 0 0
5616.91	0.00	2 0 0 1 0 0 0 0 0
5205.00	0.00	0 2 0 0 1 0 0 0 0
5190.73	0.00	0 2 0 0 0 1 0 0 0
5147.60	0.00	2 0 0 0 1 0 0 0 0
5131.46	0.00	2 0 0 0 0 1 0 0 0
5025.39	0.00	0 2 0 0 0 0 1 0 0
5018.60	0.00	0 2 0 0 0 0 0 1 0
4984.14	0.00	2 0 0 0 0 0 1 0 0
4976.63	0.00	2 0 0 0 0 0 0 1 0
4858.23	0.00	0 2 0 0 0 0 0 0 1
4850.61	0.00	0 1 2 0 0 0 0 0 0
4841.38	0.00	1 0 2 0 0 0 0 0 0
4824.89	0.00	2 0 0 0 0 0 0 0 1
4622.04	0.27	2 0 0 0 0 0 0 0 0
4622.04	0.27	2 0 0 0 0 0 0 0 0
4619.53	0.17	0 2 0 0 0 0 0 0 0
4619.53	0.17	0 2 0 0 0 0 0 0 0
4595.46	0.00	1 1 0 0 0 0 0 0 0
4462.72	0.00	0 1 0 2 0 0 0 0 0
4414.77	0.00	1 0 0 2 0 0 0 0 0
3741.78	8.87	0 0 3 0 0 0 0 0 0
3610.64	0.00	0 1 1 0 0 0 0 0 0
3601.09	0.00	1 0 1 0 0 0 0 0 0
3598.12	0.00	0 0 2 1 0 0 0 0 0
3540.91	0.00	0 1 0 0 2 0 0 0 0
3522.03	0.00	0 1 0 0 0 2 0 0 0
3501.99	0.00	1 0 0 0 2 0 0 0 0

3481.50	0.00	1	0	0	0	0	2	0	0	0
3419.12	0.00	0	0	1	2	0	0	0	0	0
3415.60	0.00	0	1	0	1	0	0	0	0	0
3384.54	0.00	1	0	0	1	0	0	0	0	0
3200.54	0.07	0	0	0	3	0	0	0	0	0
3118.80	0.00	0	1	0	0	0	0	2	0	0
3106.62	0.00	0	1	0	0	0	0	0	2	0
3099.14	0.00	1	0	0	0	0	0	2	0	0
3087.23	0.00	1	0	0	0	0	0	0	2	0
3064.73	0.00	0	0	2	0	1	0	0	0	0
3051.37	0.00	0	0	2	0	0	1	0	0	0
2931.25	0.00	0	1	0	0	1	0	0	0	0
2916.33	0.00	0	1	0	0	0	1	0	0	0
2901.47	0.00	1	0	0	0	1	0	0	0	0
2885.09	0.00	1	0	0	0	0	1	0	0	0
2859.88	0.00	0	0	2	0	0	0	1	0	0
2851.94	0.00	0	0	2	0	0	0	0	1	0
2770.84	0.00	0	1	0	0	0	0	0	0	2
2760.75	0.00	1	0	0	0	0	0	0	0	2
2740.73	0.00	0	1	0	0	0	0	1	0	0
2733.70	0.00	0	1	0	0	0	0	0	1	0
2728.12	0.00	0	0	0	2	1	0	0	0	0
2724.05	0.00	1	0	0	0	0	0	1	0	0
2717.09	0.00	1	0	0	0	0	0	0	1	0
2713.15	0.00	0	0	2	0	0	0	0	0	1
2700.14	0.00	0	0	0	2	0	1	0	0	0
2558.98	0.00	0	1	0	0	0	0	0	0	1
2557.56	0.00	0	0	0	2	0	0	1	0	0
2550.67	0.00	0	0	0	2	0	0	0	1	0
2548.86	0.00	1	0	0	0	0	0	0	0	1
2513.87	227.71	0	0	2	0	0	0	0	0	0
2513.87	227.71	0	0	2	0	0	0	0	0	0
2439.10	0.00	0	0	1	0	2	0	0	0	0
2426.39	0.00	0	0	1	0	0	2	0	0	0
2368.70	0.00	0	0	0	2	0	0	0	0	1
2355.33	0.00	0	0	1	1	0	0	0	0	0
2341.47	43.06	0	1	0	0	0	0	0	0	0
2341.47	43.06	0	1	0	0	0	0	0	0	0
2341.47	43.06	0	1	0	0	0	0	0	0	0
2334.83	50.39	1	0	0	0	0	0	0	0	0
2334.83	50.39	1	0	0	0	0	0	0	0	0
2334.83	50.39	1	0	0	0	0	0	0	0	0

2276.20	0.00	0	0	0	1	2	0	0	0	0
2260.02	0.00	0	0	0	1	0	2	0	0	0
2149.52	0.10	0	0	0	2	0	0	0	0	0
2149.52	0.10	0	0	0	2	0	0	0	0	0
2037.49	0.00	0	0	1	0	0	0	2	0	0
2026.51	0.00	0	0	1	0	0	0	0	2	0
1870.68	0.00	0	0	0	1	0	0	2	0	0
1858.84	0.00	0	0	0	1	0	0	0	2	0
1840.81	0.00	0	0	1	0	1	0	0	0	0
1827.06	0.00	0	0	1	0	0	1	0	0	0
1824.62	0.01	0	0	0	0	0	3	0	0	0
1823.78	0.00	0	0	0	0	3	0	0	0	0
1804.72	0.00	0	0	0	0	2	1	0	0	0
1799.89	0.00	0	0	0	0	1	2	0	0	0
1680.98	0.00	0	0	1	0	0	0	0	0	2
1662.43	0.00	0	0	0	1	1	0	0	0	0
1658.81	0.00	0	0	1	0	0	0	1	0	0
1652.07	0.00	0	0	1	0	0	0	0	1	0
1639.38	0.00	0	0	0	1	0	1	0	0	0
1632.66	0.00	0	0	0	0	2	0	1	0	0
1605.32	0.00	0	0	0	0	2	0	0	1	0
1601.37	0.00	0	0	0	0	0	2	0	1	0
1592.41	0.00	0	0	0	0	0	2	1	0	0
1512.29	0.00	0	0	0	1	0	0	0	0	2
1486.54	0.00	0	0	0	1	0	0	1	0	0
1479.48	0.00	0	0	0	1	0	0	0	1	0
1475.79	0.00	0	0	1	0	0	0	0	0	1
1411.10	0.00	0	0	0	0	2	0	0	0	1
1409.08	0.00	0	0	0	0	1	0	2	0	0
1389.36	0.00	0	0	0	0	0	2	0	0	1
1381.55	0.00	0	0	0	0	1	0	0	2	0
1380.57	0.00	0	0	0	0	0	1	2	0	0
1380.44	0.00	0	0	0	0	0	1	0	2	0
1300.35	0.00	0	0	0	1	0	0	0	0	1
1277.58	1717.55	0	0	1	0	0	0	0	0	0
1277.58	1717.55	0	0	1	0	0	0	0	0	0
1277.58	1717.55	0	0	1	0	0	0	0	0	0
1195.05	0.23	0	0	0	0	2	0	0	0	0
1195.05	0.23	0	0	0	0	2	0	0	0	0
1193.46	0.00	0	0	0	0	0	0	2	1	0
1189.74	0.00	0	0	0	0	0	0	1	2	0
1184.36	0.00	0	0	0	0	1	1	0	0	0

1180.84	0.36	0	0	0	0	0	2	0	0	0
1180.84	0.36	0	0	0	0	0	2	0	0	0
1126.23	0.09	0	0	0	0	0	0	3	0	0
1109.21	0.14	0	0	0	0	0	0	0	3	0
1081.36	15.72	0	0	0	1	0	0	0	0	0
1081.36	15.72	0	0	0	1	0	0	0	0	0
1081.36	15.72	0	0	0	1	0	0	0	0	0
1009.23	0.00	0	0	0	0	1	0	0	0	2
1004.69	0.00	0	0	0	0	1	0	1	0	0
998.91	0.00	0	0	0	0	0	0	2	0	1
993.90	0.00	0	0	0	0	0	1	0	0	2
991.15	0.00	0	0	0	0	1	0	0	1	0
986.18	0.00	0	0	0	0	0	0	0	2	1
983.70	0.00	0	0	0	0	0	1	1	0	0
981.50	0.00	0	0	0	0	0	1	0	1	0
824.01	0.00	0	0	0	0	0	0	1	0	2
816.71	0.00	0	0	0	0	0	0	0	1	2
803.48	0.00	0	0	0	0	0	0	1	1	0
798.98	0.00	0	0	0	0	1	0	0	0	1
783.22	0.00	0	0	0	0	0	1	0	0	1
773.67	7.24	0	0	0	0	0	0	2	0	0
773.67	7.24	0	0	0	0	0	0	2	0	0
761.97	7.67	0	0	0	0	0	0	0	2	0
761.97	7.67	0	0	0	0	0	0	0	2	0
637.03	0.01	0	0	0	0	0	0	0	0	3
613.04	0.00	0	0	0	0	0	0	1	0	1
605.89	0.00	0	0	0	0	0	0	0	1	1
591.88	0.00	0	0	0	0	1	0	0	0	0
591.88	0.00	0	0	0	0	1	0	0	0	0
591.88	0.00	0	0	0	0	1	0	0	0	0
576.82	5.22	0	0	0	0	0	1	0	0	0
576.82	5.22	0	0	0	0	0	1	0	0	0
576.82	5.22	0	0	0	0	0	1	0	0	0
426.15	0.33	0	0	0	0	0	0	0	0	2
426.15	0.33	0	0	0	0	0	0	0	0	2
395.76	10.30	0	0	0	0	0	0	1	0	0
395.76	10.30	0	0	0	0	0	0	1	0	0
395.76	10.30	0	0	0	0	0	0	1	0	0
389.51	13.22	0	0	0	0	0	0	0	1	0
389.51	13.22	0	0	0	0	0	0	0	1	0
389.51	13.22	0	0	0	0	0	0	0	1	0
213.82	8.39	0	0	0	0	0	0	0	0	1

213.82	8.39	0 0 0 0 0 0 0 0 1
213.82	8.39	0 0 0 0 0 0 0 0 1

$HRnPF_2$

Frequency (cm-1)	Intensity (km.mol-1)	Vibrational quanta
3287.97	3.26	3 0 0 0 0 0 0 0 0
3000.03	0.00	2 0 1 0 0 0 0 0 0
2996.37	0.00	2 1 0 0 0 0 0 0 0
2707.48	0.00	1 0 2 0 0 0 0 0 0
2704.13	0.00	1 2 0 0 0 0 0 0 0
2546.21	0.00	2 0 0 1 0 0 0 0 0
2540.65	0.00	2 0 0 0 0 1 0 0 0
2505.83	0.00	2 0 0 0 1 0 0 0 0
2392.17	0.21	0 3 0 0 0 0 0 0 0
2383.30	0.00	2 0 0 0 0 0 1 0 0
2370.80	0.00	0 0 3 0 0 0 0 0 0
2370.78	0.00	0 1 2 0 0 0 0 0 0
2365.25	0.00	0 2 1 0 0 0 0 0 0
2299.34	0.00	2 0 0 0 0 0 0 1 0
2281.31	0.00	2 0 0 0 0 0 0 0 1
2186.72	220.78	2 0 0 0 0 0 0 0 0
2186.72	220.78	2 0 0 0 0 0 0 0 0
2010.20	0.00	0 2 0 1 0 0 0 0 0
2006.91	0.00	0 0 2 1 0 0 0 0 0
1984.83	0.00	0 2 0 0 1 0 0 0 0
1981.67	0.00	0 0 2 0 1 0 0 0 0
1930.63	0.00	0 2 0 0 0 1 0 0 0
1928.10	0.00	0 0 2 0 0 1 0 0 0
1914.98	0.00	1 0 1 0 0 0 0 0 0
1914.22	0.00	1 1 0 0 0 0 0 0 0
1896.81	0.00	1 0 0 2 0 0 0 0 0
1845.04	0.00	1 0 0 0 2 0 0 0 0
1821.22	0.00	0 2 0 0 0 0 1 0 0
1820.53	0.00	0 0 2 0 0 0 1 0 0
1805.36	0.00	1 0 0 0 0 2 0 0 0
1692.75	0.00	0 0 2 0 0 0 0 1 0
1690.27	0.00	0 2 0 0 0 0 0 1 0
1686.66	0.00	0 2 0 0 0 0 0 0 1
1683.86	0.00	0 0 2 0 0 0 0 0 1
1632.34	0.00	0 1 0 2 0 0 0 0 0

1630.33	0.00	0	0	1	2	0	0	0	0	0
1589.62	0.12	0	2	0	0	0	0	0	0	0
1589.62	0.12	0	2	0	0	0	0	0	0	0
1584.75	0.00	0	1	1	0	0	0	0	0	0
1583.79	0.65	0	0	2	0	0	0	0	0	0
1583.79	0.65	0	0	2	0	0	0	0	0	0
1577.10	0.00	0	1	0	0	2	0	0	0	0
1575.31	0.00	0	0	1	0	2	0	0	0	0
1531.25	0.00	1	0	0	0	0	0	2	0	0
1508.45	0.00	1	0	0	1	0	0	0	0	0
1486.22	0.00	0	1	0	0	0	2	0	0	0
1485.15	0.00	0	0	1	0	0	2	0	0	0
1481.30	0.00	1	0	0	0	1	0	0	0	0
1460.91	0.00	1	0	0	0	0	1	0	0	0
1327.99	0.00	1	0	0	0	0	0	1	0	0
1319.04	0.00	1	0	0	0	0	0	0	2	0
1294.32	0.00	1	0	0	0	0	0	0	0	2
1258.65	0.00	0	0	1	0	0	0	2	0	0
1258.03	0.00	0	1	0	0	0	0	2	0	0
1241.83	0.04	0	0	0	3	0	0	0	0	0
1217.49	0.00	0	1	0	1	0	0	0	0	0
1217.39	0.00	1	0	0	0	0	0	0	1	0
1216.71	0.00	0	0	0	2	1	0	0	0	0
1215.76	0.00	0	0	1	1	0	0	0	0	0
1207.52	0.00	1	0	0	0	0	0	0	0	1
1190.37	0.00	0	1	0	0	1	0	0	0	0
1188.89	0.00	0	0	1	0	1	0	0	0	0
1184.01	0.00	0	0	0	2	0	1	0	0	0
1180.18	0.00	0	0	0	1	2	0	0	0	0
1158.19	0.03	0	0	0	0	3	0	0	0	0
1142.11	0.00	0	1	0	0	0	1	0	0	0
1140.86	0.00	0	0	1	0	0	1	0	0	0
1128.86	0.00	0	0	0	0	2	1	0	0	0
1125.58	1354.52	1	0	0	0	0	0	0	0	0
1122.01	1359.31	1	0	0	0	0	0	0	0	0
1122.01	1359.31	1	0	0	0	0	0	0	0	0
1114.64	0.00	0	0	0	1	0	2	0	0	0
1084.97	0.00	0	0	0	0	1	2	0	0	0
1067.32	0.00	0	0	0	2	0	0	1	0	0
1040.25	0.00	0	0	0	0	0	3	0	0	0
1030.30	0.00	0	0	1	0	0	0	1	0	0
1029.83	0.00	0	1	0	0	0	0	1	0	0

1004.98	0.00	0	0	1	0	0	0	0	2	0
1003.56	0.00	0	1	0	0	0	0	0	2	0
1003.07	0.00	0	0	0	0	2	0	1	0	0
991.06	0.00	0	1	0	0	0	0	0	0	2
989.39	0.00	0	0	1	0	0	0	0	0	2
939.53	0.00	0	0	0	2	0	0	0	1	0
934.22	0.00	0	0	0	2	0	0	0	0	1
927.52	0.00	0	0	0	0	0	2	1	0	0
900.84	0.00	0	0	1	0	0	0	0	1	0
900.33	0.00	0	1	0	0	0	0	0	1	0
895.42	0.00	0	1	0	0	0	0	0	0	1
894.00	0.00	0	0	1	0	0	0	0	0	1
892.15	0.00	0	0	0	0	2	0	0	1	0
877.93	0.00	0	0	0	1	0	0	2	0	0
875.49	0.00	0	0	0	0	2	0	0	0	1
838.42	0.00	0	0	0	0	1	0	2	0	0
830.53	8.01	0	0	0	2	0	0	0	0	0
830.53	8.01	0	0	0	2	0	0	0	0	0
807.68	0.00	0	0	0	0	0	1	2	0	0
804.01	0.00	0	0	0	1	1	0	0	0	0
799.70	0.00	0	0	0	0	0	2	0	1	0
798.06	140.94	0	1	0	0	0	0	0	0	0
798.04	140.87	0	1	0	0	0	0	0	0	0
798.04	140.87	0	1	0	0	0	0	0	0	0
795.45	432.91	0	0	1	0	0	0	0	0	0
794.88	432.94	0	0	1	0	0	0	0	0	0
794.88	432.94	0	0	1	0	0	0	0	0	0
793.45	0.00	0	0	0	0	0	2	0	0	1
768.81	13.30	0	0	0	0	2	0	0	0	0
768.81	13.30	0	0	0	0	2	0	0	0	0
766.73	0.00	0	0	0	1	0	1	0	0	0
737.90	0.00	0	0	0	0	1	1	0	0	0
694.02	0.16	0	0	0	0	0	2	0	0	0
694.02	0.16	0	0	0	0	0	2	0	0	0
688.94	0.01	0	0	0	0	0	0	3	0	0
650.54	0.00	0	0	0	1	0	0	1	0	0
626.63	0.00	0	0	0	1	0	0	0	2	0
617.10	0.00	0	0	0	0	1	0	1	0	0
613.28	0.00	0	0	0	1	0	0	0	0	2
605.79	0.00	0	0	0	0	1	0	0	2	0
579.87	0.00	0	0	0	0	1	0	0	0	2
579.30	0.00	0	0	0	0	0	1	1	0	0

571.87	0.00	0	0	0	0	0	0	2	1	0
561.56	0.00	0	0	0	0	0	0	2	0	1
556.46	0.00	0	0	0	0	0	1	0	2	0
541.89	0.00	0	0	0	0	0	1	0	0	2
522.50	0.00	0	0	0	1	0	0	0	1	0
517.24	0.00	0	0	0	1	0	0	0	0	1
498.04	0.00	0	0	0	0	1	0	0	1	0
486.61	0.00	0	0	0	0	1	0	0	0	1
458.33	0.21	0	0	0	0	0	0	2	0	0
458.33	0.21	0	0	0	0	0	0	2	0	0
451.73	0.00	0	0	0	0	0	1	0	1	0
445.42	0.00	0	0	0	0	0	1	0	0	1
444.69	0.00	0	0	0	0	0	0	1	2	0
427.81	0.00	0	0	0	0	0	0	1	0	2
419.62	14.24	0	0	0	1	0	0	0	0	0
418.94	14.24	0	0	0	1	0	0	0	0	0
418.94	14.24	0	0	0	1	0	0	0	0	0
392.41	24.02	0	0	0	0	1	0	0	0	0
390.91	24.00	0	0	0	0	1	0	0	0	0
390.91	24.00	0	0	0	0	1	0	0	0	0
347.39	14.66	0	0	0	0	0	1	0	0	0
347.35	14.66	0	0	0	0	0	1	0	0	0
347.35	14.66	0	0	0	0	0	1	0	0	0
338.22	0.00	0	0	0	0	0	0	1	1	0
330.79	0.00	0	0	0	0	0	0	1	0	1
316.87	0.02	0	0	0	0	0	0	0	3	0
313.31	0.00	0	0	0	0	0	0	0	2	1
301.64	0.00	0	0	0	0	0	0	0	1	2
289.94	0.00	0	0	0	0	0	0	0	0	3
231.95	6.13	0	0	0	0	0	0	1	0	0
231.42	6.13	0	0	0	0	0	0	1	0	0
231.42	6.13	0	0	0	0	0	0	1	0	0
207.25	0.01	0	0	0	0	0	0	0	2	0
207.25	0.01	0	0	0	0	0	0	0	2	0
203.90	0.00	0	0	0	0	0	0	0	1	1
193.12	0.03	0	0	0	0	0	0	0	0	2
193.12	0.03	0	0	0	0	0	0	0	0	2
104.92	2.04	0	0	0	0	0	0	0	1	0
103.92	2.04	0	0	0	0	0	0	0	1	0
103.92	2.04	0	0	0	0	0	0	0	1	0
97.38	1.01	0	0	0	0	0	0	0	0	1
97.06	1.01	0	0	0	0	0	0	0	0	1

```
      97.06       1.01     0 0 0 0 0 0 0 0 0 1
```

Direct cc-VSCF

Direct cc-VSCF data for all molecules, computed at the MP2/aug-MCP-TZP level of theory.

HRnOH

Frequency (cm-1)	Intensity (km.mol-1)	Vibrational quanta
10463.81	0.09	3 0 0 0 0 0
8843.11	0.17	2 1 0 0 0 0
7868.64	0.03	2 0 1 0 0 0
7655.24	0.00	2 0 0 1 0 0
7579.62	0.04	2 0 0 0 1 0
7556.54	0.04	2 0 0 0 0 1
7114.92	1.88	2 0 0 0 0 0
7114.92	1.88	2 0 0 0 0 0
7042.46	0.06	1 2 0 0 0 0
5326.53	2.45	1 1 0 0 0 0
5260.58	1.61	1 0 2 0 0 0
5100.69	0.06	0 3 0 0 0 0
4685.38	0.00	1 0 0 2 0 0
4474.84	0.00	1 0 0 0 0 2
4320.30	0.13	1 0 0 0 2 0
4280.26	0.35	1 0 1 0 0 0
4141.05	0.01	0 2 1 0 0 0
4132.95	0.02	1 0 0 1 0 0
4065.85	0.23	1 0 0 0 1 0
4032.13	0.13	1 0 0 0 0 1
3977.19	0.01	0 2 0 1 0 0
3957.13	0.01	0 2 0 0 1 0
3893.09	0.03	0 2 0 0 0 1
3631.75	55.53	1 0 0 0 0 0
3631.75	55.53	1 0 0 0 0 0
3451.08	23.30	0 2 0 0 0 0
3451.08	23.30	0 2 0 0 0 0
3444.95	17.14	0 1 2 0 0 0
2813.04	2.28	0 1 0 2 0 0
2639.45	0.00	0 1 0 0 0 2
2607.59	7.99	0 1 0 0 2 0

2536.38	0.95	0	0	3	0	0	0
2457.01	0.32	0	1	1	0	0	0
2331.43	0.06	0	0	2	1	0	0
2295.01	0.54	0	1	0	1	0	0
2290.78	0.01	0	0	2	0	1	0
2257.98	0.20	0	1	0	0	1	0
2233.05	6.54	0	0	2	0	0	1
2197.70	1.51	0	1	0	0	0	1
1800.97	0.02	0	0	1	2	0	0
1777.19	895.25	0	1	0	0	0	0
1777.19	895.25	0	1	0	0	0	0
1750.88	0.04	0	0	1	0	2	0
1718.13	0.34	0	0	2	0	0	0
1718.13	0.34	0	0	2	0	0	0
1618.50	0.00	0	0	0	3	0	0
1592.23	0.03	0	0	0	2	1	0
1589.80	0.00	0	0	1	0	0	2
1551.58	0.29	0	0	0	2	0	1
1439.71	0.01	0	0	0	1	0	2
1410.10	0.02	0	0	0	1	2	0
1400.60	0.01	0	0	0	0	1	2
1334.05	0.03	0	0	0	0	0	3
1332.38	1.83	0	0	0	0	2	1
1295.44	5.56	0	0	1	0	1	0
1250.49	0.10	0	0	1	1	0	0
1169.39	0.33	0	0	0	0	3	0
1149.22	0.17	0	0	1	0	0	1
1091.02	5.75	0	0	0	2	0	0
1091.02	5.75	0	0	0	2	0	0
1051.84	0.03	0	0	0	1	1	0
997.70	0.20	0	0	0	1	0	1
957.92	0.39	0	0	0	0	1	1
892.93	1.83	0	0	0	0	0	2
892.93	1.83	0	0	0	0	0	2
857.65	2.94	0	0	0	0	2	0
857.65	2.94	0	0	0	0	2	0
845.05	6.97	0	0	1	0	0	0
845.05	6.97	0	0	1	0	0	0
551.32	1.62	0	0	0	1	0	0
551.32	1.62	0	0	0	1	0	0
467.13	5.39	0	0	0	0	1	0
467.13	5.39	0	0	0	0	1	0

448.21	154.07	0 0 0 0 0 1
448.21	154.07	0 0 0 0 0 1

HRnOF

Frequency (cm-1)	Intensity (km.mol-1)	Vibrational quanta
5290.07	0.00	3 0 0 0 0 0
4573.90	0.00	2 1 0 0 0 0
4149.83	0.10	2 0 1 0 0 0
4114.39	0.01	2 0 0 1 0 0
4021.54	0.12	2 0 0 0 1 0
3771.01	0.02	1 2 0 0 0 0
3746.69	0.07	2 0 0 0 0 1
3595.89	9.29	2 0 0 0 0 0
3595.89	9.29	2 0 0 0 0 0
2934.61	1.22	1 0 2 0 0 0
2924.33	0.07	0 3 0 0 0 0
2860.94	2.04	1 0 0 2 0 0
2794.64	0.07	1 1 0 0 0 0
2663.37	0.07	1 0 0 0 2 0
2533.06	0.00	0 2 1 0 0 0
2501.90	0.00	0 2 0 1 0 0
2387.42	0.00	0 2 0 0 1 0
2385.33	0.41	1 0 1 0 0 0
2353.09	0.52	1 0 0 1 0 0
2241.60	0.84	1 0 0 0 1 0
2138.08	0.00	0 1 2 0 0 0
2116.63	0.18	1 0 0 0 0 2
2105.57	0.02	0 2 0 0 0 1
2074.35	0.00	0 1 0 2 0 0
1965.63	1.58	1 0 0 0 0 1
1957.94	1.22	0 2 0 0 0 0
1957.94	1.22	0 2 0 0 0 0
1834.05	778.57	1 0 0 0 0 0
1834.05	778.57	1 0 0 0 0 0
1834.05	778.57	1 0 0 0 0 0
1832.95	0.01	0 1 0 0 2 0
1700.17	0.04	0 0 3 0 0 0
1669.06	0.01	0 0 2 1 0 0
1634.66	0.08	0 0 1 2 0 0
1587.57	0.02	0 0 0 3 0 0

1577.92	0.14	0	0	2	0	1	0
1556.76	0.05	0	1	1	0	0	0
1524.94	0.00	0	1	0	1	0	0
1513.46	0.39	0	0	0	2	1	0
1421.65	0.00	0	0	1	0	2	0
1411.27	0.55	0	1	0	0	1	0
1387.17	0.00	0	0	0	1	2	0
1306.03	0.05	0	0	2	0	0	1
1280.31	0.03	0	1	0	0	0	2
1266.69	0.01	0	0	0	0	3	0
1237.02	0.01	0	0	0	2	0	1
1144.36	3.43	0	0	2	0	0	0
1144.36	3.43	0	0	2	0	0	0
1131.55	0.14	0	1	0	0	0	1
1106.11	0.02	0	0	1	1	0	0
1072.74	4.93	0	0	0	2	0	0
1072.74	4.93	0	0	0	2	0	0
1002.65	0.02	0	0	0	0	2	1
1001.22	0.80	0	0	1	0	1	0
983.13	8.81	0	1	0	0	0	0
983.13	8.81	0	1	0	0	0	0
983.13	8.81	0	1	0	0	0	0
968.16	0.25	0	0	0	1	1	0
877.85	0.00	0	0	1	0	0	2
849.71	1.00	0	0	0	0	2	0
849.71	1.00	0	0	0	0	2	0
840.17	0.00	0	0	0	1	0	2
730.93	0.01	0	0	0	0	1	2
727.15	1.62	0	0	1	0	0	1
692.18	0.00	0	0	0	1	0	1
579.91	0.90	0	0	0	0	1	1
576.67	16.04	0	0	1	0	0	0
576.67	16.04	0	0	1	0	0	0
576.67	16.04	0	0	1	0	0	0
543.52	2.19	0	0	0	1	0	0
543.52	2.19	0	0	0	1	0	0
543.52	2.19	0	0	0	1	0	0
453.47	0.00	0	0	0	0	0	3
427.40	142.15	0	0	0	0	1	0
427.40	142.15	0	0	0	0	1	0
427.40	142.15	0	0	0	0	1	0
302.53	0.01	0	0	0	0	0	2

302.53	0.01	0 0 0 0 0 2
151.46	2.46	0 0 0 0 0 1
151.46	2.46	0 0 0 0 0 1
151.46	2.46	0 0 0 0 0 1

HRnSH

Frequency (cm-1)	Intensity (km.mol-1)	Vibrational quanta
7725.32	0.02	3 0 0 0 0 0
6748.47	0.05	2 1 0 0 0 0
5792.73	0.00	2 0 1 0 0 0
5703.92	0.00	2 0 0 1 0 0
5638.82	0.02	1 2 0 0 0 0
5625.88	0.02	2 0 0 0 1 0
5484.76	0.00	2 0 0 0 0 1
5236.37	0.29	2 0 0 0 0 0
5236.37	0.29	2 0 0 0 0 0
4414.17	0.96	0 3 0 0 0 0
4158.56	0.82	1 1 0 0 0 0
3922.01	0.05	1 0 2 0 0 0
3587.31	0.01	1 0 0 2 0 0
3581.21	0.03	0 2 1 0 0 0
3442.38	0.04	0 2 0 1 0 0
3418.80	0.05	0 2 0 0 1 0
3381.09	0.31	1 0 0 0 2 0
3246.81	0.34	0 2 0 0 0 1
3237.74	0.06	1 0 1 0 0 0
3141.35	0.00	1 0 0 0 0 2
3112.45	0.00	1 0 0 1 0 0
3060.90	0.16	1 0 0 0 1 0
3003.83	94.10	0 2 0 0 0 0
3003.83	94.10	0 2 0 0 0 0
2892.84	0.03	1 0 0 0 0 1
2833.37	7.90	0 1 2 0 0 0
2663.10	3.69	1 0 0 0 0 0
2663.10	3.69	1 0 0 0 0 0
2663.10	3.69	1 0 0 0 0 0
2412.77	8.98	0 1 0 2 0 0
2288.08	19.59	0 1 0 0 2 0
2105.62	1.00	0 1 1 0 0 0
2022.76	0.02	0 0 3 0 0 0

2013.09	0.00	0	1	0	0	0	2
1978.67	1.39	0	1	0	1	0	0
1942.29	1.05	0	1	0	0	1	0
1784.55	0.01	0	0	2	1	0	0
1766.84	0.53	0	1	0	0	0	1
1766.34	0.01	0	0	2	0	1	0
1572.92	0.49	0	0	2	0	0	1
1534.59	1937.77	0	1	0	0	0	0
1534.59	1937.77	0	1	0	0	0	0
1534.59	1937.77	0	1	0	0	0	0
1527.35	0.01	0	0	1	2	0	0
1437.03	0.05	0	0	1	0	2	0
1379.11	0.01	0	0	0	3	0	0
1350.06	0.01	0	0	0	2	1	0
1308.74	0.22	0	0	2	0	0	0
1308.74	0.22	0	0	2	0	0	0
1244.29	0.01	0	0	0	1	2	0
1194.72	0.13	0	0	0	2	0	1
1090.28	0.24	0	0	0	0	3	0
1090.08	0.00	0	0	1	0	0	2
1058.87	0.00	0	0	1	1	0	0
1051.78	12.79	0	0	1	0	1	0
1048.80	0.82	0	0	0	0	2	1
967.45	0.00	0	0	0	1	0	2
930.06	16.62	0	0	0	2	0	0
930.06	16.62	0	0	0	2	0	0
926.07	0.00	0	0	0	0	1	2
889.34	0.00	0	0	0	1	1	0
842.78	0.04	0	0	1	0	0	1
775.91	4.89	0	0	0	0	2	0
775.91	4.89	0	0	0	0	2	0
746.60	0.01	0	0	0	0	0	3
719.88	0.11	0	0	0	1	0	1
678.17	0.20	0	0	0	0	1	1
626.38	0.57	0	0	1	0	0	0
626.38	0.57	0	0	1	0	0	0
626.38	0.57	0	0	1	0	0	0
499.19	0.37	0	0	0	0	0	2
499.19	0.37	0	0	0	0	0	2
470.63	0.85	0	0	0	1	0	0
470.63	0.85	0	0	0	1	0	0
470.63	0.85	0	0	0	1	0	0

412.47	5.11	0 0 0 0 1 0
412.47	5.11	0 0 0 0 1 0
412.47	5.11	0 0 0 0 1 0
250.31	51.93	0 0 0 0 0 1
250.31	51.93	0 0 0 0 0 1
250.31	51.93	0 0 0 0 0 1

HRnSF

Frequency (cm-1)	Intensity (km.mol-1)	Vibrational quanta
4372.03	0.05	3 0 0 0 0 0
3711.22	0.07	2 1 0 0 0 0
3441.88	0.04	2 0 1 0 0 0
3413.59	0.02	2 0 0 1 0 0
3240.53	0.29	2 0 0 0 1 0
3082.77	2.48	2 0 0 0 0 1
2985.01	71.13	2 0 0 0 0 0
2985.01	71.13	2 0 0 0 0 0
2963.74	0.01	1 2 0 0 0 0
2452.89	6.17	1 0 2 0 0 0
2391.30	9.45	1 0 0 2 0 0
2241.32	2.45	1 1 0 0 0 0
2148.92	0.06	0 3 0 0 0 0
2032.12	0.03	1 0 0 0 2 0
1996.23	1.66	1 0 1 0 0 0
1967.69	1.29	1 0 0 1 0 0
1937.56	0.00	0 2 1 0 0 0
1908.73	0.00	0 2 0 1 0 0
1773.66	2.71	1 0 0 0 1 0
1721.86	0.10	0 1 2 0 0 0
1713.62	0.13	1 0 0 0 0 2
1700.52	0.00	0 2 0 0 1 0
1663.79	0.20	0 1 0 2 0 0
1614.38	30.83	1 0 0 0 0 1
1541.73	0.02	0 2 0 0 0 1
1530.93	2024.95	1 0 0 0 0 0
1530.93	2024.95	1 0 0 0 0 0
1530.93	2024.95	1 0 0 0 0 0
1458.54	0.01	0 0 3 0 0 0
1439.71	2.65	0 2 0 0 0 0
1439.71	2.65	0 2 0 0 0 0

1429.43	0.00	0 0 2 1 0 0
1399.15	0.01	0 0 1 2 0 0
1361.15	0.01	0 0 0 3 0 0
1256.51	0.06	0 0 2 0 1 0
1242.86	0.01	0 1 0 0 2 0
1220.13	0.05	0 1 1 0 0 0
1196.97	0.15	0 0 0 2 1 0
1190.60	0.07	0 1 0 1 0 0
1097.08	0.01	0 0 2 0 0 1
1034.39	0.07	0 0 0 2 0 1
1015.53	0.00	0 0 1 0 2 0
985.27	0.00	0 0 0 1 2 0
984.01	0.08	0 1 0 0 1 0
983.97	15.65	0 0 2 0 0 0
983.97	15.65	0 0 2 0 0 0
949.83	0.00	0 0 1 1 0 0
926.50	0.18	0 1 0 0 0 2
920.80	17.97	0 0 0 2 0 0
920.80	17.97	0 0 0 2 0 0
825.55	1.28	0 1 0 0 0 1
779.50	0.00	0 0 0 0 3 0
757.14	1.42	0 0 1 0 1 0
726.94	0.16	0 0 0 1 1 0
723.47	133.55	0 1 0 0 0 0
723.47	133.55	0 1 0 0 0 0
723.47	133.55	0 1 0 0 0 0
699.93	0.02	0 0 1 0 0 2
665.47	0.00	0 0 0 1 0 2
625.08	0.01	0 0 0 0 2 1
599.07	3.16	0 0 1 0 0 1
566.91	0.00	0 0 0 1 0 1
521.41	0.14	0 0 0 0 2 0
521.41	0.14	0 0 0 0 2 0
497.22	2.70	0 0 1 0 0 0
497.22	2.70	0 0 1 0 0 0
497.22	2.70	0 0 1 0 0 0
467.32	0.02	0 0 0 0 1 2
466.87	0.59	0 0 0 1 0 0
466.87	0.59	0 0 0 1 0 0
466.87	0.59	0 0 0 1 0 0
364.91	0.46	0 0 0 0 1 1
305.42	0.00	0 0 0 0 0 3

261.55	53.26	0 0 0 0 1 0
261.55	53.26	0 0 0 0 1 0
261.55	53.26	0 0 0 0 1 0
204.31	0.01	0 0 0 0 0 2
204.31	0.01	0 0 0 0 0 2
102.47	0.40	0 0 0 0 0 1
102.47	0.40	0 0 0 0 0 1
102.47	0.40	0 0 0 0 0 1

$HRnNH_2$

Frequency (cm-1)	Intensity (km.mol-1)	Vibrational quanta
9469.40	0.03	0 3 0 0 0 0 0 0 0
9312.56	0.10	1 2 0 0 0 0 0 0 0
9300.95	0.03	3 0 0 0 0 0 0 0 0
9035.48	0.02	2 1 0 0 0 0 0 0 0
7962.01	0.10	0 2 1 0 0 0 0 0 0
7846.49	0.08	0 2 0 1 0 0 0 0 0
7805.68	28.07	2 0 1 0 0 0 0 0 0
7586.03	3.75	2 0 0 1 0 0 0 0 0
7200.89	0.00	0 2 0 0 1 0 0 0 0
7068.64	0.06	0 2 0 0 0 1 0 0 0
6947.80	0.07	2 0 0 0 1 0 0 0 0
6924.47	0.00	0 2 0 0 0 0 1 0 0
6907.58	0.02	0 2 0 0 0 0 0 1 0
6830.89	0.04	0 2 0 0 0 0 0 0 1
6828.32	3.18	2 0 0 0 0 1 0 0 0
6740.06	0.02	2 0 0 0 0 0 1 0 0
6723.70	0.69	2 0 0 0 0 0 0 1 0
6678.83	4.78	2 0 0 0 0 0 0 0 1
6394.18	0.80	0 2 0 0 0 0 0 0 0
6394.18	0.80	0 2 0 0 0 0 0 0 0
6361.62	0.00	1 0 2 0 0 0 0 0 0
6341.57	0.16	2 0 0 0 0 0 0 0 0
6341.57	0.16	2 0 0 0 0 0 0 0 0
6304.73	0.13	0 1 2 0 0 0 0 0 0
6296.61	0.48	1 1 0 0 0 0 0 0 0
6213.43	0.05	1 0 0 2 0 0 0 0 0
6202.81	0.00	0 1 0 2 0 0 0 0 0
4866.90	0.04	0 1 0 0 2 0 0 0 0
4861.28	0.00	1 0 0 0 2 0 0 0 0

4838.08	0.08	0	1	0	0	0	2	0	0	0
4811.69	0.00	1	0	1	0	0	0	0	0	0
4797.65	2.12	0	1	1	0	0	0	0	0	0
4793.31	0.02	1	0	0	0	0	2	0	0	0
4699.26	0.81	0	1	0	1	0	0	0	0	0
4668.19	1.79	1	0	0	1	0	0	0	0	0
4507.92	0.53	0	0	2	1	0	0	0	0	0
4506.73	0.10	0	0	3	0	0	0	0	0	0
4396.28	0.05	0	0	0	3	0	0	0	0	0
4389.37	0.01	0	0	1	2	0	0	0	0	0
4222.53	0.00	1	0	0	0	0	0	2	0	0
4214.97	0.12	0	1	0	0	0	0	2	0	0
4214.77	0.01	1	0	0	0	0	0	0	2	0
4203.52	0.14	0	1	0	0	0	0	0	2	0
4058.30	0.01	0	1	0	0	1	0	0	0	0
4055.93	0.00	1	0	0	0	0	0	0	0	2
4041.22	0.01	0	1	0	0	0	0	0	0	2
4037.49	0.99	1	0	0	0	1	0	0	0	0
3920.79	3.48	0	1	0	0	0	1	0	0	0
3901.76	0.01	1	0	0	0	0	1	0	0	0
3851.50	0.02	0	0	2	0	1	0	0	0	0
3773.11	0.01	1	0	0	0	0	0	1	0	0
3766.37	0.66	0	1	0	0	0	0	1	0	0
3757.15	0.03	1	0	0	0	0	0	0	1	0
3748.91	0.23	0	1	0	0	0	0	0	1	0
3740.66	0.06	0	0	2	0	0	1	0	0	0
3675.87	0.08	1	0	0	0	0	0	0	0	1
3660.76	0.27	0	1	0	0	0	0	0	0	1
3647.08	0.00	0	0	0	2	1	0	0	0	0
3554.67	0.02	0	0	2	0	0	0	1	0	0
3528.13	0.06	0	0	2	0	0	0	0	1	0
3459.54	0.10	0	0	0	2	0	1	0	0	0
3432.38	0.32	0	0	2	0	0	0	0	0	1
3376.49	0.01	0	0	0	2	0	0	0	1	0
3275.86	0.47	1	0	0	0	0	0	0	0	0
3275.86	0.47	1	0	0	0	0	0	0	0	0
3275.86	0.47	1	0	0	0	0	0	0	0	0
3267.18	0.01	0	0	0	2	0	0	1	0	0
3263.48	0.01	0	0	0	2	0	0	0	0	1
3253.92	12.10	0	1	0	0	0	0	0	0	0
3253.92	12.10	0	1	0	0	0	0	0	0	0
3253.92	12.10	0	1	0	0	0	0	0	0	0

3193.96	2.96	0	0	1	0	2	0	0	0	0
3150.48	10.38	0	0	1	0	0	2	0	0	0
3090.56	0.24	0	0	0	1	2	0	0	0	0
3075.66	62.11	0	0	2	0	0	0	0	0	0
3075.66	62.11	0	0	2	0	0	0	0	0	0
2980.91	16.46	0	0	1	1	0	0	0	0	0
2852.22	0.66	0	0	0	2	0	0	0	0	0
2852.22	0.66	0	0	0	2	0	0	0	0	0
2803.55	2.03	0	0	0	1	0	2	0	0	0
2540.41	0.02	0	0	0	0	3	0	0	0	0
2520.29	5.04	0	0	1	0	0	0	2	0	0
2503.12	4.71	0	0	1	0	0	0	0	2	0
2431.25	0.12	0	0	0	1	0	0	0	2	0
2419.23	0.72	0	0	0	1	0	0	2	0	0
2362.63	0.28	0	0	0	0	2	1	0	0	0
2352.55	0.05	0	0	0	0	1	2	0	0	0
2350.45	0.27	0	0	1	0	1	0	0	0	0
2325.92	0.05	0	0	1	0	0	0	0	0	2
2254.14	2.19	0	0	1	0	0	1	0	0	0
2235.94	0.09	0	0	0	1	1	0	0	0	0
2229.75	0.04	0	0	0	1	0	0	0	0	2
2192.89	0.00	0	0	0	0	2	0	1	0	0
2133.51	0.04	0	0	0	0	2	0	0	1	0
2090.89	2.41	0	0	0	0	0	3	0	0	0
2064.69	0.51	0	0	1	0	0	0	1	0	0
2057.36	0.66	0	0	0	0	2	0	0	0	1
2047.27	0.06	0	0	0	0	0	2	0	1	0
2045.74	0.43	0	0	1	0	0	0	0	1	0
2009.78	0.17	0	0	0	0	0	2	1	0	0
1957.04	0.03	0	0	0	1	0	0	1	0	0
1953.30	0.50	0	0	0	1	0	0	0	1	0
1946.99	0.17	0	0	1	0	0	0	0	0	1
1918.76	0.90	0	0	0	0	0	2	0	0	1
1875.30	1.20	0	0	0	1	0	1	0	0	0
1848.20	0.46	0	0	0	1	0	0	0	0	1
1831.15	0.00	0	0	0	0	1	0	2	0	0
1782.73	0.01	0	0	0	0	1	0	0	2	0
1663.47	0.01	0	0	0	0	0	1	2	0	0
1663.44	0.03	0	0	0	0	0	1	0	2	0
1638.90	1.05	0	0	0	0	2	0	0	0	0
1638.90	1.05	0	0	0	0	2	0	0	0	0
1602.19	0.00	0	0	0	0	1	0	0	0	2

1575.33	1237.20	0	0	1	0	0	0	0	0	0
1575.33	1237.20	0	0	1	0	0	0	0	0	0
1575.33	1237.20	0	0	1	0	0	0	0	0	0
1502.27	0.02	0	0	0	0	0	0	1	2	0
1495.51	0.01	0	0	0	0	0	0	2	1	0
1487.82	0.13	0	0	0	0	0	2	0	0	0
1487.82	0.13	0	0	0	0	0	2	0	0	0
1484.22	0.45	0	0	0	0	1	1	0	0	0
1448.57	0.03	0	0	0	0	0	1	0	0	2
1442.74	124.06	0	0	0	1	0	0	0	0	0
1442.74	124.06	0	0	0	1	0	0	0	0	0
1442.74	124.06	0	0	0	1	0	0	0	0	0
1434.86	0.03	0	0	0	0	0	0	3	0	0
1423.57	0.08	0	0	0	0	0	0	0	3	0
1403.10	0.24	0	0	0	0	0	0	2	0	1
1384.71	0.24	0	0	0	0	0	0	0	2	1
1338.08	0.27	0	0	0	0	1	0	1	0	0
1316.80	0.01	0	0	0	0	0	0	1	0	2
1305.56	7.74	0	0	0	0	1	0	0	1	0
1296.43	0.01	0	0	0	0	0	0	0	1	2
1210.86	0.02	0	0	0	0	1	0	0	0	1
1191.62	11.54	0	0	0	0	0	1	1	0	0
1177.92	0.05	0	0	0	0	0	0	0	0	3
1175.51	0.73	0	0	0	0	0	1	0	1	0
1063.77	0.45	0	0	0	0	0	1	0	0	1
1024.54	0.36	0	0	0	0	0	0	1	1	0
978.02	4.03	0	0	0	0	0	0	2	0	0
978.02	4.03	0	0	0	0	0	0	2	0	0
964.53	5.14	0	0	0	0	0	0	0	2	0
964.53	5.14	0	0	0	0	0	0	0	2	0
926.01	0.00	0	0	0	0	0	0	1	0	1
907.13	0.24	0	0	0	0	0	0	0	1	1
812.54	0.85	0	0	0	0	1	0	0	0	0
812.54	0.85	0	0	0	0	1	0	0	0	0
812.54	0.85	0	0	0	0	1	0	0	0	0
795.36	3.55	0	0	0	0	0	0	0	0	2
795.36	3.55	0	0	0	0	0	0	0	0	2
704.31	62.45	0	0	0	0	0	1	0	0	0
704.31	62.45	0	0	0	0	0	1	0	0	0
704.31	62.45	0	0	0	0	0	1	0	0	0
504.22	0.20	0	0	0	0	0	0	1	0	0
504.22	0.20	0	0	0	0	0	0	1	0	0

504.22	0.20	0 0 0 0 0 0 1 0 0
493.92	11.16	0 0 0 0 0 0 0 1 0
493.92	11.16	0 0 0 0 0 0 0 1 0
493.92	11.16	0 0 0 0 0 0 0 1 0
402.54	69.92	0 0 0 0 0 0 0 0 1
402.54	69.92	0 0 0 0 0 0 0 0 1
402.54	69.92	0 0 0 0 0 0 0 0 1

$\mathbf{HRnNF_2}$

Frequency (cm-1)	Intensity (km.mol-1)	Vibrational quanta
4499.70	0.51	3 0 0 0 0 0 0 0 0
4019.39	0.03	2 1 0 0 0 0 0 0 0
3953.99	0.00	2 0 1 0 0 0 0 0 0
3635.22	0.11	2 0 0 1 0 0 0 0 0
3578.25	0.03	2 0 0 0 0 1 0 0 0
3573.79	0.07	2 0 0 0 1 0 0 0 0
3459.76	0.67	2 0 0 0 0 0 1 0 0
3458.21	0.04	1 2 0 0 0 0 0 0 0
3307.70	0.32	1 0 2 0 0 0 0 0 0
3232.81	0.84	2 0 0 0 0 0 0 1 0
3229.27	0.01	2 0 0 0 0 0 0 0 1
3075.73	34.76	2 0 0 0 0 0 0 0 0
3075.73	34.76	2 0 0 0 0 0 0 0 0
2849.26	0.05	0 3 0 0 0 0 0 0 0
2760.97	0.09	0 2 1 0 0 0 0 0 0
2709.60	1.00	1 0 0 2 0 0 0 0 0
2672.54	0.02	0 1 2 0 0 0 0 0 0
2600.53	0.35	0 0 3 0 0 0 0 0 0
2591.73	2.92	1 0 0 0 2 0 0 0 0
2566.19	0.00	1 0 0 0 0 2 0 0 0
2517.87	1.11	1 1 0 0 0 0 0 0 0
2490.59	0.01	0 2 0 1 0 0 0 0 0
2443.48	0.04	1 0 1 0 0 0 0 0 0
2442.06	0.00	0 2 0 0 1 0 0 0 0
2390.15	0.07	0 2 0 0 0 1 0 0 0
2342.17	1.59	1 0 0 0 0 0 2 0 0
2326.79	0.01	0 0 2 1 0 0 0 0 0
2305.04	0.03	0 2 0 0 0 0 1 0 0
2278.90	0.00	0 0 2 0 1 0 0 0 0
2216.59	0.01	0 0 2 0 0 1 0 0 0

2145.50	0.74	1	0	0	1	0	0	0	0	0
2137.90	0.00	0	1	0	2	0	0	0	0	0
2133.80	0.05	0	0	2	0	0	0	1	0	0
2091.74	1.01	1	0	0	0	1	0	0	0	0
2067.43	1.57	1	0	0	0	0	1	0	0	0
2059.45	0.05	0	2	0	0	0	0	0	1	0
2057.80	0.02	0	0	1	2	0	0	0	0	0
2055.71	0.00	0	2	0	0	0	0	0	0	1
2041.38	0.02	0	1	0	0	2	0	0	0	0
1961.61	0.06	0	0	1	0	2	0	0	0	0
1959.14	0.46	1	0	0	0	0	0	1	0	0
1940.35	0.00	0	1	0	0	0	2	0	0	0
1904.32	6.17	0	2	0	0	0	0	0	0	0
1904.32	6.17	0	2	0	0	0	0	0	0	0
1892.53	0.05	0	0	2	0	0	0	0	1	0
1884.34	0.00	0	0	2	0	0	0	0	0	1
1882.58	0.02	1	0	0	0	0	0	0	2	0
1873.05	0.63	1	0	0	0	0	0	0	0	2
1850.55	0.01	0	0	1	0	0	2	0	0	0
1818.08	4.65	0	1	1	0	0	0	0	0	0
1756.09	0.26	0	1	0	0	0	0	2	0	0
1751.74	0.01	0	0	0	3	0	0	0	0	0
1740.57	0.61	0	0	2	0	0	0	0	0	0
1740.57	0.61	0	0	2	0	0	0	0	0	0
1725.48	10.14	1	0	0	0	0	0	0	1	0
1720.37	0.33	1	0	0	0	0	0	0	0	1
1707.34	0.00	0	0	0	2	1	0	0	0	0
1680.68	0.00	0	0	0	2	0	1	0	0	0
1668.92	0.05	0	0	1	0	0	0	2	0	0
1658.23	0.01	0	0	0	1	2	0	0	0	0
1586.69	0.01	0	0	0	0	3	0	0	0	0
1583.74	0.00	0	0	0	1	0	2	0	0	0
1582.15	0.02	0	0	0	0	2	1	0	0	0
1579.25	1657.09	1	0	0	0	0	0	0	0	0
1579.25	1657.09	1	0	0	0	0	0	0	0	0
1579.25	1657.09	1	0	0	0	0	0	0	0	0
1574.72	0.00	0	0	0	2	0	0	1	0	0
1548.38	0.48	0	1	0	1	0	0	0	0	0
1533.43	0.00	0	0	0	0	1	2	0	0	0
1498.73	0.10	0	1	0	0	1	0	0	0	0
1485.73	0.00	0	0	0	0	0	3	0	0	0
1468.75	0.05	0	0	0	0	2	0	1	0	0

1466.21	0.00	0	0	1	1	0	0	0	0	0
1449.86	1.09	0	1	0	0	0	1	0	0	0
1416.65	0.01	0	0	1	0	1	0	0	0	0
1391.43	0.00	0	0	0	0	0	2	1	0	0
1379.75	0.02	0	0	0	1	0	0	2	0	0
1363.27	0.07	0	0	1	0	0	1	0	0	0
1361.26	0.66	0	1	0	0	0	0	1	0	0
1338.34	0.01	0	0	0	2	0	0	0	1	0
1332.86	0.00	0	0	0	2	0	0	0	0	1
1320.68	0.00	0	0	0	0	1	0	2	0	0
1292.27	0.00	0	0	0	0	0	1	2	0	0
1273.25	0.09	0	0	1	0	0	0	1	0	0
1273.04	0.07	0	1	0	0	0	0	0	2	0
1265.02	0.09	0	1	0	0	0	0	0	0	2
1238.67	0.01	0	0	0	0	2	0	0	1	0
1234.67	0.01	0	0	0	0	2	0	0	0	1
1190.04	0.02	0	0	1	0	0	0	0	2	0
1177.15	0.07	0	0	1	0	0	0	0	0	2
1177.02	3.64	0	0	0	2	0	0	0	0	0
1177.02	3.64	0	0	0	2	0	0	0	0	0
1172.46	0.14	0	0	0	0	0	0	3	0	0
1151.98	0.00	0	0	0	0	0	2	0	1	0
1144.87	0.00	0	0	0	0	0	2	0	0	1
1126.12	0.04	0	0	0	1	1	0	0	0	0
1116.50	1.84	0	1	0	0	0	0	0	1	0
1111.76	0.13	0	1	0	0	0	0	0	0	1
1089.26	0.10	0	0	0	1	0	1	0	0	0
1070.81	13.31	0	0	0	0	2	0	0	0	0
1070.81	13.31	0	0	0	0	2	0	0	0	0
1038.61	0.10	0	0	0	0	1	1	0	0	0
1032.72	0.14	0	0	1	0	0	0	0	1	0
1025.60	0.13	0	0	1	0	0	0	0	0	1
992.12	0.04	0	0	0	0	0	2	0	0	0
992.12	0.04	0	0	0	0	0	2	0	0	0
989.15	12.23	0	0	0	1	0	0	1	0	0
955.53	0.07	0	0	0	0	0	0	2	1	0
954.77	240.96	0	1	0	0	0	0	0	0	0
954.77	240.96	0	1	0	0	0	0	0	0	0
954.77	240.96	0	1	0	0	0	0	0	0	0
944.42	0.00	0	0	0	0	0	0	2	0	1
934.22	0.26	0	0	0	0	1	0	1	0	0
905.60	0.00	0	0	0	1	0	0	0	2	0

896.43	0.17	0	0	0	0	0	1	1	0	0
895.11	0.01	0	0	0	1	0	0	0	0	2
874.00	111.73	0	0	1	0	0	0	0	0	0
874.00	111.73	0	0	1	0	0	0	0	0	0
874.00	111.73	0	0	1	0	0	0	0	0	0
853.98	0.00	0	0	0	0	1	0	0	2	0
846.97	0.00	0	0	0	0	1	0	0	0	2
815.64	0.01	0	0	0	0	0	1	0	2	0
803.55	0.02	0	0	0	0	0	1	0	0	2
790.17	1.65	0	0	0	0	0	0	2	0	0
790.17	1.65	0	0	0	0	0	0	2	0	0
749.99	5.48	0	0	0	1	0	0	0	1	0
744.06	0.01	0	0	0	1	0	0	0	0	1
719.21	0.00	0	0	0	0	0	0	1	2	0
702.86	0.04	0	0	0	0	0	0	1	0	2
698.64	0.01	0	0	0	0	1	0	0	1	0
694.44	4.39	0	0	0	0	1	0	0	0	1
657.08	0.05	0	0	0	0	0	1	0	1	0
650.73	0.02	0	0	0	0	0	1	0	0	1
592.81	9.66	0	0	0	1	0	0	0	0	0
592.81	9.66	0	0	0	1	0	0	0	0	0
592.81	9.66	0	0	0	1	0	0	0	0	0
560.21	0.67	0	0	0	0	0	0	1	1	0
551.32	0.00	0	0	0	0	0	0	1	0	1
541.66	9.78	0	0	0	0	1	0	0	0	0
541.66	9.78	0	0	0	0	1	0	0	0	0
541.66	9.78	0	0	0	0	1	0	0	0	0
496.85	34.05	0	0	0	0	0	1	0	0	0
496.85	34.05	0	0	0	0	0	1	0	0	0
496.85	34.05	0	0	0	0	0	1	0	0	0
474.78	0.00	0	0	0	0	0	0	0	3	0
473.40	0.00	0	0	0	0	0	0	0	2	1
468.29	0.00	0	0	0	0	0	0	0	1	2
457.37	0.00	0	0	0	0	0	0	0	0	3
399.06	47.37	0	0	0	0	0	0	1	0	0
399.06	47.37	0	0	0	0	0	0	1	0	0
399.06	47.37	0	0	0	0	0	0	1	0	0
317.36	0.01	0	0	0	0	0	0	0	2	0
317.36	0.01	0	0	0	0	0	0	0	2	0
314.17	0.03	0	0	0	0	0	0	0	1	1
305.80	0.02	0	0	0	0	0	0	0	0	2
305.80	0.02	0	0	0	0	0	0	0	0	2

159.04	2.57	0 0 0 0 0 0 0 1 0
159.04	2.57	0 0 0 0 0 0 0 1 0
159.04	2.57	0 0 0 0 0 0 0 1 0
153.31	0.04	0 0 0 0 0 0 0 0 1
153.31	0.04	0 0 0 0 0 0 0 0 1
153.31	0.04	0 0 0 0 0 0 0 0 1

$HRnPH_2$

Frequency (cm-1)	Intensity (km.mol-1)	Vibrational quanta
7147.64	0.04	1 2 0 0 0 0 0 0 0
6833.64	0.01	0 3 0 0 0 0 0 0 0
6750.13	1.55	3 0 0 0 0 0 0 0 0
6667.08	0.27	2 1 0 0 0 0 0 0 0
5911.08	0.01	0 2 1 0 0 0 0 0 0
5819.32	11.66	2 0 1 0 0 0 0 0 0
5692.80	0.00	0 2 0 1 0 0 0 0 0
5553.69	0.18	2 0 0 1 0 0 0 0 0
5201.96	0.00	0 2 0 0 1 0 0 0 0
5187.61	0.00	0 2 0 0 0 1 0 0 0
5079.69	0.00	2 0 0 0 1 0 0 0 0
5063.58	0.06	2 0 0 0 0 1 0 0 0
5021.28	0.01	0 2 0 0 0 0 1 0 0
5014.57	0.01	0 2 0 0 0 0 0 1 0
4915.40	0.22	2 0 0 0 0 0 1 0 0
4908.38	0.27	2 0 0 0 0 0 0 1 0
4861.71	0.07	0 1 2 0 0 0 0 0 0
4854.71	0.00	0 2 0 0 0 0 0 0 1
4837.36	0.00	1 0 2 0 0 0 0 0 0
4764.06	0.28	2 0 0 0 0 0 0 0 1
4603.13	0.17	0 2 0 0 0 0 0 0 0
4603.13	0.17	0 2 0 0 0 0 0 0 0
4568.60	0.27	2 0 0 0 0 0 0 0 0
4568.60	0.27	2 0 0 0 0 0 0 0 0
4551.44	0.96	1 1 0 0 0 0 0 0 0
4463.47	0.00	0 1 0 2 0 0 0 0 0
4406.28	0.03	1 0 0 2 0 0 0 0 0
3713.26	11.67	0 0 3 0 0 0 0 0 0
3618.30	0.60	0 1 1 0 0 0 0 0 0
3607.25	0.00	0 0 2 1 0 0 0 0 0
3594.23	0.08	1 0 1 0 0 0 0 0 0

3514.88	0.07	0 1 0 0 2 0 0 0 0
3492.58	0.10	0 1 0 0 0 2 0 0 0
3478.41	0.09	1 0 0 0 2 0 0 0 0
3455.24	0.06	1 0 0 0 0 2 0 0 0
3426.01	0.01	0 0 1 2 0 0 0 0 0
3420.36	0.19	0 1 0 1 0 0 0 0 0
3373.00	0.06	1 0 0 1 0 0 0 0 0
3203.79	0.07	0 0 0 3 0 0 0 0 0
3103.20	0.36	0 1 0 0 0 0 2 0 0
3092.44	0.34	0 1 0 0 0 0 0 2 0
3083.88	0.06	0 0 2 0 1 0 0 0 0
3075.21	0.11	1 0 0 0 0 0 2 0 0
3067.27	0.11	0 0 2 0 0 1 0 0 0
3064.66	0.17	1 0 0 0 0 0 0 2 0
2924.92	0.01	0 1 0 0 1 0 0 0 0
2908.63	0.31	0 1 0 0 0 1 0 0 0
2899.67	0.22	0 0 2 0 0 0 1 0 0
2892.02	0.22	0 0 2 0 0 0 0 1 0
2884.92	0.02	1 0 0 0 1 0 0 0 0
2868.35	0.03	1 0 0 0 0 1 0 0 0
2771.79	0.00	0 1 0 0 0 0 0 0 2
2747.47	0.00	1 0 0 0 0 0 0 0 2
2735.91	0.24	0 1 0 0 0 0 1 0 0
2729.16	0.05	0 1 0 0 0 0 0 1 0
2722.92	0.00	0 0 0 2 1 0 0 0 0
2721.23	5.59	0 0 2 0 0 0 0 0 1
2705.88	0.02	1 0 0 0 0 0 1 0 0
2699.27	0.15	1 0 0 0 0 0 0 1 0
2696.39	0.00	0 0 0 2 0 1 0 0 0
2560.18	0.01	0 1 0 0 0 0 0 0 1
2549.69	0.00	0 0 0 2 0 0 1 0 0
2544.04	0.00	0 0 0 2 0 0 0 1 0
2535.83	0.00	1 0 0 0 0 0 0 0 1
2521.75	228.48	0 0 2 0 0 0 0 0 0
2521.75	228.48	0 0 2 0 0 0 0 0 0
2441.70	4.02	0 0 1 0 2 0 0 0 0
2420.96	4.14	0 0 1 0 0 2 0 0 0
2369.53	0.00	0 0 0 2 0 0 0 0 1
2361.87	0.02	0 0 1 1 0 0 0 0 0
2339.37	43.11	0 1 0 0 0 0 0 0 0
2339.37	43.11	0 1 0 0 0 0 0 0 0
2339.37	43.11	0 1 0 0 0 0 0 0 0

2321.82	50.30	1	0	0	0	0	0	0	0	0
2321.82	50.30	1	0	0	0	0	0	0	0	0
2321.82	50.30	1	0	0	0	0	0	0	0	0
2264.97	0.05	0	0	0	1	2	0	0	0	0
2248.11	0.08	0	0	0	1	0	2	0	0	0
2149.95	0.10	0	0	0	2	0	0	0	0	0
2149.95	0.10	0	0	0	2	0	0	0	0	0
2020.28	13.10	0	0	1	0	0	0	2	0	0
2008.90	14.24	0	0	1	0	0	0	0	2	0
1856.70	0.12	0	0	0	1	0	0	2	0	0
1846.88	0.07	0	0	0	1	0	0	0	2	0
1845.35	0.30	0	0	1	0	1	0	0	0	0
1830.86	3.23	0	0	1	0	0	1	0	0	0
1792.05	0.00	0	0	0	0	3	0	0	0	0
1776.73	0.00	0	0	0	0	0	3	0	0	0
1770.14	0.00	0	0	0	0	2	1	0	0	0
1766.70	0.00	0	0	0	0	1	2	0	0	0
1687.12	0.03	0	0	1	0	0	0	0	0	2
1662.56	2.08	0	0	1	0	0	0	1	0	0
1657.72	0.00	0	0	0	1	1	0	0	0	0
1655.90	1.46	0	0	1	0	0	0	0	1	0
1634.74	0.30	0	0	0	1	0	1	0	0	0
1603.51	0.02	0	0	0	0	2	0	1	0	0
1573.35	0.00	0	0	0	0	2	0	0	1	0
1570.95	0.02	0	0	0	0	0	2	0	1	0
1555.98	0.08	0	0	0	0	0	2	1	0	0
1512.84	0.00	0	0	0	1	0	0	0	0	2
1482.01	11.78	0	0	1	0	0	0	0	0	1
1480.42	0.20	0	0	0	1	0	0	1	0	0
1474.10	0.03	0	0	0	1	0	0	0	1	0
1398.54	0.06	0	0	0	0	2	0	0	0	1
1380.26	0.00	0	0	0	0	1	0	2	0	0
1374.87	0.08	0	0	0	0	0	2	0	0	1
1352.42	0.02	0	0	0	0	1	0	0	2	0
1352.34	0.00	0	0	0	0	0	1	0	2	0
1348.93	0.01	0	0	0	0	0	1	2	0	0
1301.12	0.01	0	0	0	1	0	0	0	0	1
1285.01	1743.05	0	0	1	0	0	0	0	0	0
1285.01	1743.05	0	0	1	0	0	0	0	0	0
1285.01	1743.05	0	0	1	0	0	0	0	0	0
1182.17	0.23	0	0	0	0	2	0	0	0	0
1182.17	0.23	0	0	0	0	2	0	0	0	0

1166.03	0.28	0	0	0	0	1	1	0	0	0
1166.00	0.37	0	0	0	0	0	2	0	0	0
1166.00	0.37	0	0	0	0	0	2	0	0	0
1164.85	0.02	0	0	0	0	0	0	2	1	0
1162.12	0.07	0	0	0	0	0	0	1	2	0
1113.83	0.08	0	0	0	0	0	0	3	0	0
1099.78	0.12	0	0	0	0	0	0	0	3	0
1081.63	15.95	0	0	0	1	0	0	0	0	0
1081.63	15.95	0	0	0	1	0	0	0	0	0
1081.63	15.95	0	0	0	1	0	0	0	0	0
1003.93	0.00	0	0	0	0	1	0	0	0	2
989.20	0.19	0	0	0	0	1	0	1	0	0
988.36	0.00	0	0	0	0	0	1	0	0	2
985.94	0.00	0	0	0	0	0	0	2	0	1
974.74	8.42	0	0	0	0	1	0	0	1	0
974.38	0.01	0	0	0	0	0	0	0	2	1
965.93	9.22	0	0	0	0	0	1	1	0	0
965.84	0.14	0	0	0	0	0	1	0	1	0
817.67	0.01	0	0	0	0	0	0	1	0	2
810.68	0.01	0	0	0	0	0	0	0	1	2
794.11	0.01	0	0	0	0	1	0	0	0	1
787.45	0.14	0	0	0	0	0	0	1	1	0
778.12	0.01	0	0	0	0	0	1	0	0	1
761.44	7.40	0	0	0	0	0	0	2	0	0
761.44	7.40	0	0	0	0	0	0	2	0	0
750.40	7.83	0	0	0	0	0	0	0	2	0
750.40	7.83	0	0	0	0	0	0	0	2	0
636.23	0.01	0	0	0	0	0	0	0	0	3
607.15	0.20	0	0	0	0	0	0	1	0	1
600.27	0.25	0	0	0	0	0	0	0	1	1
587.02	0.00	0	0	0	0	1	0	0	0	0
587.02	0.00	0	0	0	0	1	0	0	0	0
587.02	0.00	0	0	0	0	1	0	0	0	0
571.71	5.15	0	0	0	0	0	1	0	0	0
571.71	5.15	0	0	0	0	0	1	0	0	0
571.71	5.15	0	0	0	0	0	1	0	0	0
425.85	0.33	0	0	0	0	0	0	0	0	2
425.85	0.33	0	0	0	0	0	0	0	0	2
390.13	10.23	0	0	0	0	0	0	1	0	0
390.13	10.23	0	0	0	0	0	0	1	0	0
390.13	10.23	0	0	0	0	0	0	1	0	0
383.96	13.13	0	0	0	0	0	0	0	1	0

383.96	13.13	0 0 0 0 0 0 0 1 0
383.96	13.13	0 0 0 0 0 0 0 1 0
213.75	8.38	0 0 0 0 0 0 0 0 1
213.75	8.38	0 0 0 0 0 0 0 0 1
213.75	8.38	0 0 0 0 0 0 0 0 1

$HRnPF_2$

Frequency (cm-1)	Intensity (km.mol-1)	Vibrational quanta
3244.89	2.55	3 0 0 0 0 0 0 0 0
3006.14	0.10	2 1 0 0 0 0 0 0 0
3005.58	4.29	2 0 1 0 0 0 0 0 0
2713.37	0.02	1 0 2 0 0 0 0 0 0
2712.34	0.48	1 2 0 0 0 0 0 0 0
2580.69	0.34	2 0 0 1 0 0 0 0 0
2548.69	0.29	2 0 0 0 0 1 0 0 0
2548.21	0.70	2 0 0 0 1 0 0 0 0
2395.35	24.89	2 0 0 0 0 0 1 0 0
2390.71	0.24	0 3 0 0 0 0 0 0 0
2368.08	0.00	0 0 3 0 0 0 0 0 0
2366.60	0.06	0 1 2 0 0 0 0 0 0
2361.89	0.15	0 2 1 0 0 0 0 0 0
2307.38	0.12	2 0 0 0 0 0 0 1 0
2288.37	26.51	2 0 0 0 0 0 0 0 1
2188.18	201.43	2 0 0 0 0 0 0 0 0
2188.18	201.43	2 0 0 0 0 0 0 0 0
2008.69	0.01	0 2 0 1 0 0 0 0 0
2005.08	0.00	0 0 2 1 0 0 0 0 0
1983.31	0.01	0 2 0 0 1 0 0 0 0
1980.17	0.00	0 0 2 0 1 0 0 0 0
1929.69	0.01	0 2 0 0 0 1 0 0 0
1926.87	0.01	0 0 2 0 0 1 0 0 0
1921.50	0.00	1 1 0 0 0 0 0 0 0
1920.66	36.51	1 0 1 0 0 0 0 0 0
1892.07	9.91	1 0 0 2 0 0 0 0 0
1820.27	0.01	0 2 0 0 0 0 1 0 0
1819.46	0.06	0 0 2 0 0 0 1 0 0
1814.15	22.70	1 0 0 0 2 0 0 0 0
1809.55	0.14	1 0 0 0 0 2 0 0 0
1691.37	0.00	0 0 2 0 0 0 0 1 0
1688.84	0.00	0 2 0 0 0 0 0 1 0

1685.66	0.00	0	2	0	0	0	0	0	0	1
1682.77	0.00	0	0	2	0	0	0	0	0	1
1628.33	0.02	0	1	0	2	0	0	0	0	0
1626.25	0.52	0	0	1	2	0	0	0	0	0
1588.48	0.12	0	2	0	0	0	0	0	0	0
1588.48	0.12	0	2	0	0	0	0	0	0	0
1583.49	2.69	0	1	1	0	0	0	0	0	0
1583.29	0.66	0	0	2	0	0	0	0	0	0
1583.29	0.66	0	0	2	0	0	0	0	0	0
1574.39	0.08	0	1	0	0	2	0	0	0	0
1574.37	1.18	0	0	1	0	2	0	0	0	0
1534.31	0.29	1	0	0	0	0	0	2	0	0
1515.51	1.14	1	0	0	1	0	0	0	0	0
1486.19	1.36	1	0	0	0	1	0	0	0	0
1484.81	0.01	0	1	0	0	0	2	0	0	0
1484.04	0.02	0	0	1	0	0	2	0	0	0
1465.86	0.57	1	0	0	0	0	1	0	0	0
1332.53	75.18	1	0	0	0	0	0	1	0	0
1318.49	4.05	1	0	0	0	0	0	0	2	0
1295.86	0.34	1	0	0	0	0	0	0	0	2
1256.40	0.23	0	0	1	0	0	0	2	0	0
1256.09	0.04	0	1	0	0	0	0	2	0	0
1233.25	0.04	0	0	0	3	0	0	0	0	0
1220.46	0.33	1	0	0	0	0	0	0	1	0
1215.90	0.00	0	1	0	1	0	0	0	0	0
1214.43	0.33	0	0	1	1	0	0	0	0	0
1211.42	58.09	1	0	0	0	0	0	0	0	1
1203.66	0.01	0	0	0	2	1	0	0	0	0
1188.91	0.01	0	1	0	0	1	0	0	0	0
1187.98	0.18	0	0	1	0	1	0	0	0	0
1177.16	0.01	0	0	0	2	0	1	0	0	0
1166.43	0.06	0	0	0	1	2	0	0	0	0
1150.06	0.05	0	0	0	0	3	0	0	0	0
1141.50	0.11	0	1	0	0	0	1	0	0	0
1140.59	0.77	0	0	1	0	0	1	0	0	0
1133.41	1375.53	1	0	0	0	0	0	0	0	0
1128.36	1383.52	1	0	0	0	0	0	0	0	0
1128.36	1383.52	1	0	0	0	0	0	0	0	0
1122.46	0.01	0	0	0	0	2	1	0	0	0
1109.63	0.01	0	0	0	1	0	2	0	0	0
1080.51	0.00	0	0	0	0	1	2	0	0	0
1056.93	0.28	0	0	0	2	0	0	1	0	0

1038.04	0.00	0	0	0	0	0	3	0	0	0
1029.64	0.82	0	0	1	0	0	0	1	0	0
1028.99	0.01	0	1	0	0	0	0	1	0	0
1002.24	0.56	0	0	1	0	0	0	0	2	0
1000.81	0.21	0	1	0	0	0	0	0	2	0
993.64	0.73	0	0	0	0	2	0	1	0	0
989.14	0.02	0	1	0	0	0	0	0	0	2
987.72	0.10	0	0	1	0	0	0	0	0	2
932.35	0.00	0	0	0	2	0	0	0	1	0
926.46	0.21	0	0	0	2	0	0	0	0	1
924.89	0.00	0	0	0	0	0	2	1	0	0
899.86	0.04	0	0	1	0	0	0	0	1	0
899.02	0.21	0	1	0	0	0	0	0	1	0
894.67	0.11	0	1	0	0	0	0	0	0	1
893.58	0.96	0	0	1	0	0	0	0	0	1
881.81	0.00	0	0	0	0	2	0	0	1	0
867.95	0.51	0	0	0	0	2	0	0	0	1
867.79	0.25	0	0	0	1	0	0	2	0	0
829.46	0.00	0	0	0	0	1	0	2	0	0
824.94	8.12	0	0	0	2	0	0	0	0	0
824.94	8.12	0	0	0	2	0	0	0	0	0
804.03	0.01	0	0	0	0	0	1	2	0	0
798.20	140.91	0	1	0	0	0	0	0	0	0
798.00	140.83	0	1	0	0	0	0	0	0	0
798.00	140.83	0	1	0	0	0	0	0	0	0
796.95	0.00	0	0	0	0	0	2	0	1	0
796.85	0.01	0	0	0	1	1	0	0	0	0
795.46	432.93	0	0	1	0	0	0	0	0	0
794.89	432.96	0	0	1	0	0	0	0	0	0
794.89	432.96	0	0	1	0	0	0	0	0	0
791.08	0.00	0	0	0	0	0	2	0	0	1
764.60	13.56	0	0	0	0	2	0	0	0	0
764.60	13.56	0	0	0	0	2	0	0	0	0
763.45	3.03	0	0	0	1	0	1	0	0	0
734.90	0.00	0	0	0	0	1	1	0	0	0
692.58	0.16	0	0	0	0	0	2	0	0	0
692.58	0.16	0	0	0	0	0	2	0	0	0
686.68	0.01	0	0	0	0	0	0	3	0	0
645.34	4.89	0	0	0	1	0	0	1	0	0
619.58	0.02	0	0	0	1	0	0	0	2	0
612.45	0.77	0	0	0	0	1	0	1	0	0
606.40	0.05	0	0	0	1	0	0	0	0	2

595.99	0.02	0	0	0	0	1	0	0	2	0
577.44	0.84	0	0	0	0	0	1	1	0	0
573.29	0.00	0	0	0	0	1	0	0	0	2
567.43	0.00	0	0	0	0	0	0	2	1	0
557.41	0.03	0	0	0	0	0	0	2	0	1
552.12	0.03	0	0	0	0	0	1	0	2	0
538.77	0.00	0	0	0	0	0	1	0	0	2
518.28	0.00	0	0	0	1	0	0	0	1	0
513.35	1.30	0	0	0	1	0	0	0	0	1
492.51	2.95	0	0	0	0	1	0	0	1	0
482.94	0.26	0	0	0	0	1	0	0	0	1
455.95	0.21	0	0	0	0	0	0	2	0	0
455.95	0.21	0	0	0	0	0	0	2	0	0
449.49	0.04	0	0	0	0	0	1	0	1	0
443.85	0.36	0	0	0	0	0	1	0	0	1
439.03	0.00	0	0	0	0	0	0	1	2	0
423.21	0.00	0	0	0	0	0	0	1	0	2
418.04	14.15	0	0	0	1	0	0	0	0	0
417.07	14.15	0	0	0	1	0	0	0	0	0
417.07	14.15	0	0	0	1	0	0	0	0	0
390.67	23.85	0	0	0	0	1	0	0	0	0
389.09	23.83	0	0	0	0	1	0	0	0	0
389.09	23.83	0	0	0	0	1	0	0	0	0
346.83	14.66	0	0	0	0	0	1	0	0	0
346.75	14.66	0	0	0	0	0	1	0	0	0
346.75	14.66	0	0	0	0	0	1	0	0	0
335.07	0.07	0	0	0	0	0	0	1	1	0
328.33	0.10	0	0	0	0	0	0	1	0	1
313.47	0.02	0	0	0	0	0	0	0	3	0
308.99	0.00	0	0	0	0	0	0	0	2	1
297.01	0.00	0	0	0	0	0	0	0	1	2
287.02	0.00	0	0	0	0	0	0	0	0	3
231.09	6.10	0	0	0	0	0	0	1	0	0
230.35	6.10	0	0	0	0	0	0	1	0	0
230.35	6.10	0	0	0	0	0	0	1	0	0
204.11	0.01	0	0	0	0	0	0	0	2	0
204.11	0.01	0	0	0	0	0	0	0	2	0
201.18	0.10	0	0	0	0	0	0	0	1	1
191.05	0.04	0	0	0	0	0	0	0	0	2
191.05	0.04	0	0	0	0	0	0	0	0	2
103.75	2.04	0	0	0	0	0	0	0	1	0
102.49	2.04	0	0	0	0	0	0	0	1	0

```
102.49       2.04    0 0 0 0 0 0 0 1 0
 96.70       1.01    0 0 0 0 0 0 0 0 1
 96.25       1.01    0 0 0 0 0 0 0 0 1
 96.25       1.01    0 0 0 0 0 0 0 0 1
```